



Geometry Modification Assessment and Design Optimization of Miniaturized Wideband Antennas

Muhammad Aziz UI Haq

Doctor of Philosophy

May 2019

Electrical Engineering

Reykjavík University

Ph.D. Dissertation



Geometry Modification Assessment and Design Optimization of Miniaturized Wideband Antennas

Dissertation submitted to the School of Science and Engineering
at Reykjavík University in partial fulfillment of
the requirements for the degree of
Doctor of Philosophy (Ph.D.) in Electrical Engineering

May 2019

Thesis Committee:

Slawomir Koziel, Professor, and Supervisor
Reykjavík University, Reykjavík, Iceland

Ágúst Valfells, Dean of School of Science and Engineering
Reykjavík University, Reykjavík, Iceland

Eyjólfur Ingi Ásgeirsson, Associate Professor
Reykjavík University, Reykjavík, Iceland

Kristján Leósson, General Manager
Innovation Center Iceland

Thesis Examiner:

Ivor Morrow, Senior Lecturer
Cranfield University, UK

Copyright
Muhammad Aziz Ul Haq
May 2019

Geometry Modification Assessment and Design Optimization of Miniaturized Wideband Antennas

Muhammad Aziz Ul Haq

May 2019

Abstract

Maintaining small physical dimensions of antenna structures is an important consideration for contemporary wireless communication systems. Typically, antenna miniaturization is achieved through various topological modifications of the basic antenna geometries. The modifications can be applied to the ground plane, the feed line, and/or antenna radiator. Unfortunately, various topology alteration options are normally reported on a case-to-case basis. The literature is lacking systematic investigations or comparisons of different modification methods and their effects on antenna miniaturization rate as well as electrical performance. Another critical issue—apart from setting up the antenna topology—is a proper adjustment of geometry parameters of the structure so that the optimum design can be identified. Majority of researchers utilize experience-driven parameter sweeping which typically yields designs that are acceptable, but definitely not optimal. Furthermore, in many of the cases, the authors provide a cooperative progression before and after topological modifications that generally lead to a certain reduction of the antenna size, however, with appropriate parameter adjustment missing. Consequently, suitability of particular modifications in the miniaturization context is not conclusively assessed. In order to carry out such an assessment in a reliable manner, identification of the truly optimum design is necessary. This requires rigorous numerical optimization of all antenna parameters (especially in the case of complex antenna topologies) with the primary objective being size reduction, and supplementary constraints imposed on selected electrical or field characteristics. This thesis is an attempt to carry out systematic investigations concerning the relevance of geometry modifications in the context of wideband antenna miniaturization. The studies are carried out based on selected benchmark sets of wideband antennas. In order to ensure a fair comparison, all geometry parameters are rigorously tuned through EM-driven optimization to obtain the minimum footprint while maintaining acceptable electrical performance. The results demonstrate that it is possible to conclusively distinguish certain classes of topology alterations that are generally advantageous in the context of size reduction, as well as quantify the benefits of modifications applied to various parts of the antenna structure, e.g., with feed line modifications being more efficient than the ground plane and radiator ones. Several counterexamples have been discussed as well, indicating that certain modifications can be counterproductive when introduced ad hoc and without proper parameter tuning. The results of these investigations have been utilized to design several instances of novel compact wideband antennas with the focus on isolation improvement and overall antenna size reduction in multi-input-multi-output (MIMO) systems. Experimental validations confirming the numerical findings are also provided. To the best of the author's knowledge, the presented study is the first systematic investigation of this kind in the literature and can be considered a step towards the development of better, low-cost, and more compact antennas for wireless communication systems.

Mat Á Formbreytingu og Bestun Hönnunar Á Smækkuðum Bandbreiðum Loftnetum

Muhammad Aziz Ul Haq

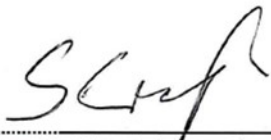
Mai 2019

Útdráttur

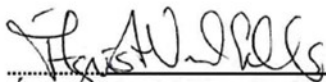
Fyrir þráðlaus fjarskiptakerfi er mikilvægt að tryggja að loftnet séu lítil að umfangi. Yfirleitt er smækkun loftneta náð með ýmis konar formbreytingum á grunngerðum þeirra. Formbreytingarnar geta verið á jarðtengingu, fæðilínu og / eða geislagjafa. Því miður er venjulega einungis sagt frá slíkum formbreytingum fyrir einstaka tilvik. Skortur er á kerfisbundnu mati og samanburði á mismunandi formbreytingum og hvaða áhrif þær hafa á smækkun og raffræðilega eiginleika loftneta. Annað mikilvægt atriði, fyrir utan að ákveða gerð formbreytingarinnar, er að velja stika sem lýsa nákvæmri lögun svo að bestuð hönnun geti átt sér stað. Flestir hönnuðir notast við þá aðferð að notast við stikaskimun sem byggir á reynslugögnum, en sú aðferð skilar almennt ásættanlegri hönnun, þó ekki bestaðri. Einnig er í mörgum tilvikum sagt frá samhliða þróun fyrir og eftir formbreytingu sem leiðir til smækkunar án þess að tilgreina breytingar á stikum. Fyrir vikið er erfitt að meta til hlítar ávinning af mismunandi formbreytingum. Til þess að framkvæma slíkt mat með áreiðanlegum hætti er nauðsynlegt að geta metið bestu hönnunarútfærslu nákvæmlega. Þetta kallar á ítarlega tölulega bestun allra stika sem lýsa loftnetinu (einkum fyrir loftnet flókinnar lögunnar) þar sem aðalmarkmiðið bestunar er smækkun en skorður eru settar af raffræðilegum eiginleikum. Í þessari ritgerð er leitast við að kerfisbundna rannsókn á mikilvægi formbreytingna í tengslum við smækkun bandbreiðra loftneta. Rannsóknin byggir á völdum söfnum viðmiðunarloftneta. Til að tryggja rétt mat eru allir stikar er varða lögun stilltir með rafsegulfræðilegri hermun til að tryggja minnst rúmtak með ásættanlegum raffræðilegum eiginleikum. Niðurstöðurnar sýna að unnt er að greina, án vafa, ákveðna flokka formbreytinga sem eru að jafnaði til þess fallnir að smækka loftnet. Auk þessa er hægt að reikna ávinning af formbreytingum mismunandi hluta loftnetsins, t.d. að breytingar á fæðilínu eru almennt hagkvæmari en breytingar á geislagjafa eða jarðtengingu. Þá er greint frá nokkrum tilvikum þar sem tilfallandi formbreytingar geta verið til tjóns ef ekki stikaval er ekki gert með réttum hætti. Niðurstöður þessara rannsókna hafa verið notaðar til að hanna nokkur nýstárleg breiðbandsloftnet með áherslu á smækkun og bættan aðskilnað fjölgátta (MIMO) loftneta. Töluleg hermun er sannreynd með tilraunum. Að bestu vitund höfundar er hér um fyrstu kerfisbundnu rannsókn þessarar gerðar að ræða og má reikna með að hún leiði til þróunar betri, ódýrari og smærri loftneta fyrir þráðlaus fjarskiptakerfi.

The undersigned hereby certify that they recommend to the School of Science and Engineering at Reykjavík University for acceptance this Dissertation entitled **Geometry Modification Assessment and Design Optimization of Miniaturized Wideband Antennas** submitted by **Muhammad Aziz Ul Haq** in partial fulfillment of the requirements for the degree of **Doctor of Philosophy (Ph.D.) in Electrical Engineering**

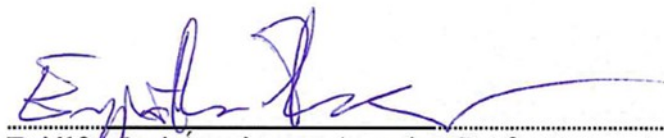
.....
Date: 17-5-2019



.....
Slawomir Koziel, Professor, Supervisor
Reykjavík University, Iceland



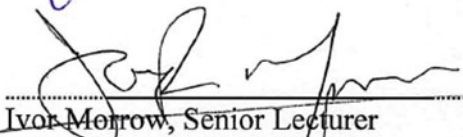
.....
Ágúst Valfell, Dean of School of Science and Engineering
Reykjavík University, Iceland



.....
Eyjólfur Ingi Ásgeirsson, Associate Professor
Reykjavík University, Iceland



.....
Kristján Leósson, General Manager
Innovation Center Iceland



.....
Ivor Morrow, Senior Lecturer
Cranfield University, UK

The undersigned hereby grants permission to the Reykjavík University Library to reproduce single copies of this Dissertation entitled **Geometry Modification Assessment and Design Optimization of Miniaturized Wideband Antennas** and to lend or sell such copies for private, scholarly or scientific research purposes only.

The author reserves all other publication and other rights in association with the copyright in the Dissertation, and except as herein-before provided, neither the Dissertation nor any substantial portion thereof may be printed or otherwise reproduced in any material form whatsoever without the author's prior written permission.

Date: 17-5-2019



Muhammad AZIZ Ul Haq
Doctor of Philosophy

Dedicated to my father Muhammad Israr Ul Haq (be mercy upon him) whose dynamic personality had always been a great source of inspiration in my life.

&

To my beloved mother, wife, children, and siblings.

Acknowledgments

I bow my head before ALLAH (SWT) in gratitude who blessed me the courage to complete this thesis. May each and every moment of my life be devoted to his praise. All respect and regards to the holy prophet Muhammad (peace be upon him), who was sent as a guide to perfect good moral character.

I am very thankful to my respected teacher and supervisor Prof. Slawomir Koziel, for his keen interest, support, guidance and intelligent suggestions throughout this research work. He was always there to advise me despite his extremely busy schedules. I am highly grateful to him for offering me a Ph.D. study under his kind supervision. May ALLAH (SWT) bless him with Iman, health, guidance, happiness, and long life (A'ameen).

No expressions, verbal or written can express my heartiest feelings for my beloved father (M. Israr Ul Haq (Late)) and mother, for their unbounded love, support and inspiration that built up my confidence to complete my study. I am really proud of them. Especially, my mother who supported me during the most tragic phase of my life and didn't let me think about to give up the masters study after the death of my father. I am truly grateful to my grandfather (M. Zahoor Ullah (be mercy upon him)) and grandmother for their love and prayers. I especially thank my younger brother (M. Mujeeb Ul Haq) for looking after my family during my stay in Iceland. I would also like to express the deepest gratitude to my siblings, parents-in-law, and uncles (M. Ihtesham Ul Haq and M. Ikram Ul Haq) for their prayers and support.

I am thankful to all my friends and group members whose encouragement and inspiration propelled me in the right direction. First and foremost I would like to thank my friend Muhammad Sulaiman Nawaz for being very supportive during my stay in Iceland. I also offer my thanks to Dr. Ubaid Ullah Yousafzai for being my lunch and coffee mate and listening to all my technical and non-technical discussions.

I would never forget the encouragement and constructive consultations of Dr. M. Arif Khan at the time of my initial research period. I am also thankful to Dr. M. Mansoor Ahmed for his kind support during my undergraduate study. I believe, without his support, my achievements in the educational journey would not have been possible.

I would like to thank the Computer Simulation Technology, Dassault Systemes, France, for making CST Microwave Studio available.

This work was supported in part by the Icelandic Centre for Research (RANNIS) Grant 163299051.

Preface

This dissertation is the original work of the author, Muhammad Aziz Ul Haq. A portion of the thesis (Chapter 3 through Chapter 9) is based upon the journal papers, published during the Ph.D. study. Note that these papers appear as per their online version in the chapters. The overall list of journal and conference papers throughout this study is listed below.

Journal papers:

1. Muhammad Aziz ul Haq, Slawomir Koziel, “Ground plane alterations for high-isolation compact wideband MIMO antennas in a parallel configuration,” *Microwave and Optical Technology Letters*. (Under review)
2. Muhammad Aziz ul Haq and Slawomir Koziel, “Ground plane alterations for design of high-isolation compact wideband MIMO antenna,” *IEEE Access*, vol. 6, pp. 48978-48983, 2018.
3. Muhammad Aziz ul Haq, Slawomir Koziel, and Qingsha S. Cheng, “Miniaturization of wideband antennas by means of feed line topology alterations,” *IET Microwaves, Antennas & Propagation*, vol. 12, Iss. 13, pp. 2128-2134, 2018.
4. Muhammad Aziz ul Haq and Slawomir Koziel, “On topology modifications for wideband antenna miniaturization,” *International Journal of Electronics and Communications*, vol. 94, pp. 215-220, 2018.
5. Slawomir Koziel and Muhammad Aziz ul Haq, “Ground plane modifications for design of miniaturized UWB antennas,” *IET Microwaves, Antennas & Propagation*, vol. 12, Iss. 8, pp. 1360-1366, 2018.
6. Muhammad Aziz ul Haq and Slawomir Koziel, “Quantitative assessment of wideband antenna geometry modifications for size-reduction-oriented design,” *International Journal of Electronics and Communications*, vol. 90, pp. 45-52, 2018.
7. Muhammad Aziz ul Haq and Slawomir Koziel, “A miniaturized UWB monopole antenna with five-section ground plane slit,” *Microwave and Optical Technology Letters*, vol. 60, Issue. 4, pp. 1001-1005, 2018.
8. Muhammad Aziz ul Haq and Slawomir Koziel, “A novel miniaturized UWB monopole with five-section stepped-impedance feed line,” *Microwave and Optical Technology Letters*, vol. 60, Issue. 1, pp. 202-207, 2018.
9. Muhammad Aziz ul Haq and Slawomir Koziel, “Simulation-based optimization for rigorous assessment of ground plane modifications in compact UWB antenna design,” *International Journal of RF and Microwave Computer-Aided Engineering*, <https://doi.org/10.1002/mmce.21204>, 2017.
10. Muhammad Aziz ul Haq and Slawomir Koziel, “Design optimization and trade-offs of miniaturized wideband antenna for Internet of Things applications,” *Metrology and Measurement Systems*, vol. 24, no. 3, pp. 463-471, 2017.

Conference papers:

1. Muhammad Aziz ul Haq and Slawomir Koziel, "EM-Driven size reduction of UWB MIMO antennas with feed line modifications," *International Applied Computational Electromagnetics Society Symp. (ACES)*, 2019.
2. Muhammad Aziz ul Haq, Slawomir Koziel, and Qingsha S. Cheng "A novel isolation improvement technique for wideband MIMO antenna systems," *European Conference on Antennas and Propagation (EuCAP)*, 2019.
3. Muhammad Aziz ul Haq and Slawomir Koziel, "Impact of ground plane modifications on element isolation in compact wideband MIMO antennas," *IEEE Loughborough Antennas and Propagation Conference (LAPC)*, 2018.
4. Muhammad Aziz ul Haq, Slawomir Koziel, and M. Arif Khan, "Systematic study of feed line and ground plane modifications for design of miniaturized wideband antennas," *IEEE MTT-S International Conference on Numerical Electromagnetic and Multiphasic Modeling and Optimization (NEMO-Iceland)*, 2018.
5. Muhammad Aziz ul Haq, Slawomir Koziel, and Qingsha S. Cheng, "Miniaturization of wideband antennas by means of ground plane modifications: A case study," *IEEE International Conference on Computational Electromagnetics (ICCEM-China)*, 2018.
6. Slawomir Koziel, and Muhammad Aziz ul Haq, "Topology considerations for compact UWB antenna design," *IEEE Loughborough Antennas and Propagation Conference (LAPC)*, 2017.
7. Muhammad Aziz ul Haq, Slawomir Koziel, and Qingsha S. Cheng, "EM-driven size reduction of UWB antennas with ground plane modifications," *International Applied Computational Electromagnetics Society Symp. (ACES-China)*, 2017.
8. Muhammad Aziz ul Haq, Slawomir Koziel, and Qingsha S. Cheng, "A structure and design optimization of compact antenna for Internet of Things applications," *International Applied Computational Electromagnetics Society Symp. (ACES-China)*, 2017.
9. Muhammad Aziz ul Haq and Slawomir Koziel, "On feed line modifications for compact wideband antenna design," *European Conference on Antennas and Propagation (EuCAP)*, 2018.
10. Muhammad Aziz ul Haq, Slawomir Koziel, "Comparison of topology modification for size-reduction-oriented wideband antenna design," *IEEE Antennas and Propagation Society (APS)*, 2018.
11. Muhammad Aziz ul Haq, Slawomir Koziel, "On compact wideband antenna design using topology modifications," *International Applied Computational Electromagnetics Society Symp. (ACES)*, 2018.

Contents

Acknowledgments	xv
Preface	xvii
Contents	xx
List of Figures	xxii
List of Tables	xxv
List of Abbreviations	xxvi
List of Symbols	xxviii
1 Introduction	2
1.1 Antenna basics	4
1.1.1 Bandwidth	5
1.1.2 Impedance matching	5
1.1.3 Radiation pattern	6
1.1.4 Radiation efficiency	6
1.1.5 Directivity.....	7
1.1.6 Gain	7
1.1.7 Mutual coupling	7
1.2 Microstrip patch antennas	8
1.2.1 Applications	8
1.3 Wideband antennas	9
1.4 Wideband antenna design techniques	10
1.4.1 Suspended plate antennas	10
1.4.2 Dielectric resonator antennas	11
1.4.3 Multilayer antenna configurations	12
1.4.4 Modified shape radiators	12
1.5 Wideband antenna applications	12
1.5.1 Wearable antennas.....	13
1.5.2 Microwave imaging.....	13
1.5.3 Internet of Things (IoT).....	14
1.5.4 Vehicular radar system.....	15
1.5.5 Summary	15
1.6 Electrically small antennas	15
1.6.1 Fundamental limitations and challenges	16
1.6.2 Antenna miniaturization techniques	16

1.7	Thesis objectives	18
1.8	Methodology and Results	19
1.9	Contributions and thesis outline.....	20
2	Antenna optimization.....	23
2.1	Antenna design as an optimization problem.....	23
2.2	Gradient-based optimization methods	24
2.3	Derivative-Free Optimization	26
2.4	Metaheuristics and Global Optimization	27
2.5	Antenna Optimization Approaches Utilized in This Work.....	27
3	Paper [J1] and [J2].....	29
4	Paper [J3].....	42
5	Paper [J4].....	56
6	Paper [J5].....	64
7	Paper [J6].....	72
8	Paper [J7].....	81
9	Paper [J8] and [J9].....	88
9.1	Introduction.....	96
9.2	Ground plane techniques for isolation improvement.....	97
9.3	Verification case studies	98
9.4	Experimental results	101
10	Conclusion and future directions.....	106
10.1	Conclusion	106
10.2	Future directions	106
	Bibliography.....	108

List of Figures

Figure 1.1: A future Internet of Things (IoT) architecture [21].	3
Figure 1.2: A typical wireless communication system.	5
Figure 1.3: Antenna equivalent circuit diagram.	7
Figure 1.4: A microstrip patch antenna with a rectangular patch.	8
Figure 1.5: Suspended plate antenna (a) conceptual geometry, (b) particular design reported in [120].	10
Figure 1.6: DRAs of different shapes.	11
Figure 1.7: Geometry of the antenna [147] (a) Isometric view, (b) Front view, (c) Left view.	12
Figure 1.8: (a) Illustration of a basic scattering mechanism [171]. (b) Proposed nature fern inspired fractal leaf antenna structure [170].	13
Figure 1.9: A measurement setup for brain imaging using a Vivaldi antenna [172].	14
Figure 1.10: Antenna configuration with a shorting post.	17
Figure 2.1: An example of minimax design specifications. For a UWB antenna, the reflection response $ S_{11} \leq -10$ dB for 3.1 GHz to 10.6 GHz is required. The response marked (- - -) does not satisfy the specifications, whereas the response marked (—) does satisfy the specs.	24
Figure 2.2: A flowchart of gradient-based simulation-driven optimization. The search process can be guided by the model response or by the response and its derivatives [221].	24
Figure 2.3: A conceptual illustration of a pattern search algorithm [221].	25
Figure 9.1: Proposed isolation enhancement technique for wideband MIMO antennas: (a) Stage 0: plain ground and the pre-optimized antenna reflection response, (b) Stage 1: L-shape stubs inserted and geometry parameters pre-adjusted using parameter sweeping followed by numerical optimization of the reflection response, (c) Stage 2: multi-stage slits below the feed lines inserted and geometry parameters optimized for best isolation with reflection constraint ($ S_{11} \leq -10$ dB).	96
Figure 9.2: Operation of the proposed isolation enhancement technique. Here, the constraints are introduced to limit physical antenna size within a certain value. A custom-designed socket is used to interface the optimizer and the EM solver. The presented framework allows for switching between various numerical optimization setups where necessary, eventually leading to the optimum results both interms of the antenna impedance matching and isolation.	97

Figure 9.3: Geometries of compact UWB-MIMO antennas utilized to validate the proposed isolation enhancement technique. (a) Antenna I, (b) Antenna II, (c) Antenna III, and (d) Antenna IV. The ground plane is shown using the light gray shade. 99

Figure 9.4: Simulated S-parameters of the optimized benchmark antennas: Antenna I (—), Antenna II (- - -), Antenna III (— -), and Antenna IV (...): (a) $|S_{11}|$ response w. r. t. the initial design, (b) $|S_{21}|$ response w. r. t. the initial design (c) $|S_{21}|$ with one-section slit, and (d) $|S_{21}|$ with two-section slits below the feed line. 99

Figure 9.5: Surface current distributions over Antenna II at 5 GHz. (a) Flat ground plane, (b) one-section slit, and (c) two-section slit below the feed line..... 100

Figure 9.6: Simulated ECC characteristics of the optimized antennas: Antenna I (—), Antenna II (---), Antenna III (- - -), and Antenna IV (...). 100

Figure 9.7: Simulated and measured S-parameters of the optimized UWB-MIMO antennas with the two-section slit below the feed line: Antenna I measured (—) and simulated (...), Antenna III measured (---), and simulated (- - -). (a) $|S_{11}|$ and (b) $|S_{21}|$ 101

Figure 9.8: Measured (—) and simulated (---) efficiencies of the optimized MIMO antennas: (a) Antenna I and (b), Antenna III. 101

Figure 9.9: Measured (—) and simulated (---) ECC and DG response of the optimized antennas: (a) Antenna I and (b) Antenna III..... 101

Figure 9.10: Simulated and measured radiation pattern of the optimized UWB-MIMO antennas with the two-section slit below the feed line: Simulated co-pol (---), measured co-pol (—), simulated cross-pol (...) and measured cross-pol (- - -). The plots from left- to right-hand side are for the frequencies 6 GHz and 8 GHz: (a) Antenna I E-plane (b) Antenna I H-plane, (c) Antenna III E-plane, and (d) Antenna III H-plane. 102

List of Tables

Table 1.1: Evolution of mobile technology.....	4
Table 1.2: Microstrip antenna applications.....	9

List of Abbreviations

1G	1 st Generation
2G	2 nd Generation
3G	3 rd Generation
4G	4 th Generation
5G	5 th Generation
ABW	Absolute Bandwidth
BCWC	Body-Centric Wireless Communication
dBd	Decibels Related to Dipole Antenna
dBi	Decibels Related to Isotropic Antenna
DRA	Dielectric Resonator Antenna
GSM	Global System for Mobile
IEEE	The Institute of Electrical and Electronics Engineers
IoT	Internet of Things
MIMO	Multiple Input Multiple Output
MTM	Metamaterial
PCS	Personal Communications Service
VRS	Vehicular Radar Systems
VSWR	Voltage Standing Wave Ratio
WiMAX	Worldwide Interoperability for Microwave Access
WLAN	Wireless Local Area Networking
ECC	Envelop Correlation Coefficient
DG	Diversity Gain

List of Symbols

Notation	Description
U	Objective function
\mathbf{R}_f	Response vector of a high-fidelity model
\mathbf{x}	Vector of antenna design variables
∇	Gradient
γ	Gradient update coefficient for Fleecher-Reeves method
$\mathbf{H}(\mathbf{x})$	Hessian
\mathbf{x}^*	Optimum design
ρ	Gain ration for trust-region framework
P	Population (in metaheuristic algorithms)
S	Parent individuals
$S(\mathbf{x})$	Maximum reflection within a frequency band of interest
$C_{eq.l}$	Equality constraints
$C_{ineq.l}$	Inequality constraints
M_{eq}	Number of equal constraints
$A(\mathbf{x})$	Antenna size
ϵ_r	Relative Permittivity
K	Wave Number

Chapter 1

1 Introduction

Communication is a fundamental tool for humans to exchange their ideas, thoughts, and feelings. It is said that the exchange of ideas between two or more persons or groups is the starting point of information dissemination and discussion. With the advent of technology, the communication media have been upgraded from verbal communication to the modern wireless communication systems. These changed our lives forever. A representative example are cell phones that provide us the means to communicate with each other regardless of how far away we are from each other.

The revolution in long distance voice communication began in 1876 with a successful experiment for an applied telephone design by Alexander Graham Bell [1]. It was a wire communication system. Afterward, the research for the development of human communication system has gone miles ahead. Then, the next revolutionary step in the context of the communication system is the design of a cordless telephone system in 1969 [2]. Using this technology, the users were able to move during the conversation. This development has changed the communication system from a fully wired-system to a partially wired one. Here, the telephone base units were connected through the wired medium and the base units to handset were a wireless one. In the subsequent phase, the partial wired-systems were replaced by the fully wireless communication systems in 1973 [3]. This invention has changed the connectivity system scenarios. Thereafter, the wireless communication system is achieving new heights day by day. This advancement in mobile communication technology is based on the standards, called “Generations.”

The first generation (1G) technology was launched in 1979 [4], where the system was able to support analog voice communication at 150 MHz band. The second generation (2G) technology was introduced in 1991 [5]–[12]. This technology was able to support digital voice communication along with a short message service (SMS). A transmission speed of 64 kbps along with a band 30-200 kHz was provided through this technology. The third-generation (3G) technology was established in 2000 along with some new features such as television signal, video message, and global roaming [13]–[15]. This technology operates at 2100 MHz frequency band with a 15-20 MHz bandwidth and 200 kbps data rate. The fourth generation (4G) technology was launched in 2008 with additional features such as online gaming, HD mobile television, cloud computing, and ultra-broadband network access to mobile devices

[16], [17]. A 100 Mbps data rate is required to handle such a wide range of applications for high mobility applications. Now, the fifth generation (5G) technology is under test which will be launched soon (nearly in the year 2020) along with a data rate of 10 Gbps [18]–[20]. It is expected that 5G technology will have access to other wireless devices simultaneously through the internet which realizes the concept “the internet of things (IoT)”. A possible design architecture illustrating the concept of IoT is shown in Figure 1.1. Table 1.1 shows the evolution of communication systems based on available services and performance.

The above outline of mobile communication technology development would not be possible without antennas which are fundamental components of any wireless communication and other systems. Antennas, especially miniaturized wideband antennas, are the main topic of this work. The specific goals will be elaborated in Section 1.7. In the remaining part of this chapter, a very generic introduction to the subject is provided, including the description of basic antenna characteristics, an overview of applications with the emphasis on wideband structures, techniques used for antenna performance evaluation, as well as a brief outline of antenna design methodologies.



Figure 1.1: A future Internet of Things (IoT) architecture [21].

Table 1.1: Evolution of mobile technology.

Generation	Launching year	Speed	Technology	Key features
1G	1979	14.4 Kbps	AMPS, NMT, TACS	Only voice services
2G	1991	64 Kbps	CDMA, TDMA	Voice and Data services
3G	2000	15-20 MHz	CDMA 2000, UMTS, EDGE	Voice, data, Multimedia, faster web browsing, video calling, and TV streaming
4G	2008	100-300 Mbps	WiMax, LTE, WiFi	High speed, HD multimedia streaming, 3D-gamming, HD video conferencing and worldwide roaming
5G	Expected from 2020	1-10 Gbps	LTE advance. OMA and NOMA	All the services from 4G, additionally, Super-fast mobile internet, IoT, autonomous driving, smart healthcare applications

1.1 Antenna basics

In a modern communication system, a wireless medium is preferred to transfer data from one end to another in order to avoid massive, costly, and complex interconnected cables. Meanwhile, the users can also feel comfortable to move around during the communication instead of having a fixed station. For this, the antenna is a critical part of any wireless system on both ends, i.e., the transmitter and the receiver ones. There are several ways to define an antenna “a device which allows for the transfer of a signal (in a wired medium) to waves that, in turn, propagate through space and can be received by another antenna” [22]. Then, the receiving antenna is responsible for the reciprocal process, i.e., transforming an electromagnetic wave into a signal or voltage for the subsequent process by the receiver. As the antenna operation is dependent on frequency, it is normally designed to operate within a specific frequency range. A block diagram illustrating the wireless communication system is shown in Figure 1.2. Although there are various antenna performance figures that are relevant for different applications, only the important ones regarding the mobile communication systems are briefly described in what follows. The provided exposition is rather superficial because the presented material is not intended to replace antenna theory textbooks but merely introduce the terminology required for other parts of the manuscript.

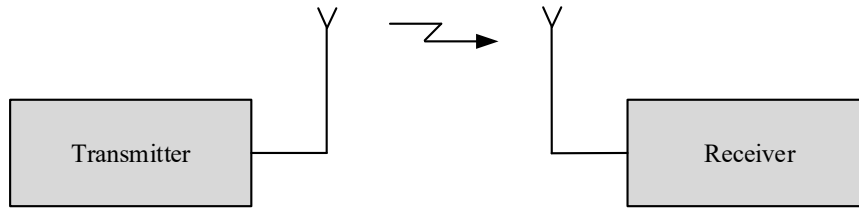


Figure 1.2: A typical wireless communication system.

1.1.1 Bandwidth

Bandwidth is the range of frequencies on the lower (f_L) and upper (f_u) side of the centre frequency (f_c) of an antenna throughout which the antenna performance remains within the acceptable limits. According to the IEEE standard terms of reference [23], it is defined as “The range of frequencies within which the performance of the antenna, concerning some characteristic, conforms to a specified standard”. Therefore, it is important for any antenna to meet the defined standard in order to operate within the band of interest. The antenna bandwidth is expressed through the absolute bandwidth (ABW) for narrowband antennas and a fractional bandwidth (FBW) for broadband antennas as:

$$ABW = f_u - f_L \quad (1.1)$$

$$FBW = 2 \frac{f_u - f_L}{f_u + f_L} \quad (1.2)$$

The center frequency (f_c) or a resonance frequency of a wideband antenna is the arithmetic mean of the upper and lower frequency bounds that can be expressed as:

$$f_c = \frac{f_u + f_L}{2} \quad (1.3)$$

1.1.2 Impedance matching

One of the most critical antenna parameters is the impedance matching. Good matching is necessary to ensure the maximum power transmission. The parameters which are associated with matching are the reflection coefficient $|S_{11}|$ and voltage standing wave ratio (VSWR). The reflection coefficient indicates how much power is reflected back towards the source from the radiator. In other words, it is a measure of the impedance mismatch between the source output and the radiator input. It can be expressed as:

$$|S_{11}| = -20 \log |\Gamma| \quad (1.4)$$

where Γ is given by:

$$|\Gamma| = \frac{Z_A - Z_C}{Z_A + Z_C} \quad (1.5)$$

Here, Z_A is the input impedance of the antenna and Z_C is the output impedance of the

source. An alternative method to represent the mismatch between the antenna and feed line impedances is VSWR, defined as:

$$VSWR = \frac{1 + |\Gamma|}{1 - |\Gamma|} \quad (1.6)$$

It is understood that the antenna is well matched if $VSWR \leq 2$ (corresponding to no more than 10% reflected power from the antenna) or $|S_{11}| \leq -10$ dB within the operating frequency range.

1.1.3 Radiation pattern

The radiation pattern of the antenna determines the radiated field strength or power distribution of the antenna as a function of the space coordinates. According to the IEEE standard terms of reference, it is defined as “the spatial distribution of a quantity that characterizes the electromagnetic field generated by the antenna” [23]. For a graphical representation, the azimuth (φ) and the elevation (θ) angles of the spherical coordinate system are selected. The most comprehensive field representation of the radiation pattern is the 3D graphical visualization. However, drawing of 3D graphics are usually difficult and sometimes unnecessary because of the pattern symmetry. Therefore, most of the time, polar plots are considered which are the planar cuts from the 3D pattern. Typically, two types of planar cuts are considered, i.e., the E-plane and the H-plane ones. The E-plane is defined as “a plane which contains an electric field vector in the direction of maximum radiation.” It is generally measured in a far-field region where the spatial (angular) distribution of the radiated power is independent of distance. Similarly, H-plane is defined as “a plane which contains a magnetic field vector in the direction of maximum radiation.”

1.1.4 Radiation efficiency

The radiation efficiency of the antenna is its capability to convert electrical signals to the radiated electromagnetic ones. According to the IEEE standard terms of reference, “The ratio of total power radiated by an antenna to the net power accepted by the antenna from connected transmitter” [23]. It can be expressed as:

$$R_{eff} = \frac{P_r}{P_i} \times 100 \quad (1.7)$$

Figure 1.3 shows an equivalent circuit diagram of the antenna. Here, L , C , R_r , and R_L denote the inductance, capacitance, radiation resistance, and the radiation inductance respectively. According to Figure 1.3, expression (1.7) can further rewritten as

$$R_{eff} = \frac{\frac{1}{2} |I|^2 R_r}{\frac{1}{2} |I|^2 R_r + \frac{1}{2} |I|^2 R_L} = \frac{R_r}{R_r + R_L} \quad (1.8)$$

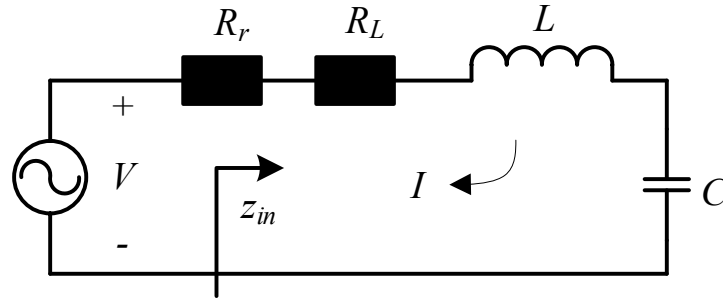


Figure 1.3: Antenna equivalent circuit diagram.

1.1.5 Directivity

The directivity of an antenna describes the radiation intensity in the direction of maximum radiation versus intensity radiated by an ideal isotropic source. According to the IEEE standard terms of reference it is defined as, “The ratio of the radiation intensity in a given direction (usually in spherical coordinate angles θ and φ) from the antenna to the radiation intensity averaged over all directions”[23]. Mathematically, it is expressed as the ratio between the radiation intensity of the radiator to the radiation intensity of an isotropic radiator. An isotropic radiator is the point source which radiates with the same intensity in all directions. The directivity is therefore given by:

$$D = \frac{U}{U_0} = \frac{4\pi U(\theta, \varphi)}{P_{rad}} \quad (1.9)$$

where, U is the radiation intensity in a given direction of the antenna and U_0 is the radiation intensity of an isotropic radiator.

1.1.6 Gain

The antenna gain is related to its directivity and the radiation efficiency [24]–[26] as:

$$\text{Gain} = \text{directivity} \times \text{radiation efficiency} \quad (1.10)$$

Usually, when the gain is calculated with respect to the isotropic source, it is expressed in dBi units. Whereas for the dipole antenna, it is expressed in dBd. Most of the time, the gain requirement depends upon the mobile application. For example, the required gain for the outdoor application is 10 – 20 dBi for the desired frequency range [27]–[30]. Usually, such a high gain is achieved using antenna arrays [31]–[36]. However, typical gain requirements for indoor applications are only 5 – 7 dBi [37]–[39].

1.1.7 Mutual coupling

The mutual coupling phenomenon is common in antenna arrays or multiple-input-multiple-out-put (MIMO) antenna systems. Usually, this occurs due to the interaction of multiple antenna elements being in close proximity of each other. Mutual coupling affects

the input impedance and radiation pattern of all antennas involved. As mentioned before, multiple antenna elements can be used to realize high gain or to provide dual-polarization (by means of two antenna elements or feeds). Additionally, multiple antenna elements can also be used to provide multiband operations for mobile communication systems within a limited space [40]–[43]. For these applications, the interference between the antenna elements should be as low as possible. Typically, for the base stations, the specification for the mutual coupling is -20 dB within the desired frequency range. However, for mobile applications such as mobile phones, multiple or wideband antennas for mobile applications, and notebook computers, the coupling may increase to -10 dB [44].

1.2 Microstrip patch antennas

The concept of a microstrip antenna was outlined in 1953 [45] and gained considerable attention at the beginning of the 1970s. Microstrip antennas are attractive due to their small size, easy design and fabrication, lightweight, as well as cost-effective and widespread applications. These type of structures are especially preferred for mobile base station applications where the weight is an important issue. A microstrip patch antenna consists of a conducting patch (with different shapes such as rectangular [46], square [47], circular [48]–[51], ring [52]–[55], triangular [56]–[60], or an elliptical one [61], [62]), a substrate, feedline and a ground plane as shown in Figure 1.4. In the original configuration, the microstrip antenna has a narrow bandwidth, which makes it more suitable for multiband applications. Numerous multiband patch antenna designs have been reported in the literature [63]–[72]. The antenna bandwidth can be enhanced by applying certain techniques such as utilization of thick and low permittivity substrates, stacked patches or cutting different shaped slots [73]–[77] in the patch, aperture coupling, modifying its ground plane [78]–[81] or the feedline structure [82].

1.2.1 Applications

The major advancements in the field of the microstrip patch antennas and arrays occurred in the early 1980s. Before, they were implemented only for defense and satellite communication systems with the aim to acquire maximum performance with a constraint on the cost of the system. On the other hand, commercial applications require a low-cost wireless system even at the expense of slight degradation of electrical performance. As the microstrip-based antennas offer low cost, lightweight, and ease of fabrication and installation, they have commonly used for the modern communication systems. Table 1.2 contains information regarding the use of microstrip patch antennas for commercial communication systems.

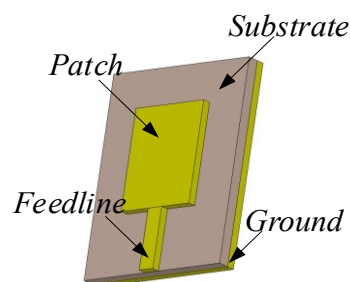


Figure 1.4: A microstrip patch antenna with a rectangular patch.

Table 1.2: Microstrip antenna applications.

Wireless applications	Frequency
Global Positioning Satellite	(1575 – 1227) MHz
GSM	(890 – 915) MHz and (935 – 960) MHz
Wireless Local Area Network	(2.40 – 2.48) GHz and 5.49 GHz
Cellular Video	28 GHz
Direct Broadcast Satellite	(11.7 – 12.5) GHz
Automatic Toll Collection	905 MHz and (5 – 6) GHz
Collision Avoidance Radar	60 GHz, 77 GHz, and 94 GHz
Wide Area Computer Networks	60 GHz
Long-Term Evolution	2300 – 2400 MHz
WiMAX	3300 – 3600 MHz
WiFi	(3650 – 3700) MHz and (5150 – 5825) MHz
Universal Mobile Telecommunication Systems	(1885 – 2200) MHz

1.3 Wideband antennas

As mentioned before, antennas belong to fundamental components of wireless communication systems. In the early days of mobile communication, devices were designed to operate for a specific frequency band such as GSM-I, GSM-II, Wi-Fi, WLAN, and PCS. Coverage of different bands required multiple antennas which affected both the volume and the cost of the system. Nowadays, an alternative solution is preferred, specifically, utilization of multiband or wideband antennas. Various circuit solutions have been developed to enable wideband operation such as using an aperture [83]–[87] or L-probe coupling [88]–[94], parasitic resonators [95]–[102], planar designs with different shapes (triangular [103], [104], rectangular [105]–[107], or circular [48], [49], [108]), multilayer antenna configuration [109], and dielectric resonators [110]–[116]. Usually, wideband antennas occupy a large space as compared to multiband antennas and the structure can be even larger in case of array configurations required to obtain high gain. Therefore, wideband antennas are mostly preferred for outdoor or indoor wireless systems instead of a mobile handset or notebook applications. In the design of wideband antennas, ensuring sufficient impedance matching only is not as challenging as handling additional criteria such as controlling gain characteristic, efficiency, or securing high isolation between the antenna elements in the context of wideband applications. Additionally, the radiator, ground plane, and the feed line of a wideband antenna can be optimized to enhance the impedance bandwidth along with other characteristics, including satisfaction of the constraints concerning the maximum allowed size (critical for applications in wireless communication devices).

1.4 Wideband antenna design techniques

One of the most common challenges in the development of antennas for contemporary wireless communication systems is to design a single antenna that can operate within a wide frequency range to support different technologies and standards. The narrowband operation is perhaps the most serious drawback of microstrip antennas, otherwise attractive due to low fabrication cost, high efficiency, and low profile. A wide variety of wideband antenna design techniques are available in the literature depending upon the wireless applications. In the following part of this section, some of the selected wideband antenna design techniques related to the modern wireless communication systems are briefly discussed.

1.4.1 Suspended plate antennas

Microstrip patch antennas possess several attractive features such as lightweight, low profile; also they are easy to fabricate and integrate with wireless devices. However, their disadvantage is inherently narrow impedance bandwidth. Nowadays, various techniques have been developed to work around this limitation so as to achieve wider bandwidth along with acceptable levels of other electrical and field performance parameters. One of the popular approaches is the suspended plate antenna (SPAs). SPAs consist of a thin-plate conductor which is positioned above the grounded low permittivity dielectric substrate (usually air) as shown in Figure 1.5. Typically, it is fed by planar strips or L- or T-shaped probes. Numerous SPA designs have been reported in the literature for wireless communication systems [117]–[122]. In [120], a wideband SPA for a wearable application using an inverted L-shape fed is presented. The feed was electromagnetically coupled both with the suspended patch using a small printed rectangle on the bottom layer of the patch, and with the shorting wall through a printed silver ink on a block of polycarbonate. This technique was useful to simplify the manufacturing process and enhance the bandwidth. The antenna operates for the frequency range 2.2 GHz to 6.44 GHz with the efficiency of more than 90%. Although the SPA technique has been successfully used to enhance the bandwidth of the antenna in the recent years, the overall size of these antennas is large as compared to the printed ones. Consequently, their installation in any compact communication device may be difficult. Moreover, the implementation of a band-notch functionality in SPAs is challenging.

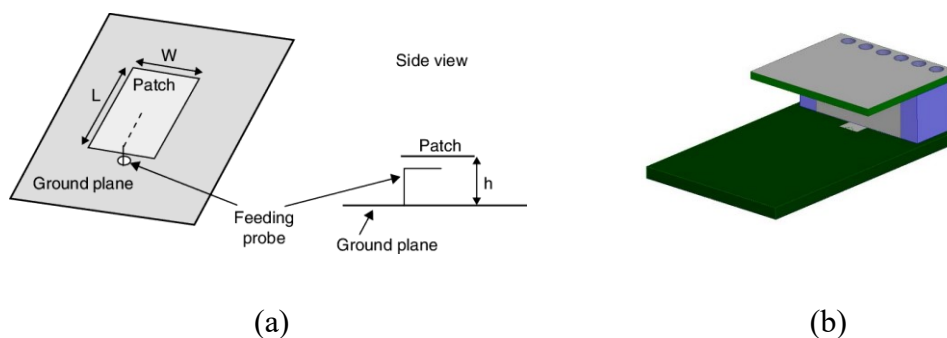


Figure 1.5: Suspended plate antenna (a) conceptual geometry, (b) particular design reported in [120].

1.4.2 Dielectric resonator antennas

Dielectric resonator antennas (DRAs) are typically composed of a block of ceramic material having different shapes (hemispherical, rectangular, cylindrical, or circular as shown in Figure 1.6), mounted on a metallic surface over a conducting ground plane. The significant advantages of DRAs are their low nominal conduction losses due to the absence of metallic resonator, low profile, high mechanical stability, ease of excitation, and convenient control over the size and the impedance bandwidth of the antenna. DRAs feature relatively lower losses as compared to the microstrip antennas (especially at higher frequencies) because of no inherent conductor loss in dielectric resonators, which leads to high efficiency. This feature has gained considerable attraction of antenna researchers, especially in the design DRAs for higher frequency applications where the conductor loss in metal fabricated antennas is high [123]–[126]. Therefore, they are usually used for WLAN applications instead of GSM bands [127], [128]. They also offer simple excitation through an aperture coupling [129]–[133], a microstrip line [134]–[137], or a coaxial probe [138], [139]. This makes them easy to integrate with planar technologies. Materials of high dielectric constant (ϵ_r) play an important role in reducing the dimensions of the resonant material. The dimensions of the DRA is calculated using the following expression $\lambda_0/\sqrt{\epsilon_r}$. Here, λ_0 is the free space wavelength and ϵ_r is the dielectric constant of the resonant material. Thus, the DRA size can be significantly reduced by choosing high values of ϵ_r . Moreover, in order to control the thermal stability, normally, the materials with dielectric constant lower than 30 are considered. The relationship between dielectric constant and DRA bandwidth is given in [140]. As the dielectric constant increases, the bandwidth decreases and vice versa. Therefore, dielectric constant is selected according to the desired antenna specifications. A lot of efforts have been observed to achieve size reduction with lower dielectric constant values [141]–[145]. Some of the designs in the context of modern communication systems have been reported in [146]–[151]. For example, in [147], a two element multiple-input-multiple-output (MIMO) DRA with wideband characteristic is presented. A wideband performance has been achieved using the mushroom-shaped dielectric resonator with trapezoidal patch excitation. The geometry of the proposed design is shown in Figure 1.7. The antenna exhibits 61% bandwidth covering frequency ranges from 5.08 GHz to 9.50 GHz. The antenna has acceptable return loss, peak gain from 3.34 to 7.40 dBi, and isolation level less than -20 dB within the desired frequency range.

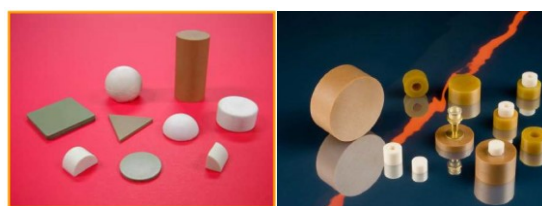


Figure 1.6: DRAs of different shapes.

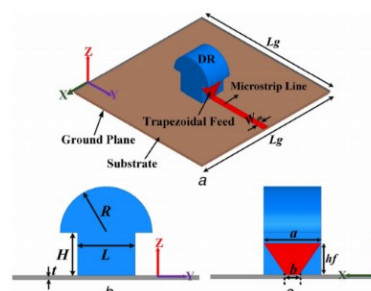


Figure 1.7: Geometry of the antenna [147] (a) Isometric view, (b) Front view, (c) Left view.

1.4.3 Multilayer antenna configurations

In a multilayer configuration, a number of patches on different layers of dielectric substrates are stacked on each other. Based on the coupling mechanism, their structures are categorized as an electromagnetically coupled or aperture coupled microstrip antennas. In [109], a concept of a bandwidth-enhanced multilayer antenna has been presented. The antenna was implemented using an alumina substrate that extended the bandwidth sixteen times as compared to a typical patch antenna. In general, although multilayer configurations may be used to achieve the desired bandwidth, this technique may considerably increase the complexity and the cost of the mobile system.

1.4.4 Modified shape radiators

Another option for enhancing the antenna bandwidth is to replace a standard radiator of the microstrip patch antennas (MPAs) such as a rectangular or a circular one, by a modified shape. Examples include a rectangular ring proposed in [152], [153], or a circular ring of [154]. In these references, the conventional topologies of the patch type antennas are perturbed which leads to the enhancement of fringing fields due to the reduced current path. As a consequence, the impedance bandwidth increases but at the cost of the low quality factor. In [155], an asymmetrical rectangular patch with the U-shaped open-slot structure has been presented. The impedance bandwidth of 122% has been achieved with -10 dB reflection. This approach is an easy and cost-effective way of improving the impedance bandwidth, which is essential for modern compact mobile devices as opposed to alternative methods requiring extra material or substrate such as in the case of DRAs or multilayer configurations, respectively.

1.5 Wideband antenna applications

Wideband antennas have received much popularity in the context of wireless communication systems due to their ability to handle different communication channels using a single structure. With a wide bandwidth, the signals can be transmitted by multi-band groups or by using ultra-short impulses. More applications and information can be carried through the radio frequency channels with a high data rate and accuracy. Also, there are numerous wideband antenna applications such as microwave imaging, wearable, IoT, satellite, and military applications that require wide bandwidth to increase the accuracy, imaging resolution, and hardware flexibility. In this section, we discuss state-of-the-art wideband antennas with the emphasis on their modern applications rather than on particular topologies, design details, or profile.

1.5.1 Wearable antennas

Body-Centric Wireless Communication (BCWC) is one of the popular research areas oriented towards the eHealth, firefighter tracking, defence, sports monitoring, and public safety applications. Antennas play a vital role in BCWC, their configuration and performance depend on on-body transceiver specifications and application environments. Wideband compact wearable antennas are crucial in the development of new wearable Body Area

Network (BAN) systems. BAN antennas should be lightweight, flexible, low cost, and compact in size. Several novel miniature wideband antennas have been designed and tested for WBAN [156]–[160], where the authors provide a clear and concise overview of their proposed design in the context of wearable antenna applications. The mentioned designs have significant advantages of wide radiation patterns over the human body for maximum coverage, small size, and less sensitive to the gap variation between the human body and the antenna. In [157], a flexible ultrawideband (UWB) antenna is presented for wearable applications. The antenna is capable to cover the frequency range 3.7–10.3 GHz with footprint $80 \text{ mm} \times 67 \text{ mm}$. In order to enhance the robustness and flexibility, the antenna is realized using conductive fabric embedded into polydimethylsiloxane polymer. Promising results are presented for free-space and wearable scenarios.

1.5.2 Microwave imaging

Microwave imaging is one of the promising techniques for screening the internal configuration and structures of the body using electromagnetic radiation at the microwave frequency range of 3 GHz to 30 GHz. A large variety of imaging techniques have been developed to visualize the internal body system [161]–[167]. Wideband antennas (working at microwave frequency) play a crucial role in the context of microwave imaging systems (MISs). In a MIS, the antenna is considered as a transmitting and receiving sensor. Signals are transmitted into the body from the transmitting end, whereas the receiving antennas collect scattered signals from the body. A typical scattering mechanism from the human breast is shown in Figure 1.8(a). The recent studies using the antenna as a sensor in a MIS have indicated that the antenna should have the specific properties ([168], [169]) such as small size, high gain, high efficiency over a wide frequency range, and directive radiation. In [170], a nature fern inspired fractal leaf antenna structure is proposed as shown in Figure 1.8(b). The impedance bandwidth of the proposed antenna is 19.7 GHz (from 1.3 to 20 GHz). Experimental results indicate a stable radiation pattern, wideband antenna feature, and acceptable group delay of less than 1 ns. The miniaturized proposed antenna structure is one of the candidates for microwave imaging system because of its ability to operate for wide frequency range, high directive gain (10 dBi), and large fidelity factor $> 90\%$. Conceptual measurement setup for brain imaging is shown in Figure 1.9.

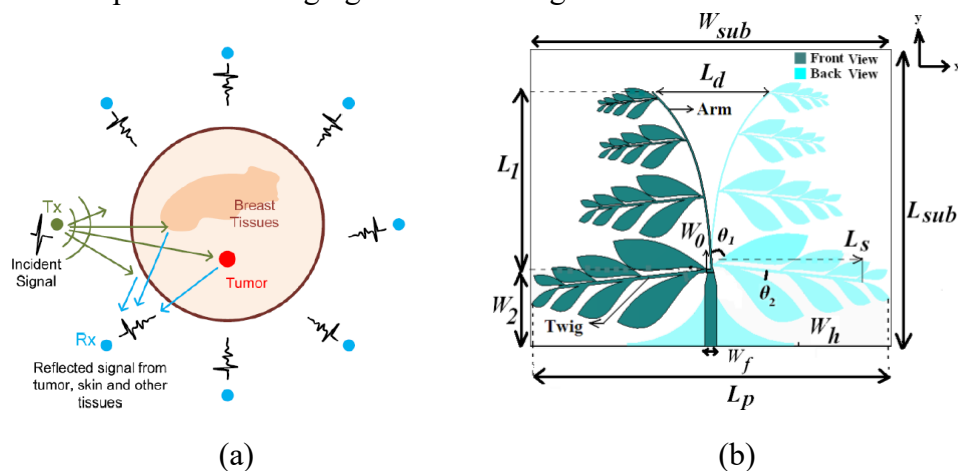


Figure 1.8: (a) Illustration of a basic scattering mechanism [171]. (b) Proposed nature fern inspired fractal leaf antenna structure [170].

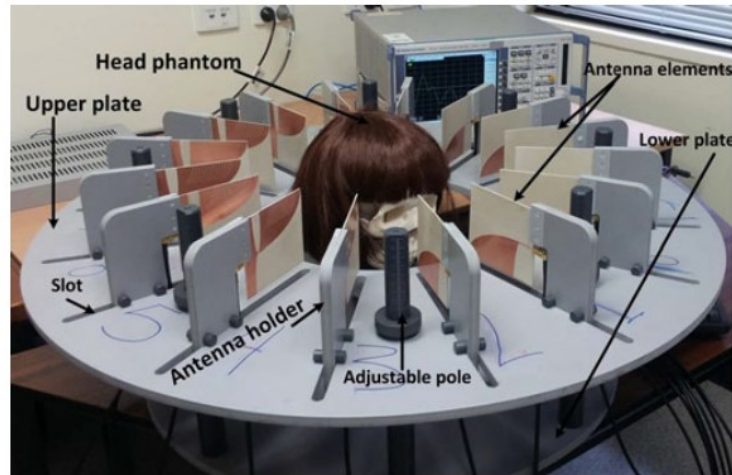


Figure 1.9: A measurement setup for brain imaging using a Vivaldi antenna [172].

1.5.3 Internet of Things (IoT)

In the modern era, the internet has revolutionized the way of gathering and processing information. An increasing number of communication devices are connected to the internet owing to their compact size and cost-effectiveness. Hence, the concept of the Internet of Things (IoT) has been introduced. A widespread use of wireless networks also promotes a shift towards modern communication devices rather than traditional ones such as desktop computers, tablets, etc. According to the recent survey, over 50 million such devices will be interconnected with each other via the internet by the end of this decade [173], [174]. The required hardware structure for IoT devices is different from traditional communication networks. Therefore, the design and manufacturing process of these devices should account for their role in the future communication systems and their specific applications. In particular, the advent of IoT calls for new wireless microwave systems which are cost-effective and compact by design, offer high data transmission rate, low power consumption and potential for use in wearable devices [175]. In recent years, there have been research efforts observed towards designing specific antennas for IoT application with a narrow bandwidth such as a miniature antenna for IoT [176], a dual-band antenna [177], or a compact reconfigurable antenna [178]. However, the selection of a specific antenna for any application may be a real challenge. Some of the research efforts are focused on identifying suitable technologies for fifth-generation communication and IoT applications, especially to allow handling all devices through one system [179]. Hence, it is actually more important to design antennas which offer a wide frequency range of operation [21]. Over the years, numerous efforts have been made to design a wideband antenna for IoT applications [180]–[182]. In [182], the authors propose a structure of a compact monopole antenna for IoT applications. Numerical optimization is performed to minimize the antenna size and to ensure its acceptable matching. The selected frequency range of interest is 5 GHz to 10 GHz. The footprint of the optimized antenna is only 44 mm². Due to its small size and good electrical performance, the antenna can be a good candidate for various IoT applications; in particular, it can be easily mounted on small wireless devices.

1.5.4 Vehicular radar system

Development in multifunction antennas for various applications, such as ships, airplanes,

automobiles, and cell phones has been attaining a momentum for the last three decades. With the phenomenal growth of wireless services, modern research has intensified the visionaries towards the need for consolidating multiple antennas into a single wideband antenna for Vehicular Radar Systems (VRS). With an antenna being a fundamental part of any wireless system, this will reduce not only the complexity of the system but also its cost. VRS operates in the 24 GHz band using directional antennas for global vehicles, provided the center frequency greater than 24.075 GHz [183]. These devices can identify the location and the movement of objects near a vehicle, enabling the features such as improved airbag activation, near-collision avoidance, and suspension systems.

1.5.5 Summary

With the explosive advancements of wireless communication, the antenna systems are entering into another phase of significant development. Modern wireless systems require antennas to cover wide frequency bands (to fulfill the demand of high data rate and speed), be small in size, and low in profile. The purpose of this chapter was to emphasize the importance of an antenna in this particular application context. The fundamental performance parameters have been presented along with the overview of design techniques for wideband antennas. Moreover, wideband antenna applications in the field of selected technologies have been highlighted as well.

1.6 Electrically small antennas

Electrically small antennas are preferred in modern communication systems due to their low cost as well as physical size constraints of compact wireless devices. An electrically small antenna is a device whose geometrical dimensions are small as compared to the wavelengths of the electromagnetic fields they radiate. In more formal terms, a small antenna is the one that fits inside a sphere of a radius $a = 1/k$, where k is the wave number associated with the electromagnetic field. The analysis of electrically small antennas was originated by Wheeler in 1947 [184], where the power factor Q was used to compute the antenna radiation. The radiation power factor is defined as the ratio of the radiated power to the stored power. By using a simple lumped circuit, it can be assessed that this ratio is equivalent to the bandwidth multiplied by the efficiency if the antenna is matched to the tuned circuit. Hence, it was confirmed mathematically that the product of efficiency and bandwidth is directly related to the radiation power factor or the volume occupied by the antenna. Based on this theory, further research was conducted by Chu [185], in which the minimum radiation quality factor Q of an antenna, which fits inside a sphere of a given radius was derived. Later, this approximate theory was extended by Harrington [186] in order to include circularly polarized antennas. In [187], Maclean re-derived a mathematical expression using non-propagating energy. In the recent years, some other efforts have been carried out to re-derive the fundamental limit on the quality factor Q using the time domain approach [188], [189]. In the following section, only the final expression (from the aforementioned work) will be discussed to highlight the concept of the fundamental limit applied on an electrically small antenna.

1.6.1 Fundamental limitations and challenges

There have been significant research efforts observed over the last years towards the development of compact antennas. Reducing the physical size of the antenna generally degrades its performance including the impedance bandwidth, efficiency, realized gain, and radiation pattern. Therefore, it is important to study the fundamental limitations and the performance trade-offs involved in size reduction. Clearly, excessive size reduction does not leave enough room for satisfying electrical performance requirements. On the other hand, reasonable trade-offs can be achieved by employing appropriate miniaturization techniques which will be discussed in the following sub-section. Some of the initial theoretical work related to antenna size reduction is discussed in [187], [190]. In [187], the author presented the exact expression for the minimum radiation factor Q with the assumption that the antenna radiates only in the spherical mode. It is

$$Q \approx \frac{1}{k^3 a^3} \quad (1.11)$$

This relationship needs to be taken into account when designing compact antennas for modern communication systems.

1.6.2 Antenna miniaturization techniques

The ability to reduce the overall antenna size without significant performance degradation has been a subject of great interest for over a half-century. Numerous antenna miniaturization techniques have been proposed, from structural modifications, lumped component loading, the use of high permittivity materials, to the more advanced implementations of metamaterials. In this particular sub-section, a review of various miniaturization techniques with the emphasis on routinely exercised approaches in the context of a patch antenna such as slots cutting, shorting posts, loading high permittivity dielectrics, and metamaterials will be discussed.

Slot cutting: one of the most popular miniaturization approaches is to create slots within the radiator. This technique is helpful for handling multiple resonances [191], [192], or to control polarization [193]. In [194], Iwasaki designed a resonant patch antenna for a circular polarization operating at the frequency of 1.15 GHz. The technique was based on a cross-slot with unequal lengths cut on a circular patch and used to facilitate antenna miniaturization. With the help of this technique, 36% size reduction was achieved. In [195], a method of cutting the slots on the ground plane was introduced in order to reduce the effect of the ground plane on the antenna performance. It was concluded that the technique was effective not only to reduce the role of the ground plane on the antenna performance but also to minimize the antenna size. More specifically, introduction of the slits on the ground plane caused the majority of the current to concentrate on the antenna radiator (without any change of its shape). Consequently, enhancement of the impedance bandwidth was obtained as well, creating a room for the antenna minimization which was achieved by adjusting selected antenna parameters using a parameter sweep tool.

Shorting posts: A microstrip patch antenna can be miniaturized by shorting posts between the patch and the ground plane as shown in Figure 1.10. Numerous studies have been conducted in the literature that presents the design or analysis of miniaturised antennas using

the shorting posts procedure [196]–[199]. Theoretical investigations of this concept have been provided by Rebekka [200]. Electrically small microstrip patch antennas (with different radiators, i.e., circular and rectangular ones) through shorting posts were investigated in [201]. Various parameters were analysed to quantify the impact of single, double, and multiple shorting posts. It was concluded that the overall size of the microstrip patch antenna could be reduced by more than a factor of three as compared to the standard antenna.

Using high-permittivity dielectrics: Another technique to reduce the antenna size is application of high-permittivity dielectrics. Usually, this method is accomplished using ceramic substrates [202], by patterning materials within the patch cavity region [203], or by placing the materials above the patch [204]. In [203], the authors employed a partially filled high-permittivity substrate in order to minimize the antenna size. A low permittivity substrate was placed with rectangular-shaped dielectric bars of high permittivity below the radiating edges of the patch. This resulted in a 50% antenna size reduction while achieving the fractional bandwidth of 10% and the gain of 6 dB.

Combination of various techniques: Numerous miniaturization techniques can be implemented simultaneously to yield the required performance. For instance, slots may be combined with shorting posts as implemented in [205]. The author has established that the size of a rectangular patch antenna can be reduced by using a high dielectric substrate, and that the bandwidth may be maintained or even improved by adding a slot. In [206], a substrate with a dielectric constant of 10.02 with size $0.13\lambda_0 \times 0.13\lambda_0$, operating at 1.7 GHz is used. Without the U-slot, the fractional bandwidth was 8%, however, with the addition of the slot, the bandwidth was extended up to 15% while maintaining the performance figures such as the realized gain of 4.5 dBi and a return loss of 25 dB.

Using metamaterials: Metamaterials (MTMs) are generally known as engineered materials, designed to exhibit the properties that are not available in “natural” materials. MTMs can be designed to realize close-to-zero permittivity values, negative permittivity or permeability, or simultaneous negative permittivity and permeability. During the past decade, numerous structures have been proposed. MMTs have also been used in many RF [207], microwave [208] and photonics devices [209] to achieve some interesting properties. In [210], three helices were placed between a circular patch and the ground plane of the antenna to reduce its overall size. This led to 60% miniaturization with a fractional bandwidth of 0.5% and a maximum gain of -7.9 dBi. In [211], overall 80% size reduction was achieved by loading a MTM transmission-line.

The outlined techniques are attractive ones in the context of antenna miniaturization. In general, an antenna can be made smaller at the expense of degrading its gain, efficiency, bandwidth, or radiation pattern. Some of these can be alleviated by modifying the structure geometry but, overall, the art of antenna miniaturization is an art of compromise.

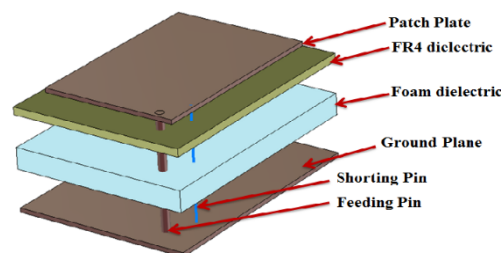


Figure 1.10: Antenna configuration with a shorting post.

1.7 Thesis objectives

Reduction of physical dimensions of the antenna structure generally leads to a degradation of both its electrical and field properties. This includes difficulties in maintaining required impedance bandwidth (particularly in the lower end of the spectrum), omnidirectional radiation pattern [212], or low level of gain variations across the operating frequency range [213]. Consequently, development of miniaturized wideband antennas with acceptable electrical performance has been a subject of intensive research. A typical strategy for antenna miniaturization is to introduce modifications to conventional antenna geometries [214]. Such modifications are often incorporated by trial and error and may include alterations of the radiator shape as well as modifications of the feeding line (e.g., adding impedance matching transformers [215]) or the ground plane [214], [216]. It is perhaps the last type of modifications that is particularly popular, arguably due to its efficiency (introducing ground plane slits and stubs is an easy way of enlarging the current path) and comes in many variations, e.g., slits below the feed line [217], ground plane stubs (I-shaped [214], L-shaped), or protruded ground plane structures [218]. Vast majority of the solutions proposed for compact antennas are case studies. Furthermore, the reduced size is usually an outcome of a particular combination of topology modifications with geometry parameters tuned to satisfy basic performance requirements. Moreover, a particular topology modification introduced to achieve compact designs may not be of any advantage in the said context. In other words, the claims of positive effects of such modifications (in terms of achieving better miniaturization rate) may or may not be justified. The final designs are hardly optimal as finding these would require rigorous numerical optimization of all geometry parameters. This cannot be achieved by means of parameter sweeping which is still the most widely used simulation-driven design approach. The works focused on explicit control of other performance figures are rare in the literature (e.g., [213], [219]). At the same time, the literature is lacking systematic studies on the effect of particular geometry modifications.

This thesis focuses on the development of reliable techniques for assessment of antenna miniaturization methods based on topology alterations. In particular, the following issues are to be addressed:

1. Topology modification is a popular approach in the design of compact antennas, but designs reported in the literature are exclusively case studies;
2. No systematic studies have been available so far concerning the general suitability of particular modifications towards antenna miniaturization;
3. A detailed performance comparison of different geometry modification has not been reported in the literature;
4. Due to complex interactions between geometry parameters and electrical/field properties of the antenna, the actual suitability of specific topology modifications is therefore unclear or even may lead to performance degradation;
5. To find the best possible design and justifying the impact of a particular modification in the context of antenna miniaturization, it is important to optimize all antenna parameters simultaneously. Unfortunately, most reported designs are still tuned using supervised parameter sweeping.

The aforementioned issues lead to a situation when design of miniaturized structures are limited to specific cases with no generic conclusions drawn concerning the relevance of particular types of geometry modifications in the context of size reduction. Given the above, the main purpose of the work is to develop the numerical optimization-based workflows that

enable identification of the most suitable types of geometry alterations in the context of antenna miniaturization. The secondary purpose is development of novel structures of compact antennas by capitalizing on the conclusions of the first part of the project.

In this work, the following research hypotheses were assumed:

1. It is possible, through appropriate numerical studies, to assess the suitability of particular types of geometry modifications for the purpose of antenna size reduction in a conclusive manner.
2. Rigorous numerical optimization of all antenna parameters is critical to determine advantageous topological alterations; the lack thereof generally leads to suboptimal designs as well as possibly wrong conclusions concerning of which antenna geometries are adequate for particular applications.
3. The results of systematic studies of topology modifications can be successfully utilized to design novel wideband antennas of compact geometries and satisfactory electrical and field performance.

1.8 Methodology and Results

This thesis is an attempt to carry out a comprehensive study in relation to wideband antenna geometry modifications (concerning a ground plane, a feed line, and a radiator one) having in mind their effect on antenna miniaturization rate. Moreover, the work puts an emphasis on the development of reliable techniques for assessment of antenna miniaturization methods based on topology alterations. In particular, the problems raised in Section 1.7 are addressed through systematic simulation- and experimental-based studies involving benchmark sets of wideband antennas, the modifications under study are applied to. The purpose of this section is to describe the methodological approaches assumed in the project.

From a methodology point of view, the work can be divided into three phases. In the first phase, two different kinds of modifications (i.e., ground plane and feed line) are applied on the same wideband monopole antenna. Initially, a monopole antenna undergoes ground plane modifications in the form of five-section slits below the feed line. The purpose of this study is to investigate the antenna miniaturization rate that can be achieved by increasing the number of degrees of freedom in the ground plane. All antenna dimensions are tuned through rigorous EM-driven design optimization as discussed in Chapter 2. Afterward, a combination of the ground plane and feed line modification is considered (on the same antenna structure). In all cases, antenna parameters are carefully optimized in order to achieve meaningful results. Based on the discussed study, further investigation in the context of defected ground structure (here, in the form of a rectangular and elliptical slit below the feed line) on achievable miniaturization rate of a wideband antenna is performed. For the assessment purposes, a benchmark set of four wideband monopole antennas is considered. The goal is to determine which modification technique leads to a higher miniaturization rate of the antenna structure. The result was in the favour of elliptical slit rather than the rectangular slit below the feed line. From this conclusion, the complexity of the ground plane alterations below the feed line is increased up to two sections. The results indicate that the one-section elliptical slit is more advantageous than the one-section rectangular slit. However, the situation is the opposite in the case of two-section slits. Therefore, a rectangular slit was considered for further investigations. In the next stage, a benchmark set of the monopole antenna is selected to enhance the complexity below the feed line until the section-number where the minimum size of the antenna is achieved. A similar approach was also adopted for the case of feed line

modifications. To conclude this study with generic remarks, a comprehensive study related to component modifications (pertinent to the feed line, the ground plane, and the radiator) of wideband antennas in the context of antenna miniaturization (using a benchmark set) is performed.

The second phase of the thesis was carried out to demonstrate that particular topology modifications incorporated into the antenna structure with the intention of improving its performance (here, to achieve smaller footprint) may not lead to the expected results. In order to illustrate this point, three antenna structures are selected from the available literature and geometry parameters are rigorously optimized (by employing the same methodology as discussed before) to find the minimum-size designs. It is shown that proper parameter tuning led to disappearance of the said modifications while achieving footprint areas smaller than in the source publications. This not only proves that appropriate EM-driven design closure is essential but also, and more importantly, that the topological changes introduced ad hoc may be and often are counterproductive.

The third phase of the thesis was focused on capitalizing on the results obtained in the first part of the work and using them to design novel and high-performance wideband antenna structures. The particular case study considered was a wideband multiple-input-multiple-output (MIMO) antenna designed for high isolation between radiators. The adopted methodology was incorporation of the n -section rectangular slits below the feed line aimed at improving the impedance matching, thus create a performance margin that can be used to improve isolation. The effect of the number of degrees of freedom on antenna performance was also investigated.

1.9 Contributions and thesis outline

The contributions of the thesis have been described in eight journal publications that constitute Chapters 2 through 9 of the thesis. These are publications selected from the overall record of the candidate (ten journal and eleven conference papers) prepared during his Ph.D. study. Their common theme is miniaturization of wideband antennas for wireless communication.

- [J1] Muhammad Aziz ul Haq and Slawomir Koziel, "A miniaturized UWB monopole antenna with five-section ground plane slit," *Microwave and Optical Technology Letters*, vol. 60, Issue. 4, pp. 1001-1005, 2018.
- [J2] Muhammad Aziz ul Haq and Slawomir Koziel, "A novel miniaturized UWB monopole with five-section stepped-impedance feed line," *Microwave and Optical Technology Letters*, vol. 60, Issue. 1, pp. 202-207, 2018.
- [J3] Muhammad Aziz ul Haq and Slawomir Koziel, "Simulation-based optimization for rigorous assessment of ground plane modifications in compact UWB antenna design," *International Journal of RF and Microwave Computer-Aided Engineering*, <https://doi.org/10.1002/mmce.21204>, 2017.
- [J4] Slawomir Koziel and Muhammad Aziz ul Haq, "Ground plane modifications for design of miniaturized UWB antennas," *IET Microwaves, Antennas & Propagation*, vol. 12, Iss. 8, pp. 1360-1366, 2018.
- [J5] Muhammad Aziz ul Haq, Slawomir Koziel, and Qingsha S. Cheng, "Miniaturization of wideband antennas by means of feed line topology alterations," *IET Microwaves, Antennas & Propagation*, vol. 12, Iss. 13, pp. 2128-2134, 2018.

- [J6] Muhammad Aziz ul Haq and Slawomir Koziel, "Quantitative assessment of wideband antenna geometry modifications for size-reduction-oriented design," *International Journal of Electronics and Communications*, vol. 90, pp. 45-52, 2018.
- [J7] Muhammad Aziz ul Haq and Slawomir Koziel, "On topology modifications for wideband antenna miniaturization," *International Journal of Electronics and Communications*, vol. 94, pp. 215-220, 2018.
- [J8] Muhammad Aziz ul Haq and Slawomir Koziel, "Ground plane alterations for design of high-isolation compact wideband MIMO antenna," *IEEE Access*, vol. 6, pp. 48978-48983, 2018.
- [J9] Muhammad Aziz ul Haq and Slawomir Koziel, "Ground plane alterations for high-isolation compact wideband MIMO antennas in a parallel configuration," *Microwave and Optical Technology Letters*. (Under review)

Chapter 2 presents the exposition of antenna design task as an optimization problem. Conventional numerical optimization techniques including derivative-free and gradient-based methods have been discussed briefly. Reference [J1], [J2] (Chapter 3) discusses the structure and design of a miniaturized monopole antenna in order to investigate the effect of different types of topological modifications on the antenna miniaturization rate. Reference [J3] (Chapter 4) deals with an investigation in the context of defected ground structure (here, in the form of a rectangular and elliptical slit below the feed line) on achievable miniaturization rate in the case of wideband antenna structures. Reference [J4] (Chapter 5) carries out systematic investigations concerning the relevance of ground plane modifications in the context of antenna size reduction. Here, a specific ground plane modification in the form of n -section rectangular slit below the feedline is considered. Reference [J5] (Chapter 6) contains a systematic analysis of the two types of feed lines (a stepped-impedance line and a multi-section taper one) to study their effect on achievable minimum footprint in the case of wideband antennas. Reference [J6] (Chapter 7) presents a comprehensive study related to wideband antenna geometry modifications (concerning a ground plane, a feed line, and a radiator) having in mind their effect on antenna miniaturization rate. The study is performed using a benchmark set of two wideband monopole antennas. The feed line and a ground plane modifications considered here are slits below the feed line and multi-section stepped-impedance lines respectively. For a radiator, circular, elliptical, and rectangular slits are investigated. Reference [J7] (Chapter 8) demonstrates that particular topology modifications introduce to achieve compact designs may or may not be advantageous in the context of the antenna size reduction as well as that numerical optimization is critical to conclusively assess their suitability for the said purpose. Reference [J8], [J9] (Chapter 9) discusses the impact of multi-section ground plane slits for isolation improvement in the case of wideband multiple-input-multiple-output (MIMO) antenna system. Chapter 10 concludes the thesis and discusses the important possible future directions.

Chapter 2

2 Antenna optimization

This chapter provides a short overview of numerical optimization within the scope relevant to the thesis. A brief summary of conventional optimization techniques, including gradient-based and derivative-free methods, as well as population-based metaheuristics are also part of the discussion.

2.1 Antenna design as an optimization problem

The antenna optimization problem is formulated as the following nonlinear minimization task [220]:

$$\mathbf{x}^* = \underset{\mathbf{x}}{\operatorname{argmin}} U(\mathbf{R}_f(\mathbf{x})) \quad (2.1)$$

Here, $\mathbf{R}_f \in R^m$ denotes the response vector of a high-fidelity, EM-simulated model of the antenna, e.g., the modulus of the reflection coefficient $|S_{11}|$ evaluated at m different frequencies; $\mathbf{x} \in R^n$ is a vector of antenna design variables, and U is a given scalar merit function, e.g., a minimax function with upper and lower specifications. Vector \mathbf{x}^* is the optimum design to be determined. The notation $U(\mathbf{R}_f(\mathbf{x}))$ denotes an objective function. The function U is defined so that better designs correspond to the smaller values of U . Figure 2.1 shows the example of minimax specifications for the reflection response, i.e., $|S_{11}| \leq -10$ dB, corresponding to the UWB frequency range. In this case, the value of $U(\mathbf{R}_f(\mathbf{x}))$ is a maximum violation of the design specifications within the frequency band of interest.

For the rest of the chapter, a symbol $f(\mathbf{x})$ will be used as an abbreviation instead of $U(\mathbf{R}_f(\mathbf{x}))$. As a matter of fact, the problem (2.1) is always a constrained one. Three different types of constraints can be considered:

- Lower and upper bounds for design variables, i.e., $l_b \leq x_b \leq u_b$, $b = 1, \dots, m$;
- Equality constraints, i.e., $c_{eq,l}(\mathbf{x}) = 0$, $l = 1, \dots, M_{eq}$, where M_{eq} is the number of constraints;
- Inequality constraints, i.e., $c_{ineq,l}(\mathbf{x}) \leq 0$, $l = 1, \dots, M_{ineq}$, where M_{ineq} is the number of constraints.

Normally, constraints are introduced to ensure the physical dimensions (length, width,

area) of the antenna within the specified bounds. Furthermore, the constraints can be helpful in order to make sure that the antenna structure that is to be evaluated by the EM solver is physically valid (e.g., certain parts of the structure do not overlap, etc.).

Figure 2.2 shows a typical flow of simulation-driven design optimization. Generally, it is an iterative process where the designs obtained by the optimizer are verified by evaluating the antenna model using the EM solver. Furthermore, the search process is guided either by the model response itself or by the response gradients. In the following parts of the section, we briefly discuss gradient-based optimization techniques as well as derivative-free methods, including population-based metaheuristics.

2.2 Gradient-based optimization methods

Gradient-based techniques belong to the most popular optimization methods [214]. The search process is based on the derivatives of the objective function. Assuming that the objective function $f(\mathbf{x})$ is sufficiently smooth or at least continuously differentiable, the gradient $\nabla f = [\partial f/\partial x_1 \ \partial f/\partial x_2 \ \dots \ \partial f/\partial x_n]^T$ gives the information about the descent of f in the vicinity of the design at which the gradient is calculated. In particular,

$$f(\mathbf{x} + \mathbf{h}) \cong f(\mathbf{x}) + \nabla f(\mathbf{x}) \cdot \mathbf{h} \quad (2.2)$$

for a vector \mathbf{h} if $\nabla f(\mathbf{x}) \cdot \mathbf{h} < 0$. In particular, $\mathbf{h} = -\nabla f(\mathbf{x})$ determines the direction of the steepest descent. While it is advantageous to follow this direction when away from the optimum, steepest descent methods exhibit poor overall performance and are not used in practice [222]. A practical technique is a conjugate-gradient method which utilizes the combination of the previous direction \mathbf{h}_{i-1} and the current gradient in order to find the search direction, i.e.,

$$\mathbf{h} = -\nabla f(\mathbf{x}^i) + \gamma \mathbf{h}_{i-1} \quad (2.3)$$

A popular technique for selecting the coefficient γ is a Fleecher-Reeves method where

$$\gamma = \frac{\nabla f(\mathbf{x})^T \nabla f(\mathbf{x})}{\nabla f(\mathbf{x}_{i-1})^T \nabla f(\mathbf{x}_{i-1})} \quad (2.4)$$

The next design \mathbf{x}^{i+1} is computed from the current one \mathbf{x}^i as:

$$\mathbf{x}^{i+1} = \mathbf{x}^i + \alpha \cdot \mathbf{h} \quad (2.5)$$

The choice of the step size $\alpha > 0$ can be based on the line search or acquiring information from the second-order derivatives [223].

An alternative class of optimization techniques is Newton and quasi-Newton methods. If f is at least twice continuously differentiable, a second-order Taylor expansion of f can be written as:

$$f(\mathbf{x} + \mathbf{h}) \cong f(\mathbf{x}) + \nabla f(\mathbf{x}) \cdot \mathbf{h} + \frac{1}{2} \mathbf{h} \cdot \mathbf{H}(\mathbf{x}) \cdot \mathbf{h} \quad (2.6)$$

Here, $\mathbf{H}(\mathbf{x})$ is the Hessian of f at \mathbf{x} , that is, $\mathbf{H}(\mathbf{x}) = [\partial^2 f/\partial x_j \partial x_k]_{j,k=1,\dots,n}$. This implies that

the next approximation of the optimum can be determined as:

$$\mathbf{x}^{i+1} = \mathbf{x}^i + [H(\mathbf{x})]^{-1}\nabla f(\mathbf{x}) \quad (2.7)$$

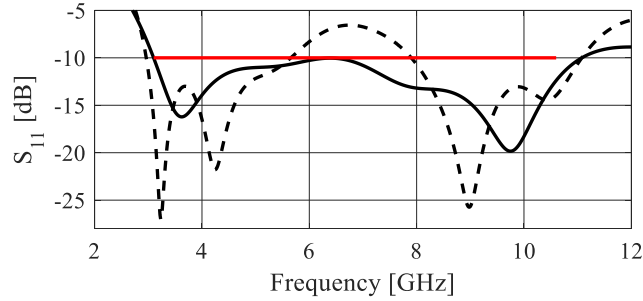


Figure 2.1: An example of minimax design specifications. For a UWB antenna, the reflection response $|S_{11}| \leq -10$ dB for 3.1 GHz to 10.6 GHz is required. The response marked (- -) does not satisfy the specifications, whereas the response marked (—) does satisfy the specs.

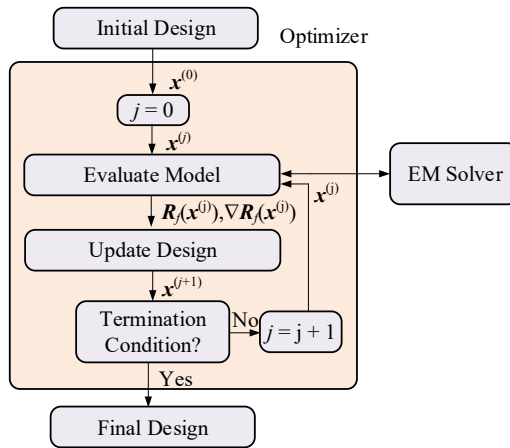


Figure 2.2: A flowchart of gradient-based simulation-driven optimization. The search process can be guided by the model response or by the response and its derivatives [221].

The algorithm (2.7) features very fast (quadratic) convergence rate but only works if the starting point is sufficiently close to the optimum and the Hessian is positive definite at all iterations [222]. These conditions are difficult to satisfy, which makes (2.7) impractical. Instead, various types of damped Newton techniques are used [223].

Another group of gradient-based optimization methods is trust-region (TR) algorithms. A TR procedure iteratively finds a local minimum of the cost function f by producing a series of approximations $\mathbf{x}^{(i)}$, $i = 0, 1, \dots$, to the optimum design \mathbf{x}^* . These are typically found by optimizing the linear expansion model

$$\mathbf{L}(i)(\mathbf{x}) = f(\mathbf{x}(i)) + \nabla f(\mathbf{x}(i)) \cdot (\mathbf{x} - \mathbf{x}(i)) \quad (2.8)$$

In the i^{th} iteration of the TR algorithm, the following problem is solved

$$\mathbf{x}^{(i+1)} = \arg \min_{\mathbf{x}; -\mathbf{d}^{(i)} \leq \mathbf{x} - \mathbf{x}^{(i)} \leq \mathbf{d}^{(i)}} U(\mathbf{L}^{(i)}(\mathbf{x})) \quad (2.9)$$

The vector $\mathbf{d}^{(i)}$ is the TR region size adjusted using the standard rules [224], i.e., based on the gain ratio $\rho = [U(\mathbf{R}(\mathbf{x}^{(i+1)})) - U(\mathbf{R}(\mathbf{x}^{(i)}))]/[U(\mathbf{L}^{(i)}(\mathbf{x}^{(i+1)})) - U(\mathbf{L}^{(i)}(\mathbf{x}^{(i)}))]$ (actual versus linear-model predicted objective function improvement). The inequalities $-\mathbf{d}^{(i)} \leq \mathbf{x} - \mathbf{x}^{(i)} \leq \mathbf{d}^{(i)}$ in (2.9)

are understood component-wise. Because the variable ranges in antenna structures may be dramatically different for various parameters (e.g., fractions of millimetre for gaps, and tens of millimetres for ground plane width), the search region is defined here, as a hypercube rather than a ball $\|\mathbf{x} - \mathbf{x}^{(i)}\| \leq \delta^{(i)}$ (Euclidean norm with scalar TR radius). This—when setting up the initial size vector $\mathbf{d}^{(0)}$ proportional to the design space sizes—allows for ensuring similar treatment of variables with significantly different ranges. TR algorithms are the major technique utilized in this work.

In the context of EM-driven antenna optimization, utilization of gradient-based method is relatively expensive because of the necessity of evaluating the response gradient through finite differentiation and the high cost of EM analysis. In some cases, it is possible to speed up the process by utilizing adjoint sensitivities but these are only available—among commercial solvers—through CST [225] and HFSS [226], and only in a limited number of practical cases.

2.3 Derivative-Free Optimization

In some cases, gradient-based methods are not the best choice, e.g., if the objective function is discontinuous or noisy, or derivative information is not available. Derivative-free methods enable the search for a local (or global, cf. Section 2.4) minimum merely based on the objective function value. Popular examples include pattern search methods. A conceptual demonstration of this method is shown in Figure 2.3. In the most popular version, the search process is restricted to the rectangular grid and explores a grid-restricted neighbourhood of the current design. Upon an unsuccessful move, the grid is refined to allow smaller steps. Numerous varieties of the pattern search methods are presented in [227]. A large size of the initial grid may allow us to utilize these techniques for a quasi-global search.

Another popular derivative-free method is the Nelder-Mead algorithm [222] also known as the simplex method. Here, the search process depends upon moving the vertices of the simplex in the design space in such a way that the vertex corresponding to the highest value of the objective function is updated by the new one at the location where the objective function value is expected to be improved. The simplex algorithm is reliable but slowly convergent.

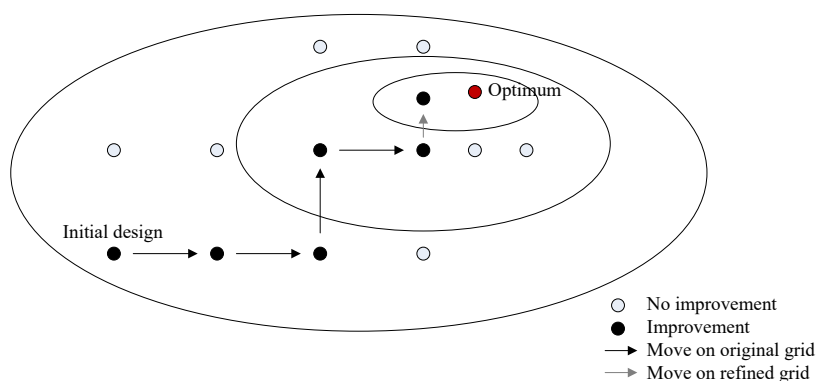


Figure 2.3: A conceptual illustration of a pattern search algorithm [221].

2.4 Metaheuristics and Global Optimization

Metaheuristics are global search methods, inspired by the natural processes such as biological or social systems. Metaheuristics are capable to avoid getting stuck in local optima and converge (with reasonable probability) towards a globally optimal solution of the problem. Moreover, they can handle non-differentiable, noisy, and discontinuous objective functions. The most popular types of metaheuristic algorithms are genetic algorithms (GAs) [228], evolutionary algorithms (EAs) [229], evolution strategies (ES) [229], particle swarm optimizers (PSO) [230], differential evolution (DE) [231], and, firefly algorithm [222].

A generic flow of the metaheuristic algorithm, pertinent to methods such as GAs or EAs, is the following [221]:

1. Initialize population P (a random process);
2. Evaluate population P ;
3. Select parent individuals S from P ;
4. Apply recombination operators to create a new population P from parent individuals S ;
5. Apply mutation operators to introduce local perturbations in individuals of P ;
6. If termination condition is not satisfied go to 2;
7. END.

In the context of antenna design, metaheuristics are attractive approaches for those problems where evaluation time is not of concern and where multiple local optima are expected. Therefore, metaheuristics are highly preferred for antenna array optimization problems for pattern synthesis [232], [233], as long as the array is evaluated using the analytical array factor model. On the other hand, due to their inherently high computational complexity, population-based metaheuristics are generally not recommended for handling full-wave electromagnetic antenna models.

2.5 Antenna Optimization Approaches Utilized in This Work

The problem considered in this work is to find the minimum-footprint antenna that satisfies the condition $S(\mathbf{x}) \leq -10$ dB, where $S(\mathbf{x})$ is the maximum reflection in the frequency band of interest, and \mathbf{x} stands for adjustable geometry parameters of the structure at hand. The antenna size will be denoted as $A(\mathbf{x})$. The design problem is therefore formulated as:

$$\mathbf{x}^* = \underset{\mathbf{x}}{\operatorname{argmin}}\{A(\mathbf{x})\}, \quad S(\mathbf{x}) \leq -10 \text{ dB} \quad (2.10)$$

The problem (2.10) is solved here using the pattern search algorithm [218], starting from the design obtained by minimizing $S(\mathbf{x})$ (to ensure a feasible initial point).

A pattern search implementation utilized here [234] is a derivative-free stencil-based search routine where grid-restricted line search (with search direction obtained from objective function gradient estimated using on-grid perturbations) is interleaved with poll-type search and grid refinement (in case of the failure of the neighbor search).

Optimization for minimum reflection is arranged differently, namely, we utilize a trust-region (TR) [224] gradient search algorithm (cf. (2.8), (2.9)) with the antenna response Jacobians estimated through finite differentiation. TR-embedded gradient-based routine is generally faster, however, it is not suitable for handling explicit constraints (as in (2.9)). Practical computational complexity of both pattern search and gradient-based routine (the

latter is used here with numerical derivatives) is more or less quadratic with respect to the design space dimension, meaning that the number of EM simulations required for algorithm convergence is typically between a few dozen to two hundred depending upon the antenna structure at hand. Occasionally, a particle swarm optimization (PSO) algorithm [230] is used at the initial stage of the optimization process in order to identify a good starting point for the local search.

Chapter 3

3 Paper [J1] and [J2]

Muhammad Aziz ul Haq, and Slawomir Koziel

A Miniaturized UWB Monopole Antenna with Five-Section Ground Plane Slit

Published: *Microwave and Optical Technology Letters*, vol. 60, Issue. 4, pp. 1001-1005, 2018.

DOI: <https://doi.org/10.1002/mop.31099>

REFERENCES

- [1] Lacroix B, Papapolymerou J. A triple-mode X-band microstrip ring resonator filter. In IEEE MTT-S International Microwave Symposium Digest, 2011, 1–4.
- [2] He ZS, Shao ZH, You CJ. Parallel feed bandpass filter with high selectivity and wide stopband. *Electron Lett*. 2016;52(10):844–846.
- [3] Chen RS, Wong SW, Zhu L, Chu QX. Wideband bandpass filter using u-slotted substrate integrated waveguide (SIW) cavities. *IEEE Microw Wirel Comp Lett*. 2015;25(1):1–3.
- [4] Zheng CY, Xu F. Compact bandpass filter based on one-third equilateral triangular resonator of substrate integrated waveguide. *Electron Lett*. 2015;51(19):1505–1507.
- [5] Zheng CY, Xu F. A compact wideband filter designed on single one-third equilateral triangular cavity. *Microw Opt Technol Lett*. 2016;58(8):1993–1996.
- [6] Cariou M, Potelon B, Quendo C, et al. Compact X-band filter based on substrate integrated advanced coaxial line stubs using advanced multilayer PCB technology. *IEEE Trans Microw Theory Technol*. 2017;65(2):496–503.
- [7] Hong JS, Lancaster MJ. *Microstrip Filters for RF/Microwave Applications*. New York: John Wiley & Sons, 2001.

How to cite this article: Zheng Y, Sheng W. Compact X-band bandpass filter using stub-loaded T-shape resonator with source-load coupling. *Microw Opt Technol Lett*. 2018;60:996–1001. <https://doi.org/10.1002/mop.31096>

Received: 5 September 2017

DOI: 10.1002/mop.31099

A miniaturized UWB monopole antenna with five-section ground plane slit

Muhammad Aziz Ul Haq  |Slawomir Koziel 

Engineering Optimization & Modeling Center, School of Science and Engineering, Reykjavik University, 101 Reykjavik, Iceland

Correspondence

Muhammad Aziz ul Haq, Engineering Optimization & Modeling Center, School of Science and Engineering, Reykjavik University, 101 Reykjavik, Iceland.

Email: muhammadu16@ru.is

Funding information

Icelandic Centre for Research (RANNIS), Grant/Award Number: 163299051

Abstract

A practical miniaturized ultra-wideband monopole antenna with a five-section ground plane slit is proposed. The structure is a modification of a reference antenna designed with the two-section ground plane slit and featuring the footprint area of 216 mm². To reduce the antenna size, a ground plane modification was introduced in the form of a five-section slit below the feeding line. Furthermore, all geometry parameters of the structure were simultaneously optimized. The final design exhibits a small size of only 22.5 × 7.9 mm² with footprint of 178 mm² and good electrical and field characteristics. Experimental validation and comparisons with recently reported designs are also provided.

KEYWORDS

experimental validation, five-section slit, geometry parameters, optimization, size reduction

1 | INTRODUCTION

Modern communication systems require smart, low cost, omnidirectional radiation pattern, and high-bandwidth antennas.¹ In the context of ultra-wideband (UWB) applications, monopole antenna appear to be attractive solutions. On the other hand, one of the important prerequisites in the design of UWB antennas, especially for wearable devices,² microwave imaging,³ and internet of things (IoT),⁴ is a compact size. Unfortunately, design of a compact size UWB antenna is a quite challenging task due to certain limitations. For example, the major difficulty is that the reduction of the physical dimensions of the antenna generally leads to degradation of its performance figures such as gain, efficiency, and radiation pattern. There have been a number of techniques proposed to overcome this problem by introducing various geometry modifications. The most successful of these concerns a ground plane, for example, slits and L-shape stubs,⁴ an inverted T-shape slit,⁵ a dielectric resonator within the ground plane,⁶ a CPW square slot at the ground plane,⁷ protruded ground plane structures,⁸ or a tapered fed region.⁹ To achieve the minimum antenna size, topological modifications have to be accompanied by simultaneous adjustment of all antenna parameters. This can only be accomplished by rigorous EM-driven design optimization.¹⁰

In this article, we discuss a structure and design of a miniaturized monopole antenna. The purpose of this study is to investigate the antenna miniaturization rate by increasing the number of degrees of freedom in the ground plane. The antenna is a modification of the design reported in ref. [11]. To increase the number of degrees of freedom, a ground

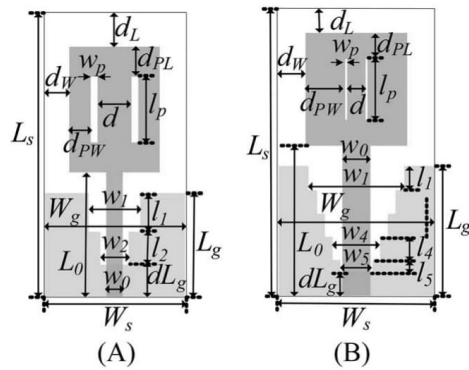


FIGURE 1 UWB monopole antennas prototype. A, Reference antenna. B, Modified antenna with five-section slit below the feed line

plane modification is incorporated in the form of a five-section slit below the feed line. All antenna dimensions are adjusted through rigorous EM-driven design optimization.¹⁰ Simulation-based optimization of all antenna parameters with constraints imposed on reflection characteristics leads to the design featuring a small footprint of only 178 mm² and acceptable electrical and field properties for the entire UWB frequency range. Experimental validation of the fabricated antenna prototype is provided and compared with simulation results.

2 | ANTENNA DESIGN

The proposed antenna is a modification of the design of ref. [11], incorporating two radiator slots as shown in Figure 1A and featuring the footprint area of 216 mm². Here, a modified ground plane is introduced in the form of an n -section

slit below the feeding line as shown in Figure 1B. Here, $n = 3, 4,$ and 5 . The structure is realized on a 1.55-mm-thick FR-4 substrate ($\epsilon_r = 4.4$). The reference antenna is described by the following vector of geometry parameters $x = [L_0 \ L_P \ w_P \ d \ d_L \ d_{PL} \ d_{PW} \ d_W \ l_1 \ w_1 \ l_2 \ w_2 \ d_{Lg}]^T$ (all dimensions in mm). For the sake of design optimization, a computational model is implemented in CST Microwave Studio¹² and evaluated using time-domain solver. The model contains the SMA connector. To emphasize the importance of geometry parameter optimization, the reference antenna has been re-optimized for minimum size using the pattern search algorithm¹³ with additional requirements on the reflection response (maximum in-band reflection to be not higher than -10 dB, enforced through an explicit constraint). The optimized parameter vector is $x^{*1} = [11.36 \ 6.02 \ 0.75 \ 2.00 \ 0.00 \ 2.75 \ 2.55 \ 0.00 \ 3.50 \ 4.00 \ 1.25 \ 0.77 \ 2.59]^T$. The antenna footprint is 198 mm², which is considerably smaller than for the reference design of ref. [11]. To increase the number of degrees of freedom for antenna miniaturization, 3, 4, and 5 section slits below the feed line have been considered. Furthermore, to emphasize the effect of the slit by itself, another variation of the antenna, with flat ground, has also been optimized. The effect on antenna footprint due to the particular ground plane topology is shown in Table 1. It can be observed that increasing the number of sections contributes to improving achievable miniaturization rate. Here, however, $n = 5$ is considered as the maximum structure complexity. Upon applying the five-section ground plane modification of Figure 1B, the geometry parameter vector was extended $x = [L_0 \ L_P \ w_P \ d \ d_L \ d_{PL} \ d_{PW} \ d_W \ l_1 \ w_1 \ l_2 \ w_2 \ l_3 \ w_3 \ l_4 \ w_4 \ l_5 \ w_5 \ dL_g]^T$. Its optimized values are $x^{*2} = [13.27 \ 5.14 \ 0.15 \ 1.28 \ 0.02 \ 2.05 \ 3.17 \ 0.00 \ 4.01 \ 5.48 \ 2.08 \ 1.67 \ 1.15 \ 1.59 \ 0.29 \ 0.87 \ 0.20 \ 0.53 \ 1.35]^T$. The antenna footprint is only 178 mm². It should be emphasized that the core antenna dimensions are significantly different in x^{*1} and x^{*2} which indicates that

TABLE 1 Footprint area of optimized antenna with section slit below the feed line

Optimized antenna foot print [mm ²]				
Flat ground	Reference antenna	3-section slit	4-section slit	5-section slit
264	198	190	186	178

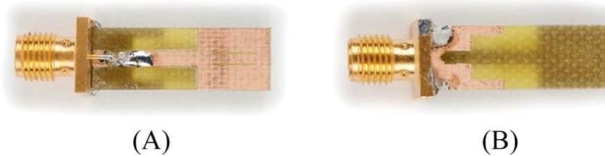


FIGURE 2 Photographs of the fabricated antenna prototype. A, Top layer. B, Bottom layer [Color figure can be viewed at wileyonlinelibrary.com]

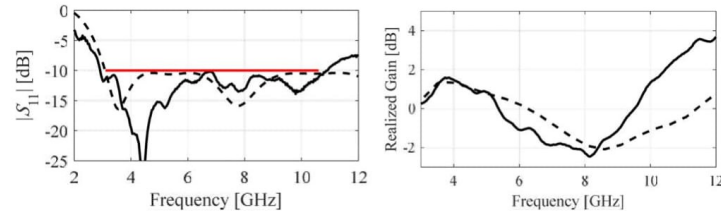


FIGURE 3 Simulated (---) and measured (—) antenna characteristics: A, reflection response and B, realized gain [Color figure can be viewed at wileyonlinelibrary.com]

advantages of particular geometry modifications can only be fully exploited if accompanied by adjustment of all relevant antenna parameters.

3 | RESULTS AND DISCUSSIONS

The final antenna design has been fabricated (Figure 2) and measured. The results have been shown in Figures 3–5. Figure 3 shows the antenna reflection response and realized gain. It is observed that the measured reflection response is well under -10 dB for the entire UWB frequency range. Meanwhile, antenna realized gain also shows an acceptable agreement with the simulated gain. Figure 4A,B shows the H-plane and E-plane patterns of the modified antenna. It is observed that the radiation pattern is nearly omnidirectional, which is one of the fundamental requirements for UWB antennas. However, it can also be noticed that for lower frequency, that is, 4 GHz, the measured E-plane pattern is

slightly deviating from the simulations that might be due to the soldering effect on the antenna. This phenomenon usually happens due to the change of material properties by soldering copper especially for small-size antennas.

The proposed antenna exhibits very good radiation pattern stability. More specifically, its pattern stability factor (PSF) is 0.92, with PSF being¹⁴

$$\text{PSF} = \int_{\Omega} C(\vec{R}) ds / \int_{\Omega} ds \quad (1)$$

where Ω is the range of operating directions (following ref. [10], we consider the H-plane so that Equation 1 is reduced to a linear integral), $C(\vec{R})$ and is the frequency-domain correlation pattern

$$C(\vec{R}) = \int_{\Omega} F^2(\vec{R}, \vec{r}) ds / \int_{\Omega} ds \quad \text{with}$$

$$F^2(\vec{R}, \vec{r}) = \int_{\text{BW}} E(\vec{r}, f) E^*(\vec{R}, f) df / \left[\int_{\text{BW}} |E(\vec{r}, f)|^2 df \int_{\text{BW}} |E(\vec{r}, f)|^2 df \right]$$

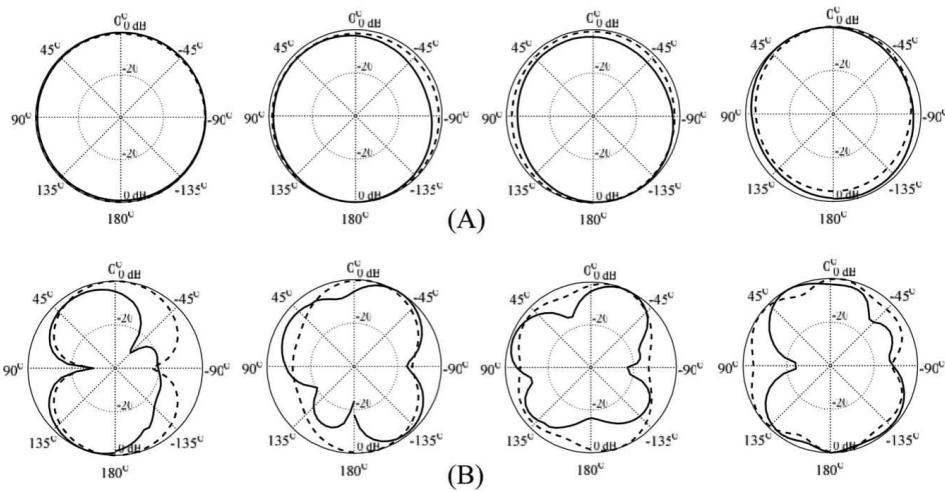


FIGURE 4 Simulated (---) and measured (—) radiation patterns of the proposed antenna. The plots (from left to right) are for frequencies 4, 6, 8, and 10 GHz: A, H-plane patterns and B, E-plane patterns

TABLE 2 Comparison of a comparative set of UWB antennas in term of size, frequency, and gain

Ref.	Size (mm × mm)	Operating bandwidth (GHz)	Antenna footprint (λ_g^2) ^a	Realized gain range (dB)
[11]	18 × 12	3.12–12.73	0.29	–
[15]	20 × 16	4.8–14.5	0.43	1.9–4.4
[16]	10 × 32.5	3.1–10.6	0.43	1.25–3.5
[17]	22 × 15.8	3.1–10.6	0.26	–
[18]	28 × 20	2.85–11.85	0.54	–0.8–3.2
[19]	24 × 16	3.1–10.9	0.50	2–4
This work	22.5 × 7.9	2.9–10.9	0.23	–2.2–3.8

^a λ_g denotes the antenna footprint in terms of the guided wavelength.

where $E(\vec{r}, f)$ is the far-field electric field in direction, is a reference direction, and * denotes the complex conjugate.

Similarly, the proposed antenna features good pulse fidelity factor (PFF) which describes time-domain correlations between the input and transmitted electric field waveforms.¹⁴ More specifically, the PFF values for the H-plane (azimuth angles of 0°, 30°, ..., 330°) are 0.89, 0.90, 0.89, 0.82, 0.86, 0.89, 0.90, 0.89, 0.86, 0.82, 0.89, and 0.90, respectively.

Figure 5 shows the normalized input and output electric field waveforms for selected azimuth angles.

4 | COMPARISON OF PROPOSED ANTENNA SPECIFICATIONS

The proposed antenna performance was compared with the recently reported UWB monopole antennas,^{11,15–19} in terms

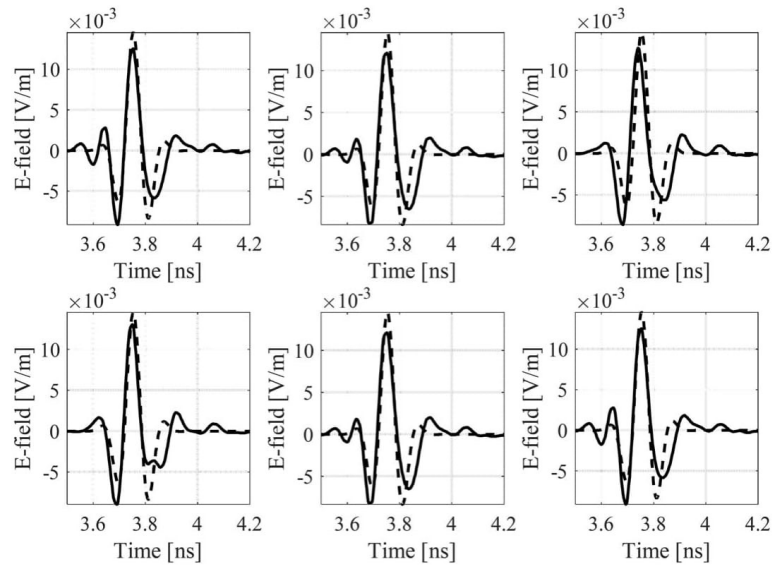


FIGURE 5 (Normalized) electric field waveforms for the proposed antenna in the H-plane for the azimuth angles of 30°, 60°, 120°, 180°, 270°, and 330°. Shifted version of the input waveform (---) $e(t - \tau)$ is shown that maximizes the convolution integral $\int v(t)e(t - \tau)dt$ (cf. ref. [14]) with the output waveform (—)

of bandwidth, size, and realized gain (Table 2). Antennas footprint was expressed in term of a guided wavelength to ensure a fair comparison between substrates of various properties. The guided wave length was defined by 50Ω line impedance operating at 6 GHz. It can be observed that the antenna structure proposed in this article is competitive with respect to both the operating bandwidth and the size. Comparison of pattern stability and pulse fidelity was not possible because no relevant results have been reported in the benchmark antennas.

5 | CONCLUSION

In this article, a structure of a UWB monopole antenna with a five-section ground plane slit has been presented. As demonstrated, introduction of more complex ground plane modification along with simultaneous adjustment of all geometry parameters leads to considerably reduction of the antenna size, from 216 mm^2 for the reference antenna to only 178 mm^2 (dimensions of $22.5 \times 7.9 \text{ mm}^2$). The structure exhibits reflection below -10 dB in 2.9 GHz to over 10.9 GHz frequency range. The radiation characteristic of the antenna is omnidirectional with good radiation pattern stability and decent pulse fidelity.

ACKNOWLEDGMENT

This work has been partially supported by the Icelandic Centre for Research (RANNIS) Grant 163299051.

ORCID

Muhammad Aziz Ul Haq  <http://orcid.org/0000-0003-3380-4745>

Slawomir Koziel  <http://orcid.org/0000-0002-9063-2647>

REFERENCES

- [1] Vendik IB, Rusakov A, Kanjanasit K, Hong J, Filonov D. Ultra-wideband (UWB) planar antenna with single-, dual-, and triple-band notched characteristic based on electric ring resonator. *IEEE Antennas Wireless Propag Lett.* 2017;16:1597–1600.
- [2] Abbasi QH, Rehman MU, Yang X, Alomainy A, Qaraqe K, Serpedin E. Ultrawideband band-notched flexible antenna for wearable applications. *IEEE Antennas Wireless Propag Lett.* 2013;12:1606–1609.
- [3] Moosazadeh M, Kharkovskiy S, Toby J, Samali B. Miniaturized UWB antipodal vivaldi antenna and its application for detection of void inside concrete specimens. *IEEE Antennas Wireless Propag Lett.* 2017;16:1317–1320.
- [4] Bekasiewicz A, Koziel S. Compact UWB monopole antenna for internet of things applications. *Electron Lett.* 2016;52(7):492–494.
- [5] Mohammadi B, Valizade A, Rezaei P, Nourinia J. New design of compact dual band-notch ultra-wideband band pass filter based on coupled wave canceller inverted T-shaped stubs. *IET Microwave Antennas Propag.* 2015;9(1):64–72.
- [6] Yang N, Leung K, Lu K, Wu N. Omnidirectional circularly polarized dielectric resonator antenna with logarithmic spiral slots in the ground. *IEEE Trans Antennas Propag.* 2017;65(2):839–844.
- [7] Shokri M, Rafii V, Karamzadeh S, Amiri Z, Virdee B. Miniaturised ultra-wideband circularly polarised antenna with modified ground plane. *Electron Lett.* 2014;50(24):1786–1788.
- [8] Li J, Chu Q, Li Z, Xia X. Compact dual band-notched UWB MIMO antenna with high isolation. *IEEE Trans Antennas Propag.* 2013;61(9):4759–4766.
- [9] Manohar M, Kshetrimayum RS, Gogoi AK. Printed monopole antenna with tapered feed line, feed region and patch for super wideband applications. *IET Microwave Antennas Propag.* 2014;8(1):39–45.
- [10] Koziel S, Bekasiewicz A. "Multi-objective design of antennas using surrogate models," World Scientific, 2016.
- [11] Ojaroudi M, Ghobadi C, Nourinia J. Small square monopole antenna with inverted T-shaped notch in the ground plane for UWB application. *IEEE Antennas Wireless Propag Lett.* 2009;8:728–731.
- [12] CST Microwave Studio, ver. 2015. CST AG, Bad Nauheimer Str. 19, D-64289 Darmstadt, Germany, 2015.
- [13] Koziel S. Computationally efficient multi-fidelity multi-grid design optimization of microwave structures. *Appl Comput Electromagn Soc J.* 2010;25(7):578–586.
- [14] Liu J, Esselle KP, Hay SG, Zhong S. Effects of printed UWB antenna miniaturization on pulse fidelity and pattern stability. *IEEE Trans Antennas Propag.* 2014;62(8):3903–3910.
- [15] Shakib M, Moghavvemi NM, Mahadi WNL. Design of a compact planar antenna for ultra-wideband operation. *Appl Comput Electromagn Soc J.* 2015;20(2):222–229.
- [16] Liu YF, Wang P, Qin H. Compact ACS-fed UWB monopole antenna with extra bluetooth band. *Electron Lett.* 2014;50(18):1263–1264.
- [17] Bekasiewicz A, Koziel S. Structure and computationally-efficient simulation-driven design of compact UWB monopole antenna. *IEEE Antennas Wireless Propag Lett.* 2015;14:1282–1285.
- [18] Nikolaou S, Abbasi MAB. Design and development of a compact UWB monopole antenna with easily-controllable return loss. *IEEE Trans Antennas Propag.* 2017;65(4):2063–2067.
- [19] Alsath MGN, Kanagasabai M. Compact UWB monopole antenna for automotive communication. *IEEE Trans Antennas Propag.* 2015;63(9):4204–4208.

How to cite this article: Ul Haq MA, Koziel S. A miniaturized UWB monopole antenna with five-section ground plane slit. *Microw Opt Technol Lett.* 2018;60:1001–1005. <https://doi.org/10.1002/mop.31099>

Muhammad Aziz ul Haq, and Slawomir Koziel

A Novel Miniaturized UWB Monopole with Five-Section Stepped-Impedance Feed Line

Published: *Microwave and Optical Technology Letters*, vol. 60, Issue. 1, pp. 202-207, 2018.

DOI: <https://doi.org/10.1002/mop.30936>

ACKNOWLEDGMENTS

The authors acknowledge, IIT Kanpur for allowing to use facility available in “Microwave Antenna Laboratory” for Antenna Measurement.

ORCID

A. Gangwar  <http://orcid.org/0000-0001-7023-2614>

REFERENCES

- [1] Pei J, Wang AG, Gao S, Leng W. Miniaturized triple-band antenna with a defected ground plane for WLAN/WiMAX applications. *IEEE Antennas Wirel Propag Lett.* 2011;10:298–301.
- [2] Liu P, Zou Y, Xie B, Liu X, Sun B. Compact CPW-fed tri-band printed antenna with meandering split-ring slot for WLAN/WiMAX applications. *IEEE Antennas Wirel Propag Lett.* 2012;11:1242–1244.
- [3] Chen H, Yang X, Yin YZ, Wu JJ, Cai YM. Tri-band rectangle-loaded monopole antenna with inverted-I slot for WLAN/WiMAX applications. *Electron Lett.* 2013;49:1261–1262.
- [4] Verma S, Kumar P. Compact triple-band antenna for WiMAX and WLAN applications. *Electron Lett.* 2014;50:484–486.
- [5] Li Y, Yu W. A miniaturized triple band monopole antenna for WLAN and WiMAX applications. *Int J Antennas Propag.* 2015;1–5.
- [6] Li L, Zhang X, Yin X, Zhou L. A compact triple-band printed monopole antenna for WLAN/WiMAX applications. *IEEE Antennas Wirel Propag Lett.* 2016;15:1853–1855.
- [7] Pushkar P, Gupta VR. A metamaterial based Tri-band antenna for WiMAX/WLAN application. *Microwave Opt Technol Lett.* 2016;58:558–561.
- [8] Hamid M, Hamid R. Equivalent circuit of dipole antenna of arbitrary length. *IEEE Trans Propag.* 1997;45:1695–1696.
- [9] Gangwar AK, Alam MS. A SSRR based multiband antenna for mobile phone. In: *2016 Twenty Second National Conference on Communication (NCC)*, Guwahati; 2016:1–4.
- [10] Advanced Design System (ADS), Agilent Technologies, Inc., Palo Alto, CA, www.keysight.com; 2016.
- [11] Gangwar AK, Alam MS. A SSRR based multiband reconfigurable monopole antenna. In: *2016 IEEE student technology symposium (TechSym)*, Kharagpur, India, 2016:208–211.
- [12] Ali MSM, Rahim SKA, Sabran MI, Abedian M, Eteng A, Islam MT. Dual band miniaturized microstrip slot antenna for WLAN applications. *Microwave Opt Technol Lett.* 2016;58:1358–1362.
- [13] Gronwald F, Gluge S, Nitsch J. on network representations of antennas inside resonating environments. *Adv Radio Sci.* 2007;5:157–162.
- [14] Collin RE. *Antennas and Radio Wave Propagation*. Vol. 6, McGraw-Hill, New York, NY, 1985.
- [15] Milligan TA. *Modern Antenna Design*. John Wiley & Sons, Hoboken, NJ; 2005:17–18.

How to cite this article: Gangwar A, Alam MS. A high FoM monopole antenna with asymmetrical L-slots for WiMAX and WLAN applications. *Microw Opt Technol Lett.* 2017;60:196–202. <https://doi.org/10.1002/mop.30941>

Received: 19 June 2017

DOI: 10.1002/mop.30936

A novel miniaturized UWB monopole with five-section stepped-impedance feed line

Muhammad Aziz Ul Haq  |

Slawomir Koziel 

Engineering Optimization & Modeling Center, Reykjavik University, Reykjavik, Iceland

Correspondence

Muhammad Aziz Ul Haq, Engineering Optimization & Modeling Center, Reykjavik University, Reykjavik, Iceland.
Email: muhammadu16@ru.iskoziel@ru.is

Funding information

Icelandic Centre for Research (RANNIS), Grant/Award number: 163299051

Abstract

A structure and design procedure of a compact ultra-wideband (UWB) monopole antenna is proposed. In order to achieve additional size reduction, a modified-shape feed line and a five-section rectangular slit below the feed line is incorporated into a reference antenna featuring a two-section rectangular slit below the feed line and two radiator slots. The minimum-size is obtained by adjustment of all geometry parameters of the structure using rigorous numerical optimization. An explicit constraint on antenna reflection characteristic is imposed in order to ensure sufficient matching in the entire UWB frequency range. The footprint area of the final design is only 167 mm² with antenna dimensions of 22.46 mm × 7.45 mm. Experimental validation confirms good electrical and field properties. Thorough benchmarking indicates that the proposed antenna is competitive to recently reported designs.

KEYWORDS

compact antennas, design optimization, modified feed line, modified ground plane, wideband antennas

1 | INTRODUCTION

Ultra-wideband (UWB) antennas play an important role in wireless communication systems due to their inherent

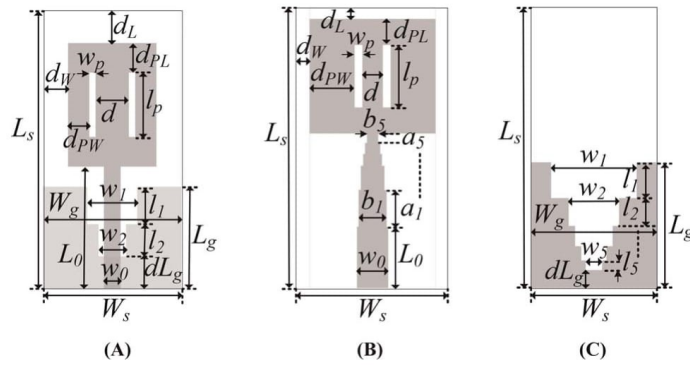


FIGURE 1 Proposed UWB monopole antenna. A, Reference antenna [], B, top layer of the proposed antenna, and C, bottom layer of the proposed antenna



FIGURE 2 Photographs of the fabricated antenna prototype. A, Top layer, and B, bottom layer. [Color figure can be viewed at wileyonlinelibrary.com]

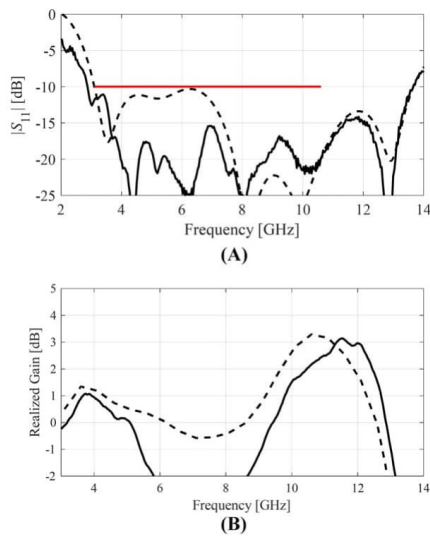


FIGURE 3 Simulated (---) and measured (-) antenna characteristics. A, Reflection response, and B, realized gain. [Color figure can be viewed at wileyonlinelibrary.com]

features such as low cost, omnidirectional radiation patterns, low power consumption, a potential for high data rate transmission, and high efficiency.¹ In UWB systems, small size of antennas is highly recommended or even mandatory due to the compact size of the modern communication devices. Nevertheless, the reduction in size may lead to degradation of the electrical and field properties of the antenna. Consequently, design of compact antennas is a real challenge for researchers. A number of techniques have been proposed in the literature, mostly based on modifications, eg, slits and L-shape stubs,² an inverted T-shape slit,³ slots in the ground plane,⁴ CPW-fed circularly polarized square slot,⁵ protruded ground plane structures,⁶ or tapered feed region.⁷ However, in order to exploit true potential of a novel antenna topology, in particular, to achieve the smallest possible antenna size, simultaneous adjustment of all the antenna parameters is required, which can be realized by means of a rigorous EM-driven design optimization.⁸

In this letter, we consider a novel UWB monopole with a modified-shape feed line and a five-section rectangular slit below the feed line. Simultaneous optimization of all geometry parameters of the antenna leads to a design featuring a small footprint of only 167 mm² and acceptable electrical and field properties.

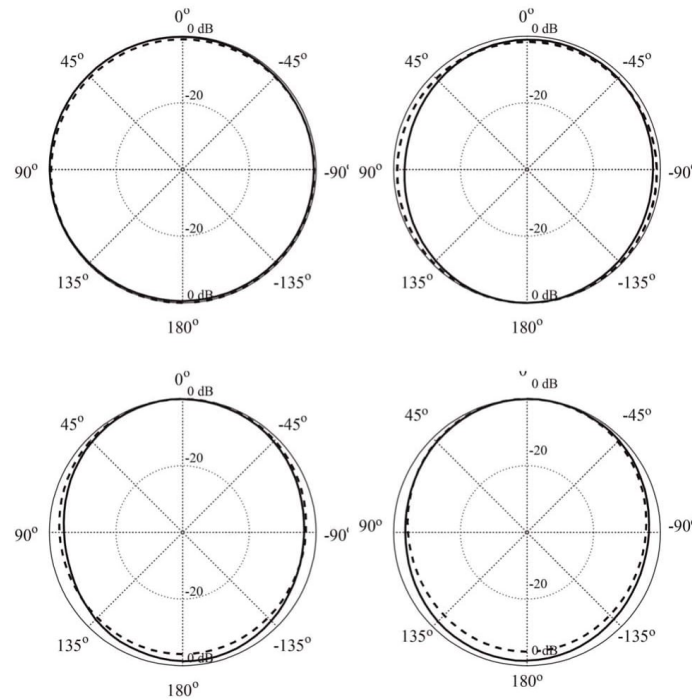


FIGURE 4 Simulated (---) and measured (—) H -plane radiation patterns of the proposed antenna. The plots (from left top to right bottom) are for frequencies 4, 6, 8, and 10 GHz

2 | ANTENNA DESIGN AND OPTIMIZATION

The proposed antenna is a modified version of the design reported by Ojaroudi et al.⁹ with two-section slit below the feed line (cf. Figure 1A), and featuring the footprint area of 216 mm². In this letter, a modified-shape feed line and a five-section rectangular slit below the feed is incorporated to increase the number of degrees of freedom for antenna miniaturization as shown in Figure 1B,C. The structure is realized on 1.5 mm-thick FR-4 substrate with $\epsilon_r = 4.4$. The reference antenna is described using the following vector of geometry parameters $x = [L_0 \ l_p \ w_p \ d \ d_L \ d_{PL} \ d_{PW} \ d_W \ l_1 \ w_1 \ l_2 \ w_2 \ dL_g]^T$ (all dimensions in mm). Upon applying an additional modification in the feed line and ground plane as shown in Figure 1B,C, the parametric vector extended as $x = [L_0 \ l_p \ w_p \ d \ d_L \ d_{PL} \ d_{PW} \ d_W \ l_1 \ w_1 \ l_2 \ w_2 \ l_3 \ w_3 \ l_4 \ w_4 \ l_5 \ w_5 \ dL_g \ a_1 \ b_1 \ a_2 \ b_2 \ a_3 \ b_3 \ a_4 \ b_4 \ a_5 \ b_5]^T$. For the sake of design optimization, a computational model is implemented in CST Microwave Studio¹⁰ and evaluated using its time-domain solver. The model

includes the SMA connector in order to improve the agreement between simulation and measurement results of the antenna prototype.

The antenna of Figure 1B,C has been optimized for minimum size using the pattern search algorithm.¹¹ The design constraint was imposed on the reflection response so as to ensure that the reflection is not higher than -10 dB in the entire UWB frequency range. The optimized parametric vector of the reference antenna is $x^{*1} = [11.36 \ 6.02 \ 0.75 \ 2.00 \ 0.00 \ 2.75 \ 2.55 \ 0.00 \ 3.50 \ 4.00 \ 1.39 \ 0.09 \ 2.59]^T$. The optimized values for the proposed structure are $x^{*2} = [5.13 \ 5.25 \ 0.18 \ 1.30 \ 0.04 \ 2.19 \ 2.88 \ 0.00 \ 4.03 \ 5.44 \ 2.34 \ 1.34 \ 1.28 \ 1.41 \ 0.44 \ 0.81 \ 0.25 \ 0.22 \ 1.50 \ 3.09 \ 1.78 \ 2.02 \ 1.52 \ 0.99 \ 1.19 \ 0.91 \ 0.97 \ 0.60 \ 0.72]^T$. The antenna footprint exhibits only 167 mm², which is 15% smaller than the reference antenna. It should be emphasized that the corresponding dimensions in x^{*1} and x^{*2} are clearly different which is a clear indication that smaller size was not achieved merely by introducing the feed line modifications but also by simultaneous adjustment of all antenna parameters.

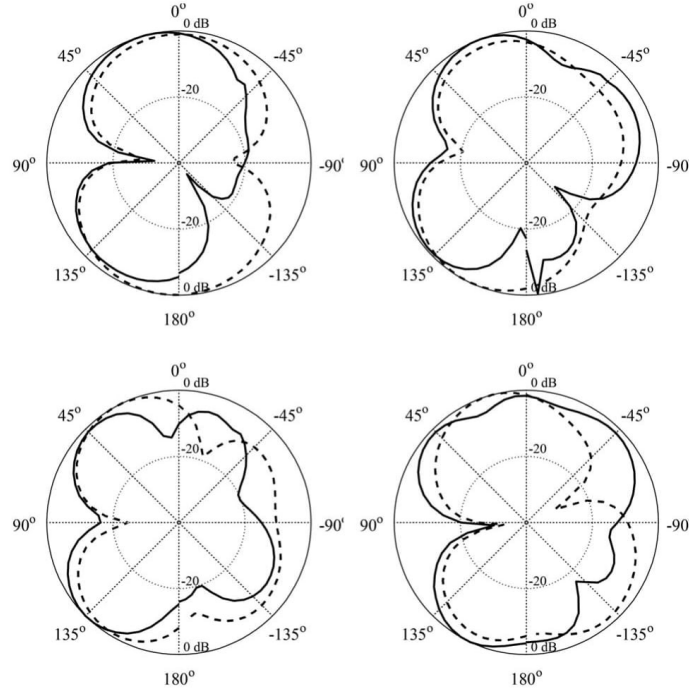


FIGURE 5 Simulated (---) and measured (—) E -plane radiation patterns of the proposed antenna. The plots (from left top to right bottom) are for frequencies 4, 6, 8, and 10 GHz

3 | RESULTS AND DISCUSSION

Figure 2 shows the photograph of the fabricated antenna prototype. The simulation and measurement results have been shown in Figures 3–6. Figure 3A shows the reflection response and realized gain of the proposed UWB antenna. It is observed that the measured reflection response is well under -10 dB for the entire UWB frequency range. Similarly, the measured realized gain (cf. Figure 3B) also demonstrates a good agreement with the simulations. Figures 4 and 5 show the radiation patterns of the proposed antenna that exhibits the omnidirectional characteristics. Misalignments between simulations and measurements (mostly in the E -plane) are due to the shadowing effects of the measurement setup.

In order to verify the radiation pattern stability of the proposed antenna, a pattern stability factor (PSF) has been evaluated following the work by Koziel.¹² The PSF is calculated as

$$\text{PSF} = \frac{\int_{\Omega} C(\vec{R}) ds}{\int_{\Omega} ds} \quad (1)$$

with Ω being the range of operating directions (here, corresponding to the H -plane), and $C(\vec{R})$ being the frequency-domain correlation pattern $C(\vec{R}) = \int_{\Omega} F^2(\vec{R}, \vec{r}) ds / \int_{\Omega} ds$, with $F^2(\vec{R}, \vec{r}) = |\int_{\text{BW}} E(\vec{r}, f) E^*(\vec{R}, f) df| / [\int_{\text{BW}} |E(\vec{r}, f)|^2 df \int_{\text{BW}} |E(\vec{R}, f)|^2 df]$. In the above equations, $E(\vec{r}, f)$ is the far-field electric field in direction \vec{r} , \vec{R} is a reference direction; the symbol * stands for complex conjugate. The PSF of our antenna is 0.94.

In order to evaluate time-domain properties of the antenna, the pulse fidelity factor (PFF) has been evaluated which essentially describes time-domain correlations between the input and transmitted electric field waveforms (cf. Ref. [12]). The PFF values for the H -plane (azimuth angles of $0^\circ, 30^\circ, \dots, 330^\circ$) are 0.88, 0.89, 0.90, 0.87, 0.88, 0.90, 0.90, 0.90, 0.88, 0.87, 0.90, and 0.89, respectively. Normalized input/output electric field waveforms for selected azimuth angles have been shown in Figure 6.

4 | COMPARISON OF PROPOSED ANTENNA SPECIFICATIONS

Table 1 shows the comparison between the proposed and recently reported UWB monopole antennas in the

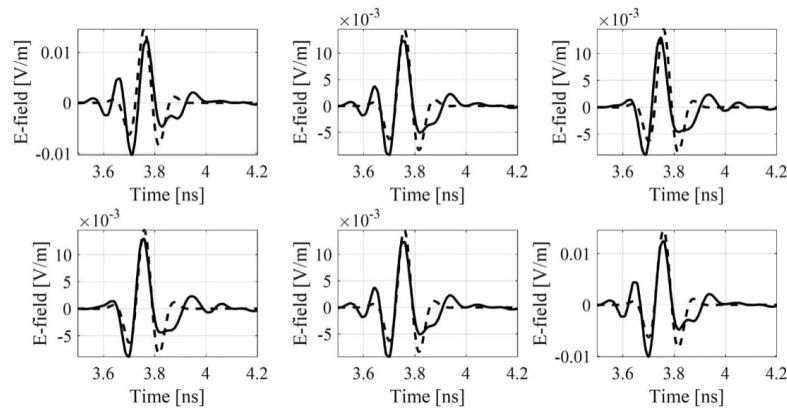


FIGURE 6 (Normalized) electric field waveforms for the proposed antenna in the H -plane for the azimuth angles of 60° , 180° , and 300° . Shifted version of the input waveform ($- -$) $e(t - \tau)$ is shown that maximizes the convolution integral $\int v(t)e(t - \tau)dt$ (cf. Ref. [12]) with the output waveform ($-$)

TABLE 1 Benchmarking: comparison of footprint areas and electrical performance parameters for recently reported of UWB antenna designs

Refs.	Size mm \times mm	Operational bandwidth (GHz)	Antenna footprint (λ_g^2) ^a	Realized gain range (dB)
[9]	18 \times 12	3.12–12.73	0.29	N/A
[13]	20 \times 16	4.8–14.5	0.43	1.9–4.4
[14]	24 \times 22	3.1–11	0.36	–1 to 4
[15]	22 \times 15.8	3.1–10.6	0.26	N/A
[16]	28 \times 20	2.85–11.85	0.54	–0.8 to 3.2
[17]	24 \times 16	3.1–10.9	0.50	0–5
[18]	25 \times 25	3.6–11	0.83	1.8–7
This work	22.46 \times 7.45	3.1–13.65	0.22	–2 to 3

^a λ_g denotes the antenna footprint in terms of the guided wavelength.

literature.^{9,13–18} The antenna footprint was expressed in the form of guided wavelength to ensure the fair comparison between different substrate properties. The guided wavelength was defined by 50- Ω line impedance operating at 6 GHz. The benchmarking provided in Table 1 indicates that that the antenna structure proposed in this letter offers a high bandwidth and smaller size as compared to other designs.

5 | CONCLUSION

In this letter, a novel design of UWB monopole antenna has been proposed. By incorporating a multi-section below the feed line and stepped-impedance feed line with rigorous adjustment of all geometry parameters of the antenna

through constrained optimization, the design featuring a footprint area of only 167 mm² has been obtained. The assumed optimization task formulation ensures achieving minimum size while maintaining required maximum in-band reflection level (here ≤ -10 dB). Experimental verification indicates good electrical and field properties of the proposed structure, in particular acceptable level of pattern stability as well as omnidirectional radiation pattern.

ACKNOWLEDGMENTS

The authors thank Computer Simulation Technology AG, Darmstadt, Germany, for making CST Microwave Studio Available. This work has been partially supported by the Icelandic Centre for Research (RANNIS) Grant 163299051.

ORCID

Muhammad Aziz Ul Haq  <http://orcid.org/0000-0003-3380-4745>

Slawomir Koziel  <http://orcid.org/0000-0002-9063-2647>

REFERENCES

- [1] Vendik IB, Rusakov A, Kanjanasit K, Hong J, Filonov D. Ultra-wideband (UWB) planar antenna with single-, dual-, and triple-band notched characteristic based on electric ring resonator. *IEEE Antennas Wireless Propag Lett.* 2017;16:1600–1597.
- [2] Bekasiewicz A, Koziel S. Compact UWB monopole antenna for internet of things applications. *Electron Lett.* 2016;52(7):492–494.
- [3] Mohammadi B, Valizade A, Rezaei P, Nourinia J. New design of compact dual band-notch ultra-wideband band pass filter based on coupled wave canceller inverted T-shaped stubs. *IET Microwave Antennas Propag.* 2015;9(1):64–72.
- [4] Yang N, Leung K, Lu K, Wu N. Omnidirectional circularly polarized dielectric resonator antenna with logarithmic spiral slots in the ground. *IEEE Trans Antenna Propag.* 2017;56(2):839–844.
- [5] Shokri M, Rafii V, Karamzadeh S, Amiri Z, Virdee B. Miniaturised ultra-wideband circularly polarised antenna with modified ground plane. *Electron Lett.* 2014;50(24):1786–1788.
- [6] Li J, Chu Q, Li Z, Xia X. Compact dual band-notched UWB MIMO antenna with high isolation. *IEEE Trans Antenna Propag.* 2013;61(9):4759–4766.
- [7] Manohar M, Kshetrimayum RS, Gogoi AK. Printed monopole antenna with tapered feed line, feed region and patch for super wideband applications. *IET Microwave Antennas Propag.* 2014;8(1):39–45. Iss.pp
- [8] Koziel S, Bekasiewicz A. Multi-objective design of antennas using surrogate models. *World Sci.* 2016.
- [9] Ojaroudi M, Ghobadi C, Nourinia J. Small square monopole antenna with inverted T-shaped notch in the ground plane for UWB application. *IEEE Antennas Wireless Propag Lett.* 2009;8:728–731.
- [10] CST Microwave Studio, ver. 2015. CST AG, Bad Nauheimer Str. 19, D-64289 Darmstadt, Germany, 2015.
- [11] Liu J, Esselle KP, Hay SG, Zhong S. Effects of printed UWB antenna miniaturization on pulse fidelity and pattern stability. *IEEE Trans Antenna Propag.* 2014;62(8):3903–3910.
- [12] Koziel S. Computationally efficient multi-fidelity multi-grid design optimization of microwave structures. *Appl Comput Electromagn Soc J.* 2010;25(7):578–586.
- [13] Shakib M, Moghavvemi NM, Mahadi WNL. Design of a compact planar antenna for ultra-wideband operation. *Appl Comput Electromagn Soc J.* 2015;20(2):222–229.
- [14] Orazi H, Soleiman H. Miniaturisation of UWB triangular slot antenna by the use of DRAF. *IET Microwave Antennas Propag.* 2017;11(4):450–456.
- [15] Bekasiewicz A, Koziel S. Structure and computationally-efficient simulation-driven design of compact UWB monopole antenna. *IEEE Antennas Wireless Propag Lett.* 2015;14:1282–1285.
- [16] Nikolaou S, Abbasi MAB. Design and development of a compact UWB monopole antenna with easily-controllable return loss. *IEEE Trans Antenna Propag.* 2017;65(4):2063–2067.
- [17] Alsath MGN, Kanagasabai M. Compact UWB monopole antenna for automotive communication. *IEEE Trans Antenna Propag.* 2015;63(9):4204–4208.
- [18] Ellis MS, Zhao Z, Wu J, Nie Z, Liu QH. Small planar monopole ultra-wideband antenna with reduced ground plane effect. *IET Microwave Antennas Propag.* 2015;9(10):1028–1034.

How to cite this article: Ul Haq MA, Koziel S. A novel miniaturized UWB monopole with five-section stepped-impedance feed line. *Microw Opt Technol Lett.* 2017;60:202–207. <https://doi.org/10.1002/mop.30936>

Received: 19 June 2017

DOI: 10.1002/mop.30945

Design of balanced power divider with wide common-mode suppression band

Ching-Her Lee¹  | Chung-I G. Hsu² | Wen-Xuan Chen¹

¹Graduate Institute of Communications Engineering, National Changhua University of Education, 1 Jin-De Road, Changhua, Taiwan 500, Republic of China

²Department of Electrical Engineering, National Yunlin University of Science and Technology, 123 University Road, Section 3, Douliou, Yunlin, Taiwan 640, Republic of China

Correspondence

Ching-Her Lee, Graduate Institute of Communications Engineering, National Changhua University of Education, 1 Jin-De Road, Changhua, Taiwan 500, Republic of China.
Email: iecher@cc.ncue.edu.tw

Funding information

Ministry of Science and Technology, Taiwan, Grant Number: MOST 105-2221-E-018-004

Abstract

In this paper, a balanced power divider (PD) is designed and implemented in a three-layer configuration. It consists of two tightly stacked microstrip Wilkinson PDs with a shared ground plane in the middle layer. With both dumbbell-shaped and partially interdigital open-ended slots embedded in the common ground, the designed balanced PD can yield a high common-mode (CM) suppression level over a very wide frequency band without

Chapter 4

4 Paper [J3]

Muhammad Aziz ul Haq, and Slawomir Koziel

Simulation-Based Optimization for Rigorous Assessment of Ground Plane Modifications in Compact UWB Antenna Design

Published: International Journal of RF and Microwave Computer-Aided Engineering

DOI: <https://doi.org/10.1002/mmce.21204>

Simulation-based optimization for rigorous assessment of ground plane modifications in compact UWB antenna design

Muhammad Aziz Ul Haq  | Slawomir Koziel 

Engineering Optimization and Modeling Center, Reykjavik University, Reykjavik, Iceland

Correspondence
Muhammad Aziz Ul Haq, Engineering Optimization and Modeling Center, Reykjavik University, Reykjavik, Iceland.
Email: muhammadu16@ru.is, koziel@ru.is

Funding information
Icelandic Centre for Research (RANNIS) Grant, Grant Number: 163299051

Abstract

Introducing ground plane modifications is a popular approach in the design of compact UWB antennas. Yet, specific topological alterations are normally reported on case to case basis without thorough investigations concerning their general suitability for antenna miniaturization. In particular, detailed performance comparison of different ground plane modifications is lacking in the literature. In this article, the effect of selected ground plane modifications on achievable miniaturization rate is considered based on a set of four UWB antennas. EM-driven optimization is carried out to minimize the antenna footprints while maintaining acceptable matching within the UWB frequency range. In each case, all geometry parameters of the respective structures are utilized in the design process. For the sake of fair comparison, all antennas are implemented on the same dielectric substrate. Our results indicate a clear performance pattern, here, an advantage of the elliptical ground plane slit below the feed line over the rectangular one (average size reduction ratio of 26% versus 19% across the benchmark set). Our conjectures are confirmed by physical measurements of the fabricated antenna prototypes.

KEYWORDS

antenna miniaturization, design optimization, EM-driven design, ground plane modifications, ultra-wideband (UWB) antennas

1 | INTRODUCTION

Ultra-wideband antennas play an important role in wireless communication systems due to their inherent features such as compact size, omnidirectional radiation pattern, high data rate, low power consumption and high efficiency.¹ Small size of UWB antennas is critical for many space-limited applications, including wearable devices,² internet of things (IoT),³ and medical imaging.⁴ Unfortunately, size reduction directly affects antenna electrical properties due to disturbance of the current path, leading to a violation of acceptable reflection level. Furthermore, miniaturization may affect field properties such as gain or radiation pattern stability.⁵ Working around these limitations, in particular, achieving small size while satisfying stringent electrical performance requirement becomes a serious challenge for antenna engineers.

There has been considerable research effort observed over the recent years focused on novel designs of compact UWB antennas.^{6–12} Typically, various geometrical modifications of conventional topologies (monopoles, uniplanar antennas, slot antennas) are proposed, involving ground plane and/or radiator modifications. Popular approaches include radiator slots,⁵ slits below the feed line,⁶ L-/I-shape ground plane stubs,^{3,7–9} introduction of a dielectric resonator within the ground plane,¹⁰ or a CPW square slot at the ground plane.¹¹ It should be emphasized that the designs reported in the literature are almost exclusively case studies oriented towards specific application areas.^{13–16} There have been no systematic studies undertaken so far concerning general suitability of particular topology modifications in the context of antenna miniaturization.

Another issue pertinent to the design of miniaturized UWB antennas is adjustment of geometry parameters. In a

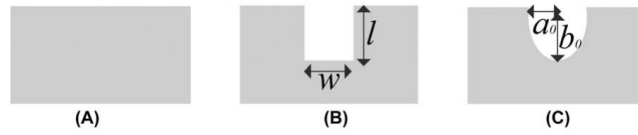


FIGURE 1 Ground plane modifications considered in this work: A, flat ground (reference), B, rectangular slit, C, elliptical slit. Both slits are parameterized using two geometry parameters

vast majority of cases, compact size is a result of applied geometry modifications with antenna footprint rarely optimized explicitly. Instead, dimension sizing is typically oriented towards ensuring acceptable electrical performance and realized through experience-driven parameter sweeping. In order to obtain a truly optimum design, simultaneous adjustment of all antenna parameters using rigorous numerical optimization routines is recommended.¹⁷ Furthermore, for the sake of evaluation reliability, computational models utilized in the design process should incorporate environmental components such as connectors. A large variety of optimization algorithms have been utilized and proposed for antenna design, including local search methods (both gradient-based,^{17–19} and derivative-free^{20–25}) as well as global algorithms, mostly population-based metaheuristics (genetic algorithms,²⁶ particle swarm optimizers,²⁷ differential evolution,²⁸ etc.). Recently, surrogate-based optimization methods have been applied for computationally-efficient optimization of antenna structures,²⁹ including compact antennas.³⁰

The purpose of this paper is to investigate the effect of a particular type of defected ground structure (here, in the form of a slit below the feed line) on achievable miniaturization rate of UWB antennas. We consider two types of slits, a rectangular and an elliptical one. In order to ensure conclusive results, rigorous EM-driven optimization is carried out over a set of representative UWB monopole antennas to determine size reduction that can be achieved. The design optimization process is constrained to maintain the maximum in-band reflection at the acceptable level of -10 dB. The obtained

results clearly indicate advantage of the elliptical slit over the rectangular one with the average miniaturization rate of 26% versus 19% for the rectangular slit. At the same time, the improved size reduction ratio was obtained without compromising electrical or field properties of the respective antennas. Experimental verification of the fabricated antenna prototypes is also provided and confirms correctness of the numerical data.

The remaining part of the paper is organized as follows. Section 2 introduces the considered ground plane modifications as well as benchmark antenna structures. Design optimization approach is described in Section 2.1. Numerical results and experimental validation are provided in Sections 4 and 5, respectively. Section 4 concludes the paper.

2 | TOPOLOGICAL MODIFICATIONS AND BENCHMARK ANTENNA STRUCTURES

In this section, we first describe topological modifications (here, pertinent to the ground plane) considered in our study, then introduce four antenna structures utilized as a benchmark set.

2.1 | Ground plane modifications for antenna miniaturization studies

In this work, for the sake of illustration of the comparison and assessment strategy utilized in this study, we consider

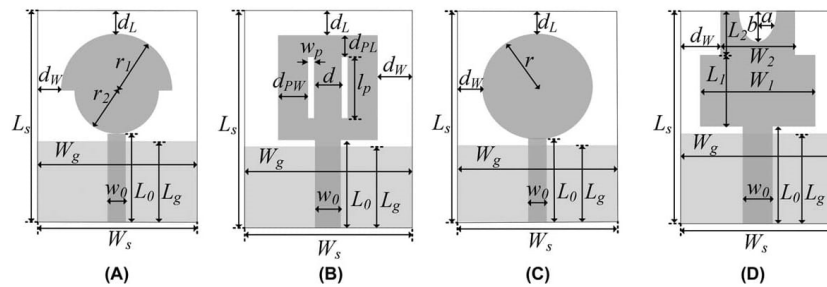


FIGURE 2 Benchmark set of four UWB monopole antennas: A, Antenna I [25], B, Antenna II,²⁶ C, Antenna III,²⁷ and D, Antenna IV.²⁸ Ground plane marked using a lighter shade of gray

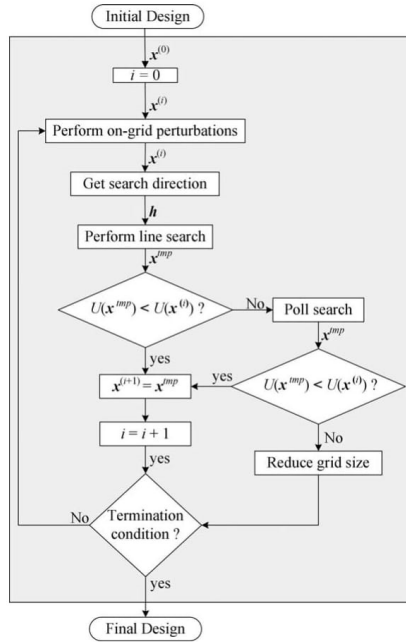


FIGURE 3 A flowchart of the pattern search optimization procedure. The symbol U denotes the objective function optimized by the algorithm. The termination condition is based on convergence in argument as well as on the minimum grid size (both user-defined)

two types of ground plane modifications, both in the form of slits below the feeding line as shown in Figure 1. The objective is to determine which modification may lead to a higher miniaturization rate of the antenna structure it is applied to.

2.2 | Benchmark antennas

As a benchmark set, we utilize four UWB monopole antennas recently reported in the literature^{31–34} and shown in

TABLE 1 Optimized sizes of antennas I-IV

Antenna	Ground plane modification					
	Reference (flat ground)		Rectangular		Elliptical	
	Size (mm ²)	Reduction ratio (%) ^a	Size (mm ²)	Reduction ratio (%) ^a	Size (mm ²)	Reduction ratio (%) ^a
I	802	-	617	23.1	571	28.8
II	264	-	241	7.9	235	11.0
III	875	-	469	46.4	356	59.3
IV	281	-	276	1.8	265	5.7

^aSize reduction ratio with respect to the antenna with the flat ground plane.

Figure 2. All structures are realized on 1.55-mm thick FR-4 substrate ($\epsilon_r = 4.4$). Computational models of the structures are implemented in CST Microwave Studio.³⁵ For the sake of design optimization, all geometry parameters of the antennas are adjustable. Design variable vectors for Antennas I-IV are as follows: $\mathbf{x}_1 = [L_g, L_0, r_1, r_2, d_w]^T$, $\mathbf{x}_2 = [L_g, L_0, L_P, W_P, d, d_L, d_{PL}, d_{PW}]^T$, $\mathbf{x}_3 = [L_g, L_0, d_w, r]^T$, and $\mathbf{x}_4 = [L_g, L_0, L_1, L_2, W_1, W_2, d_w, a, b]^T$ (all dimensions in mm). Upon applying a particular ground plane modifications, the respective vectors are extended by the slit parameters. The initial values of geometry parameters are based on the literature: $\mathbf{x}_1^{(0)} = [14, 14, 0.9, 11, 6.4]^T$, $\mathbf{x}_2^{(0)} = [4.4, 7.8, 9.8, 0.24, 3.9, 5, 2.84, 3.6]^T$, $\mathbf{x}_3^{(0)} = [13, 14.24, 5.32, 8.9]^T$, and $\mathbf{x}_4^{(0)} = [3.8, 5.8, 12.8, 7.6, 15.7, 9.7, 4.4, 0.9, 0.1]^T$. The EM models are equipped with the SMA connectors in order to permit reliable experimental validation of the optimized designs. The antennas are supposed to operate in the standard UWB frequency range (3.1 GHz to 10.6 GHz).

3 | DESIGN OPTIMIZATION APPROACH

The objective is to find the minimum-footprint antenna that satisfies the condition $S(\mathbf{x}) \leq -10$ dB, where $S(\mathbf{x})$ is the maximum reflection in the UWB band (from 3.1 GHz to 10.6 GHz) and \mathbf{x} stands for adjustable geometry parameters of the structure at hand (cf. Section 2). The antenna size will be denoted as $A(\mathbf{x})$. The design problem is therefore formulated as

$$\mathbf{x}^* = \arg \min_{\mathbf{x}} \{A(\mathbf{x})\}, \quad S(\mathbf{x}) \leq -10 \text{ dB} \quad (1)$$

Here, a pattern search algorithm²⁰ is utilized to solve (1), starting from the design obtained by minimizing $S(\mathbf{x})$ (to ensure a feasible initial point).

A pattern search implementation utilized here²⁴ is a derivative-free stencil-based search routine where grid-restricted line search (with search direction obtained from objective function gradient estimated using on-grid

TABLE 2 Optimized dimensions of antennas I-IV

Antenna	Ground plane modification	Geometry parameters (mm)										
Antenna I		L_g	L_0	r_1	r_2	d_w	G_1	G_2				
	Flat ground	13.8	14.4	0.7	9.1	3.9	-	-				
	Rectangular slit	13.9	14.5	0.6	8.8	1.4	2.7	3.3				
	Elliptical slit	13.6	15.1	0.6	8	1.9	6.8	1.4				
Antenna II		L_g	L_0	L_p	W_p	d	d_L	d_{PL}	d_{PW}	d_w	G_1	G_2
	Flat ground	4.4	7.7	9.7	0.2	3.2	0.9	2.8	3.6	0	-	-
	Rectangular slit	10.2	8.6	9.8	0.2	2.9	0	2.4	3	0.3	1.8	2.3
	Elliptical slit	5.5	9	8.5	0.4	2.6	0.5	2.4	3.3	0	3	1.1
Antenna III		L_g	L_0	d_w	r	G_1	G_2					
	Flat ground	12.9	14	4.7	8.9	-	-					
	Rectangular slit	14.5	16.8	2.8	5.5	3.9	4.1					
	Elliptical slit	13.3	16.8	1	5.4	6.3	2.6					
Antenna IV		L_g	L_0	L_1	L_2	W_1	W_2	d_w	a	b	G_1	G_2
	Flat ground	4.3	7.6	10.3	6.4	11.5	7.4	2	0.1	0.1	-	-
	Rectangular slit	4.5	8	11.9	4.2	9.5	7.1	2.1	0.1	0.1	1	3.4
	Elliptical slit	5.5	9	11.7	3.2	9.4	7.9	1.5	0.4	0.1	1.9	1.3

G_1 stands for w for rectangular slit and b_0 for elliptical slit; G_2 stands for l for rectangular slit and a_0 for elliptical slit.

perturbations) is interleaved with poll-type search and grid refinement (in case of the failure of the neighbor search).

Optimization for minimum reflection is arranged differently, namely, we utilize a trust-region (TR)³⁶ gradient

search algorithm with the antenna response Jacobians estimated through finite differentiation. TR-embedded gradient-based routine is generally faster, however, it is not suitable for handling explicit constraints (as in (1)). Practical

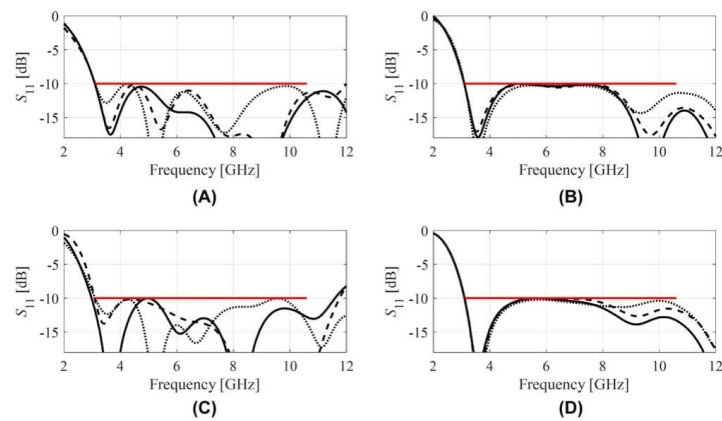


FIGURE 4 Reflection responses of size-optimized antennas with flat ground (···), rectangular slit (- - -), and elliptical slit (—): A, Antenna I, B, Antenna II, C, Antenna III, and D, Antenna IV

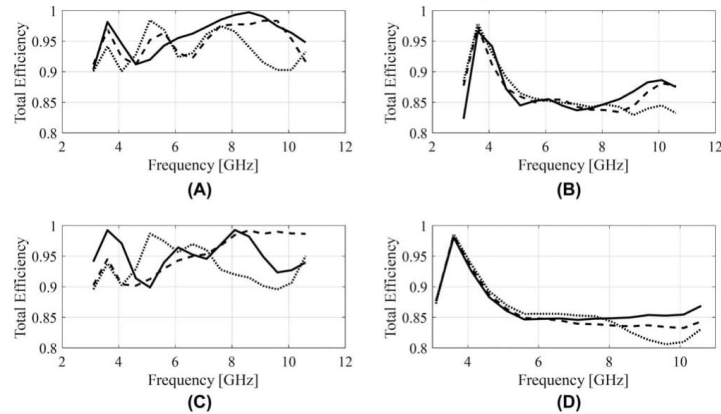


FIGURE 5 Total efficiency of size-optimized antennas with flat ground (···), rectangular slit (---), and elliptical slit (—): A, Antenna I, B, Antenna II, C, Antenna III, and D, Antenna IV

computational complexity of both pattern search and gradient-based routine (the latter is used here with numerical derivatives) is more or less quadratic with respect to the design space dimension, meaning that the number of EM simulations required for algorithm convergence is typically between a few dozen to two hundred depending on a particular antenna structure within the benchmark set. A flowchart of the pattern search algorithm has been shown in Figure 3.

4 | NUMERICAL RESULTS

The antenna structures of Figure 2 have been optimized for minimum reflection, and, subsequently, for minimum size.

For each antenna, three cases of the ground plane were considered as shown in Figure 1, that is, the flat ground (no modifications), rectangular slit (Figure 1b), and elliptical slit (Figure 1c). The results have been shown in Table 1 (footprint areas) and Table 2 (detailed structure dimensions). The miniaturization rate has been computed with respect to the reference case (flat ground plane). It can be observed that utilization of the elliptical slit allows for consistently higher size reduction ratio than the rectangular one. The average (across the considered antenna set) miniaturization ratio is 26% for elliptical slit versus 19% for the rectangular one. However, comparison of the absolute values of the antenna footprints is even more meaningful: in case of Antenna I, elliptical slit permits additional reduction of the antenna size

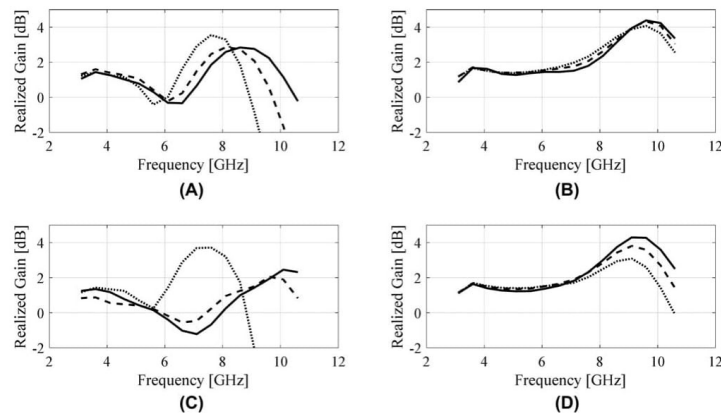


FIGURE 6 Realized gain of size-optimized antennas with flat ground (···), rectangular slit (---), and elliptical slit (—): A, Antenna I, B, Antenna II, C, Antenna III, and D, Antenna IV

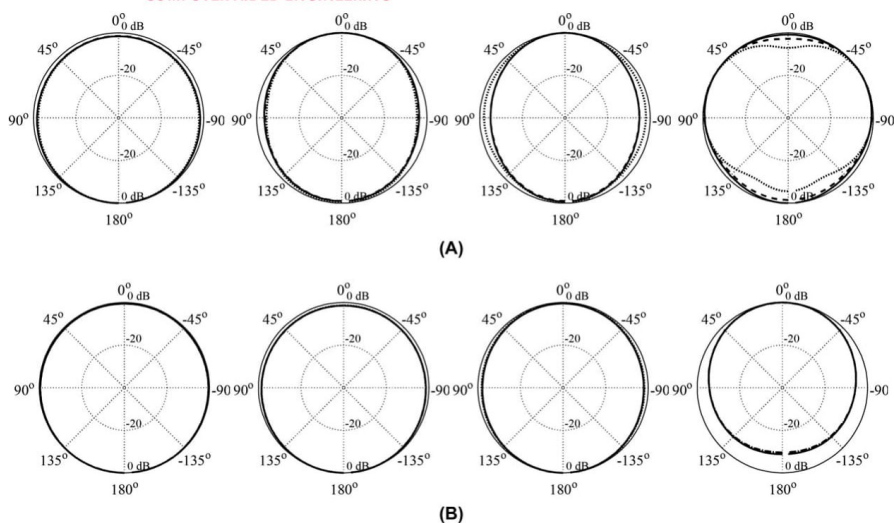


FIGURE 7 H-plane patterns of antennas with flat ground (···), rectangular slit (---), and elliptical slit (—): A, Antenna I, B, Antenna II. The plots (from left to right) are for frequencies 4 GHz, 6 GHz, 8 GHz, and 10 GHz

by 46 mm^2 (compared to rectangular slit), whereas for Antenna III, the difference is 113 mm^2 . In general, the results allow us to conclude that the elliptical slit is a better ground plane modification in the context of antenna miniaturization.

Figures 4–10 show a comparison of reflection, total efficiency, gain, and radiation patterns for the considered

antennas. The first observation is that—in all cases—the maximum in-band reflection is almost exactly at -10 dB , which means that the obtained designs indeed represent optimum antenna dimensions (further size reduction would lead to violating the -10 dB threshold for the reflection response). Thus, the optimization process has been

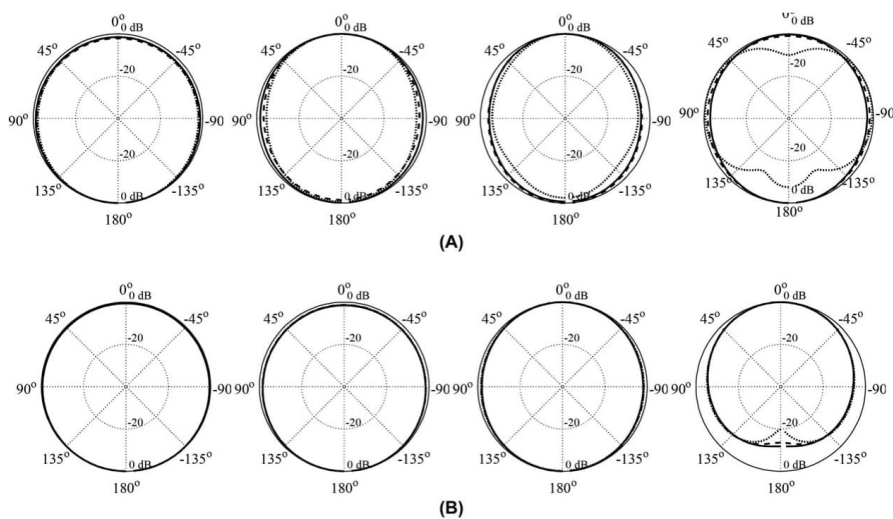


FIGURE 8 H-plane patterns of antennas with flat ground (···), rectangular slit (---), and elliptical slit (—): A, Antenna III, B, Antenna IV. The plots (from left to right) are for frequencies 4 GHz, 6 GHz, 8 GHz, and 10 GHz

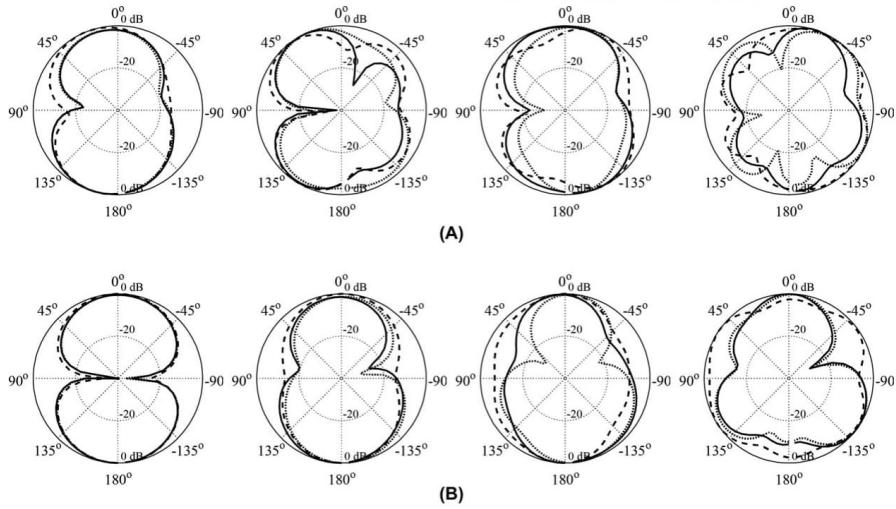


FIGURE 9 E-plane patterns of antennas with flat ground (····), rectangular slit (---), and elliptical slit (—): A, Antenna I, B, Antenna II. The plots (from left to right) are for frequencies 4 GHz, 6 GHz, 8 GHz, and 10 GHz

accomplished successfully. Consequently, the comparison of the antenna structures is fair and meaningful.

In terms of both electrical and field properties, the structures utilizing either rectangular or elliptical slits are very similar. This observation applies to reflection characteristics, efficiency, gain, but also radiation patterns, particularly in

the H-plane. This means that the additional size reduction due to a particular slit (here, elliptical) is not achieved at the expense of antenna performance degradation. The differences are more noticeable for the reference antennas (with unmodified ground plane) and the structures with either of the slits. This is particularly the case for Antennas I and III, where

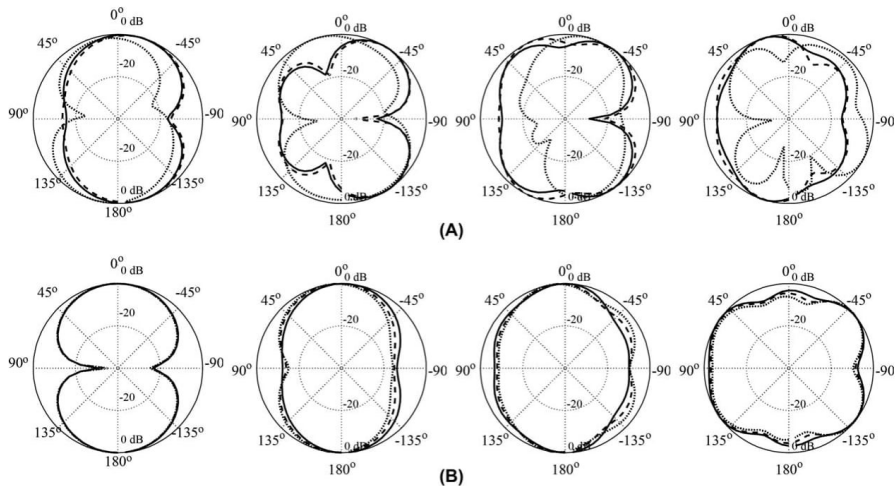


FIGURE 10 E-plane patterns of antennas with flat ground (····), rectangular slit (---), and elliptical slit (—): A, Antenna III, B, Antenna IV. The plots (from left to right) are for frequencies 4 GHz, 6 GHz, 8 GHz, and 10 GHz

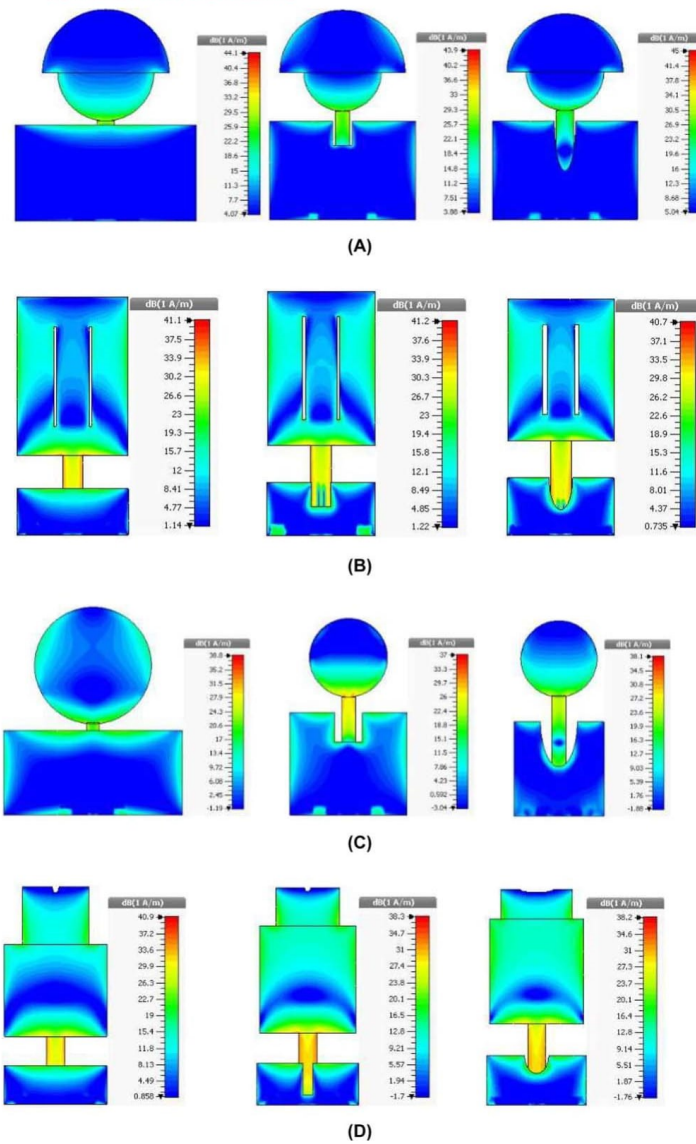


FIGURE 11 Current distributions of the optimized UWB antennas at 8 GHz. The plots from the left to right are for the flat ground, rectangular slit, and elliptical slit, respectively: A, Antenna I, B, Antenna II, C, Antenna III, and D, Antenna IV

application of ground plane modifications results in dramatic reduction of the structure size. For other antennas, the differences are minor.

It should be noticed that all antennas exhibit good efficiency. Average efficiencies for Antennas I through IV are

0.95, 0.87, 0.95, and 0.86 (rectangular slit), and 0.96, 0.87, 0.95, and 0.87 (elliptical slit), despite the fact that all structures are implemented on FR-4 substrate ($\tan\delta = 0.02$).

Gain characteristics are also very similar for structures with rectangular and elliptical slits. Radiation characteristics

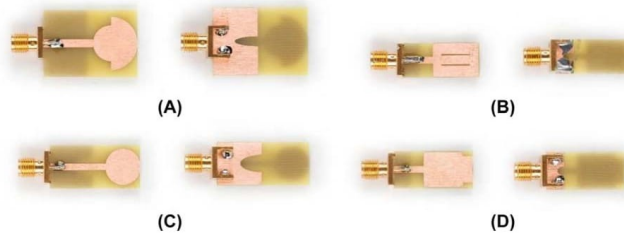


FIGURE 12 Photographs of fabricated antenna prototypes (with elliptical slit): A, Antenna I, B, Antenna II, C, Antenna III, and D, Antenna IV

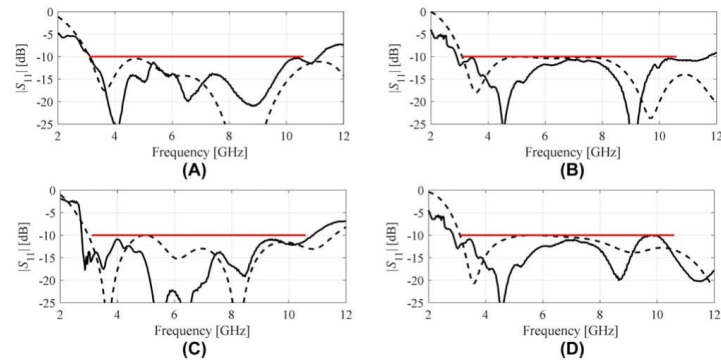


FIGURE 13 Simulated (---) and measured (—) reflection responses: A, Antenna I, B, Antenna II, C, Antenna III, and D, Antenna IV

shown in Figures 7–10 indicate that all antennas are omnidirectional in the H-plane for the entire UWB frequency range and the characteristics are close to each other for both considered ground plane modifications. In case of the E-plane, the differences are more pronounced in some cases (e.g., Antennas I and II). Furthermore, miniaturization using

ground plane modifications generally leads to improvement of the omnidirectional character of the patterns, particularly at higher frequencies. Figure 11 shows the simulated electric current distribution for all considered antenna structures at 8 GHz. It can be observed that some amount of current is present on the flat ground plane of all antennas. As a result,

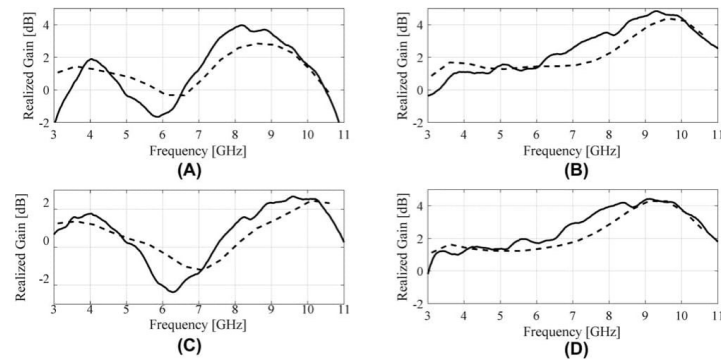


FIGURE 14 Simulated (---) and measured (—) realized gain characteristics: A, Antenna I, B, Antenna II, C, Antenna III, and D, Antenna IV

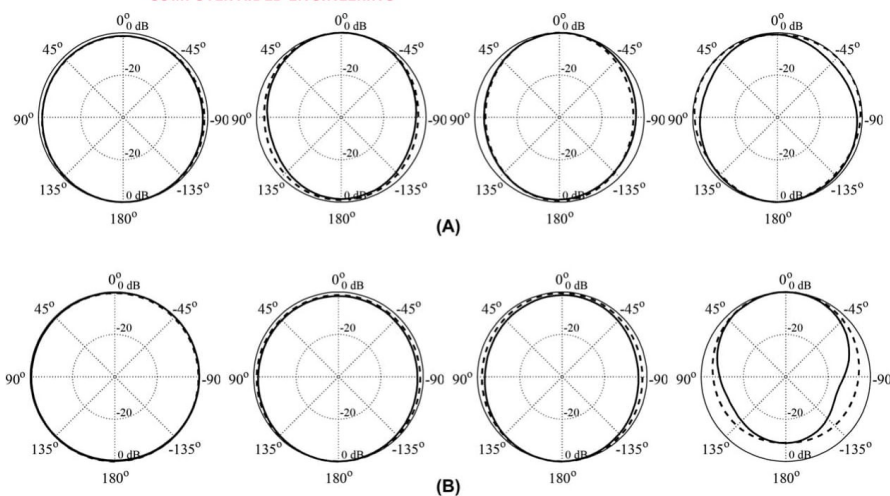


FIGURE 15 Simulated (---) and measured (—) H-plane radiation patterns: A, Antenna I and B, Antenna II. The plots (from left to right) are for frequencies 4 GHz, 6 GHz, 8 GHz, and 10 GHz

the ground plane also acts as a radiator and any change in the dimensions of the ground plane directly effects the electrical properties of antennas. In order to shift the amount of current from ground plane to radiator, a rectangular and elliptical slits are introduced just below the feed line. It is clear from the figure that introduction of both slits is responsible

for diverting the current towards the radiator which results in improvement of the antenna impedance. This creates a room to further reduction of antenna dimensions while maintaining acceptable electrical performance. Here, the elliptical slit turns to be more efficient in diverting current from the ground plane to the radiator; consequently, a higher

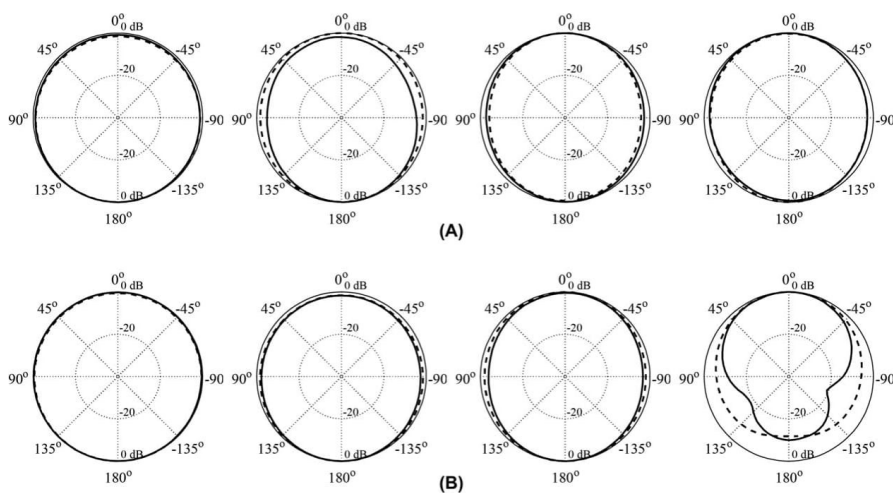


FIGURE 16 Simulated (---) and measured (—) H-plane radiation patterns: A, Antenna III and B, Antenna IV. The plots (from left to right) are for frequencies 4 GHz, 6 GHz, 8 GHz, and 10 GHz

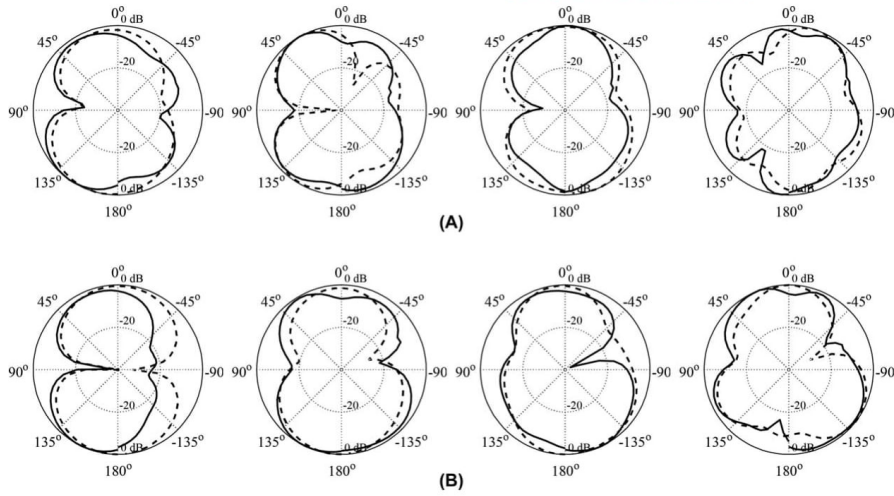


FIGURE 17 Simulated (---) and measured (—) E-plane radiation patterns: A, Antenna I and B, Antenna II. The plots (from left to right) are for frequencies 4 GHz, 6 GHz, 8 GHz, and 10 GHz

miniaturization rate can be achieved as compared to the rectangular slit.

5 | EXPERIMENTAL VALIDATION

For the sake of additional verification, selected antenna designs (specifically, Antennas I-IV with elliptical slits) have been fabricated and measured. Figure 12 shows the

photographs of the antenna prototypes, whereas Figures 13–18 show comparison of simulated and measured reflection responses, gain, and radiation patterns. The agreement between simulations and measurements is acceptable with the discrepancies being mainly a result of antenna assembly inaccuracy (connector soldering, etc.) as well as the shadowing effects of the antenna mounting (particularly for the E-plane measurements).

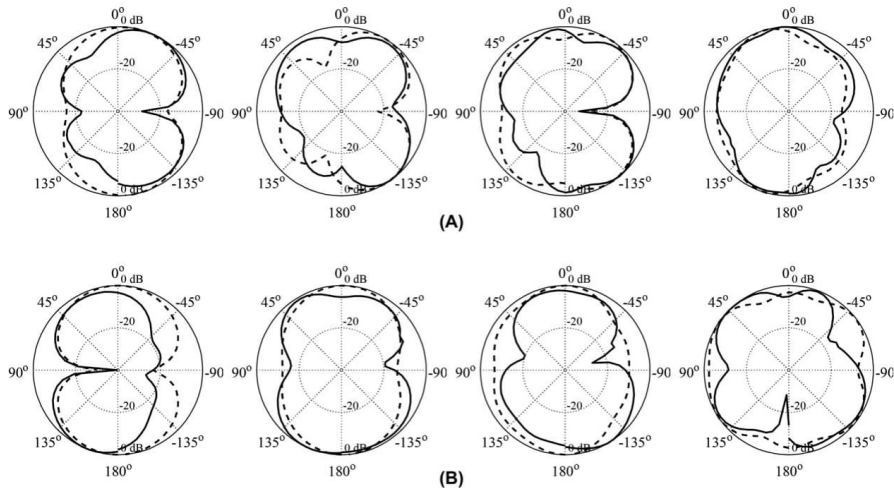


FIGURE 18 Simulated (---) and measured (—) E-plane radiation patterns: A, Antenna III, and B, Antenna IV. The plots (from left to right) are for frequencies 4 GHz, 6 GHz, 8 GHz, and 10 GHz

6 | CONCLUSION

In this paper, investigations of the effect of ground plane modifications on achievable miniaturization rate of UWB antennas have been presented. Two ground plane modifications have been considered, a rectangular and an elliptical slit below the feed line. Numerical studies have been carried out, specifically, size-reduction-oriented optimization, conducted for a representative set of four UWB monopole antennas. Our results indicate that the elliptical slit allows for a higher size reduction rate (on average, 26% of miniaturization rate compared to 19% for the rectangular slit), and its superiority is consistent throughout the entire benchmark set of considered antenna structures. Both numerical and experimental results confirm that additional this size reduction is obtained without compromising electrical and field properties of the respective antennas. The presented study can be considered as a step towards development of systematic rather than case-to-case based design of compact UWB antennas.

ACKNOWLEDGMENTS

The authors thank Computer Simulation Technology, Darmstadt, Germany, for making CST Microwave Studio available. This work has been partially supported by the Icelandic Centre for Research (RANNIS) Grant 163299051.

ORCID

Muhammad Aziz Ul Haq  <http://orcid.org/0000-0003-3380-4745>

Slawomir Koziel  <http://orcid.org/0000-0002-9063-2647>

REFERENCES

- [1] Wu C, Chen Y, Liu W. A compact ultrawideband slotted patch antenna for wireless USB dongle application. *IEEE Antennas Wirel Propag Lett.* **2012**;11:596–599.
- [2] Abbasi QH, Rehman MU, Yang X, Alomainy A, Qaraqe K, Serpedin Q. Ultrawideband band-notched flexible antenna for wearable applications. *IEEE Antennas Wirel Propag Lett.* **2013**;12:1606–1609.
- [3] Bekasiewicz A, Koziel S. Compact UWB monopole antenna for internet of things applications. *Electron Lett.* **2016**;52(7):492–494.
- [4] Sugita T, Kubo S, Taya A, Xiao X, Kikkawa T. A compact 4×4 planar UWB antenna array for 3-d breast cancer detection. *IEEE Antennas Wirel Propag Lett.* **2013**;12:733–736.
- [5] Chen ZN, See TSP, Qing X. Small printed ultrawideband antenna with reduced ground plane effect. *IEEE Antenna Wirel Propag Lett.* **2007**;55(2):383–388. no.
- [6] Li W, Tu Z, Chu Q, Wu X. Differential stepped-slot UWB antenna with common-mode suppression and dual sharp-selectivity notched bands. *IEEE Antenna Wirel Propag Lett Vol. 11* **2016**;15:1120–1123.
- [7] Naghar A, Falcone F, Alejos A, Aghzout O, Alvarez D. A simple UWB tapered monopole antenna with dual wideband-notched performance by using single SRR-slot and single SRR-shaped conductor-backed plane. *Appl Comput Electromagn Soc J.* **2016**;31:1048–1055.
- [8] Dissanayake T, Esselle KP. UWB performance of compact I-shaped wide slot antennas. *IEEE Antenna Wirel Propag Lett.* **2008**;56(4):1183–1187.
- [9] Li L, Cheung SW, Yuk TI. Compact MIMO antenna for portable devices in UWB applications. *IEEE Antenna Wirel Propag Lett.* **2013**;61(8):4257–4264.
- [10] Ryu KS, Kishk AA. Ultra wideband dielectric resonator antenna with broadside patterns mounted on a vertical ground plane edge. *IEEE Trans. Ant. Prop.* **2010**;58(4):1047–1053.
- [11] Felegari N, Nourini J, Ghobadi C, Pourahmadaz J. Broadband CPW-Fed circularly polarized square slot antenna with three inverted-I-shape grounded strips. *IEEE Antenna Wirel Propag Lett.* **2011**;10:274–277.
- [12] Alibakhshi-Kenari M, Naser-Moghaddasi M, Sadeghzadeh RA, Singh Virdee B, Limiti E. New compact antenna based on simplified CRLH-TL for UWB wireless communications systems. *Int J RF Microwave CAE* **2016**;26(3):217–225.
- [13] Bod M, Hassani HR, Taheri MMS. Compact UWB printed slot antenna with extra Bluetooth, GSM, and GPS bands. *IEEE Antenna Wirel Propag Lett.* **2012**;11:531–534.
- [14] Liu Y, Wang P, Qin H. Compact ACS-fed UWB monopole antenna with extra Bluetooth band. *Electron. Lett.* **2014**;50(18):1263–1264.
- [15] Chu Q, Mao C, Zhu H. A compact notched band UWB slot antenna with sharp selectivity and controllable bandwidth. *IEEE Antenna Wirel Propag Lett.* **2013**;61(8):3961–3966. no.
- [16] Pourahmadaz J, Ghobadi C, Nourinia J, Felegari N, Shirzad H. Broadband CPW-fed circularly polarized square slot antenna with inverted-L strips for UWB applications. *IEEE Antenna Wirel Propag Lett.* **2011**;10:369–372.
- [17] Koziel S, Bekasiewicz A. *Multi-Objective Design of Antennas Using Surrogate Models*. Singapore: World Scientific; **2017**.
- [18] Nocedal J, Wright S. *Numerical Optimization*. 2nd ed. New York: Springer; **2006**.
- [19] Koziel S, Bekasiewicz A. EM-simulation-driven design optimization of compact microwave structures using multi-fidelity simulation models and adjoint sensitivities. *Int J RF Microwave CAE* **2016**;26(5):442–448.
- [20] Kolda TG, Lewis RM, Torczon V. Optimization by direct search: new perspectives on some classical and modern methods. *SIAM Rev.* **2003**;45(3):385–482.
- [21] Koziel S, Bekasiewicz A. Expedited simulation-driven design optimization of UWB antennas by means of response features. *Int J RF Microw CAE* **2017**;27(6):e21102 no.
- [22] Koziel S, Bekasiewicz A. Computationally feasible narrow-band antenna modeling using response features. *Int J RF Microw CAE* **2017**;27(4):e21077 no.

- [23] Koziel S, Bekasiewicz A. On rapid re-design of UWB antennas with respect to substrate permittivity. *Metrol Meas Syst.* **2016**;23(4):513–520.
- [24] Koziel S. Computationally efficient multi-fidelity multi-grid design optimization of microwave structures. *Appl Comput Electromagn Soc J.* **2010**;25(7):578–586.
- [25] Zhou B, Cheng CH, Cheng Y, Wang X, Wang Z, Hu S. Tuning space mapping with tuning exponent of T-matrix. *Int J RF Microw CAE* **2016**;26(3):232–239. no.
- [26] Ha BV, Mussetta M, Pirinoli P, Zich RE. Modified compact genetic algorithm for thinned array synthesis. *IEEE Antenna Wirel Propag Lett.* **2016**;15:1105–1108.
- [27] Papadopoulos KA, Papagianni CA, Gkonis PK, Venieris IS, Kaklamani DI. Particle swarm optimization of antenna arrays with efficiency constraints. *Prog Electromagn Res.* **2011**;17:237–251.
- [28] Deb A, Roy JS, Gupta B. Performance comparison of differential evolution, particle swarm optimization and genetic algorithm in the design of circularly polarized microstrip antennas. *IEEE Trans Antennas Propag.* **2014**;62(8):3920–3928. no.
- [29] Koziel S, Ogurtsov S. *Antenna Design by Simulation-Driven Optimization*, Springer Briefs in Optimization. Cham, Switzerland: Springer International Publishing; **2014**.
- [30] Bekasiewicz A, Koziel S. Structure and computationally-efficient simulation-driven design of compact UWB monopole antenna. *IEEE Antenna Wirel Propag Lett.* **2015**;14:1282–1285.
- [31] Koohestani M, Pires N, Skrivervik AK, Moreira AA. Performance study of a UWB antenna in proximity to a human arm. *IEEE Antenna Wirel Propag Lett.* **2013**;12:555–558.
- [32] Ojaroudi M, Ghobadi C, Nourinia J. Small square monopole antenna with inverted T-shaped notch in the ground plane for UWB application. *IEEE Antenna Wirel Propag Lett Vol 8* **2009**; 8:728–731.
- [33] Ghanbari L, Keshtkar A, Ghanbari S, Jarchi S. Planar low VSWR monopole antenna for UWB and LTE communication. *16th Mediterranean Microw Symp (MMS)* **2016**;1:1–4.
- [34] Xu K, Zhu Z, Li H, Huangfu J, Li C, Ran L. A printed single-layer UWB monopole antenna with extended ground plane stubs. *IEEE Antenna Wirel Propag Lett.* **2013**;12:237–240.
- [35] CST Microwave Studio, ver. **2015**. CST AG, Bad Nauheimer Str. 19, D-64289 Darmstadt, Germany, **2015**.
- [36] Conn AR, Gould NIM, Toint PL. *Trust Region Methods*, MPS-SIAM Series on Optimization. Society for Industrial and Applied Mathematics; **2000**.

AUTHOR BIOGRAPHIES



Muhammad Aziz ul Haq received his BS and MS degrees in electronic engineering from Mohammad Ali Jinnah University, Karachi (Islamabad campus), Pakistan, in 2011 and 2014, respectively. He has been involved in several projects in the field of contemporary antenna design for microwave imaging, eHealth and future wireless communication systems such as 5G and Internet of Things (IoT) since 2014 to 2016. He is currently pursuing his Ph.D. degree with the School of Science and Engineering, Reykjavik University, Iceland. His research interests include compact antenna design and optimization methods for selected classes of antenna structures.



Slawomir Koziel received the M.Sc. and Ph.D. degrees in electronic engineering from Gdansk University of Technology, Poland, in 1995 and 2000, respectively. He also received the M.Sc. degrees in theoretical physics and in mathematics, in 2000 and 2002, respectively, as well as the PhD in mathematics in 2003, from the University of Gdansk, Poland. He is currently a Professor with the School of Science and Engineering, Reykjavik University, Iceland. His research interests include CAD and modeling of microwave and antenna structures, simulation-driven design, surrogate-based optimization, space mapping, circuit theory, analog signal processing, evolutionary computation and numerical analysis.

How to cite this article: Aziz Ul Haq M, Koziel S. Simulation-based optimization for rigorous assessment of ground plane modifications in compact UWB antenna design. *Int J RF Microw Comput Aided Eng.* 2017:e21204. <https://doi.org/10.1002/mmce.21204>

Chapter 5

5 Paper [J4]

Slawomir Koziel and Muhammad Aziz ul Haq

Ground plane modifications for design of miniaturized UWB antennas

Published: *IET Microwaves, Antennas & Propagation*, vol. 12, Iss. 8, pp. 1360-1366, 2018.

DOI: 10.1049/iet-map.2017.1111

Ground plane modifications for design of miniaturised UWB antennas

ISSN 1751-8725
 Received on 24th November 2017
 Revised 5th February 2018
 Accepted on 10th February 2018
 E-First on 10th April 2018
 doi: 10.1049/iet-map.2017.1111
 www.ietdl.org

Slawomir Koziel¹, Muhammad Aziz Ul Haq¹ ✉

¹Engineering Optimization and Modeling Center, School of Science and Engineering, Reykjavik University, 101 Reykjavik, Iceland

✉ E-mail: muhammadu16@ru.is

Abstract: This study investigates a particular type of ground plane modifications in ultra-wideband (UWB) antennas and the effect they have on achievable amount of miniaturisation of the structure at hand. The focus is on n -section rectangular slits below the feeding line. The authors analyse possible size reduction as a function of the number n of slit sections. In order to ensure that the minimum antenna footprint is obtained in each case, rigorous numerical optimisation of all antenna parameters has been carried out. The optimisation process is constrained to guarantee that the antenna exhibits acceptable in-band matching at the level of -10 dB. For the sake of generality, the study has been performed using a benchmark set of four representative UWB monopoles. The results clearly indicate a significant advantage of increasing the number of degrees of freedom of the ground plane slit but also the saturation effect, i.e. decreasing advantages of introducing additional slit sections beyond a certain value of n . The average amount of miniaturisation for $n = 5$ versus $n = 1$ is around 40%. For selected designs, numerical results have been validated experimentally.

1 Introduction

Ultra-wideband (UWB) antennas are fundamental components of wireless communication systems. Their advantages include low fabrication cost, omnidirectional radiation pattern, low power consumption, as well as potential for high data rate communication [1]. Small size is an important consideration for antennas in general and UWB structures in particular, which is due to the increasing role of space-limited applications such as wearable devices [2] or a growing area of the Internet of things [3]. A challenge in the design of compact UWB antennas is that reduction in physical dimensions generally leads to degradation of both electrical and field properties, such as in-band reflection, flat gain characteristic [4], or sufficient radiation pattern stability [5].

Development of miniaturised UWB antennas has been a subject of intensive research. A typical strategy is to introduce modifications to conventional antenna geometries [6–8]. Such modifications are often incorporated by trial and error and may include alterations of the radiator shape as well as modifications of the feeding line (e.g. adding impedance matching transformers [9]) or the ground plane [7, 10, 11]. It is perhaps the last type of modifications that is particularly popular, arguably due to its efficiency (introducing ground plane slits and stubs is an easy way of enlarging the current path) and comes in many variations, e.g. slits below the feed line [10], ground plane stubs (I-shaped [7], L-shaped), or protruded ground plane structures [11].

The vast majority of the solutions proposed for compact antennas are case studies. Furthermore, the reduced size is usually an outcome of a particular combination of topology modifications with geometry parameters tuned to satisfy basic performance requirements. The final designs are hardly optimal as finding these would require rigorous numerical optimisation of all geometry parameters. This cannot be achieved by means of parameter sweeping which is still the most widely used simulation-driven design approach. The works focused on explicit control of other performance figures are rare in the literature (e.g. [4, 12, 13]). At the same time, the literature is lacking systematic studies on the effect of particular geometry modifications.

As indicated in the literature (e.g. [14]), optimum designs can only be obtained by simultaneous adjustment of relevant antenna parameters using numerical procedures. If the objective is size reduction, the optimisation task is a constrained problem because

of necessity of satisfying, given electrical performance requirements. Explicit size reduction through constrained optimisation has been demonstrated to provide much better results, both in single- [11] and multi-objective setting [14], also using adjoint sensitivities [15].

This paper is an attempt to carry out systematic investigation concerning the relevance of geometry modifications of the antenna structure in the context of miniaturisation. We consider a specific ground plane modification, which is an n -section rectangular slit below the feeding line. Owing to the nature of modification, the technique is not applicable for coplanar waveguide-fed antenna structures where the ground plane is placed on a same layer as the feed line. Rigorous numerical optimisation of all antenna parameters is applied to investigate the effects of the number of slit sections on achievable amount of miniaturisation of the antenna. Our numerical experiments are performed using a representative set of four UWB monopoles. The results indicate the benefits of increasing the number of degrees of freedom of the slit: the amount of miniaturisation is between 25% and almost 60% when comparing one- and five-section slits. On the other hand, a saturation effect is observed which, however, occurs for relatively high value of n (around four or five). At the same time, no considerable degradation of antenna field properties is noticed due to the additional size reduction. The analysis of the optimised dimensions confirms fundamental importance of simultaneous adjustment of all antenna parameters as a mean to obtain the best amount of miniaturisation possible. This is demonstrated by observing that the values of all antenna parameters are subject to change for the minimum-size designs obtained for various section count. The conclusions are consistent for the entire set of benchmark structures. Numerical results are validated experimentally.

2 Case studies ground plane modifications

This work is a systematic investigation of a particular type of ground plane modification in the form of an n -section slit below the feeding line. We consider various values of n from one through five as shown in Fig. 1. The purpose of the study is to determine achievable miniaturisation ratio of the antenna structure as a function of n . Four UWB monopole antennas recently reported in the literature ([16–19]) are utilised as a benchmark set [16–19].

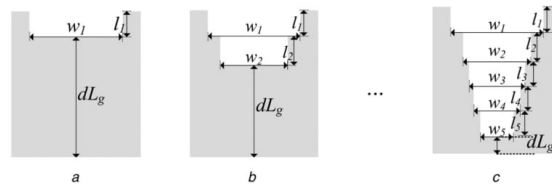


Fig. 1 Sample ground plane modifications considered in this work: n -section rectangular slit

The pictures shown the slit for (a) $n=1$, (b) $n=2$, (c) $n=5$

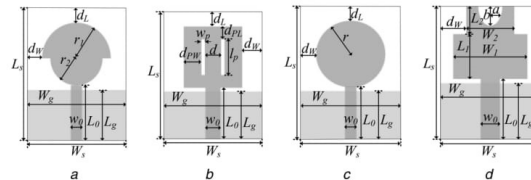


Fig. 2 Sample benchmark set of four UWB monopole antennas

(a) Antenna I [16], (b) Antenna II [17], (c) Antenna III [18], (d) Antenna IV [19]

Table 1 Optimised size of UWB antennas

Ground plane mod.	Antenna footprints							
	Antenna I		Antenna II		Antenna III		Antenna IV	
	mm ²	ka ^a	mm ²	ka ^a	mm ²	ka ^a	mm ²	ka ^a
flat ground	802	1.308	264	0.859	875	1.365	281	0.876
rect. slit ($n=1$)	617	1.178	241	0.829	469	1.059	276	0.870
rect. slit ($n=2$)	482	1.074	198	0.795	303	0.905	249	0.845
rect. slit ($n=3$)	384	0.993	190	0.792	259	0.861	222	0.825
rect. slit ($n=4$)	330	0.946	186	0.791	232	0.834	205	0.805
rect. slit ($n=5$)	271	0.860	177	0.773	218	0.819	205	0.803

^aka values are calculated at lowest operating frequency, i.e. 3.1 GHz; $k=2\pi/\lambda$ is a wave number, and a is the radius of the minimum size sphere which the antenna can fit in.

The structures have been shown in Fig. 2. All antennas are realised on 1.55 mm thick FR-4 substrate ($\epsilon_r=4.4$). The computational models of the structures are implemented in CST Microwave Studio [20] and simulated using its time-domain solver. All models incorporate SMA connectors in order to improve the reliability of subsequent experimental validation.

For the sake of design optimisation, all geometry parameters of the antennas are made adjustable. Design variable vectors for antennas I through IV are as follows:

- $\mathbf{x}_1 = [L_g, L_0, r_1, r_2, d_W]^T$,
- $\mathbf{x}_2 = [L_g, L_0, l_P, w_P, d, d_L, d_{PL}, d_{PW}]^T$,
- $\mathbf{x}_3 = [L_g, L_0, d_W, r]^T$,
- $\mathbf{x}_4 = [L_g, L_0, L_1, L_2, W_1, W_2, d_W, a, b]^T$

All dimensions are in millimetre. Upon applying particular ground plane modifications, the respective vectors are extended by the slit parameters as shown in Fig. 1. The initial values of geometry parameters are based on the literature: $\mathbf{x}_1^{(0)} = [14, 14.6, 0.9, 11, 6.4]^T$, $\mathbf{x}_2^{(0)} = [4.4, 7.8, 9.8, 0.24, 3.9, 5, 2.8, 3.6]^T$, $\mathbf{x}_3^{(0)} = [13, 14.24, 5.32, 8.9]^T$, and $\mathbf{x}_4^{(0)} = [3.8, 5.8, 12.8, 7.6, 15.7, 9.7, 4.4, 0.9, 0.1]^T$.

The conventional monopole antenna (with flat ground) is considered as a reference model to compare the obtained results from the proposed ground plane modifications. The antennas are supposed to operate in the standard UWB frequency range (3.1–10.6 GHz).

3 Antenna miniaturisation by EM-driven design

In this work, minimum-size antenna designs are obtained by appropriate adjustment of geometry parameters. In particular, electromagnetic-driven design optimisation is carried out using numerical optimisation in which the primary goal is to minimise the antenna footprint $A(\mathbf{x})$, with \mathbf{x} being a vector of geometry parameters of the structure at hand (cf. Section 2). At the same time, we want to ensure sufficient matching in the entire UWB frequency range, i.e. to satisfy the condition $S(\mathbf{x}) \leq -10$ dB, where $S(\mathbf{x})$ is the maximum reflection from 3.1 to 10.6 GHz.

Given the above, the design problem can be formulated as a constrained non-linear minimisation task of the form

$$\mathbf{x}^* = \arg \min_{\mathbf{x}} \{A(\mathbf{x})\}, \quad S(\mathbf{x}) \leq -10 \text{ dB} \quad (1)$$

Here, the optimisation routine of choice is pattern search [21], which is a stencil-based algorithm involving grid-restricted linear search and polling (neighbour search) with adaptive adjustment of the grid size [21]. The pattern search requires the starting point which is feasible from the point of view of the aforementioned matching requirement. Such a point is obtained by minimising $S(\mathbf{x})$.

4 Numerical results

All antenna structures from the benchmark set of Section 2 have been optimised for minimum size in their basic configurations (flat ground plane) and the n -section slit for $n=1, \dots, 5$. The results have been gathered in Tables 1–5 as well as Figs. 3–8. The design task was formulated as explained in Section 3, i.e. as a constrained problem with the acceptance threshold on maximum in-band reflection being -10 dB. It is important to observe (cf. Fig. 3) that the matching constraint is active for all considered cases which indicates that the obtained designs do represent the minimum

Table 2 Geometry parameter values (mm) for optimised designs of antenna I

n	L_g	L_0	r_1	r_2	d_W	d_{L_g}	l_1	l_2	l_3	l_4	l_5	w_1	w_2	w_3	w_4	w_5
0	13.8	14.4	6.8	9.1	3.9	—	—	—	—	—	—	—	—	—	—	—
1	—	15.4	5.4	8.9	1.4	10.6	0.24	—	—	—	—	0.13	—	—	—	—
2	—	15.8	4.7	7.7	0.8	5.3	0.2	0.36	—	—	—	0.18	0.1	—	—	—
3	—	15.9	4.0	7.0	0.03	6.9	0.15	0.21	0.1	—	—	0.32	0.1	0.1	—	—
4	—	15.7	4.2	6.2	0.02	6.6	0.17	0.17	0.06	0.08	—	0.35	0.3	0.18	0.15	—
5	—	15.1	3.8	5.5	0.02	4.6	0.22	0.22	0.05	0.08	0.1	0.46	0.3	0.14	0.17	0.07

n denotes the number of rectangular slits below the feed line.

Table 3 Geometry parameter values (mm) for optimised designs of antenna II

n	L_g	L_0	l_p	w_p	d	d_L	d_{PL}	d_{PW}	d_{L_g}	l_1	l_2	l_3	l_4	l_5	w_1	w_2	w_3	w_4	w_5
0	4.4	7.7	9.7	0.2	3.2	0.9	2.8	3.6	—	—	—	—	—	—	—	—	—	—	—
1	—	8.6	9.8	0.3	2.9	0.0	2.4	3.0	8.4	0.52	—	—	—	—	0.22	—	—	—	—
2	—	11.3	6.0	0.7	2.0	0.0	2.7	2.5	2.5	0.47	0.17	—	—	—	0.47	0.09	—	—	—
3	—	11.6	5.4	0.2	1.5	0.0	2.9	3.18	0.4	0.43	0.37	0.13	—	—	0.43	0.1	0.08	—	—
4	—	11.6	5.3	0.2	1.5	0.0	2.9	3.13	8.3	0.2	0.17	0.06	0.01	—	0.2	0.17	0.06	0.02	—
5	—	13.2	5.1	0.15	1.2	0.0	2.0	3.17	1.3	0.4	0.21	0.1	0.03	0.02	0.4	0.2	0.2	0.1	0.06

n denotes the number of rectangular slits below the feed line.

Table 4 Geometry parameter values (mm) for optimised designs of antenna III

n	L_g	L_0	d_W	r	d_{L_g}	l_1	l_2	l_3	l_4	l_5	w_1	w_2	w_3	w_4	w_5
0	13.0	14	4.7	8.9	—	—	—	—	—	—	—	—	—	—	—
1	—	16.8	2.8	5.5	10.3	0.28	—	—	—	—	0.24	—	—	—	—
2	—	15.0	1.0	5.0	7.2	0.17	0.2	—	—	—	0.4	0.3	—	—	—
3	—	14.6	0.5	4.8	6.8	0.2	0.1	0.17	—	—	0.5	0.3	0.12	—	—
4	—	14.5	0.25	4.6	6.6	0.23	0.08	0.15	0.06	—	0.7	0.28	0.24	0.05	—
5	—	14.3	0.07	4.5	2.9	0.32	0.13	0.12	0.05	0.1	0.82	0.34	0.22	0.23	0.18

n denotes the number of rectangular slits below the feed line.

Table 5 Geometry parameter values (mm) for optimised designs of antenna IV

n	L_g	L_0	L_1	L_2	W_1	W_2	d_W	a	b	d_{L_g}	l_1	l_2	l_3	l_4	l_5	w_1	w_2	w_3	w_4	w_5
0	4.3	7.6	10.3	6.4	11.5	7.4	2	0.1	0.1	—	—	—	—	—	—	—	—	—	—	—
1	—	8.0	11.9	4.2	10.8	7.11	2.1	0.1	0.1	1.1	0.75	—	—	—	—	0.12	—	—	—	—
2	—	10.0	11.6	2.2	9.8	4.5	2.9	0.8	0.1	1.2	0.4	0.38	—	—	—	0.3	0.1	—	—	—
3	—	11.3	10.1	2	9.3	4.5	2.4	0.2	0.11	1.3	0.48	0.029	0.36	—	—	0.32	0.13	0.05	—	—
4	—	12.7	8.7	1.6	8.7	3.5	2.6	0.28	0.26	2.5	0.3	0.07	0.03	0.0008	—	0.45	0.13	0.004	0.25	—
5	—	12.7	8.7	1.6	8.7	3.5	2.6	0.27	0.25	2.6	0.5	0.11	0.06	0.01	0.005	0.45	0.09	0.07	0.2	0.24

n denotes the number of rectangular slits below the feed line.

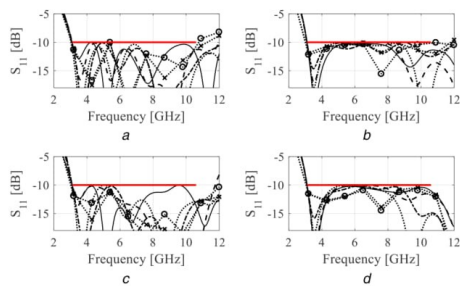


Fig. 3 Reflection responses of size-optimized antennas with flat ground (continuous line), one-section slit (dashed line), two-section slit (dotted line), three-section slit (dashed dot), four-section slits (line with multi symbol), and five-section slit (line with circle) (a) Antenna I, (b) Antenna II, (c) Antenna III, (d) Antenna IV

possible antenna footprints. On the other hand, satisfaction of the reflection constraint is critical for fair comparison of the designs corresponding to different values of n .

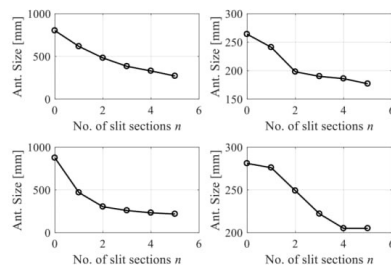


Fig. 4 Comparison of optimized antenna size as a function of the number of slit sections (zero refers to the flat ground case). Plots from the top left to bottom right-hand-side are for the antenna I, antenna II, antenna III, and antenna IV, respectively

Table 1 indicates the physical and electrical lengths of the optimized antennas. Here, the electrical lengths are calculated as ka , where $k = 2\pi/\lambda$ is a wave number values at the lowest frequency, i.e. 3.1 GHz, whereas a is the radius of the minimum sphere containing the antenna. It can be observed that increasing the

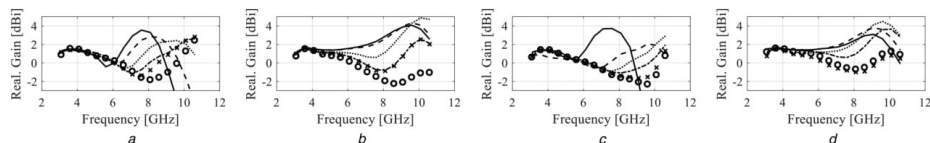


Fig. 5 Realised gain of size-optimised antennas with flat ground (continuous line), one-section slit (dashed line), two-section slit (dotted line), three-section slit (dashed-dot line), four-section slits (multi-symbol), and five-section slit (circles)
(a) Antenna I, (b) Antenna II, (c) Antenna III, (d) Antenna IV

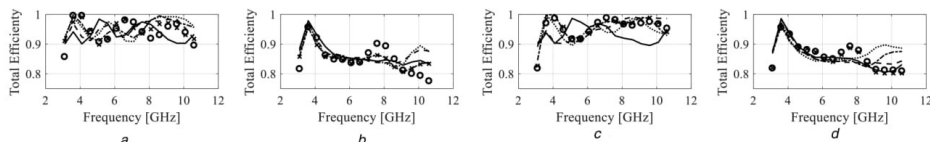


Fig. 6 Total efficiency of size-optimised antennas with flat ground (continuous line), one-section slit (dashed line), two-section slit (dotted line), three-section slit (dashed-dot line), four-section slits (multi-symbol), and five-section slit (circles)
(a) Antenna I, (b) Antenna II, (c) Antenna III, (d) Antenna IV

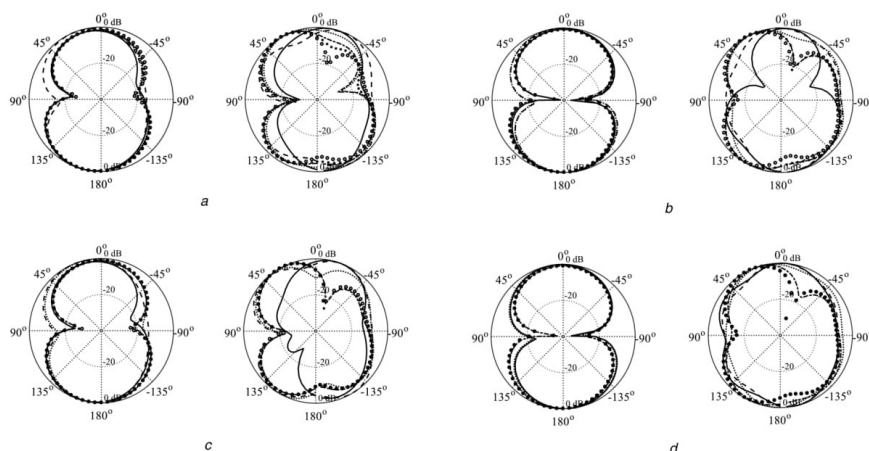


Fig. 7 E -plane pattern of size-optimised antennas with flat ground (continuous line), one-section slit (dashed line), two-section slit (dotted line), three-section slit (dashed-dot line), four-section slits (multi-symbol), and five-section slit (circles)
(a) Antenna I, (b) Antenna II, (c) Antenna III, (d) Antenna IV. The left- and right-hand-side plots are for the frequencies of 4 and 8 GHz, respectively

number of slit section has a dramatic effect on the antenna size for all antenna structures. Although increasing the number of sections beyond two or three may seem to be a minor modification, it still has a considerable effect on the antenna footprint as indicated in Table 1. Beyond $n=4$, the advantages of increasing the slit complexity become less pronounced; however, they are still noticeable, particularly for antennas I and III. Clearly, simultaneous adjustment of all antenna parameters is critical to achieve this effect (detailed antenna dimensions are not shown for the sake of brevity). Fig. 4 contains visualisation of the data of Table 1. The saturation effect can be observed; however, further benefits are expected when increasing n for all antennas except antenna IV.

Regarding other performance figures, increasing the slit section number n leads to slight degradation of the antenna gain for higher frequencies (but only when $n>3$). Usually, this phenomenon occurs as a consequence of using high-loss substrate (e.g. FR-4) and for physically small antennas. Here, this effect is much more pronounced as antenna size decreases (cf. Fig. 5). At the same time, it should be noted that the gain of miniaturised antennas (with the slit) is higher than the gain of the reference antenna (with flat ground) towards the end of the UWB frequency range (around 9 GHz and beyond). No significant effect on antenna efficiency can be observed (cf. Fig. 6). However, certain efficiency improvement

can be noted for all antennas at the frequencies >6 GHz (when compared with the reference structures). The above effects, although generally beneficial, were by-products of the optimisation process since neither gain nor efficiency have been directly handled.

Similarly, there are minor changes of radiation patterns in the E -plane (cf. Fig. 7). All antennas exhibit consistent omnidirectional characteristics in the H -plane (cf. Fig. 8). Thus, it can be concluded that additional size reduction due to increasing the number of sections of the slit have overall minor effect on both electrical and field properties of the antennas. Tables 2–5 show the optimised parametric values of each antenna. The slit dimensions are relative to the corresponding ground plane to ensure physical consistency of the antenna structure (in particular, that the slit is entirely allocated within the ground plane during the optimisation process).

5 Experimental validation

Figs. 9–11 show the comparison of simulation and measurement data for antennas I through IV. For the sake of brevity, only the smallest antennas with five-section slit below the feed line included. Fig. 12 exhibits the photographs of the fabricated antennas.

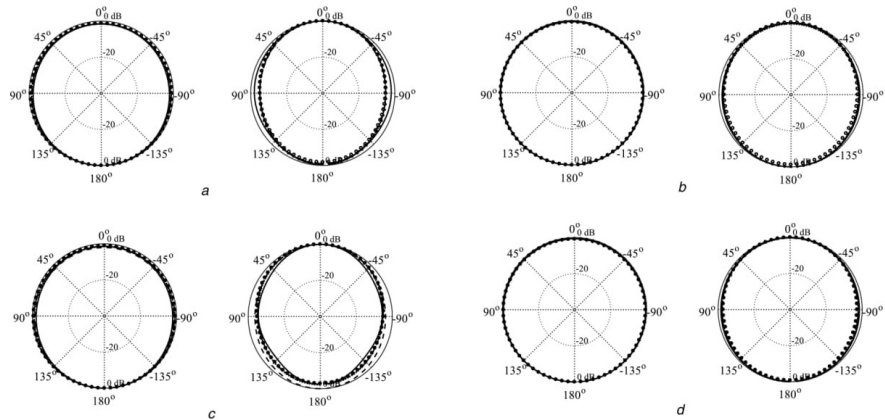


Fig. 8 *H*-plane pattern of size-optimised antennas with flat ground (continuous line), one-section slit (dashed line), two-section slit (dotted line), three-section slit (dashed dot line), four-section slits (multi symbol), and five-section slit (circles)
 (a) Antenna I, (b) Antenna II, (c) Antenna III, (d) Antenna IV. The left- and right-hand-side plots are for the frequencies of 4 and 8 GHz, respectively

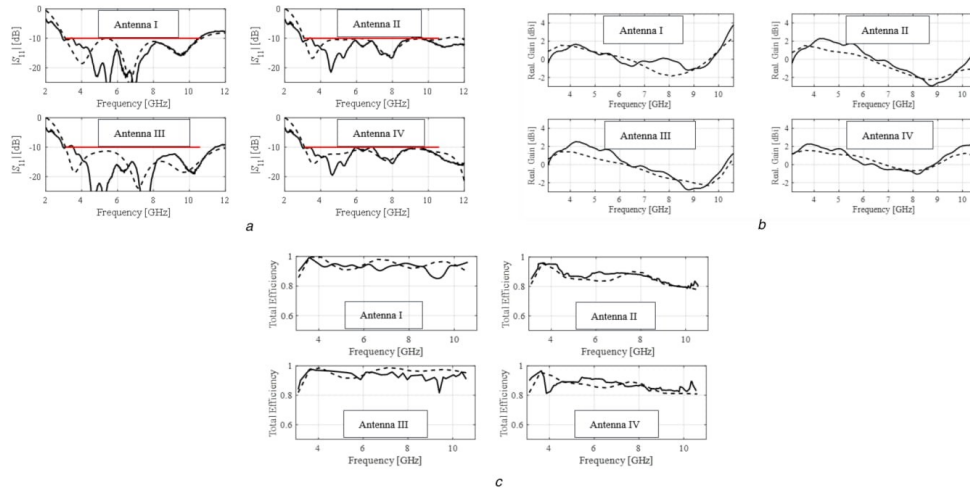


Fig. 9 Simulated (dashed line) and measured (continuous line) reflection response, realised gain, and total efficiency characteristics (with five-section slit below the feed line)
 (a) Reflection response, (b) Realised gain, (c) Total efficiency

Fig. 9a indicates that the measured reflection response is well under -10 dB for the entire UWB frequency range. Similarly, Fig. 9b shows an acceptable agreement between the simulated and measured gain. Simulated and measured total efficiency is shown in Fig. 9c. The simulated and measured characteristics are well aligned. The radiation pattern for frequencies 4 and 10 GHz is shown in Figs. 10 and 11. The radiation pattern is omnidirectional which is the requirement for UWB antennas (especially for communication application). However, in the case of *E*-plane, an inconsistency is being observed for the lower frequencies, e.g. 4 GHz that is mainly due to the shadowing effect of the measurement setup (in particular, the 90° bend utilised to mount the antenna) as well as the connector-soldering factor. Similar, but significantly less pronounced effect can be observed at 10 GHz.

6 Conclusion

In this paper, a comprehensive study concerning the effects of a particular ground plane modification (a slit below the feeding line)

on achievable amount of miniaturisation of UWB antennas has been conducted. Rigorous numerical optimisation of all antenna parameters has been applied to ensure that the designs featuring minimum size are generated. Our numerical results obtained for a benchmark set of four recent compact UWB monopoles indicate that increasing the number of degrees of freedom of the slit has a significant effect on antenna size even for relatively large number of the slit sections. At the same time, the size reduction obtained this way does not affect electrical performance of the respective antennas in a significant way. The two effects that have been observed include certain degradation of realised gain for higher frequencies (>6 GHz), which is more pronounced for increasing number of the slit sections n , as well as slight improvement of efficiency at higher frequencies. The presented study can be considered as a step towards systematic analysis of importance and advantages of topological modifications in the context of antenna miniaturisation.

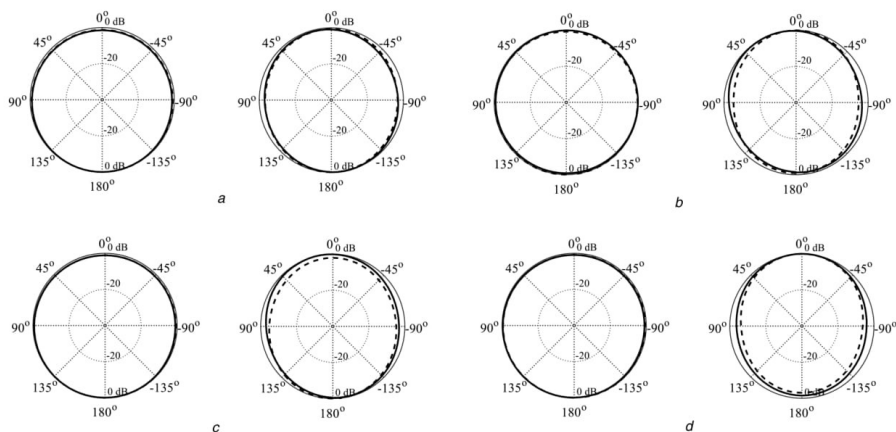


Fig. 10 Simulated (dashed line) and measured (continuous line) H-plane radiation patterns (with five-section slit below the feed line) (a) Antenna I, (b) Antenna II, (c) Antenna III, (d) Antenna IV. The plots (from left to right) are for frequencies 4 and 10 GHz

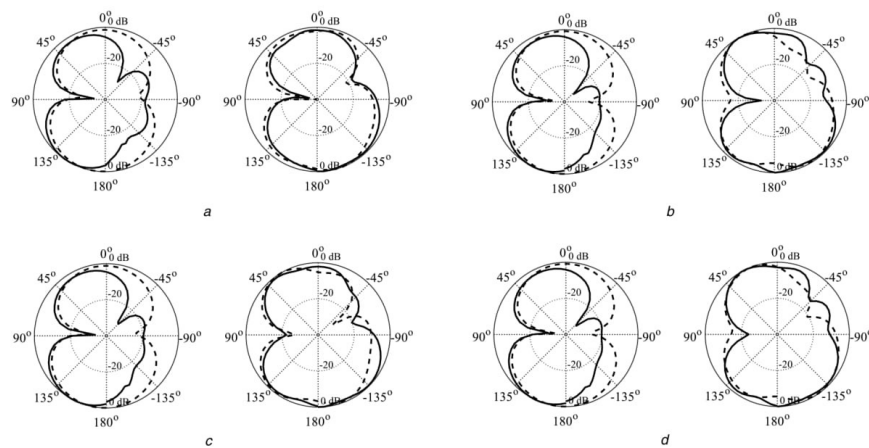


Fig. 11 Simulated (dashed line) and measured (continuous line) E-plane radiation patterns (with five-section slit below the feed line) (a) Antenna I, (b) Antenna II, (c) Antenna III, (d) Antenna IV. The plots (from left to right) are for frequencies 4 and 10 GHz

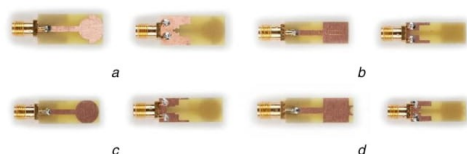


Fig. 12 Photographs of fabricated antenna prototypes (with five-section slit below the feed line)

(a) Antenna I, (b) Antenna II, (c) Antenna III, (d) Antenna IV

7 Acknowledgments

The authors thank Computer Simulation Technology AG, Darmstadt Germany for making CST Microwave Studio available. This work is partially supported by the Icelandic Centre for Research (RANNIS) grant 174114051, and by National Science Centre of Poland Grant 2015/17/B/ST6/01857.

8 References

- [1] Wu, C., Chen, Y., Liu, W.: 'A compact ultrawideband slotted patch antenna for wireless USB dongle application', *IEEE Antennas Wirel. Propag. Lett.*, 2012, **11**, pp. 596–599
- [2] Abbasi, Q.G., Rehman, M.U., Yang, X., *et al.*: 'Ultrawideband band-notched flexible antenna for wearable applications', *IEEE Antennas Wirel. Propag. Lett.*, 2013, **12**, pp. 1606–1609
- [3] Bekasiewicz, A., Koziel, S.: 'Compact UWB monopole antenna for internet of things applications', *Electron. Lett.*, 2016, **52**, (7), pp. 492–494
- [4] Chiu, Y.H., Chen, Y.S.: 'Multi-objective optimization for UWB antennas in impedance matching, gain, and fidelity factor'. *IEEE Int. Symp. Antennas and Propagation*, 2015, pp. 1–2
- [5] Liu, J., Esselle, K.P., Hay, S.G., *et al.*: 'Effects of printed UWB antenna miniaturization on pulse fidelity and pattern stability', *IEEE Trans. Antennas Propag.*, 2014, **62**, (8), pp. 3903–3910
- [6] Felegari, N., Nourini, J., Ghobadi, C., *et al.*: 'Broadband CPW-fed circularly polarized square slot antenna with three inverted-l-shape grounded strips', *IEEE Antennas Wirel. Propag. Lett.*, 2011, **10**, pp. 274–277
- [7] Li, L., Cheung, S.W., Yuk, T.I.: 'Compact MIMO antenna for portable devices in UWB applications', *IEEE Trans. Antennas Propag.*, 2013, **61**, (8), pp. 4257–4264
- [8] Qing, X., Chen, Z.N.: 'Compact coplanar waveguide-fed ultra-wideband monopole-like slot antenna', *IET Microw. Antennas Propag.*, 2009, **3**, (5), pp. 889–898
- [9] Bekasiewicz, A., Koziel, S.: 'A novel structure and design optimization of miniaturized UWB slot antenna'. *Int. Symp. Antennas and Propagation*, 2016, pp. 1313–1314

- [10] Li, J.F., Chu, Q.X., Li, Z.H., *et al.*: 'Compact dual band-notched UWB MIMO antenna with high isolation', *IEEE Trans. Antennas Propag.*, 2013, **61**, (9), pp. 4759–4766
- [11] Bekasiewicz, A., Koziel, S., 'Structure and computationally-efficient simulation-driven design of compact UWB monopole antenna', *IEEE Antennas Wirel. Propag. Lett.*, 2015, **14**, pp. 1282–1285
- [12] Tian, B., Li, Z., Wang, C.: 'Boresight gain optimization of an UWB monopole antenna using FDTD and genetic algorithm', *IEEE Int. Conf. Ultra-Wideband*, 2012, **1**, pp. 1–4
- [13] Koziel, S., Bekasiewicz, A., Cheng, Q.S., *et al.*: 'On ultra-wideband antenna miniaturization involving efficiency and matching constraints', *IEEE European Antennas and Propagation Conf.*, 2017, pp. 3264–3268
- [14] Koziel, S., Bekasiewicz, A.: '*Multi-objective design of antennas using surrogate models*', (Word Scientific, London, 2016)
- [15] Koziel, S., Bekasiewicz, A.: 'Fast EM-driven size reduction of antenna structures by means of adjoint sensitivities and trust regions', *IEEE Antennas Wirel. Propag. Lett.*, 2015, **14**, pp. 1681–1684
- [16] Koohestani, M., Pires, N., Skrivervik, A.K., *et al.*: 'Performance study of a UWB antenna in proximity to a human arm', *IEEE Antennas Wirel. Propag. Lett.*, 2013, **12**, pp. 555–558
- [17] Ojaroudi, M., Ghobadi, C., Nourinia, J.: 'Small square monopole antenna with inverted T-shaped notch in the ground plane for UWB application', *IEEE Antennas Wirel. Propag. Lett.*, 2009, **8**, pp. 728–731
- [18] Ghanbari, L., Keshkar, A., Ghanbari, S., *et al.*: 'Planar low VSWR monopole antenna for UWB and LTE communication'. 16th Mediterranean Microwave Symp. (MMS), 2016, pp. 1–4
- [19] Xu, K., Zhu, Z., Li, H., *et al.*: 'A printed single-layer UWB monopole antenna with extended ground plane stubs', *IEEE Antennas Wirel. Propag. Lett.*, 2013, **12**, pp. 237–240
- [20] CST Microwave Studio, ver. 2015. CST AG, Darmstadt, Germany, 2015
- [21] Koziel, S.: 'Computationally efficient multi-fidelity multi-grid design optimization of microwave structures', *Appl. Comput. Electromagn. Soc. J.*, 2010, **25**, (7), pp. 578–586

Chapter 6

6 Paper [J5]

Muhammad Aziz ul Haq, Slawomir Koziel, and Qingsha S. Cheng


Miniaturization of wideband antennas by means of feed line topology alterations

Published: *IET Microwaves, Antennas & Propagation*, vol. 12, Iss. 13, pp. 2128-2134, 2018.

DOI: 10.1049/iet-map.2018.5197


Miniaturisation of wideband antennas by means of feed line topology alterations

ISSN 1751-8725
Received on 11th September 2017
Revised 23rd April 2018
Accepted on 26th June 2018
E-First on 27th September 2018
doi: 10.1049/iet-map.2018.5197
www.ietdl.org

Muhammad Aziz Ul Haq¹, Slawomir Koziel¹ , Qingsha S. Cheng²

¹Engineering Optimization and Modeling Center, School of Science and Engineering, Reykjavik University, 101 Reykjavik, Iceland

²Department of Electrical and Electronic Engineering, Southern University of Science and Technology, Shenzhen, People's Republic of China

 E-mail: koziel@ru.is

Abstract: It is a common practice to achieve reduction of wideband antenna size by incorporating appropriate geometrical modifications into conventional antenna topologies (e.g. monopoles or uniplanar structures). The authors investigate a particular type of modification, which is changing the geometry of the feed line. The two basic geometries include a taper and a stepped-impedance line. They carry out systematic investigations concerning the effect of these feed line geometries on obtainable antenna miniaturisation rates. For the sake of generality, feed line geometries of various complexities are considered (from two to six sections). An automated adjustment of antenna geometry parameters through numerical optimisation is performed to ensure design optimality for each combination of antenna/feed structure. The optimisation process is formulated as an explicit size reduction task with a constraint on the maximum in-band reflection level. The investigations are performed using two selected ultra-wideband monopoles. The results indicate clear advantage of the stepped-impedance feed line over the tapered one. On the other hand, considerable size reduction can be obtained by increasing the geometrical complexity of the feed line, although the design problem becomes more challenging due to the increased number of antenna parameters. Numerical results are validated experimentally for selected antenna prototypes.

1 Introduction

The attractive features of ultra-wideband (UWB) systems include the ability of high-data-rate transmission and wireless connectivity, as well as applicability in radar and imaging systems [1]. The critical components of the UWB systems are UWB antennas characterised by low-fabrication cost, omnidirectional radiation pattern, and low-power consumption [2]. Due to the stringent performance requirements imposed on contemporary communication systems, the antenna design process has to take into account a number of electrical and field properties such as reflection response, gain variability [3], efficiency, and radiation pattern stability [4]. Furthermore, for an increasing number of applications (e.g. wearable devices [5], internet of things [6], cognitive radio [7], or medical imaging [8]), achieving small size of the antenna structure becomes one of the most important design objectives. Unfortunately, the reduction of the antenna footprint leads to the degradation of the structure performance. One of the well-known effects is the reduction of the impedance bandwidth, in particular, difficulties in ensuring sufficient matching at lower UWB frequencies due to the shortening of the current path. Other problems include degradation of the radiation pattern omnidirectionality and antenna efficiency or increased gain variability. In general, any practical design is a trade-off between geometry constraints and electrical performance.

Literature review reveals that the majority of novel UWB antenna structures are developed by modifying conventional structures (e.g. monopoles or slot antennas) [9–13]. There is a large variety of modifications utilised in practical designs, involving alterations of the radiator shape, feed line shape (e.g. incorporating impedance matching transformers [14, 15]), or – probably the most popular – modifications of the ground plane [10, 16, 17]. Examples within the last group include slits below the feed line [16], ground plane stubs (I-shaped [10] and L-shaped), or protruded ground plane structures [17]. Although the number of novel compact wideband antennas reported in the literature is quite large, virtually all of the proposed structures are presented as case studies (typically, as antennas oriented towards particular applications). Often, researchers describe an ‘evolution’ of the structure that

illustrates the effects of the introduced topological changes. Typically, however, reduction of the antenna size is a by-product of a particular antenna topology: adjustment (or optimisation) of geometry parameters usually aims at satisfying selected performance requirements, such as sufficient in-band matching. There are a very limited number of papers addressing explicit control of other performance figures (e.g. [3, 18, 19]). On the other hand, there are no systematic studies (performed on the benchmark sets of antenna structures) investigating the effects of the particular geometry modifications on antenna performance.

Having the antenna topology selected, design closure has to be performed in order to obtain the best possible design. Due to the complexity of contemporary antenna structures, this cannot be achieved using traditional means (e.g. parameter sweeping); rigorous numerical optimisation is required instead [20]. In case of size reduction, the design optimisation task becomes more challenging: the necessity of satisfying electrical performance requirements imposed on the antenna makes the problem a constrained one. Some of the recent works have reported explicit size reduction of antenna structures both in single-objective [17] and multi-objective [20] context. Explicit optimisation-based antenna miniaturisation using adjoint sensitivities has also been reported [21].

In this work, we carry out a systematic investigation of two types of feed lines in the context of their effect on the achievable miniaturisation rate of the UWB antennas. More specifically, we consider a stepped-impedance line and a multi-section taper. For both types of lines, the complexity is controlled by the number n of sections (steps or tapers, respectively), with n varying from two to six. The minimum structure size for any particular configuration of the antenna-feed is obtained by optimising all geometry parameters. The benchmark set contains two UWB monopoles. The obtained results clearly indicate the advantage of the stepped-impedance line, which allows for well over 50% size reduction as compared with the reference case (conventional feed line). Furthermore, increasing the number of feed line sections leads to considerable improvement of the miniaturisation rate (at the expense of more challenging design process). It is also of fundamental importance that all antenna parameters are adjusted

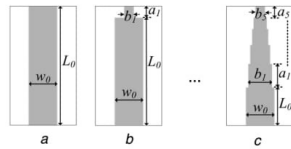


Fig. 1 Stepped-impedance feed line
(a) Conventional (unmodified) line, (b) Two sections, (c) Five sections

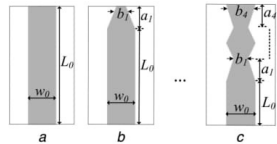


Fig. 2 Multi-section taper feed line
(a) Conventional (unmodified) line, (b) Two sections, (c) Five sections

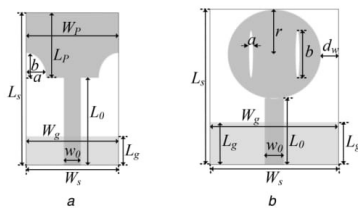


Fig. 3 Benchmark set of two UWB monopole antennas
(a) Antenna I, (b) Antenna II

Table 1 Footprint areas of the optimised antennas

Feed line modif.	Antenna footprint area, mm ²			
	Stepped-impedance line		Taper line	
	Antenna I	Antenna II	Antenna I	Antenna II
flat feed	539	780	539	780
($n = 2$)	472	544	490	558
($n = 3$)	374	463	453	456
($n = 4$)	344	406	410	418
($n = 5$)	282	372	367	394
($n = 6$)	230	356	—	—

n denotes the number of sections in the feed line.

simultaneously. This is evident by observing the fact that all antenna dimensions (not only feed-related ones) are different at the respective optimum designs for various values of the number of sections n . Experimental results have been provided for selected antenna prototypes for the sake of supplementary verification. The main contributions of the work can be summarised as follows: (i) systematic investigation of particular types of feeding structures and their effect on antenna miniaturisation capability, (ii) comprehensive study concerning feed complexity versus minimum antenna footprint that can be obtained for a given number of degrees of freedom of the feed, (iii) demonstration of the numerical optimisation tools that can be used to determine the most suitable geometry modifications (here, feed-related) in a given design context (here, size reduction). None of these have been reported in the literature so far.

2 Feed line modifications and case studies

This research presents a systematic investigation of two types of feed line geometries, namely, a stepped-impedance and a multi-section taper one. The objective is to determine the miniaturisation ratio that can be achieved by means of endowing the antenna structure with the above feed lines. Various structural complexities of the lines are considered controlled by the number n of sections

as shown in Figs. 1 and 2. The benchmark set of two monopole antennas has been shown in Fig. 3. The antennas are implemented on a Rogers substrate with a thickness of 0.76 mm and $\epsilon_r = 3.55$. The computational models of the structures are implemented in CST Microwave Studio [22] and simulated using their time domain solver. The models incorporate the SubMiniature version A connectors in order to ensure better agreement between simulated and measured results. Initially, the antennas are designed and optimised using a conventional (unmodified) feed line. These structures are used as reference designs. Design parameters for both antennas are as follows: $x^1 = [L_g \ L_0 \ L_p \ W_p \ a \ b]^T$ and $x^2 = [L_g \ L_0 \ r \ a \ b \ d_w]^T$. All dimensions are in mm. The numerical values for the optimised reference antennas are $x^{*1} = [8.910.214.821.80.430.38]^T$ and $x^{*2} = [9.289.4810.30.405.174.0]^T$. Upon applying a particular feed line modification, antenna geometry parameters are extended as shown in Figs. 1 and 2. The reference antennas are used to compare the results with the modified feed line antennas, in particular, to evaluate the effect of a particular feed line technique on the miniaturisation rate of the structures. For the sake of design optimisation, all antenna geometry parameters are made adjustable. The antennas are supposed to operate in the entire UWB frequency range (3.1–10.6 GHz).

3 Antenna miniaturisation through numerical optimisation

As mentioned in the introduction, finding the optimum values of geometry parameters is an important (and challenging) part of the design process. Here, the design is oriented towards reducing the antenna size, represented by $A(x)$, where x is a vector of independent parameters of the structure at hand. In this work, we consider a single constraint, which is to maintain acceptable antenna matching within the UWB frequency range. Thus, the design optimisation problem can be written as

$$x^* = \arg \min_x \{A(x), S(x) \leq -10 \text{ dB}\}, \quad (1)$$

where $S(x)$ denotes the maximum in-band reflection level. Here, the constraint is treated explicitly, and the optimisation method of choice is a pattern search algorithm [23], which is a derivative-free, stencil-based routine, incorporating grid-restricted line search, and a neighbour search. Since pattern search requires a feasible starting point, the initial design is the one optimised for the best matching (problem formulation: $x^* = \text{argmin}\{x; S(x)\}$). It should be emphasised that the formulation (1) is generic and can be used to handle antenna structures with any types of feeding structures.

4 Results and discussion

The benchmark antenna structures of Fig. 3 have been optimised for minimum size using the unmodified feed line, and, subsequently, the stepped-impedance and the tapered lines of various complexities. The optimisation process was carried out as described in Section 3, i.e. to ensure the reflection response does not exceed -10 dB for the entire UWB frequency range. The optimised antenna footprints corresponding to each feed line variation have been collected in Table 1. From the results, it can be inferred that increasing the feed line complexity has a clear (and positive) effect on the miniaturisation rate obtained and that the stepped-impedance line outperforms the tapered one. The results are consistent for both antenna structures; however, the difference is more pronounced for Antenna I. Fig. 4 shows a visualisation of the antenna footprint dependence on the feed line complexity. The plots indicate that further increase of the feed line complexity might be beneficial in terms of providing an additional size reduction.

The reflection response corresponding to each feed-line section is shown in Fig. 5a. It should be noted that all responses satisfy the requirement $|S_{11}| < -10$ dB for the entire UWB frequency range. Furthermore, bandwidth enhancement beyond 10.6 GHz is

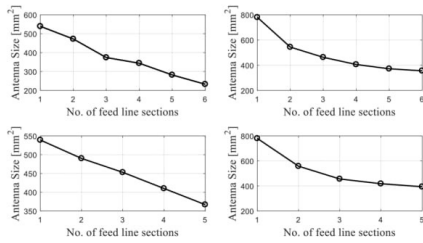


Fig. 4 Optimised antenna size as a function of the number of feed line sections. From top-left to the bottom-right panel, shown are: Antenna I with stepped-impedance feed line, Antenna II with stepped-impedance feed, Antenna I with the tapered line, and Antenna II with the tapered line, respectively

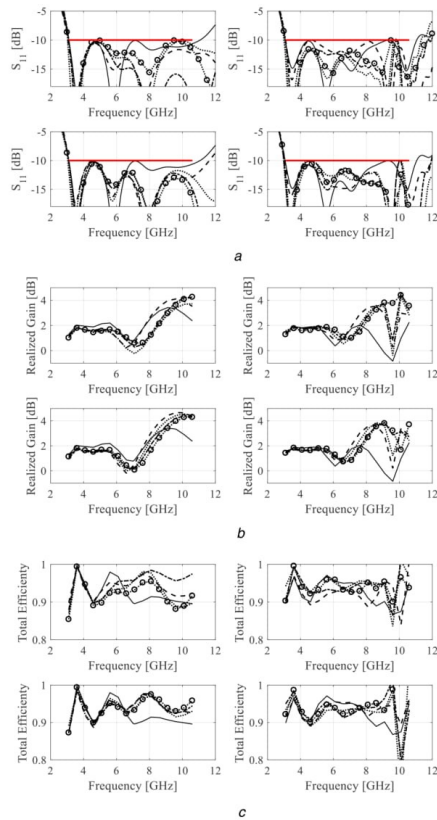


Fig. 5 Reflection response, realised gain, and total efficiency of size-optimised antennas with unmodified feed line (—), two-sections (---), three-sections (....), four-sections (-.-), five-sections (ooo), and six-sections (xxx). The top and bottom plots correspond to the stepped-impedance and multi-section feed line of Antenna I and Antenna II, respectively (a) Reflection response, (b) Realised gain and (c) Total efficiency

observed as a result of utilising the considered feed-line configuration as compared with the unmodified feed line. This is, however, just a by-product benefit as the bandwidth enhancement has not been the objective of this work. The realised gain characteristics have been shown in Fig. 5b. No overall degradation is being observed due to the feed-line modifications. In contrast, gain improvement is observed at higher frequencies as a

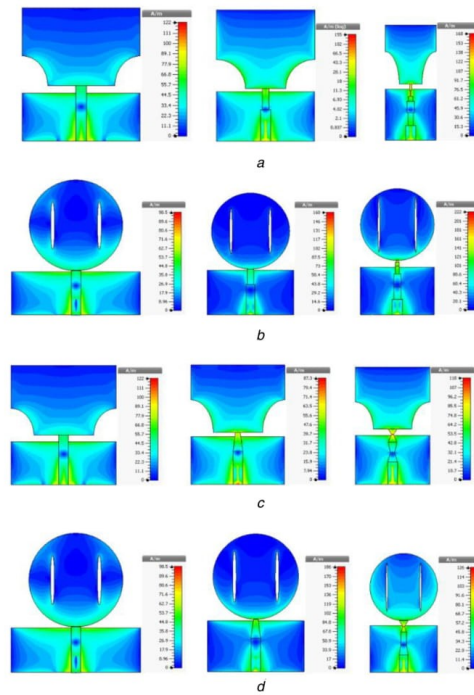


Fig. 6 Current distributions of the optimised UWB antennas at 7 GHz (a) Antenna I with unmodified feed, two- and six-section stepped-impedance feed line, (b) Antenna II with unmodified feed, two and six-section stepped-impedance feed line, (c) Antenna I with unmodified feed, two and five-section tapered feed line, and (d) Antenna II with unmodified feed, two and five-section tapered line

consequence of the applied feed-line configurations. Fig. 5c shows the total efficiency of the antenna structures which is above 90% for the entire UWB frequency range. This is another indication that feed line modification is a practical way to reduce the antenna size (upon proper adjustment of all antenna dimensions) without degrading the electrical and field properties. Fig. 6 shows the current distribution over the antenna surface at 7 GHz. It can be inferred from the figure that the energy from the source provided to the radiator has been transformed due to the feed line modifications and the current density has been increased along the edges of the radiator. It was also clear from the animation that more and more of energy from the source is transmitted to the edges of the radiator as the frequency increases (especially in the case of the modified feed line structures). Meanwhile, the current density starts decreasing at the ground plane and, consequently, creates a room for antenna miniaturisation. Figs. 7 and 8 show the E - and H -plane radiation patterns of the optimised antennas. All the antennas exhibit a consistent omnidirectional characteristic in E - and H -plane which is the fundamental requirement for UWB wireless applications. A minor effect on the E -plane is observed at 8 GHz frequency. What is important, additional size reduction obtained by increasing the complexity of the feed lines has a minor effect on the radiation characteristics. The Tables 2–5 show the optimised parametric values of each antenna structure due to a particular feed line modification. An important observation is that the geometry parameters of the antenna are considerably different. This means that obtaining a truly optimum design requires simultaneous adjustment of all parameters (not just those of the feed line).

5 Experimental validation

The selected antenna structures have been fabricated (Fig. 9) and measured. For the sake of brevity, only measurements of the

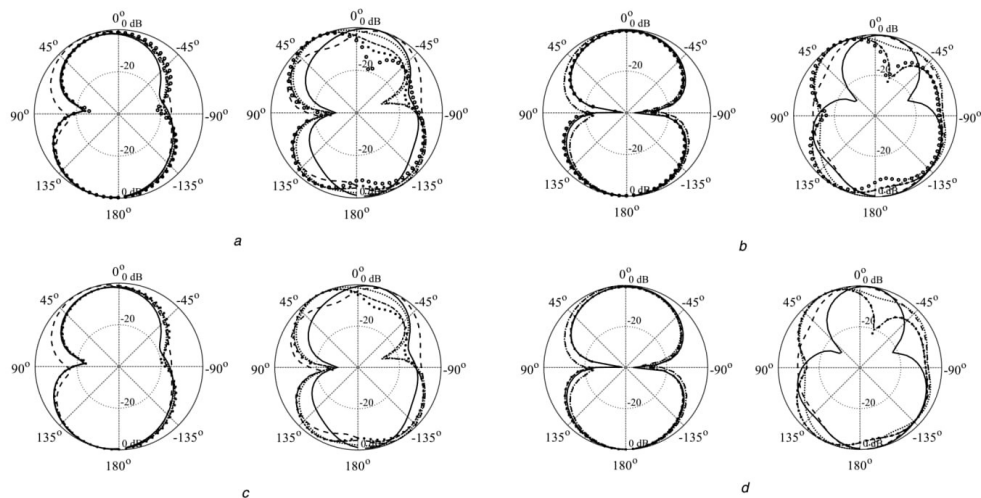


Fig. 7 *E*-plane patterns of size-optimised antennas with unmodified feed line (—), two-sections (---), three-sections (...), four-sections (- · -), five-sections (xx) and six-sections (ooo)
 (a) Antenna I with stepped-impedance feed line, (b) Antenna II with stepped-impedance feed line, (c) Antenna I with a tapered feed line, and (d) Antenna II with a tapered line. The left- and right-hand side plots are for the frequencies 4 and 8 GHz, respectively

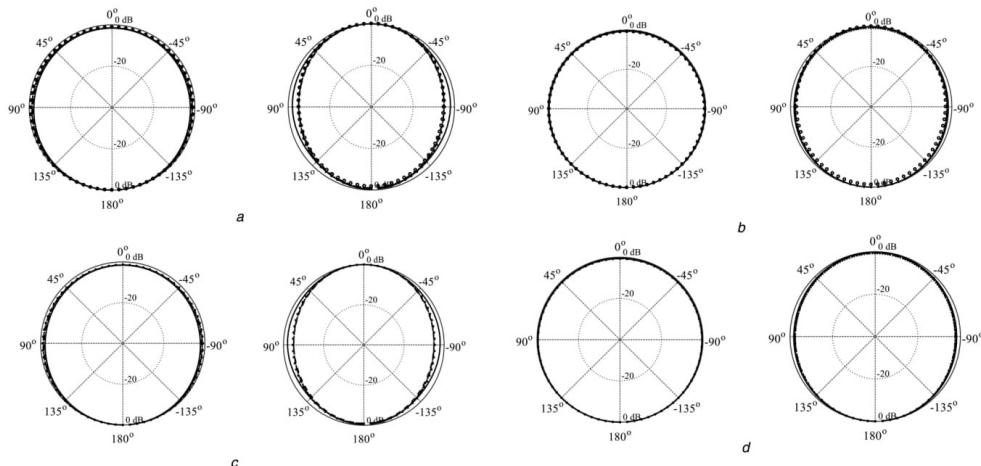


Fig. 8 *H*-plane pattern of size-optimised antennas with unmodified feed line (—), two-sections (---), three-sections (...), four-sections (- · -), five-sections (xx) and six-sections (ooo)
 (a) Antenna I with stepped-impedance feed line, (b) Antenna II with stepped-impedance feed line, (c) Antenna I with a tapered feed line, and (d) Antenna II with a tapered line. The left- and right-hand side plots are for the frequencies 4 and 8 GHz, respectively

Table 2 Geometry parameter values for optimised designs of Antenna I with the stepped-impedance feed line

<i>n</i>	Geometry parameters, mm																	
	L_g	L_0	L_p	W_p	a	b	a_1	a_2	a_3	a_4	a_5	b_1	b_2	b_3	b_4	b_5	L_s	W_s
1	9.9	10.2	14.5	21.7	4.6	4.1	—	—	—	—	—	—	—	—	—	—	24.81	21.72
2	9.4	6.0	15.1	18.7	5.5	3.3	4.0	—	—	—	—	1.22	—	—	—	—	25.14	18.75
3	9.8	4.0	13.1	15.5	4.4	3.0	3.9	2.98	—	—	—	1.21	1.44	—	—	—	24.00	15.5
4	9.3	3.7	12.9	14.4	3.5	2.9	3.0	2.9	1.03	—	—	1.40	1.27	0.73	—	—	23.71	15.5
5	9.4	3.2	13.1	11.9	2.7	2.6	1.95	3.12	1.11	1.07	—	1.36	1.27	0.59	0.35	—	23.58	11.96
6	10.2	2.9	11.8	10.1	2.7	2.7	2.51	2.32	1.0	1.2	1.25	1.00	1.46	0.88	0.15	0.37	23.00	10.00

n denotes the number of steps in the feed line.

Table 3 Geometry parameter values for optimised designs of Antenna II with the stepped-impedance feed line

n	Geometry parameters, mm																	
	L_g	L_0	r	a	b	d_w	a_1	a_2	a_3	a_4	a_5	b_1	b_2	b_3	b_4	b_5	L_s	W_s
1	9.2	9.4	9.7	0.4	5.1	3.7	—	—	—	—	—	—	—	—	—	—	258.97	26.91
2	10.2	7.0	8.7	0.3	5.2	0.92	3.5	—	—	—	—	1.37	—	—	—	—	28.08	19.38
3	10	4.5	7.8	0.2	5.4	0.85	3.7	2.99	—	—	—	1.37	1.28	—	—	—	26.89	17.30
4	9.5	3.3	7.7	0.2	5.4	0.08	3.6	2.22	1.44	—	—	1.37	1.28	0.97	—	—	26.07	15.59
5	9.5	3.3	7.3	0.2	5.4	0.0	2.6	2.33	1.49	0.89	—	1.37	1.36	0.99	0.46	—	25.32	14.67
6	9.4	3.0	7.1	0.2	5.4	0.0	2.5	2.58	1.50	0.78	0.33	1.38	1.36	0.74	0.70	0.40	25.00	14.23

n denotes the number of steps in the feed line.

Table 4 Geometry parameter values for optimised designs of Antenna I with the tapered feed line

n	Geometry parameters, mm													L_s	W_s			
	L_g	L_0	L_p	W_p	a	b	a_1	a_2	a_3	a_4	b_1	b_2	b_3			b_4		
1	9.9	10.2	14.5	21.7	4.6	4.1	—	—	—	—	—	—	—	—	—	—	24.81	21.72
2	9.9	6.91	14.1	19.5	4.5	4.6	3.99	—	—	—	1.00	—	—	—	—	—	25.00	19.57
3	9.9	6.45	13.9	18.2	4.6	3.8	2.73	1.73	—	—	0.68	2.11	—	—	—	—	24.86	18.22
4	10.1	4.71	13.4	16.7	4.35	3.6	2.80	2.00	1.53	—	1.00	1.94	0.30	—	—	—	24.48	16.67
5	10.0	4.6	12.7	15.2	0.48	0.43	1.89	2.11	1.62	1.11	0.84	1.79	0.37	1.84	—	—	24.00	15.22

n denotes the number of steps in the feed line.

Table 5 Geometry parameter values for optimised designs of Antenna II with the tapered feed line

n	Geometry parameters, mm													L_s	W_s			
	L_g	L_0	r	a	b	d_w	a_1	a_2	a_3	a_4	b_1	b_2	b_3			b_4		
1	9.2	9.4	9.7	0.4	5.1	3.7	—	—	—	—	—	—	—	—	—	—	28.97	26.91
2	10.4	6.7	8.7	0.3	5.3	1.1	4.0	—	—	—	0.88	—	—	—	—	—	28.27	19.73
3	10.8	5.5	8.0	0.3	5.27	0.17	3.0	3.0	—	—	0.93	1.41	—	—	—	—	27.75	6.44
4	10.6	4.21	7.5	0.22	5.33	0.22	3.30	2.86	1.40	—	1.0	1.07	0.66	—	—	—	26.89	15.55
5	10.3	3.9	7.4	0.20	5.34	0.0	2.11	2.90	1.22	1.30	1.19	1.23	0.31	2.04	—	—	26.36	14.95

n denotes the number of steps in the feed line.

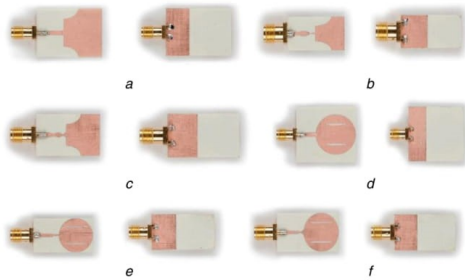


Fig. 9 Photographs of the fabricated antenna prototypes
 (a) Antenna I with an unmodified feed line, (b) Antenna I with stepped-impedance feed, (c) Antenna I with tapered feed, (d) Antenna II with an unmodified feed line, (e) Antenna II with stepped-impedance feed, (f) Antenna II with tapered feed

smallest antennas with six section stepped-impedance and five section tapered feed line are shown. Fig. 10a shows the simulated and measured reflection response that fulfils the criteria for UWB antennas, i.e. below -10 dB for the entire UWB frequency range. It is also noticed that for lower frequencies, i.e. below 8 GHz, the measured response is better than the simulated one. Above 8 GHz, the agreement is very good. Furthermore, a bandwidth enhancement beyond 10.6 GHz (as described in Section 4) is confirmed by the measurements. Fig. 10b shows an acceptable agreement between the simulated and measured realised gain characteristics. The gain varies from 1 to 5 dB in the 3.1–10.6 GHz frequency range. The increase of realised gain is also observed for higher frequencies as it was in the case of simulated gain (cf. Fig. 6).

Figs. 11 and 12 show the simulated and the measured E - and H -plane radiation patterns at 8 and 10 GHz frequencies for co- and cross-polarisation, respectively. It has been observed that the radiation pattern of the size-optimised antennas is almost omnidirectional which is in accordance with the requirements for UWB applications. Furthermore, the measured results exhibit a good agreement with the simulated ones. Here, it can be concluded that the feed line topology alterations permit reduction of the antenna size without affecting its omnidirectional characteristics.

6 Conclusion

In this study, a comprehensive study regarding feed line geometries and their effect in terms of the possible achievable miniaturisation rate on wideband antenna structures has been presented. A benchmark set of two different monopole antennas is used to investigate two different n -sections feed line topologies, namely, the stepped-impedance and the tapered feed lines. A rigorous numerical optimisation of all antenna geometry parameters has been carried out to ensure the minimum size for all antenna-feed configurations.

The results clearly indicate the advantage of the step-impedance feed line over the tapered one. Also, the increasing complexity of the feed line has a significant effect on the miniaturisation rate (both types of feeds). It has also been observed that the electrical performance of the antennas did not degrade due to applying different feedline topologies. Hence, it can be concluded that feed line modifications are a convenient tool for miniaturisation of wideband antennas (under the assumption that the appropriate design closure is conducted in order to yield optimum antenna dimensions). This research can be considered as a step towards the development of systematic procedures for the design of compact monopole antennas. Furthermore, the presented study focuses only on monopole antennas and can be a benchmark to explore the

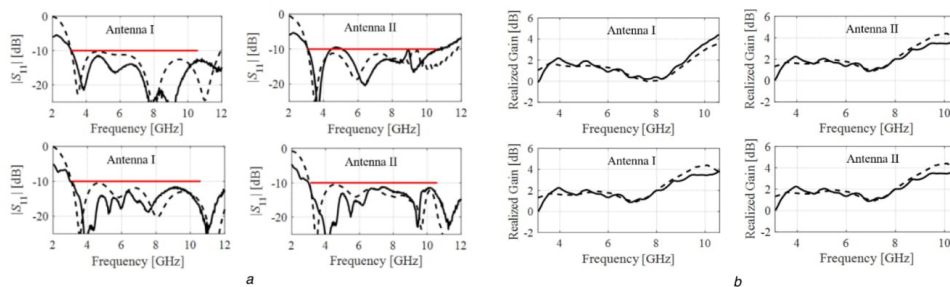


Fig. 10 Simulated (---) and measured (—) reflection responses and realised gain characteristics with six section stepped-impedance and five section tapered feed line: The top and bottom plots correspond to the stepped-impedance and multi-section feed line, respectively
 (a) Reflection response, (b) Realised gain

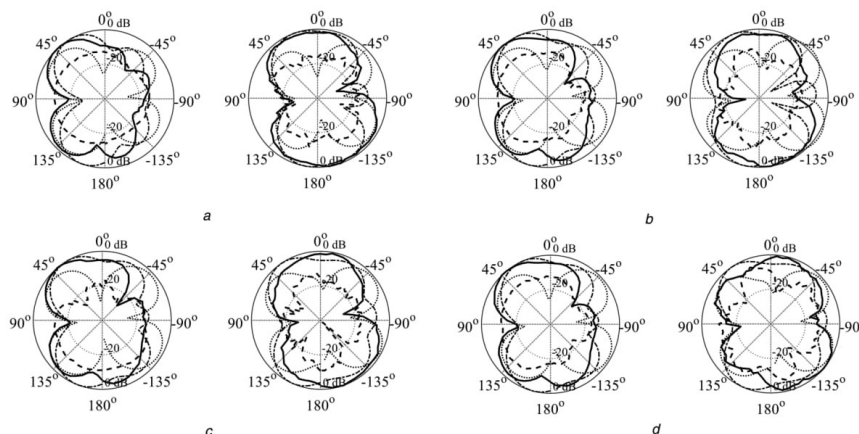


Fig. 11 Simulated and measured E-plane patterns of the size optimised antennas with measured co- (—), simulated co- (---), measured cross- (---), and simulated cross-polarisation (---) with six section stepped-impedance and five section tapered feed line
 (a) Antenna I with stepped-impedance feed line, (b) Antenna II with stepped-impedance feed line, (c) Antenna I with a tapered feed line, and (d) Antenna II with a tapered line. The left- and right-hand side plots are for the frequencies 8 and 10 GHz, respectively

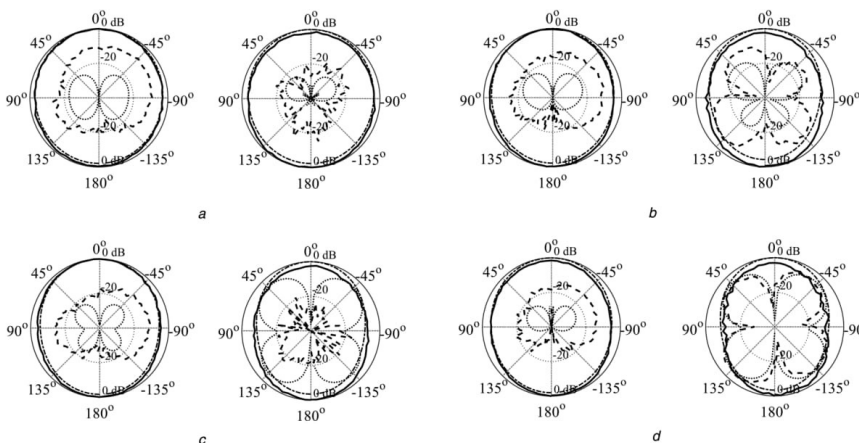


Fig. 12 Simulated and measured H-plane patterns of the size optimised antennas with measured co- (—), simulated co- (---), measured cross- (---), and simulated cross-polarisation (---) with six section stepped-impedance and five section tapered feed line
 (a) Antenna I with stepped-impedance feed line, (b) Antenna II with stepped-impedance feed line, (c) Antenna I with a tapered feed line, and (d) Antenna II with a tapered line. The left- and right-hand side plots are for the frequencies 8 and 10 GHz, respectively

effect of feed line modifications for other types of antenna structures such as monopolar, uniplanar and others.

7 Acknowledgments

The authors would like to thank the Computer Simulation Technology AG, Darmstadt, Germany, for making CST Microwave Studio available. This work was supported in part by the Icelandic Centre for Research (RANNIS) grant no. 174114051, and by the National Science Centre of Poland Grant 2015/17/B/ST6/01857, and by the National Natural Science Foundation of China Grant 61471258.

8 References

- [1] Vendik, I.B., Rusakov, A., Kanjanasit, K., *et al.*: 'Ultrawideband (UWB) planar antenna with single-, dual-, and triple-band notched characteristic based on electric ring resonator', *IEEE Antennas Wirel. Propag. Lett.*, 2017, **16**, pp. 1597–1600
- [2] Wu, C., Chen, Y., Liu, W.: 'A compact ultrawideband slotted patch antenna for wireless USB dongle application', *IEEE Antennas Wirel. Propag. Lett.*, 2012, **11**, pp. 596–599
- [3] Chiu, Y.H., Chen, Y.S.: 'Multi-objective optimization for UWB antennas in impedance matching, gain, and fidelity factor'. IEEE Int. Symp. on Antennas Propagation, Vancouver, BC, Canada, 2015, pp. 1–2
- [4] Liu, J., Esselle, K.P., Hay, S.G., *et al.*: 'Effects of printed UWB antenna miniaturization on pulse fidelity and pattern stability', *IEEE Trans. Antennas Propag.*, 2014, **62**, (8), pp. 3903–3910
- [5] Abbasi, Q.G., Rehman, M.U., Yang, X., *et al.*: 'Ultrawideband band-notched flexible antenna for wearable applications', *IEEE Antennas Wirel. Propag. Lett.*, 2013, **12**, pp. 1606–1609
- [6] Bekasiewicz, A., Koziel, S.: 'Compact UWB monopole antenna for internet of things applications', *Electron. Lett.*, 2016, **52**, (7), pp. 492–494
- [7] Srivastava, G., Mohan, A., Chakrabarty, A.: 'Compact reconfigurable UWB slot antenna for cognitive radio applications', *IEEE Antennas Wirel. Propag. Lett.*, 2017, **16**, pp. 1139–1142
- [8] Sugita, T., Kubo, S., Toya, A., *et al.*: 'A compact 4 × 4 planar UWB antenna array for 3-D breast cancer detection', *IEEE Antennas Wirel. Propag. Lett.*, 2013, **12**, pp. 733–736
- [9] Felegari, N., Nourini, J., Ghobadi, C., *et al.*: 'Broadband CPW-Fed circularly polarized square slot antenna with three inverted-L-shape grounded strips', *IEEE Antennas Wirel. Propag. Lett.*, 2011, **10**, pp. 274–277
- [10] Li, L., Cheung, S.W., Yuk, T.I.: 'Compact MIMO antenna for portable devices in UWB applications', *IEEE Antennas Wirel. Propag. Lett.*, 2013, **61**, (8), pp. 4257–4264
- [11] Qing, X., Chen, Z.N.: 'Compact coplanar waveguide-fed ultra-wideband monopole-like slot antenna', *IET Microw. Antennas Propag.*, 2009, **3**, (5), pp. 889–898
- [12] Nikolaou, S., Abbasi, M.A.B.: 'Design and development of a compact UWB monopole antenna with easily-controllable return loss', *IEEE Trans. Antennas Propag.*, 2017, **65**, (4), pp. 2063–2067
- [13] Srivastava, G., Mohan, A.: 'Compact MIMO slot antenna for UWB applications', *IEEE Antennas Wirel. Propag. Lett.*, 2016, **15**, pp. 1057–1060
- [14] Bekasiewicz, A., Koziel, S.: 'A novel structure and design optimization of miniaturized UWB slot antenna'. Int. Symp. on Antennas Propagation, Fajardo, Puerto Rico, 2016, pp. 1313–1314
- [15] Liu, J., Esselle, K.P., Hay, S.G., *et al.*: 'Achieving ratio bandwidth of 25:1 from a printed antenna using a tapered semi-ring feed', *IEEE Antennas Wirel. Propag. Lett.*, 2011, **10**, pp. 1333–1336
- [16] Li, J.F., Chu, Q.X., Li, Z.H., *et al.*: 'Compact dual band-notched UWB MIMO antenna with high isolation', *IEEE Trans. Antennas Propag.*, 2013, **61**, (9), pp. 4759–4766
- [17] Bekasiewicz, A., Koziel, S.: 'Structure and computationally-efficient simulation-driven design of compact UWB monopole antenna', *IEEE Antennas Wirel. Propag. Lett.*, 2015, **14**, pp. 1282–1285
- [18] Tian, B., Li, Z., Wang, C.: 'Boresight gain optimization of an UWB monopole antenna using FDTD and genetic algorithm'. IEEE Int. Conf. on Ultra-Wideband, Nanjing, China, 2010, vol. 1, pp. 1–4
- [19] Koziel, S., Bekasiewicz, A., Cheng, Q.S., *et al.*: 'On ultra-wideband antenna miniaturization involving efficiency and matching constraints'. IEEE European Antennas and Propagation Conf., Paris, France, 2017
- [20] Koziel, S., Bekasiewicz, A.: 'Multi-objective design of antennas using surrogate models' (World Scientific, London, 2016)
- [21] Koziel, S., Bekasiewicz, A.: 'Fast EM-driven size reduction of antenna structures by means of adjoint sensitivities and trust regions', *IEEE Antennas Wirel. Propag. Lett.*, 2015, **14**, pp. 1681–1684
- [22] CST Microwave Studio, ver. 2015. CST AG, Bad Nauheimer Str. 19, D-64289 Darmstadt, Germany, 2015
- [23] Koziel, S.: 'Computationally efficient multi-fidelity multi-grid design optimization of microwave structures', *Appl. Comput. Electromagn. Soc. J.*, 2010, **25**, (7), pp. 578–586

Chapter 7

7 Paper [J6]

Muhammad Aziz ul Haq, and Slawomir Koziel

Quantitative assessment of wideband antenna geometry modifications for size-reduction-oriented design

Published: International Journal of Electronics and Communications, vol. 90, pp. 45-52, 2018.

DOI: <https://doi.org/10.1016/j.aeue.2018.04.007>



Contents lists available at ScienceDirect

Int. J. Electron. Commun. (AEÜ)

journal homepage: www.elsevier.com/locate/aeue

Regular paper

Quantitative assessment of wideband antenna geometry modifications for size-reduction-oriented design



Muhammad Aziz ul Haq*, Slawomir Koziel

Engineering Optimization & Modeling Center, Reykjavik University, Reykjavik, Iceland

ARTICLE INFO

Keywords:

Wideband antennas
Antenna miniaturization
Ground plane modifications
Feed line
Radiator
EM-driven optimization

ABSTRACT

Incorporation of various topological modifications to basic antenna structures is a common strategy in the context of size-reduction-oriented design. Modifications can be applied to the ground plane, the feed line, and/or antenna radiator, and may lead to achieving smaller physical dimensions of the antenna at hand. Unfortunately, various topology alteration options are normally reported on a case-to-case basis; systematic comparisons of different modification types are lacking in the literature. In this paper, thorough investigations of selected topological changes in terms of their effect on antenna size reduction are carried out. Numerical experiments are performed using two ultra-wideband monopoles. In order to ensure a fair comparison, for each antenna topology, all geometry parameters are rigorously optimized to obtain the minimum footprint while maintaining acceptable electrical performance. The results clearly indicate the advantage of feed line modifications (56% average physical size reduction) over a ground plane and radiator ones (43% and 2.15% respectively). Experimental validations confirming the numerical findings are also provided.

1. Introduction

In modern communication systems, miniaturization of wideband antennas is an important design criterion, originating from the necessity of mounting them within compact devices such as wearable ones [1] or related to the Internet of Things (IoT) [2], cognitive radio [3], microwave imaging [4], Wi-Fi, Wi-MAX, and UWB applications [5]. At the same time, reduction of the physical dimensions of the antenna affects its electrical properties due to disturbance of the current path and may result in performance degradation, among others, difficulties in ensuring required impedance bandwidth. Moreover, size reduction may also affect field properties such as radiation pattern stability, gain, and efficiency [6]. Consequently, the design of miniaturized wideband antennas with acceptable performance is not a trivial task.

Perhaps the most widely used approach to antenna size reduction is incorporation of various geometry modifications into the basic antenna structures. There are plenty of examples available in the literature, e.g., an exponential slot edge applied in a Vivaldi antenna [7], a C-shape radiator [8], a bending microstrip feed line [9], rectangular slots edge on a radiator [10], or a differential stepped slot [11]. These and other examples represent case studies, and hardly any systematic investigations have reported in the literature regarding the comparison of different topology modification techniques and their effects on antenna miniaturization rate and electrical performance.

Another critical issue—apart from setting up the antenna topology—is a proper adjustment of geometry parameters of the structure so that an accurate optimum design can be obtained. Majority of researchers utilize experience-driven parameter sweeping [12], which typically yields designs that are acceptable, but definitely not optimal. Especially in case of complex antenna topologies, simultaneous adjustment of all geometry parameters through numerical optimization is a necessity due to various and sometimes subtle interactions between parameters that cannot be detected by handling one or two parameters at a time [13]. There is a large variety of optimization algorithms available, including local search methods (gradient-based [14] and derivative-free [15,16]), as well as global search algorithms such as genetic algorithms [17], particle swarm optimizers [18], and differential evolution [19]. Many of these algorithms have been applied for antenna design [20–22].

In this work, a comprehensive study has been carried out in relation to wideband antenna geometry modifications (concerning a ground plane, a feed line, and a radiator) having in mind their effect on antenna miniaturization rate. The study is performed using a benchmark set of two wideband monopole antennas. The feed line and a ground plane modifications considered here are multi-section stepped-impedance lines and slits below the feed line, respectively. For a radiator, rectangular, circular and elliptical slits are investigated. EM-driven optimization is performed to obtain minimum-size designs with acceptable

* Corresponding author.

E-mail addresses: muhammadu16@ru.is (M.A. ul Haq), koziel@ru.is (S. Koziel).<https://doi.org/10.1016/j.aeue.2018.04.007>

Received 27 November 2017; Accepted 4 April 2018

1434-8411/ © 2018 Elsevier GmbH. All rights reserved.

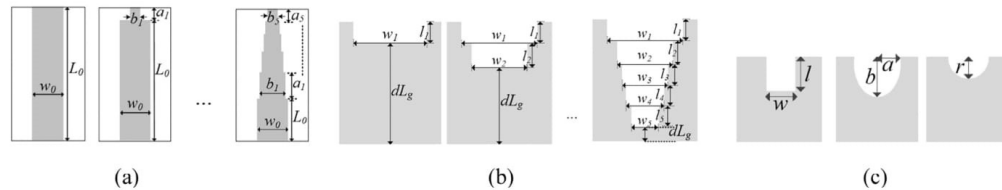


Fig. 1. Selected topological modifications for benchmark UWB monopole antennas. (a) Stepped-impedance feed line complexity, (b) ground plane modifications up to five-section slit, and (c) radiator modifications: rectangular, elliptical and circular, respectively.

electrical performance. The results indicate superiority of feed line modification (average miniaturization rate of 56%) over a ground plane and radiator modifications (miniaturization rates of 43% and 2.15%, respectively). Experimental results are also provided for selected antenna prototypes for the sake of auxiliary verification.

2. Antenna modifications and case studies

In this work, a detailed study related to the topological modifications of conventional wideband antenna structures is carried out. Specific selected modifications are applied to antenna ground plane, feed line and radiator as shown in Fig. 1. The purpose of this study is to determine the overall effect of the considered modifications on physical size of the antenna, in particular, on its achievable miniaturization rate. Two monopole wideband antennas shown in Fig. 2 are used as a benchmark set. Both antennas are implemented on a 0.762 mm thick RF-35 substrate with ($\epsilon_r = 3.5$). CST Microwave Studio [23] is used to simulate the computational models of the structures. Antenna models are also integrated with SMA connectors to ensure better agreement between simulated and measured results. The design variable vectors for Antenna I and II are $\mathbf{x}_1 = [L_g L_p W_p a b]^T$ and $\mathbf{x}_2 = [L_g L_0 r a b d_w]^T$. All dimensions are in mm. The initial numerical values for both antenna design structures are $\mathbf{x}_1^{(0)} = [8.9 \ 10.2 \ 14.8 \ 21.8 \ 0.43 \ 0.38]^T$ and $\mathbf{x}_2^{(0)} = [9.28 \ 9.48 \ 10.3 \ 0.40 \ 5.17 \ 4.0]^T$. Both vectors are extended upon applying particular modifications to antenna components as shown in Fig. 1. The antennas are to operate in the standard UWB frequency range (3.1–10.6 GHz).

3. Design optimization approach

The objective is to determine the minimum antenna footprint while satisfying the condition $S(\mathbf{x}) \leq -10$ dB. Here, $S(\mathbf{x})$ is the maximum reflection level for the entire UWB frequency range (from 3.1 GHz to 10.6 GHz) and \mathbf{x} denotes the adjustable geometry parameters of the structure to be optimized (cf. Section 2). $A(\mathbf{x})$ denotes the antenna size. The design problem is therefore formulated as

The design problem is therefore formulated as

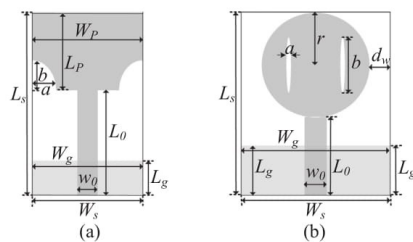


Fig. 2. Benchmark set of two UWB monopole antennas: (a) Antenna I, (b) Antenna II.

$$\mathbf{x}^* = \underset{\mathbf{x}}{\operatorname{argmin}}\{A(\mathbf{x})\}, \quad S(\mathbf{x}) \leq -10 \text{ dB} \quad (1)$$

The problem (1) is solved using a pattern search algorithm [17]. The starting point is a design obtained by minimizing $S(\mathbf{x})$. The reason for such a procedure is twofold: (i) the pattern search routine requires a feasible starting point, (ii) optimization-wise, the problem (1) is easier to solve when starting from the best possible $S(\mathbf{x})$, i.e., the interior of the feasible region rather than by traversing the feasible region boundary.

A pattern search implementation utilized here [18] is a derivative-free stencil-based search routine that consists of several steps executed sequentially:

- Estimation of the objective function gradients based on on-grid design perturbations.
- Grid-restricted line search.
- Poll search (i.e., nearest neighbor search) in case of a failure of the line search, further extended in the direction of the best design found.
- Grid refinement in case of a failure of the poll search.

Termination condition for the pattern search is grid refinement beyond a user-defined minimum size (here, 10^{-3}).

Optimization for minimum reflection is arranged differently,

Table 1
Antenna dimensions with feed line modifications.

Antenna #	Optimized antenna footprint area [mm ²]					
	Ref. antenna	$n = 2$	$n = 3$	$n = 4$	$n = 5$	$n = 6$
Antenna I	539	472	374	344	282	233
Antenna II	780	544	463	406	372	356

ⁿ n denotes number of feed-line sections.

Table 2
Antenna dimensions with ground plane modifications.

Antenna #	Optimized antenna footprint area [mm ²]					
	Ref. antenna	$n = 1$	$n = 2$	$n = 3$	$n = 4$	$n = 5$
Antenna I	539	491	431	326	270	238
Antenna II	780	635	557	496	458	435

ⁿ n denotes number of ground plane sections.

Table 3
Antenna dimensions with radiator modifications.

Antenna #	Optimized antenna footprint area [mm ²]			
	Ref. antenna	Rect. slit	Ellipt. slit	Circ. slit
Antenna I	539	538	533	528
Antenna II	780	751	768	746

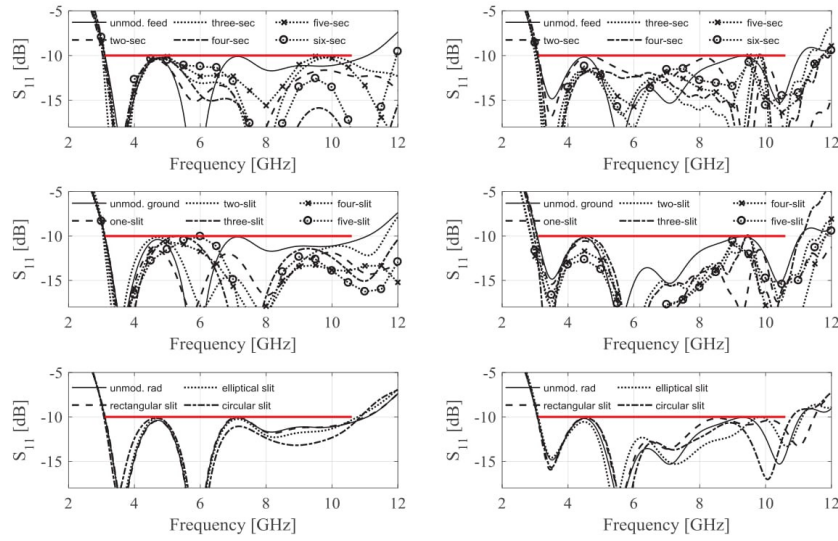


Fig. 3. Reflection coefficient of size-optimized antennas. The left- and right-hand side plots correspond to Antenna I and Antenna II, respectively.

namely, we utilize a trust-region (TR) [24] gradient search algorithm with the antenna response Jacobians estimated through finite differentiation. TR-embedded gradient-based routine is generally faster, however, it is not suitable for handling explicit constraints (as in (1)).

4. Numerical results

The benchmark antennas have been optimized for minimum size using the methodology of Section 3. Tables 1–3 show the optimized

antenna footprints for the three types of geometry modifications discussed in Section 2, respectively. It can be observed that increasing the complexity of the feed line and the ground plane has a significant effect on antenna miniaturization rate. Furthermore, numerical results of Tables 2 and 3 illustrate the superiority of feed line modifications (in the context of antenna miniaturization) as compared to the ground plane modifications. On the other hand, Table 3 indicates a minor impact of radiator modifications compared to the feed and ground plane ones. Yet, it is still noticeable for Antenna II. Hence, it can be

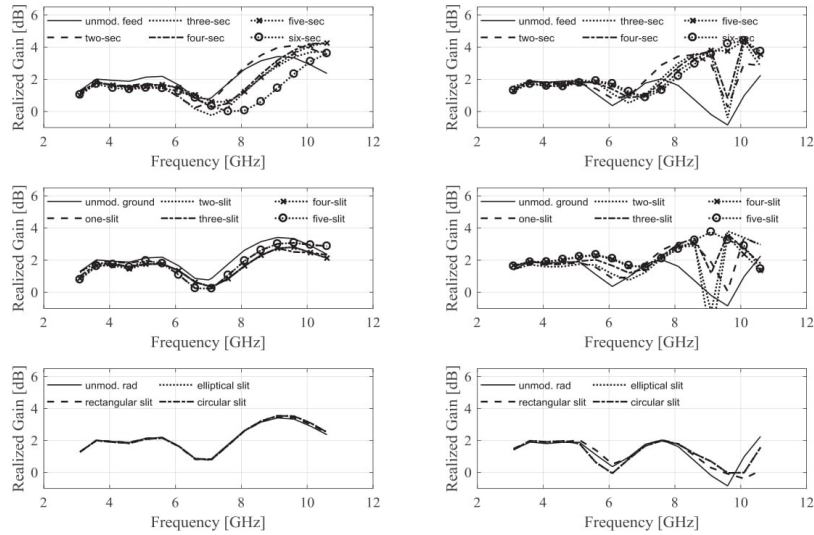


Fig. 4. Realized gain of size-optimized antennas. The left- and right-hand side plots correspond to Antenna I and Antenna II, respectively.

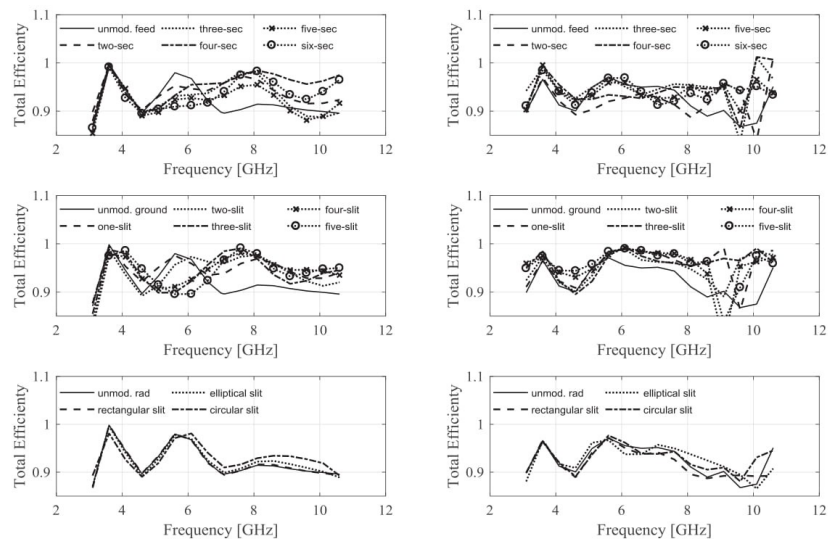


Fig. 5. Total efficiency of size-optimized antennas. The left- and right-hand side plots correspond to Antenna I and Antenna II, respectively.

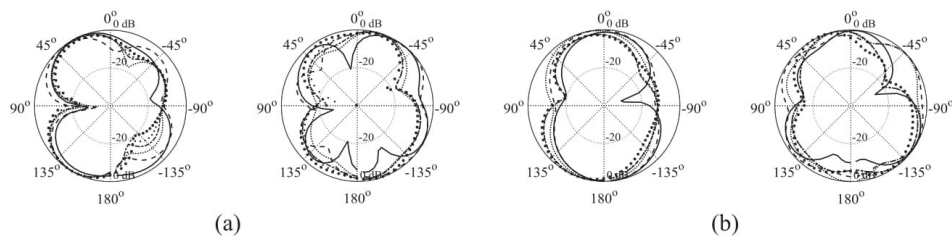


Fig. 6. Feed line modifications. E-Plane patterns of size-optimized antennas with unmodified feed line (—), two-sections (---), three-sections (····), four-sections (— · —), five-sections (xxx) and six-sections (ooo): (a) Antenna I, and (b) Antenna II. The left- and right-hand side plots are for the frequencies 6 GHz and 10 GHz, respectively.

concluded that radiator modification technique may or may not be suitable for antenna miniaturization depending upon the structure of the radiator. In short, modifying the feed line turns out to be a more efficient technique in the context of antenna miniaturization as compared to the ground plane and radiator ones. It should be reiterated that simultaneous adjustment of all geometry parameters of respective antennas (both related to particular modifications and the basic structure itself) is critical to obtain the optimum design and, therefore, to properly assess the importance of specific topological alterations. Note that for the sake of brevity, only the overall antenna footprints (instead of particular antenna geometry parameter values) are shown in Tables 1–3.

Figs. 3–8 show simulated characteristics of the benchmark antennas with and without modifications. It is worth noticing that the maximum in-band reflection for all designs is very close to -10 dB which confirms desired performance of the optimization procedure but also the fact that the obtained designs are the optimum ones. More specifically, as size reduction is in conflict with maintaining the required impedance bandwidth, the constraint $S(x) \leq -10$ dB is expected to be active at the minimum-size designs which is actually the case. Furthermore, an

interesting phenomenon is observed, which is the extension of the bandwidth (especially at higher frequencies) as compared to unmodified antennas. The characteristics of Fig. 4 indicate that size reduction due to topology modifications is achieved without gain degradation. As a matter of fact, in majority of cases, realized gain is improved at higher frequencies. Total efficiency is above 90% for entire UWB band in most of the cases. Furthermore, as a consequence of antenna modifications, an efficiency improvement can be observed at higher frequencies.

Figs. 6–8 show the E-plane radiation patterns of the antennas at 6 GHz and 10 GHz frequency. Almost an omnidirectional characteristic has been observed which is the fundamental requirement for any antenna to operate in UWB frequency range.

5. Experimental validation

Selected designs of Section 4 have been fabricated and measured. Fig. 9 shows the photographs of the antenna prototypes. Figs. 10–14 show the measured and simulated results for Antenna I and Antenna II. For the sake of brevity, only the results corresponding to the smallest

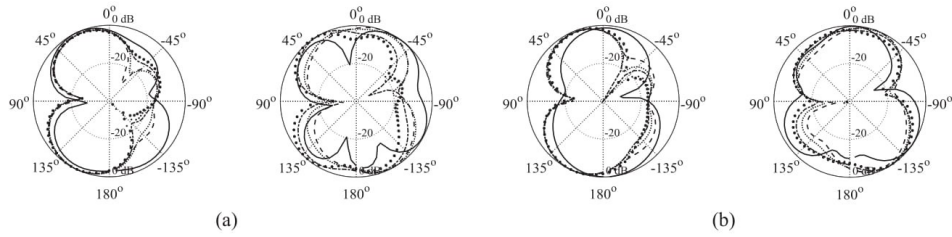


Fig. 7. Ground plane modifications. E-Plane patterns of size-optimized antennas with unmodified ground plane (—), two-sections (---), three-sections (...), four-sections (-.-), five-sections (xxx) and six-sections (ooo): (a) Antenna I, and (b) Antenna II. The left- and right-hand side plots are for the frequencies 6 GHz and 10 GHz, respectively.

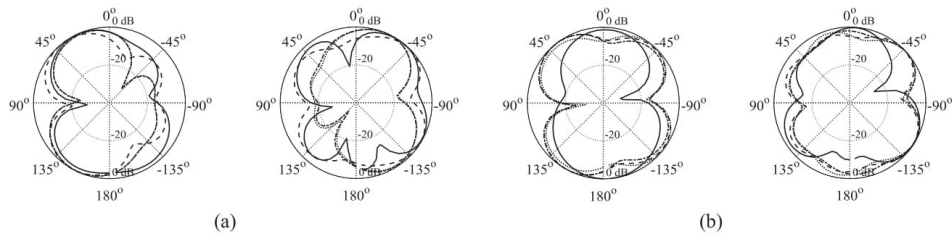


Fig. 8. Radiator modifications. E-Plane patterns of size-optimized antennas with unmodified radiator (—), two-sections (---), three-sections (...), four-sections (-.-), five-sections (xxx) and six-sections (ooo): (a) Antenna I, and (b) Antenna II. The left- and right-hand side plots are for the frequencies 6 GHz and 10 GHz, respectively.

antennas (for each case of feed line, ground plane and radiator modification) have been shown. The reflection responses of all antennas satisfy the condition $S_{11} \leq -10$ dB (cf. Fig. 10). The phenomena of bandwidth enhancement is also confirmed through the measured results as discussed in Section 4. Fig. 11 indicates acceptable agreement

between simulated and measured realized gain. Figs. 12–17 show the E- and H-plane characteristics of all antennas (for all considered modification cases) in term of co- and cross-polarization at 6 and 10 GHz. The basic reason to illustrate the radiation pattern is to confirm omnidirectional characteristics of all antennas within the UWB frequency

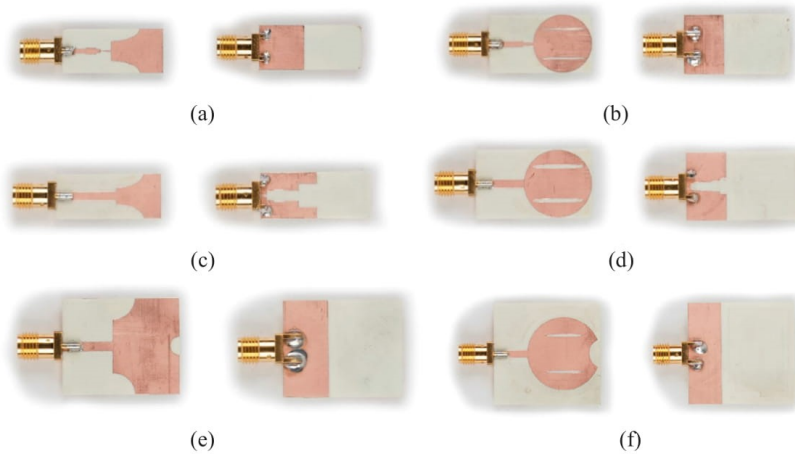


Fig. 9. Photographs of the fabricated antenna prototypes: (a) Antenna I with stepped-impedance feed, (b) Antenna II with stepped-impedance feed, (c) Antenna I with ground plane modification, (d) Antenna II with ground plane modification, (e) Antenna I with a circular slit at radiator, (f) Antenna II with circular slit at radiator.

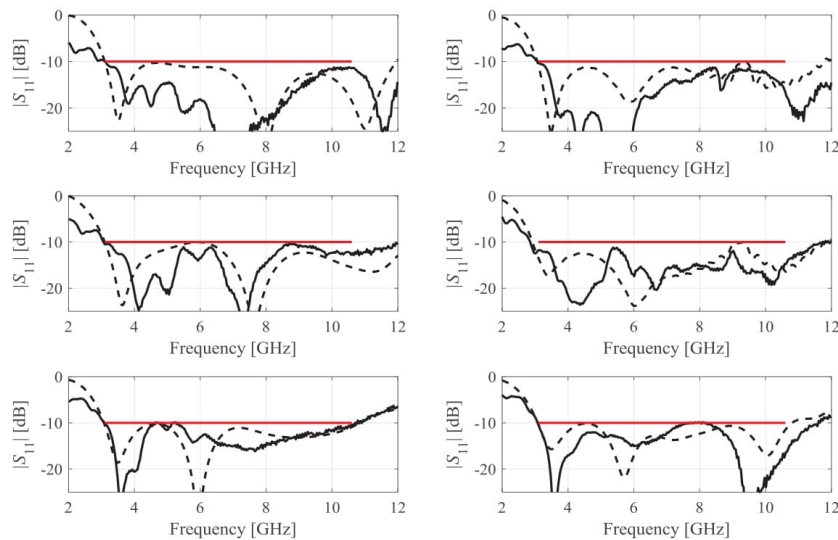


Fig. 10. Simulated (—) and measured (---) reflection of size-optimized antennas. The left- and right-hand side plots are corresponding to Antenna I and Antenna II, respectively.

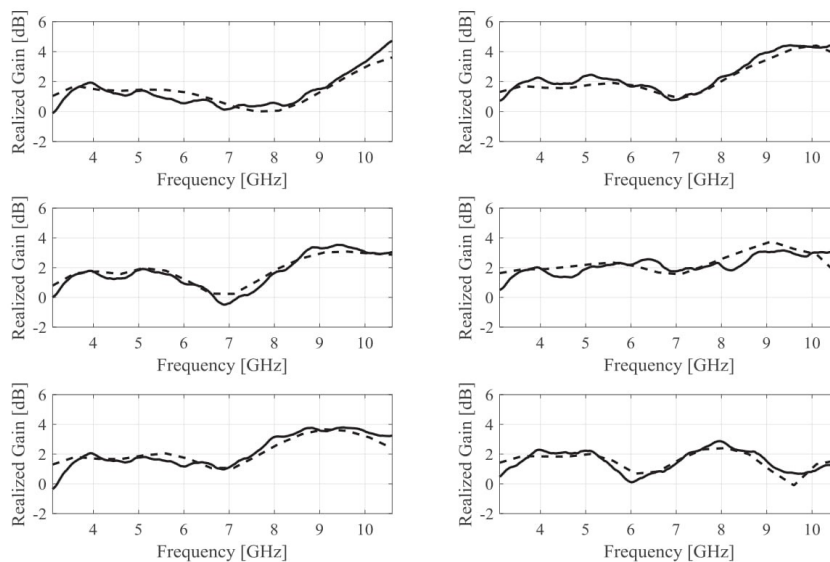


Fig. 11. Simulated (—) and measured (---) realized gain of size-optimized antennas. The left- and right-hand side plots are corresponding to Antenna I and Antenna II, respectively.

range. In short, the measured results verify acceptable performance of the modified antennas from the point of view of UWB applications.

6. Conclusion

In this paper, a comprehensive study related to component modifications (pertinent to the feed line, the ground plane, and the radiator)

of wideband antennas and their effects on antenna miniaturization has been presented. Rigorous numerical optimization of all antenna geometry parameters has been executed to minimize physical dimensions of the antenna structures while ensuring acceptable electrical properties. Our numerical results indicate superiority of feed line modifications with the average of 56% physical size reduction, as compared to a ground plane and radiator modification (43% and 2.15% size

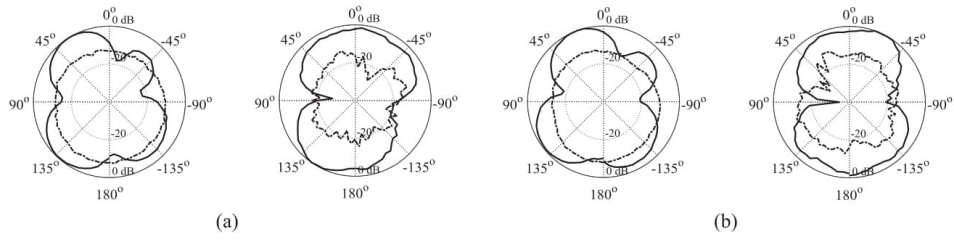


Fig. 12. Measured E-plane Co- (—) and Cross-polarization (---) of size-optimized antennas with six section stepped-impedance feed line: (a) Antenna I, (b) Antenna II. The left- and right-hand side plots are for the frequencies 6 GHz and 10 GHz, respectively.

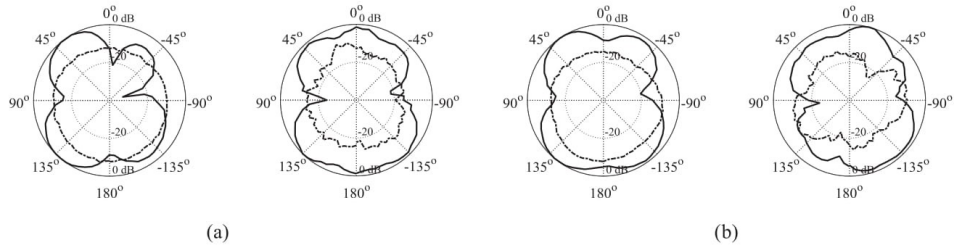


Fig. 13. Measured E-plane Co- (—) and Cross-polarization (---) of size-optimized antennas with five section ground plane slit: (a) Antenna I, (b) Antenna II. The left- and right-hand side plots are for the frequencies 6 GHz and 10 GHz, respectively.

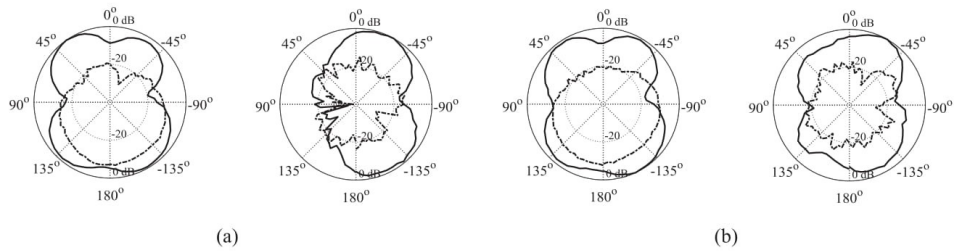


Fig. 14. Measured E-plane Co- (—) and Cross-polarization (---) of size-optimized antennas with circular slit on the radiator: (a) Antenna I, (b) Antenna II. The left- and right-hand side plots are for the frequencies 6 GHz and 10 GHz, respectively.

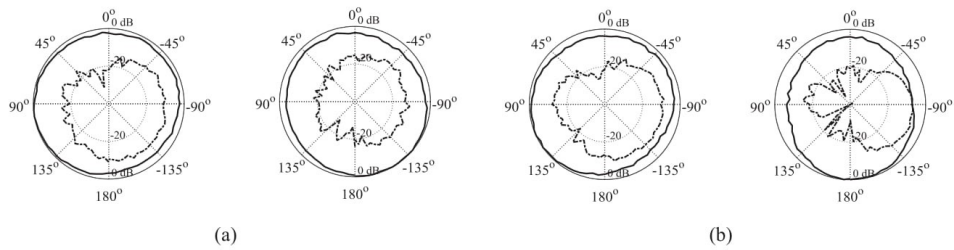


Fig. 15. Measured H-plane Co- (—) and Cross-polarization (---) of size-optimized antennas with six section stepped-impedance feed line: (a) Antenna I, (b) Antenna II. The left- and right-hand side plots are for the frequencies 6 GHz and 10 GHz, respectively.

reduction, respectively). The measured results confirm the correctness of numerical findings. The presented study can be considered a step towards systematic investigation of topology modifications in the context of wideband antenna miniaturization. In particular, similar studies

performed on large antenna benchmark sets may be used to determine the most beneficial classes of geometry alterations as well as their effects on overall performance of antenna structures for particular applications.

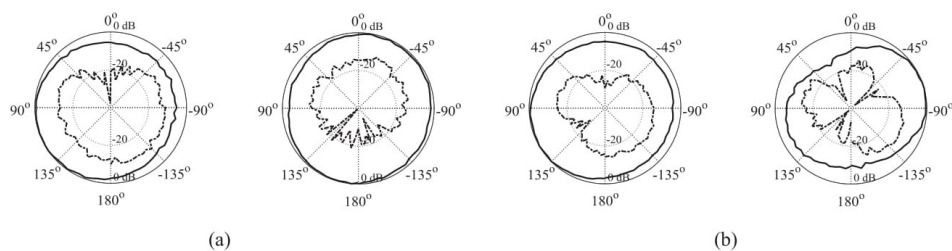


Fig. 16. Measured H-plane Co- (—) and Cross-polarization (---) of size-optimized antennas with five section ground plane slit: (a) Antenna I, (b) Antenna II. The left- and right-hand side plots are for the frequencies 6 GHz and 10 GHz, respectively.

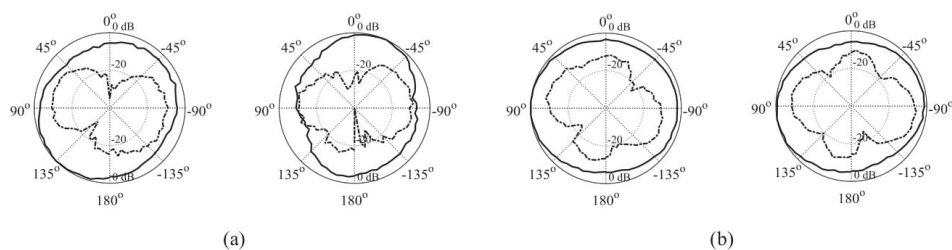


Fig. 17. Measured H-plane Co- (—) and Cross-polarization (---) of size-optimized antennas with circular slit on the radiator: (a) Antenna I, (b) Antenna II. The left- and right-hand side plots are for the frequencies 6 GHz and 10 GHz, respectively.

References

- [1] Abbasi QH, Rehman MU, Yang X, Alomainy A, Qaraqe K, Serpedin Q. Ultrawideband band-notched flexible antenna for wearable applications. *IEEE Antennas Wirel Propag Lett* 2013;12:1606–9.
- [2] Haq MA, Koziel S. Design optimization and trade-offs of miniaturized wideband antenna for internet of things applications. *Metrol Meas Syst* 2017;24(3):463–71.
- [3] Srivastava G, Mohan A, Chakrabarty A. Compact reconfigurable UWB slot antenna for cognitive radio applications. *IEEE Antennas Wirel Propag Lett* 2017;16:1139–42.
- [4] Moosazadeh M, Kharkovsky S, Case JT, Samali B. Improved radiation characteristics of small antipodal Vivaldi antenna for microwave and millimeter-wave imaging applications. *IEEE Antennas Wirel Propag Lett* 2017;16:1961–4.
- [5] Khariche S, Reddy GS, Mukherjee B, Gupta R, Mukherjee J. MIMO antenna for Bluetooth, Wi-Fi, Wi-MAX and UWB applications. *Prog Electromagn Res C* 2014;52:53–62.
- [6] Chen ZN, See TSP, Qing X. Small printed ultrawideband antenna with reduced ground plane effect. *IEEE Trans Antennas Propag* 2007;55(2):383–8.
- [7] Oliveira AMD, Perotoni MB, Kofuji ST, Justo JF. A palm tree antipodal Vivaldi antenna with exponential slot edge for improved radiation pattern. *IEEE Antennas Wirel Propag Lett* 2015;14:1334–7.
- [8] Tang H, Wang K, Wu R, Yu C, Zhang J, Wang X. A novel broadband circularly polarized monopole antenna based on C-shaped radiator. *IEEE Antennas Wirel Propag Lett* 2017;16:964–7.
- [9] Pandey GK, Verma H, Meshram MK. Compact antipodal Vivaldi antenna for UWB applications. *Electron Lett* 2015;51(4):308–10.
- [10] Teni G, Zhang N, Qiu J. Research on a novel miniaturized antipodal Vivaldi antenna with improved radiation. *IEEE Antennas Wirel Propag Lett* 2013;12:417–20.
- [11] Li W, Tu Z, Chu Q, Wu X. Differential stepped-slot UWB antenna with common-mode suppression and dual sharp-selectivity notched bands. *IEEE Antennas Wirel Propag Lett* 2016;11:1120–3.
- [12] Karmokar DK, Esselle KP. Periodic U-slot-loaded dual-band half-width microstrip leaky-wave antennas for forward and backward beam scanning. *IEEE Trans Antennas Propag* 2015;63(12):5372–81.
- [13] Koziel S, Bekasiewicz A. Multi-objective design of antennas using surrogate models. World Scientific; 2016.
- [14] Nocedal J, Wright S. Numerical optimization. 2nd ed. New York: Springer; 2006.
- [15] Kolda TG, Lewis RM, Torczon V. Optimization by direct search: new perspectives on some classical and modern methods. *SIAM Rev* 2003;45:385–482.
- [16] Koziel S. Computationally efficient multi-fidelity multi-grid design optimization of microwave structures. *Appl Comput Electromagn Soc J* 2010;25(7):578–86.
- [17] Ha BV, Mussetta M, Pirinoli P, Zich RE. Modified compact genetic algorithm for thinned array synthesis. *IEEE Antennas Wirel Propag Lett* 2016;15:1105–8.
- [18] Papadopoulos KA, Papagianni CA, Gkonis PK, Venieris IS, Kaklamani DI. Particle swarm optimization of antenna arrays with efficiency constraints. *Prog Electromagn Res* 2011;17:237–51.
- [19] Deb A, Roy JS, Gupta B. Performance comparison of differential evolution, particle swarm optimization and genetic algorithm in the design of circularly polarized microstrip antennas. *IEEE Trans Antennas Propag* 2014;62(8):3920–8.
- [20] Koziel S, Bekasiewicz A, Cheng QS, Li S. On ultra-wideband antenna miniaturization involving efficiency and matching constraints. *IEEE European ant. prop. conf.*; 2017.
- [21] Haq MA, Koziel S. A novel miniaturized UWB monopole with five-section stepped-impedance feed line. *Microwave Opt Tech Lett* 2017:202–7.
- [22] Haq MA, Koziel S. Simulation-based optimization for rigorous assessment of ground plane modifications in compact UWB antenna design. *Int J RF Microw Comput Aided Eng* 2017:1–13.
- [23] CST Microwave Studio, ver. 2016. CST AG, Bad Nauheimer Str. 19, D-64289 Darmstadt, Germany; 2016.
- [24] Conn AR, Gould NIM, Toint PL. Trust region methods. MPS-SIAM series on optimization; 2000.

Chapter 8

8 Paper [J7]

Muhammad Aziz ul Haq, and Slawomir Koziel

On Topology Modifications for Wideband Antenna Miniaturization

Published: International Journal of Electronics and Communications, vol. 94, pp. 215-220, 2018.

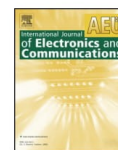
DOI: <https://doi.org/10.1016/j.aeue.2018.07.006>



Contents lists available at ScienceDirect

Int. J. Electron. Commun. (AEÜ)

journal homepage: www.elsevier.com/locate/aeue



Regular paper

On topology modifications for wideband antenna miniaturization

Muhammad Aziz Ul Haq*, Slawomir Koziel

Engineering Optimization & Modeling Center, Reykjavik University, Reykjavik, Iceland



ARTICLE INFO

Keywords:

Wideband antennas
Antenna miniaturization
Topology modifications
Design optimization
Simulation-driven design

ABSTRACT

Introducing various topological modifications is a common practice in the design of miniaturized wideband antennas. Some examples of successful alterations include ground plane stubs or slits below the feed line. In general, novel antenna topologies are reported on the case-to-case basis, often in the form of geometry evolution supported by parameter sweeps, supposedly demonstrating the benefits of the particular changes made to the device. The fundamental problem of such approaches is that neither the reference nor the modified structures are properly optimized. Due to complex interactions between geometry parameters and electrical/field properties of the antenna, the actual suitability of specific topology modifications is therefore unclear or even may lead to performance degradation. In order to illustrate this point, three antenna structures selected from the available literature are considered with geometry parameters rigorously optimized in order to find the minimum-size designs, with and without particular topology changes introduced by the authors of the respective papers. The results indicate that the optimization process virtually removes the said modifications and the optimized antenna footprints are smaller without these. The major message of the work is that conclusive assessment of the suitability of any geometry changes requires proper optimization of all relevant antenna parameters. Numerical results presented in the paper are validated experimentally.

1. Introduction

Ultra-wideband (UWB) antennas are essential components of wireless communication systems due to their inherent features such as high data rate, omnidirectional radiation pattern, high efficiency and low cost [1–3]. In recent years, it has become more and more important to maintain small size of wideband antennas [4–6], which is critical for many applications, including wearable devices [7], Internet of Things (IoT) [8], and cognitive radio [9]. It is a matter of fact that physical size reduction of the antenna structure directly influences its electrical and field properties, in particular, it may lead degradation of radiation pattern, realized gain, reflection response, as well as efficiency [10]. Due to the necessity of ensuring sufficient performance, antenna miniaturization poses considerable practical difficulties. Some promising miniaturized techniques based on the metamaterial or artificial concept are reported in [11–13].

Usually, size reduction is achieved by introducing various topological modifications to the antenna radiator, the feed line, or the ground plane. Some of the recent circuit solutions in this regard include an exponential slot edge applied in a Vivaldi antenna [14], a C-shape radiator [15], a bending microstrip feed line [16], rectangular slots edge on a radiator [17], or a differential stepped slot [18]. It should be noted

that the reported designs are based on case studies oriented towards specific applications without drawing any general conclusions concerning potential contribution of the considered modifications in the context of antenna electrical performance and miniaturization. Furthermore, in the majority of cases [19–21], the authors provide a cooperative progression before and after topological modifications that generally lead to a certain reduction of the antenna size, however, with appropriate parameter adjustment lacking. The reason is that parameter sweeping typically utilized to yield the final design does not account for parameter interactions. Consequently, suitability particular modifications in the miniaturization context is not conclusively assessed. In order to carry out such an assessment in a reliable manner, identification of the optimum design is necessary. This requires rigorous numerical optimization of all antenna parameters with the primary objective being size reduction, and supplementary constraints imposed on selected electrical or field characteristics. The latter permits finding the designs that satisfy given performance specifications. The literature offers a large variety of algorithms, e.g., [22–27], many of have been applied for antenna design [28–31].

The purpose of this paper is to demonstrate, using antenna examples from the literature (specifically [20;21]), that particular topology modifications introduce to achieve compact designs, may not be of any

* Corresponding author.

E-mail addresses: muhammadu16@ru.is (M. Aziz Ul Haq), koziel@ru.is (S. Koziel).

<https://doi.org/10.1016/j.aeue.2018.07.006>

Received 9 April 2018; Accepted 11 July 2018

1434-8411/ © 2018 Elsevier GmbH. All rights reserved.

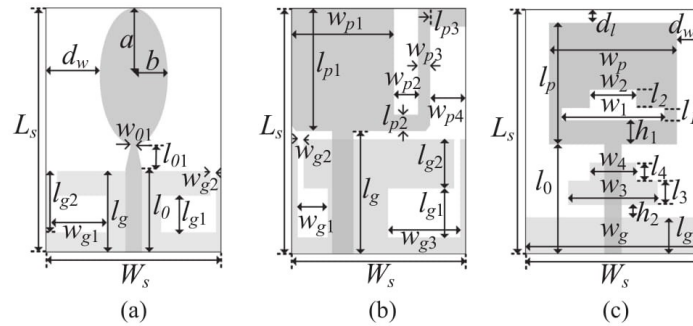


Fig. 1. Geometries of UWB monopole antennas: (a) Antenna I [20], (b) Antenna II [20] and (c) Antenna III [21].

Table 1
Geometry Parameters of Antennas I through III.

	l_g	l_0	l_{01}	w_{01}	a	b	d_w	l_{g1}	w_{g1}	l_{g2}	w_{g2}			
x^I	14.5	12.8	2.0	0.2	9.6	8.6	7.8	2.8	5.6	10	0.5			
x^{*I}	14.2	12.4	2.0	0.2	8.4	4.3	7	0	0	0	0			
	l_g	l_0	l_{p1}	w_{p1}	l_{p2}	w_{p2}	w_{p3}	l_{p4}	w_{p4}	l_{g1}	w_{g1}	l_{g2}	w_{g2}	w_{g3}
x^{II}	13.2	15.0	12.9	14.5	0.8	2.6	1.9	0.14	5.4	5.1	1.4	5.1	0.5	13.3
x^{*II}	7.25	8.9	14.4	14.7	4.7	1.3	1.8	0.17	8.0	0	0	0	0	0
	l_g	l_0	l_p	w_p	l_1	w_1	l_2	w_2	l_3	w_3	l_4	w_4	h_1	h_2
x^{III}	3.5	7	10	10	0.5	8	2.5	4	1	5	0.5	4	1	1
x^{*III}	6.3	10.3	11.5	9.6	0.4	1.9	0	0	0	0	0	0	2.7	0.5

x^* denotes the optimized parametric values.

Table 2
Footprints of Antennas I through III.

	Antenna I	Antenna II	Antenna III
Reported size ($L \times W$) [#]	35 × 32	25 × 25	18 × 12
Optimized size ($L \times W$)	31.3 × 22.7	23.36 × 25.9	21.9 × 9.7
Reported footprint area [mm ²] [#]	1120	625	216
Optimized footprint area [mm ²]	710.5	605	212

[#] The antenna dimensions reported in the original papers [12] (Antenna I and II), and [13] (Antenna III).

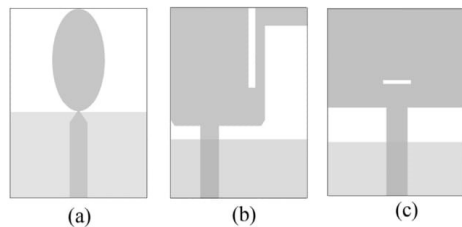


Fig. 2. Topologies of the size-optimized antennas of Fig. 1: (a) Antenna I, (b) Antenna II, and (c) Antenna III.

advantage in the said context. All antennas are optimized for minimum size with the initial dimensions as reported in the respective references. A rigorous constrained numerical optimization is carried out which not only leads to the effective disappearance of originally introduced modifications (the slots on ground plane [20], and a stair-like rectangular slots on the patch with inverted L shape stub at the ground plane

[21]) but also to smaller designs than those reported in the said references. At the same time, electrical and field characteristics are not affected significantly.

2. Topological alterations and benchmark Antenna structures

In this section, we illustrate the issues discussed in the introduction, in particular, the fact that particular topology modifications incorporated into an antenna structure with the intent of improving its performance (here, allow for achieving a smaller footprint) may not be lead to the expected results. Furthermore, we demonstrate that numerical optimization of all antenna parameters is mandatory for conclusive assessment of the suitability of such modifications, and—needless to say—to yield a truly optimum design with respect to whatever set of performance specifications is utilized in the design process.

Three reported wideband antennas are selected, specifically UWB antennas of [20] and [21]. Geometries of the respective structures have been shown in Fig. 1. In all antennas, particular types of modifications are introduced: the slots within ground plane in Antenna I and II, and a rectangular slots on a patch with an inverted L-shape ground plane stub in Antenna III. For a fair investigation on the relevance of the said modifications, all antennas are implemented using the same substrate as reported in the literature [20,21], i.e., Antenna I and III on 1.55 mm thick FR-4 substrate with $\epsilon_r = 4.6$, and Antenna II on 1.524 mm thick Rogers substrate with $\epsilon_r = 3.38$. The computational models of the structures are implemented using CST Microwave Studio [32]. The design parameters for Antenna I through III are $x^I = [l_g, l_0, l_{01}, w_{01}, a, b, d_w, l_{g1}, w_{g1}, l_{g2}, w_{g2}]^T$, $x^{II} = [l_g, l_0, l_{p1}, w_{p1}, l_{p2}, w_{p2}, w_{p3}, l_{p4}, w_{p4}, l_{g1}, w_{g1}, l_{g2}, w_{g2}, w_{g3}]^T$, and $x^{III} = [l_g, l_0, l_p, w_p, l_1, w_1, l_2, w_2, l_3, w_3, l_4, w_4, h_1, h_2]^T$ (all dimensions in mm). In order to ensure better consistency between simulated and measured results, the computational models of all antennas include

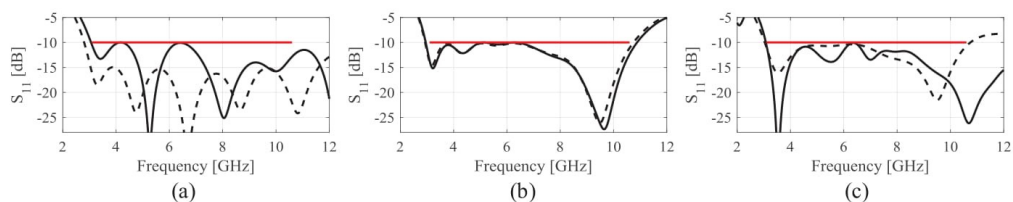


Fig. 3. Reflection responses of the antennas before and after the size optimization is denoted by the dotted and solid lines, respectively: (a) Antenna I, (b) Antenna II, and (c) Antenna III.

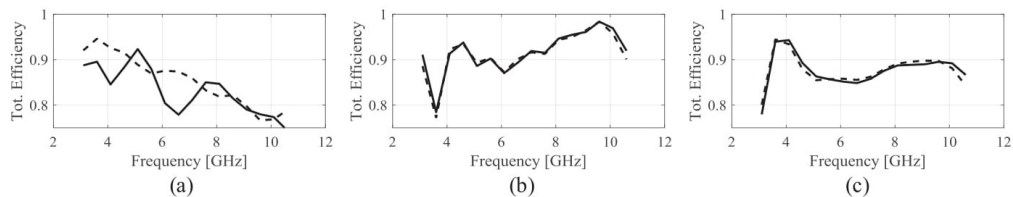


Fig. 4. Total efficiency of the antennas before and after the size optimization is denoted by the dotted and solid lines, respectively: (a) Antenna I, (b) Antenna II, and (c) Antenna III.

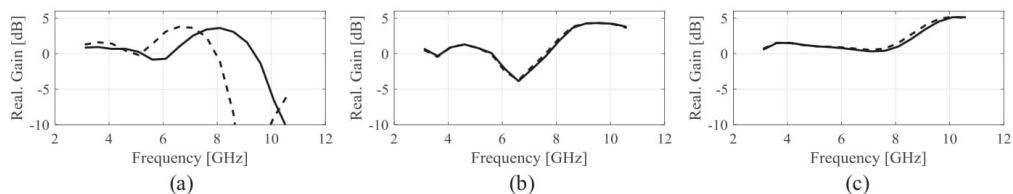


Fig. 5. Realized gain of the antennas before and after the size optimization is denoted by the dotted and solid lines, respectively: (a) Antenna I, (b) Antenna II, and (c) Antenna III.

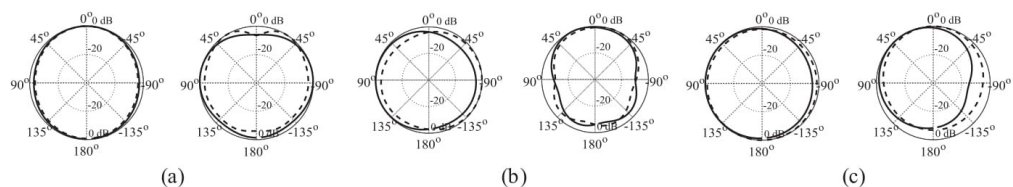


Fig. 6. H-plane patterns of the antennas before and after the size optimization is denoted by the dotted and solid lines, respectively: (a) Antenna I, (b) Antenna II, and (c) Antenna III. The plots (from left to right) are for frequencies 6 GHz and 10 GHz.

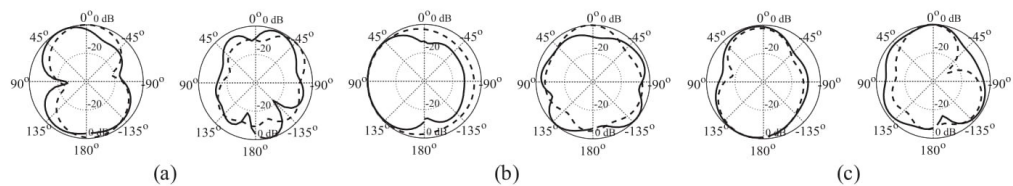


Fig. 7. E-plane patterns of the antennas before and after the size optimization is denoted by the dotted and solid lines, respectively: (a) Antenna I, (b) Antenna II, and (c) Antenna III. The plots (from left to right) are for frequencies 6 GHz and 10 GHz.

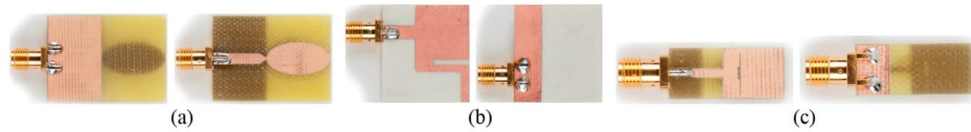


Fig. 8. Photographs of fabricated antenna prototypes: (a) Antenna I, (b) Antenna II, and (c) Antenna III.

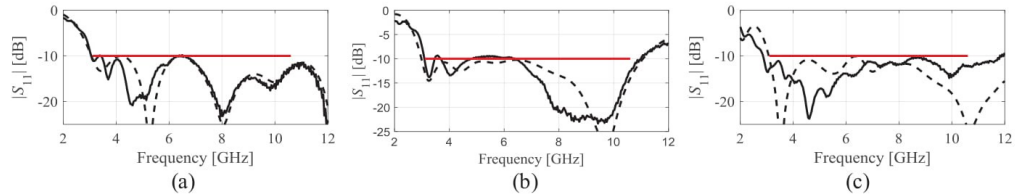


Fig. 9. Simulated (---) and measured (—) reflection responses of size-optimized antenna: (a) Antenna I, (b) Antenna II, and (c) Antenna III.

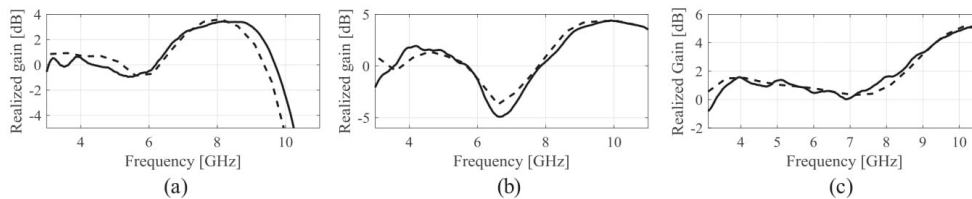


Fig. 10. Simulated (---) and measured (—) realized gain characteristics of size-optimized antenna: (a) Antenna I, (b) Antenna II, and (c) Antenna III.

the SMA connectors. Antennas are supposed to operate in the UWB frequency range (3.1 GHz to 10.6 GHz).

3. Antenna Minimization by numerical optimization

Here, we are interested in minimum-size designs. Consequently, the primary objective is a reduction of the antenna footprint area. At the same time, we want to ensure sufficient matching, represented by a condition $S(x) \leq -10$ dB, where $S(x)$ is the maximum reflection in the UWB band (from 3.1 GHz to 10.6 GHz) and x stands for adjustable geometry parameters of the structure at hand (cf. Section 2). The antenna size will be denoted as $A(x)$. Using this notation, the design problem is can be formulated as

$$x^* = \underset{x}{\operatorname{argmin}} \{A(x), S(x) \leq -10 \text{ dB}\} \quad (1)$$

The optimization engine utilized in this work is a pattern search algorithm [24]. The initial design for size reduction is the best matching design found by minimizing $S(x)$ (to ensure a feasible initial point as required by the pattern search routine). A particular implementation of the pattern search follows [24]. It is a derivative-free stencil-based search routine where the candidate solutions are identified on a

rectangular grid of a certain size (further refined during the optimization run).

Minimization of $S(x)$ is realized using a trust-region (TR) [33] gradient search algorithm with the antenna response Jacobians estimated through finite differentiation. TR-based algorithms typically exhibit faster convergence rate but they are not suitable for handling explicit constraints (as in (1)).

4. Results and discussions

Antennas I through III (cf. Section 2) have been optimized for minimum size using the procedure of Section 3. The intermediate step is optimization for best matching (in order to provide a feasible starting point for size optimization). The values of geometry parameter after this step are $x^I = [14.5 \ 12.8 \ 2.0 \ 0.2 \ 9.6 \ 8.6 \ 7.8 \ 5.6 \ 10 \ 0.5]^T$, $x^{II} = [13.2 \ 15.0 \ 12.9 \ 14.5 \ 0.8 \ 2.6 \ 1.9 \ 0.14 \ 5.4 \ 5.1 \ 1.4 \ 5.1 \ 0.5 \ 13.3]^T$, and $x^{III} = [3.5 \ 7 \ 10 \ 10 \ 0.5 \ 8 \ 2.5 \ 4 \ 1 \ 5 \ 0.5 \ 4 \ 1]^T$ respectively. The final (size-optimized) parameter values of all antennas have been gathered in Table 1. Table 2 indicates the antenna overall footprints before and after size optimization. It can be observed that geometry modifications that supposed to help in achieving small size actually disappear in all

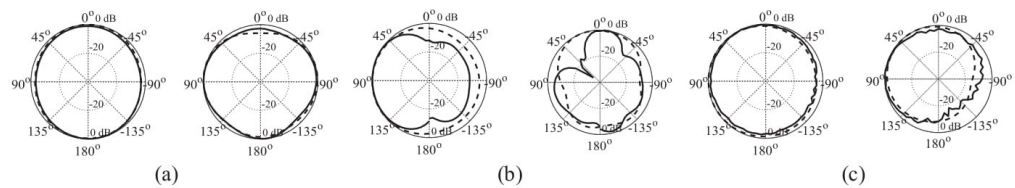


Fig. 11. Measured (—) and simulated (---) H-plane pattern of size-optimized antenna: (a) Antenna I, (b) Antenna II, and (c) Antenna III. The plots (from left to right) are for frequencies 6 GHz and 10 GHz.

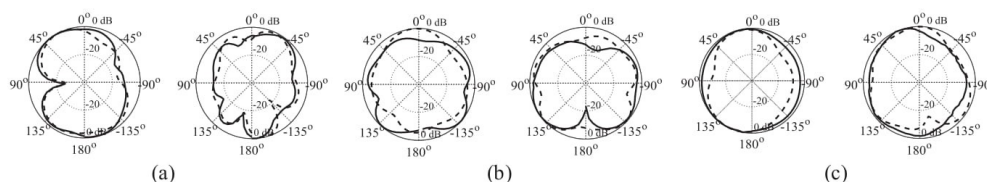


Fig. 12. Measured (—) and simulated (---) E-plane pattern of size-optimized antenna: (a) Antenna I, (b) Antenna II, and (c) Antenna III. The plots (from left to right) are for frequencies 6 GHz and 10 GHz.

antennas after optimization as indicated in Fig. 2. Furthermore, the optimized antenna footprints are smaller than those reported in the original papers. In particular, the dimensions of Antenna I and II (as reported in [20]) are 35 mm × 32 mm (footprint of 1120 mm²) and 25 mm × 25 mm (footprint of 625 mm²), respectively. Whereas proper size optimization leads to dimensions 31.3 mm × 22.7 mm (footprint of 710.5 mm²) and 23.36 mm × 25.9 mm (footprint of 605 mm²), respectively. For Antenna III, the reported size is 18 mm × 12 mm (footprint of 216 mm²), whereas optimization leads to dimensions 21.9 mm × 9.7 mm (footprint of 212 mm²). It should be noted that the size reduction for Antenna I is much more significant than for Antennas II and III, which is because the original Antenna I design is characterized by low reflection (around -15 dB) which leaves considerable room for miniaturization. This is not the case for the remaining structures.

Figs. 3 through 5 show the electrical performance before and after the optimization process. It can be observed that size optimization does not affect electrical characteristics in a significant manner. Fig. 3 indicates that the reflection for all antennas is under -10 dB for the entire UWB range. Total efficiency and realized gain are shown in Figs. 4 and 5, respectively. It should be noted that disappearance of the mentioned modifications does not lead to performance degradation. The H-plane and E-plane radiation patterns are shown in Figs. 6 and 7. Again, size reduction has a minor effect on field characteristics of the antennas.

For the sake of additional validation, the optimized antennas have been fabricated and measured. Fig. 8 shows the antenna prototypes, whereas Figs. 9 through 12 show the measured characteristics. Fig. 9 illustrates the simulated and measured reflection response of size-optimized antennas. It can be seen that the measured reflection responses satisfy the condition $|S_{11}| \leq -10$ dB for the entire UWB range. Also, the measured characteristics are better than the simulated ones for most of the frequencies. However, a slight inconsistency due to fabrication tolerance is observed for some of the frequencies in case of Antenna II. Fig. 10 shows the measured and optimized realized gain. An acceptable agreement can be observed. Figs. 11 and 12 show the measured H- and E-plane pattern of all size optimized antennas at 6 GHz and 10 GHz frequencies. An omnidirectional characteristic has been observed for all the cases which is the fundamental requirement of monopole antennas operating for UWB applications.

5. Conclusion

In the paper, the relevance of geometry modifications in the context of size reduction of wideband antennas has been investigated. Using three case studies of wideband antennas recently reported in the literature, we demonstrated that certain modifications may not lead to the expected results. We also demonstrated that conclusive assessment of the importance of particular modifications requires rigorous optimization of all antenna parameters. In other words, a truly optimum design has to be found in order to verify whether a given modification actually leads to antenna miniaturization. For the case studies considered, size-reduction-oriented alterations disappear during the optimization process, indicating that they are—as a matter of fact—irrelevant. More

specifically, disappearance of the said alterations during the optimization process means that they do not serve the purpose they were introduced for. At the same time, the obtained antenna footprints are smaller than reported in the original papers (by 36.56%, 3.2%, and 1.85%, respectively).

Acknowledgment

The authors thank Dassault Systemes, France, for making CST Microwave Studio available. This work has been partially supported by the Icelandic Centre for Research (RANNIS) Grant 163299051.

References

- [1] Wu C, Chen Y, Liu W. A compact ultrawideband slotted patch antenna for wireless USB dongle application. *IEEE Antennas Propag Lett* 2012;11:596–9.
- [2] Ali WA, Ibrahim AA. A compact double sided MIMO antenna with an improved isolation for UWB applications. *AEU Int J Electron Commun* 2017;7:1–3.
- [3] Li Y, Yang X, Yang Q, Li C. Compact coplanar waveguide fed ultra wideband antenna with a notch band characteristic. *AEU Int J Electron Commun* 2011;961–96.
- [4] Xu H, Wang G, Qi M, Zhang C, Liang J, Gong J, Zhou Y. Analysis and design of two-dimensional resonant-type composite right/left-handed transmission lines with compact gain-enhanced resonant antennas. *IEEE Trans Antenn Propag* 2013;61(2):735–47.
- [5] Xu H, Wang G, Tao Z, Cai T. Compact fractal left-handed structures for improved cross-polarization radiation pattern. *IEEE Trans Antenn Propag* 2014;62(2):546–54.
- [6] Xu H, Wang G, Tao Z, Cai T. An octave-bandwidth half maxwell fish-eye lens antenna using three-dimensional gradient-index fractal metamaterials. *IEEE Trans Antenn Propag* 2014;62(9):4823–8.
- [7] Abbasi QH, Rehman MU, Yang X, Alomainy A, Qaraqe K, Serpedin Q. Ultrawideband band-notched flexible antenna for wearable applications. *IEEE Antenn Propag Lett* 2013;12:1606–9.
- [8] Haq MA, Koziel S. Design optimization and trade-offs of miniaturized wideband antenna for internet of things applications. *Metrologia* 2017;24(3):463–71.
- [9] Srivastava G, Mohan A, Chakrabarty A. Compact reconfigurable UWB slot antenna for cognitive radio applications. *IEEE Antenn Propag Lett* 2017;16:1139–42.
- [10] Chen ZN, See TSP, Qing X. Small printed ultrawideband antenna with reduced ground plane effect. *IEEE Antenn Propag Lett* 2007;55(2):383–8.
- [11] Xu H, Wang G, Qi MQ, Li L, Cui TJ. Three-dimensional super lens composed of fractal left-handed materials. *Adv Opt Mater* 2014;2(6):572–80.
- [12] Xu H, Wang G, Ma K, Cui TJ. Superscatterer illusions without using complementary media. *Adv Opt Mater* 2013;1(7):495–502.
- [13] Xu H, Wang G, Cai T. Miniaturization of 3-D anisotropic zero-refractiveindex metamaterials with application to directive emissions. *IEEE Trans Antenn Propag* 2014;62(6):3141–9.
- [14] Oliveira AMD, Perotoni MB, Kofuji ST, Justo JF. A palm tree antipodal vivaldi antenna with exponential slot edge for improved radiation pattern. *IEEE Antenn Propag Lett* 2015;14:1334–7.
- [15] Tang H, Wang K, Wu R, Yu C, Zhang J, Wang X. A novel broadband circularly polarized monopole antenna based on C-shaped radiator. *IEEE Antenn Propag Lett* 2017;16:964–7.
- [16] Pandey GK, Verma H, Meshram MK. Compact antipodal Vivaldi antenna for UWB applications. *Electron Lett* 2015;51(4):308–10.
- [17] Teni G, Zhang N, Qiu J. Research on a novel miniaturized antipodal Vivaldi antenna with improved radiation. *IEEE Antenn Propag Lett* 2013;12:417–20.
- [18] Li W, Tu Z, Chu Q, Wu X. Differential stepped-slot UWB antenna with common-mode suppression and dual sharp-selectivity notched bands. *IEEE Antenn Propag Lett* 2016;11:1120–3.
- [19] Prombutr N, Kirawanich P, Akkaraekthalin P. Bandwidth enhancement of UWB microstrip antenna with a modified ground plane. *Int J Micro Sci Technol* 2009;1–7.
- [20] Lu Y, Huang Y, Chattha HT, Shen Y. Technique for minimising the effects of ground plane on planar ultra-wideband monopole antennas. *IET Microw Antenn Propag* 2012;6(5):510–8.
- [21] Ojaroudi M, Yazdanifard S, Ojaroudi N, Moghaddasi MN. Small square monopole antenna with enhanced bandwidth by using inverted T-shaped slot and conductor-backed plane. *IEEE Trans Antenn Propag* 2011;59(2):670–4.

- [22] Nocedal J, Wright S. Numerical Optimization, 2nd ed. New York: Springer; 2006.
- [23] Kolda TG, Lewis RM, Torczon V. Optimization by direct search: new perspectives on some classical and modern methods. *SIAM Rev* 2003;45:385–482.
- [24] Koziel S. Computationally efficient multi-fidelity multi-grid design optimization of microwave structures. *Appl Comput Electromag Soc J* 2010;25(7):578–86.
- [25] Ha BV, Mussetta M, Pirinoli P, Zich RE. Modified compact genetic algorithm for thinned array synthesis. *IEEE Anten Wirel Propag Lett* 2016;15:1105–8.
- [26] Papadopoulos KA, Papagianni CA, Gkonis PK, Venieris IS, Kalamani DL. Particle swarm optimization of antenna arrays with efficiency constraints. *Prog Electromag Res* 2011;17:237–51.
- [27] Deb A, Roy JS, Gupta B. Performance comparison of differential evolution, particle swarm optimization and genetic algorithm in the design of circularly polarized microstrip antennas. *IEEE Trans Anten Propag* 2014;62(8):3920–8.
- [28] Koziel S, Bekasiewicz A, Cheng QS, Li S. On topology modifications for wideband antenna miniaturization. *IEEE Eur Anten Propag Conf* 2017.
- [29] Haq MA, Koziel S. Quantitative assessment of wideband antenna geometry modifications for size-reduction-oriented design. *AEU Int J Electron Commun* 2018;90:45–52.
- [30] Haq MA, Koziel S. A novel miniaturized UWB monopole with five-section stepped-impedance feed line. *Microw Opt Technol Lett* 2017;60(1):202–7.
- [31] Haq MA, Koziel S. Simulation-based optimization for rigorous assessment of ground plane modifications in compact UWB antenna design. *Int J RF Microw Comput Aided Eng* 2017;1–13.
- [32] CST Microwave Studio. ver. 2015. CST AG. Bad Nauheimer Str. 19. D-64289 Darmstadt. Germany; 2015.
- [33] Conn A.R., Gould N.I.M., Toint P.L. Trust Region Methods. *MPS-SIAM Series on Optimization*; 2000.

Chapter 9

9 Paper [J8] and [J9]

Muhammad Aziz ul Haq, and Slawomir Koziel

Ground Plane Alterations for Design of High-Isolation Compact Wideband MIMO Antenna

Published: *IEEE Access*, vol. 6, pp. 48978-48983, 2018.

DOI: 10.1109/ACCESS.2018.2867836

Ground Plane Alterations for Design of High-Isolation Compact Wideband MIMO Antenna

MUHAMMAD AZIZ UL HAQ AND SLAWOMIR KOZIEL[✉], (Senior Member, IEEE)

Engineering Optimization and Modeling Center, School of Science and Engineering, Reykjavik University, 101 Reykjavik, Iceland

Corresponding author: Slawomir Koziel (koziel@ru.is)

This work was supported in part by the Icelandic Centre for Research (RANNIS) under Grant 174114051 and in part by the National Science Centre of Poland under Grant 2014/15/B/ST7/04683.

ABSTRACT In this paper, a simple technique for improving element isolation in wideband multiple-input multiple-output (MIMO) antenna is investigated. We consider n -section rectangular slits below the feed line and analyze the effects of the number of sections on achievable isolation. The effect of the slits is indirect by improving the impedance matching, which creates a room for isolation enhancement through rigorous optimization of all antenna parameters. The results obtained for an exemplary antenna structure indicate the advantages of increasing the slit complexity as well as a saturation effect beyond $n = 3$. Using these considerations, a compact MIMO antenna is developed and optimized to operate in the ultrawideband (UWB) (3.1–10.6 GHz) frequency range. The final design features $|S_{11}| \leq -10$ dB and isolation $|S_{21}| \leq -20$ dB in the entire UWB range, as well as small dimensions of only 25×32 mm². Excellent performance figures, including envelop coefficient correlation (< 0.005), diversity gain (> 9.99 dB), and total efficiency ($> 80\%$ by average), demonstrate that the considered structure is suitable for practical applications and competitive to the state-of-the-art antennas reported in the literature. Experimental validation of the design is also provided.

INDEX TERMS EM-simulation-driven design, ground plane alterations, MIMO antenna, size reduction.

I. INTRODUCTION

Wideband antennas have gained popularity owing to their attractive features such as high data rate, simultaneous multi-channel connectivity, low power consumption as well as ability to provide high-resolution images [1], [2]. The Federal Communications Commission (FCC) authorized the frequency range (3.1 – 10.6 GHz) for ultrawideband (UWB) systems to be used for commercial applications in 2002 [3], which started advancements towards development of UWB antennas for wideband applications such as wearable devices [4], Internet of Things [5], and cognitive radio [6]. However, the critical issue associated with UWB systems is their suitability for a short range communication only, which is due to low power transmission allowed by FCC. Furthermore, considerable environmental scattering causes a multipath fading that leads to degradation of the transmission quality. Finally, a single wideband antenna has its own limitations in handling multi-channel communication over a wide range.

A multiple-input-multiple-output (MIMO) technology has been used to overcome the aforementioned problems.

An important characteristic of MIMO structures is separation between the antenna elements, high level of which is essential to avoid mutual coupling and to ensure reliable communication [7], [8]. Also, stronger mutual coupling between the antenna elements results in decreasing the data transfer capacity and efficiency of the MIMO system [9]. Notably, this phenomenon becomes more pronounced in compact communication systems where a limited space is allocated to mount the antenna on. Consequently, design of compact MIMO antennas with high isolation for space-limited communication devices is a considerable challenge. From the system point of view, isolation level of -20 dB is considered sufficient in the context of quality of wireless communication [9]. Yet, achieving it while maintaining the compact size of the antenna structure along with sufficient levels of other performance figures is a considerable design challenge.

There have been significant research efforts observed over the last few years to deal with mutual coupling issues. The most popular approach is to place antenna elements orthogonal to each other [10], [11], which makes it easy to handle mutual coupling. However, orthogonally-allocated

antenna structures increase complexity of the feeding structure in compact communication devices. Other techniques to improve isolation include utilization of parasitic structures [12], Electromagnetic Band Gap (EBG) structures [13], neutralizing lines [14], and Defected Ground Structures (DGS) [15]. Although the aforementioned techniques are very attractive in the context of isolation improvement, their implementation for wideband and ultra wideband applications is difficult, especially for contemporary communication devices. Therefore, these techniques have not yet been in practical use in UWB-MIMO antenna structures to the best of authors' knowledge.

Alternative methods include a wide range of ground plane alterations. In [16], a compact UWB-MIMO antenna with F-shaped stubs in the ground plane has been proposed. High isolation ($|S_{21}| < -20$ dB) is achieved by the stub evolution in the ground plane. In [17], a bi-planar Yagi-like MIMO antenna has been proposed with isolation better than -17 dB. Two L-shape inverted parasitic strips with smaller L-shape stubs have been introduced in [18] to achieve improved isolation. The main problem associated with the above structures is their large size, as well as the fact that element isolation is not explicitly handled in the design process, therefore, it is only a byproduct of the introduced modifications. To achieve better control, explicit formulation of requirements concerning relevant performance figures is necessary along with suitable geometry alterations that are capable of controlling respective characteristics. At the same time, rigorous optimization needs to be carried out so as to account for parameter and antenna responses interrelations.

In this paper, a technique for element isolation improvement in compact UWB-MIMO antennas is proposed and investigated. Our approach involves introduction of n -section slits below the feed line. The slits permit impedance matching improvement of individual antenna elements [19], which is further utilized to enhance isolation through rigorous constrained optimization of all antenna elements and balancing reflection level (at -10 dB within the operating band of the antenna) and isolation (at -20 dB), while maintaining the compact footprint. The number $n = 2$ of the slit sections has been found to be the best compromise between efficiency (in terms of isolation improvement but also maintaining the small size) and structural complexity. The presented concept has been demonstrated for a UWB-MIMO structure based on two monopole antenna elements, placed parallel to each other with a common ground plane. Inverted L-shape stubs are utilized in the ground plane to enhance the matching. The simulated and measured results confirm the applicability of the considered antenna for contemporary modern communication devices, among others, due to its very low ECC and high diversity gain.

II. BENCHMARK MIMO ANTENNA STRUCTURE AND ANALYSIS

Our considerations are illustrated using the UWB-MIMO antenna shown in Fig. 1. Two monopole antenna elements

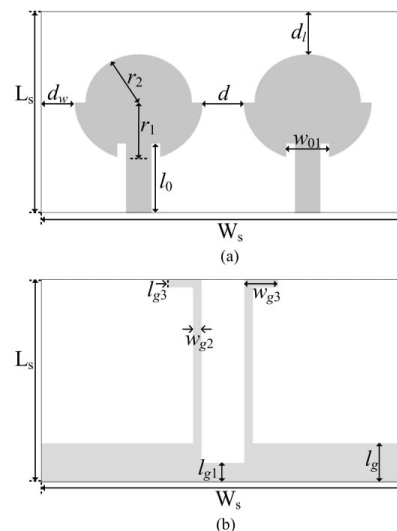


FIGURE 1. The geometry of a compact UWB-MIMO Antenna I used to demonstrate the proposed isolation enhancement concept. (a) Top and (b) Bottom view.

are positioned parallel to each other with a common ground plane and fed by 50Ω impedance lines.

The structure is implemented on 1.55-mm-thick FR-4 substrate with $\epsilon_r = 4.3$. The antenna geometry is described using the following vector of parameters: $\mathbf{x}_0 = [l_g \ l_0 \ r_1 \ r_2 \ d \ d_w \ l_{g1} \ w_{g2} \ l_{g3} \ w_{g3} \ w_{01}]^T$. The numerical values are $\mathbf{x}_0^{(0)} = [3 \ 5.7 \ 7 \ 0.9 \ 7 \ 3 \ 3 \ 0.3 \ 0.2 \ 0.5 \ 2 \ 5]^T$ mm. The computational model is implemented in CST Microwave Studio [20] ($\sim 770,000$ mesh cells, simulation time 2 minutes). In order to ensure reliable experimental validation, the model includes the SMA connectors. The antennas are supposed to operate in the UWB frequency range (3.1 GHz to 10.6 GHz). Figure 2(a) shows the reflection response of the initial design which is not satisfying the condition $|S_{11}| \leq -10$ dB. Therefore, our first goal was to optimize the antenna for the maximum in-band reflection not exceeding -10 dB. Here, a pattern search algorithm [21] has been utilized with reflection constrained handled implicitly (through a penalty function approach [22]). The reflection response of optimized antenna is shown in Fig. 2(b) which indicates that

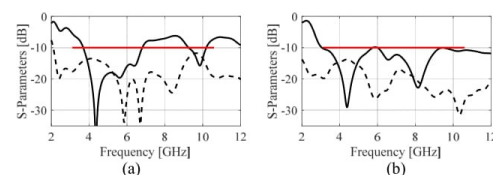


FIGURE 2. Simulated S-parameters of Antenna I: (—) S_{11} , and (---) S_{21} . (a) The initial design, (b) Optimized design.

the MIMO antenna is operating for entire UWB frequency range (3.1 GHz to 10.6 GHz). The numerical values of optimized antenna (called Antenna I) are as follows: $\mathbf{x}_1^{(0)} = [4.0 \ 5.8 \ 6.7 \ 0.9 \ 2.9 \ 5.6 \ 3.3 \ 0.5 \ 1.5 \ 1.2 \ 1.0 \ 3.5]^T$.

III. ANTENNA EVOLUTION TOWARDS ISOLATION IMPROVEMENT

A proposed way of improving element isolation are multi-section slits below the feed lines. To analyze the impact of these ground plane alterations on the UWB-MIMO antenna, the optimized Antenna I has undergone systematic modifications. At the first stage, a rectangular slit below the feed line was introduced as shown in Fig. 3(a) (the structure referred to as Antenna II). Upon applying this modification, the design variable vector was extended to $\mathbf{x}_2 = [l_g \ l_0 \ r_1 \ r_2 \ d \ d_l \ d_w \ l_{g1} \ w_{g2} \ l_{g3} \ w_{g3} \ w_{01} \ l_1 \ w_1]^T$. Here, l_1 and w_1 are the length and width of the introduced slit below the feed line. Antenna II was optimized using the same procedure as described before. For a fair comparison between the isolation of Antenna I and Antenna II, the overall antenna size was fixed during the optimization. The S-parameters of Antenna II are shown in Fig. 4 (a). It can be observed that isolation (S_{21}) between the two ports of the MIMO antenna elements was improved considerably. The optimized numerical values of Antenna II are: $\mathbf{x}_2^{(0)} = [4.6 \ 5.5 \ 7.0 \ 0.9 \ 1.2 \ 5.0 \ 2.9 \ 0.6 \ 2.0 \ 1.8 \ 2.2 \ 3.7 \ 2.6 \ 1.9]^T$.



FIGURE 3. Evolution progression of the considered UWB-MIMO antenna. The ground plane is shown using the dark gray shade. (a) Antenna II, (b) Antenna III.

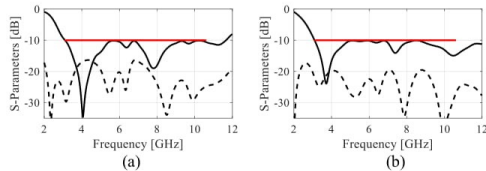


FIGURE 4. Simulated S-parameters of optimized UWB-MIMO antenna. (—) S_{11} , and (---) S_{21} . (a) Antenna II, (b) Antenna III.

At the next stage, another section of the slit has been added as shown in Fig. 3(b) (the structure referred to as Antenna III). The design variable vector of Antenna III is $\mathbf{x}_3 = [l_g \ l_0 \ r_1 \ r_2 \ d \ d_l \ d_w \ l_{g1} \ w_{g2} \ l_{g3} \ w_{g3} \ w_{01} \ l_1 \ w_1 \ l_2 \ w_2]^T$. Again, the same optimization procedure with fixed antenna size was performed. Figure 4(b) shows the S-parameters of the optimized Antenna III. The results clearly indicate that two-section slit below the feed line makes a dramatic impact

on isolation ($|S_{21}| \leq -20$ dB) as compared to Antenna II. The numerical values of geometry parameters are: $\mathbf{x}_3^{(0)} = [5.7 \ 7.0 \ 7.4 \ 0.8 \ 1.3 \ 5.4 \ 0.7 \ 1.0 \ 3.0 \ 4.2 \ 1.8 \ 4.2 \ 3.8 \ 0.2 \ 0.9 \ 0.8]^T$.

Further increase of the number of slit sections does not bring noticeable improvement of the isolation, therefore, Antenna III is considered a final design. Other performance figures such as total efficiency, Envelop Coefficient Correlation, and diversity gain have also been considered for all antenna structures. The purpose of this study was to analyze the impact of antenna modifications on the mentioned characteristics. Figure 5 shows the total efficiency of all antennas for the entire UWB frequency range. The average efficiency is similar for all antenna structures and larger than 80% and despite high-loss substrate (FR-4). One of the critical performance figures of a MIMO antenna, reflecting the signal correlation, is the Envelop Correlation Coefficient (ECC). For an ideal MIMO antenna, ECC value should be zero, however, $ECC < 0.5$ is considered acceptable for an uncorrelated MIMO antenna system. The ECC can be calculated using the field radiation pattern [23] as:

$$ECC = \frac{\left| \iint_{4\pi} [\vec{F}_1(\theta, \Phi) \cdot \vec{F}_2(\theta, \Phi)] d\Omega \right|^2}{\iint_{4\pi} |\vec{F}_1(\theta, \Phi)|^2 d\Omega \iint_{4\pi} |\vec{F}_2(\theta, \Phi)|^2 d\Omega} \quad (1)$$

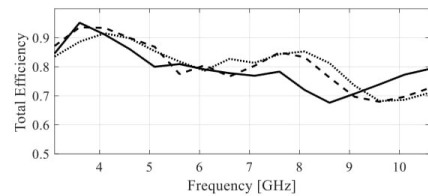


FIGURE 5. Simulated efficiencies of the optimized antennas: Antenna I (—), Antenna II (---), and Antenna III (—).

Where, $\vec{F}_i(\theta, \Phi)$ is the field radiation pattern of the MIMO antenna element when port i is excited (here, $i = 1, 2$) and other port is terminated with the 50Ω load. Figure 6(a) shows the ECC for Antennas I through III. Here, again, isolation-improvement-oriented antenna modification did not degrade the ECC within the entire UWB frequency range.

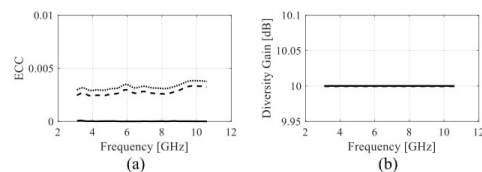


FIGURE 6. Simulated response of the optimized antennas: Antenna I (—), Antenna II (---), and Antenna III (—). (a) ECC, (b) Diversity Gain.

Diversity gain of the MIMO antenna can be calculated using the following equation:

$$DG = 10\sqrt{1 - ECC^2} \quad (2)$$

Figure 6(b) shows DG for all considered antennas. As before, improving isolation through ground plane modifications is not achieved at the expense of DG degradation.

A. CURRENT DISTRIBUTIONS

The impact of the considered ground plane alteration on antenna isolation was further analyzed using the surface current distribution over the modified MIMO antennas at 3.1 GHz as shown in Fig. 7. It is clear from Fig. 7(a) that with Port 1 excited, a significant amount of current is coupled along Port 2. This coupling effect is reduced by one-section slit below the feed line up as shown in Fig. 7(b). Introduction of the two-section slit improves the situation dramatically as illustrated in Fig. 7(c). Only a negligible amount of current is observed at the surface of the second antenna. Consequently, high isolation is achieved.

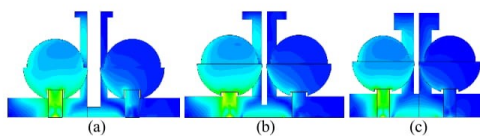


FIGURE 7. Surface current distribution at 4.1 GHz: (a) initial design, (b) design with a one-section slit, and (c) design with a two-section slit below the feed line.

B. EXPERIMENTAL VALIDATIONS

To verify the performance of the antenna, the optimized UWB-MIMO structure was fabricated (cf. Fig. 8). During the measurement process, Port 1 was excited, while Port 2 was terminated with a 50Ω load. Figure 9 shows the measured and simulated S-parameters of the considered antenna.

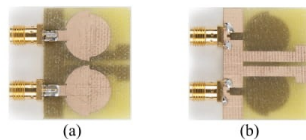


FIGURE 8. Photographs of the fabricated UWB-MIMO antenna: (a) top view, (b) bottom view.

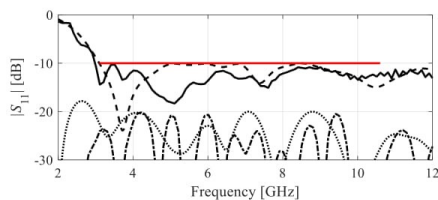


FIGURE 9. Simulated and measured S-parameters of the optimized UWB-MIMO antennas with the two-section slit below the feed line: S_{11} simulated (---), S_{11} measured (—), S_{21} simulated (···) and S_{21} measured (— · —).

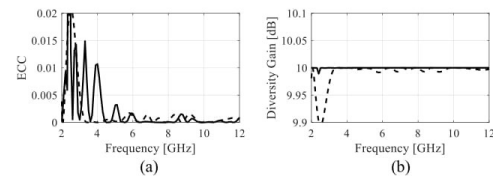


FIGURE 10. Simulated (---) and measured (—) response of the optimized UWB-MIMO antenna (a) Envelop Correlation Coefficient (b) Diversity Gain.

The measured results confirm the capability of the design to operate within the UWB range. A slight discrepancy might be due to fabrication tolerance and inconsistency of the dielectric constant of the substrate. Figure 10 shows the simulated and measured ECC and DG of the antenna. As our experimental facilities do not allow to measure the 3D field pattern, the measured scattering parameters has been used for ECC evaluation using the expression [23]:

$$ECC = \frac{|S_{11}^* S_{12} + S_{21}^* S_{22}|^2}{(1 - |S_{11}|^2 - |S_{21}|^2)(1 - |S_{12}|^2 - |S_{22}|^2)} \quad (3)$$

It is clear from the Fig. 10 that ECC is lower than 0.005 and DG is higher than 9.99 dB for the entire UWB range. The important observation is that the ECC and DG responses by using the field radiation pattern or scattering parameters are well aligned over the entire frequency range. The considered antenna can be a good candidate for modern communication devices due to very low ECC and high DG. To the best of authors knowledge, the antenna exhibits a much better performance (especially, in terms of ECC and DG) than recently reported designs [16]–[18], [24]–[26] for the UWB range. The detailed performance comparison has been provided in Table 1. For a fair comparison, only parallel-fed antenna designs were considered. Figure 11 shows the simulated and measured total efficiency of the antenna. The measured results indicate that the average efficiency of the antenna is higher than 80% which also confirms the applicability of the structure for modern communication devices. Another important characteristic is the radiation pattern. Figure 12 shows the E- and H-plane patterns at 6 GHz and 8 GHz. The radiation is omnidirectional. Some discrepancies can be found due to the

TABLE 1. Comparison of the recently reported UWB-MIMO antennas.

Ref #	Size [mm ²] (l × w)	Size (λ _g × λ _g)	Frequency [GHz]	Isolation [dB]	ECC	Diversity Gain [dB]
[16]	30×50	1.09×1.82	2.5–14.5	< -20	< 0.04	> 7.5
[17]	50×80	1.65×2.65	3.1–10.6	< -17	< 0.056	NA
[18]	30×40	1.09×1.46	2.4, 3.1–10.6	< -11.5	< 0.15	NA
[24]	40×50	1.46×1.82	2.5–11	< -15	< 0.02	NA
[25]	60×40	2.19×1.46	3.1–10.6	< -20	< 0.06	> 9.89
[26]	37×46	1.01×1.26	2–10.6	< -20	< 0.02	> 9.9
This work	25×32	0.91×1.17	3.1–10.6	< -20	< 0.005	> 9.99

^a Here, λ_g denotes the antenna size in term of the guided wavelength (defined by 50 Ω impedance feed line operating at 6 GHz) corresponding to the substrate properties.

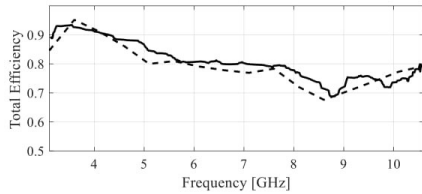


FIGURE 11. Simulated and measured total efficiency of the optimized UWB-MIMO antennas with the two-section slit below the feed line: Simulated (---), and Measured ones (—).

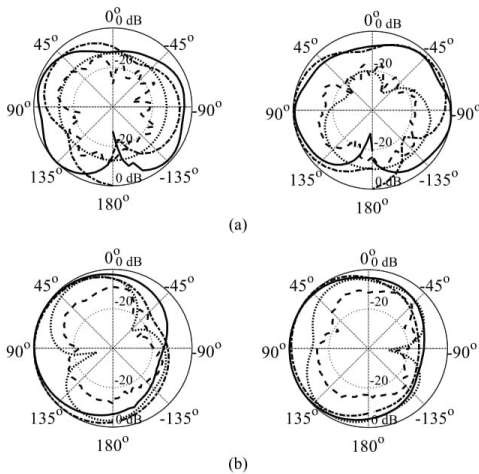


FIGURE 12. Simulated and measured radiation pattern of the optimized UWB-MIMO antenna with the two-section slit below the feed line: Simulated co-pol (---), measured co-pol (—), simulated cross-pol (...) and measured cross-pol (-.-). The plots from left- to right- hand side are for the frequencies 6 GHz and 8 GHz: (a) E- and (b) H-plane.

substrate characteristics, and (especially for the E plane) due to utilization of the 90-degree bend to mount the antenna.

IV. CONCLUSION

In this paper, a technique for isolation improvement of compact wideband MIMO antennas has been proposed, and demonstrated using an exemplary UWB MIMO structure. High isolation was achieved by using an n -section slit below the feed line. Systematic ground plane modifications have been investigated leading to a conclusion that $n = 2$ gives an optimum trade-off between the structure complexity and performance. Also, rigorous design closure of the antenna has been carried out using numerical optimization to ensure its best possible performance. The measured results ($|S_{21}| \leq -20$ dB, ECC < 0.005, DG > 9.99dB) confirm suitability of the antenna for modern communication systems. The considered structure also exhibits satisfactory field properties, in particular, high efficiency and omnidirectional radiation characteristics. The presented work can be used as a

benchmark for future investigations of the impact of specific topology alterations on MIMO antenna performance.

ACKNOWLEDGMENT

The authors thank Dassault Systemes, France, for making CST Microwave Studio available.

REFERENCES

- [1] C. M. Wu, Y. L. Chen, and W. C. Liu, "A compact ultrawideband slotted patch antenna for wireless USB dongle application," *IEEE Antennas Wireless Propag. Lett.*, vol. 11, pp. 596–599, 2012.
- [2] H. Bahramiabarghouei, E. Porter, A. Santorelli, B. Gosselein, M. Popović, and L. A. Rusch, "Flexible 16 antenna array for microwave breast cancer detection," *IEEE Trans. Biomed. Eng.*, vol. 62, no. 10, pp. 2516–2525, Oct. 2015.
- [3] *Federal Communications Commission Revision of Part 15 of the Commission's Rules Regarding Ultrawideband Transmission System From 3.1 to 10.6 GHz*, document ET-Docket 98-153, Federal Communications Commission, Washington, DC, USA, 2002.
- [4] Q. H. Abbasi, M. U. Rehman, X. Yang, A. Alomainy, K. Qaraqe, and E. Serpedin, "Ultrawideband band-notched flexible antenna for wearable applications," *IEEE Antennas Wireless Propag. Lett.*, vol. 12, pp. 1606–1609, 2013.
- [5] A. Bekasiewicz and S. Koziel, "Compact UWB monopole antenna for Internet of Things applications," *Electron. Lett.*, vol. 52, no. 7, pp. 492–494, 2016.
- [6] G. Srivastava, A. Mohan, and A. Chakrabarty, "Compact reconfigurable UWB slot antenna for cognitive radio applications," *IEEE Antennas Wireless Propag. Lett.*, vol. 16, pp. 1139–1142, 2017.
- [7] S. Koziel and A. Bekasiewicz, "Electromagnetic-simulation-driven design of compact ultra-wideband multiple-input–multiple-output antenna," *IET Microw., Antennas Propag.*, vol. 10, no. 15, pp. 1721–1724, 2016.
- [8] S. Tripathi, A. Mohan, and S. Yadav, "A compact Koch fractal UWB MIMO antenna with WLAN band-rejection," *IEEE Antennas Wireless Propag. Lett.*, vol. 14, pp. 1565–1568, 2015.
- [9] P.-S. Kildal and K. Rosengren, "Correlation and capacity of MIMO systems and mutual coupling, radiation efficiency, and diversity gain of their antennas: Simulations and measurements in a reverberation chamber," *IEEE Commun. Mag.*, vol. 42, no. 12, pp. 104–112, Dec. 2004.
- [10] S. Koziel, A. Bekasiewicz, and Q. S. Cheng, "Conceptual design and automated optimisation of a novel compact UWB MIMO slot antenna," *IET Microw., Antennas Propag.*, vol. 11, no. 8, pp. 1162–1168, 2017.
- [11] L. Liu, S. W. Cheung, and T. I. Yuk, "Compact MIMO Antenna for portable devices in UWB applications," *IEEE Trans. Antennas Propag.*, vol. 61, no. 8, pp. 4257–4264, Aug. 2013.
- [12] Z. Li, Z. Du, M. Takahashi, K. Saito, and K. Ito, "Reducing mutual coupling of MIMO antennas with parasitic elements for mobile terminals," *IEEE Trans. Antennas Propag.*, vol. 60, no. 2, pp. 473–481, Feb. 2012.
- [13] Q. Li, A. P. Feresidis, M. Mavridou, and P. S. Hall, "Miniaturized double-layer EBG structures for broadband mutual coupling reduction between UWB monopoles," *IEEE Trans. Antennas Propag.*, vol. 63, no. 3, pp. 1168–1171, Mar. 2015.
- [14] S. Zhang and G. F. Pedersen, "Mutual coupling reduction for UWB MIMO antennas with a wideband neutralization line," *IEEE Antennas Wireless Propag. Lett.*, vol. 15, pp. 166–169, 2016.
- [15] R. Anitha, V. P. Sarin, P. Mohanan, and K. Vasudevan, "Enhanced isolation with defected ground structure in MIMO antenna," *Electron. Lett.*, vol. 50, no. 24, pp. 1784–1786, 2014.
- [16] A. Iqbal, O. A. Saraereh, A. W. Ahmad, and S. Bashir, "Mutual coupling reduction using F-shaped stubs in UWB-MIMO antenna," *IEEE Access.*, vol. 6, pp. 2755–2759, 2018.
- [17] S. S. Jehangir and M. S. Sharawi, "A miniaturized UWB biplanar Yagi-like MIMO antenna system," *IEEE Antennas Wireless Propag. Lett.*, vol. 16, pp. 2320–2323, 2017.
- [18] J.-Y. Deng, L.-X. Guo, and X.-L. Liu, "An ultrawideband MIMO Antenna with a high isolation," *IEEE Antennas Wireless Propag. Lett.*, vol. 15, pp. 182–185, 2016.
- [19] S. Koziel and M. A. U. Haq, "Ground plane modifications for design of miniaturised UWB antennas," *IET Microw., Antennas Propag.*, vol. 12, no. 8, pp. 1360–1366, 2018.
- [20] *CST Microwave Studio, Version 2015*. CST AG, Darmstadt, Germany, 2015.

- [21] S. Koziel, "Computationally efficient multi-fidelity multi-grid design optimization of microwave structures," *Appl. Comput. Electromagn. Soc. J.*, vol. 25, no. 7, pp. 578–586, 2010.
- [22] A. R. Conn, N. I. M. Gould, and P. L. Toint, *Trust Region Methods* (MPS-SIAM Series on Optimization). Philadelphia, PA, USA: MPS, 2000.
- [23] S. Blanch, J. Romeu, and I. Corbella, "Exact representation of antenna system diversity performance from input parameter description," *Electron. Lett.*, vol. 39, no. 9, pp. 705–707, May 2003.
- [24] G.-S. Lin, C.-H. Sung, J.-L. Chen, L.-S. Chen, and M.-P. Hong, "Isolation improvement in UWB MIMO antenna system using carbon black film," *IEEE Antennas Wireless Propag. Lett.*, vol. 16, pp. 222–225, 2017.
- [25] C.-X. Mao, Q.-X. Chu, Y.-T. Wu, and Y.-H. Qian, "Design and investigation of closely-packed diversity UWB slot-antenna with high isolation," *Prog. Electromagn. Res. C*, vol. 41, pp. 13–25, 2013.
- [26] S. U. Kharche, G. S. Reddy, B. Mukherjee, R. K. Gupta, and J. Mukherjee, "MIMO antenna for Bluetooth, Wi-Fi, Wi-MAX and UWB applications," *Prog. Electromagn. Res. C*, vol. 52, pp. 53–62, 2014.



SLAWOMIR KOZIEL received the M.Sc. and Ph.D. degrees in electronic engineering from the Gdansk University of Technology, Poland, in 1995 and 2000, respectively, the M.Sc. degree in theoretical physics and the M.Sc. and Ph.D. degrees in mathematics from the University of Gdansk, Poland, in 2000, 2002, and 2003, respectively. He is currently a Professor with the School of Science and Engineering, Reykjavik University, Iceland. His research interests include CAD and modeling of microwave and antenna structures, simulation-driven design, surrogate-based optimization, space mapping, circuit theory, analog signal processing, evolutionary computation, and numerical analysis.

...



MUHAMMAD AZIZ UL HAQ received the B.S. and M.S. degrees in electronic engineering from Mohammad Ali Jinnah University, Karachi (Islamabad campus), Pakistan, in 2011 and 2014, respectively. He is currently pursuing the Ph.D. degree with the School of Science and Engineering, Reykjavik University, Iceland. He has been involved in several projects in the field of contemporary antenna design for microwave imaging, eHealth, and future wireless communication systems, such as 5G and Internet of Things, from 2014 to 2016. His research interests include compact antenna design and optimization methods for selected classes of antenna structures.

Muhammad Aziz ul Haq, and Slawomir Koziel

Ground Plane Alterations for High-Isolation Compact Wideband MIMO Antennas In a Parallel Configuration

Under review: Microwave and Optical Technology Letters.

Abstract: This paper presents a novel mutual coupling reduction technique for wideband multiple-input-multiple-output (MIMO) antennas in a parallel configuration. Our approach is based on ground plane alterations. We consider n -section rectangular slits below the feed line and analyze the effect of multiple sections on achievable isolation levels. A benchmark set of four wideband MIMO antenna is utilized to examine the actual impact of the considered alterations on radiator isolation. Rigorous numerical optimization of all geometry parameters is carried out to ensure the minimum size of the structures while satisfying two performance constraints: reflection $|S_{11}| \leq -10$ dB, and isolation $|S_{21}| \leq -20$ dB, both within the operational bandwidth. Other performance figures obtained for the considered antennas such as Envelop Coefficient Correlation ($ECC < 0.005$), diversity gain ($DG > 9.99$ dB), and total efficiency approximately $> 80\%$ also demonstrate that high isolation is achieved without compromising the important MIMO antenna characteristics. Numerical results are verified experimentally.

9.1 Introduction

Multiple-Input-Multiple-Output (MIMO) antenna systems have significantly enhanced reliability and data capacity of communication channels over single antenna systems without using extra bandwidth or power consumption [a]. Multiple antenna installation (at the receiving or transmitting end) featuring low mutual coupling is essential for reliable communication [b]. The size has always been an important issue for designers in the context of mounting antennas in physically small devices. On the other hand, densely arranged MIMO antenna elements lead to a coupling issue that degrades the MIMO system performance. Design of compact MIMO antennas with high isolation for space-limited communication devices remains a challenge for the researchers. In some applications, such as imaging and radar systems [c], where transmitting and receiving antenna elements are placed close to each other, a high level of isolation is required to ensure adequate operation and performance.

There have been significant research efforts observed over the last few years to address the aforementioned issues. One of the simplest methods to reduce the mutual coupling effect is to place the antenna elements orthogonal to each other [d], [e]. However, for certain applications such as imaging and radar systems where a large number of antenna elements are required to enhance the system resolution, practical issues arise related to the complexity of the feeding structure (problematic for compact communication devices). Other approaches include introduction of a rectangular strip between the antenna elements [f], a parasitic coupling element [g], [h], a neutralization line [i], [j], a coupled-resonator decoupling network (CRDN) [k], Electromagnetic Band Gap (EBG) structures [l], as well as metamaterial-inspired antennas [m]. These techniques have been successfully applied to reduce the mutual coupling phenomena, but at the cost of their own limitations. In particular, they are typically applied to narrowband structures, whereas their implementation for compact wideband and ultrawideband systems is much more complicated. Some geometry-modification-based techniques intended to achieve improved isolation for wideband applications have been reported in [n]-[p].

It should be emphasized that the development of a particular antenna topology, including appropriate alterations such as those discussed in the previous paragraph, is not sufficient to achieve a satisfactory design. Another, often overlooked stage, is a proper adjustment of antenna geometry parameters concerning all performance figures involved. A conventional approach here is parameter sweeping, which is laborious and does not lead to optimum results due to complex interactions between various parameters. Rigorous numerical optimization ensures superior results and should be carried out not only to achieve the best possible antenna performance but also to validate the relevance of particular topological changes introduced into the antenna structure [q].

In this paper, a technique for isolation improvement in the context of wideband MIMO antennas in a parallel configuration is proposed. Our approach is based on appropriate ground plane modifications, primarily multi-section slits below the feed lines. These allow us to improve the antenna matching without enlarging the footprint. The “safety” margin between the maximum in-band reflection and the -10 dB acceptance limit obtained this way, permits—along with rigorous optimization of antenna parameters—for enhancing isolation. The technique is generic as demonstrated using four UWB structures of various radiator shapes. Isolation at the level of -20 dB is obtained in all cases, along with satisfactory values of other performance figures (ECC, DG, radiation pattern). Experimental validation is provided.

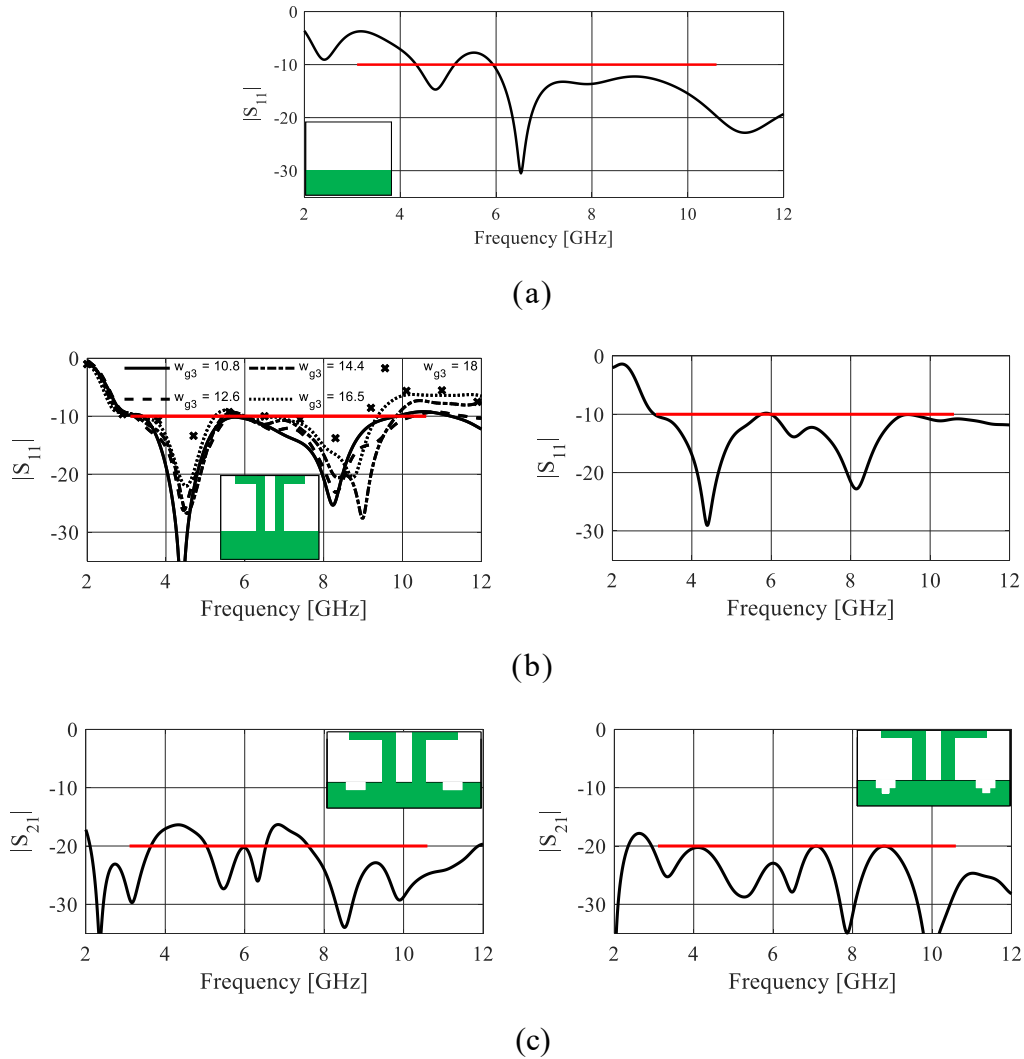


Figure 9.1: Proposed isolation enhancement technique for wideband MIMO antennas: (a) Stage 0: plain ground and the pre-optimized antenna reflection response, (b) Stage 1: L-shape stubs inserted and geometry parameters pre-adjusted using parameter sweeping followed by numerical optimization of the reflection response, (c) Stage 2: multi-stage slits below the feed lines inserted and geometry parameters optimized for best isolation with reflection constraint ($|S_{11}| \leq -10$ dB).

9.2 Ground plane techniques for isolation improvement

This section discusses the proposed systematic approach to isolation enhancement for wideband MIMO antenna design. The procedure has been conceptually explained in Fig. 1, where subsequent stages of ground plane development have been illustrated. For the sake of clarity, only the ground plane (but not the radiators) has been shown. The starting point is a plain ground (Figure 9.1 (a)), with a possibly good antenna performance achieved through parameter sweeping and/or numerical optimization. In the next stage, the L-shape stubs are inserted (Figure 9.1 (b)). The primary purpose of these is an improvement of the reflection response. The geometry parameter adjustment at this stage is first realized using a parameter sweeping, then (upon producing a reasonable initial design), through numerical optimization (cf. Figure 9.1(b)). The second stage provides a good initial design for the last stage, which consists of inserting multi-section slits below the radiator feed lines, followed by rigorous

constrained optimization of the antenna parameters. The optimization algorithm of choice is a trust-region gradient search with numerical derivatives [r] and implicit constraint handling using by means of a penalty function approach [s]. Figure 9.2 shows a flowchart of the procedure. At particular stages of the process, the optimizer switches between a parameter sweeping routine and the gradient-based algorithm, as well as appropriately selects the design objectives and constraints. Note that the last stage involves a constraint on the reflection response with the primary objective being isolation improvement. As demonstrated in the remaining parts of the letter, the proposed decomposition of the design preferences and constraints, as well as sequential introduction of ground plane modifications interleaved by parameter optimization allows us to obtain consistent and competitive results. Furthermore, comprehensive verification carried out for a variety of radiators indicates the versatility of the techniques.

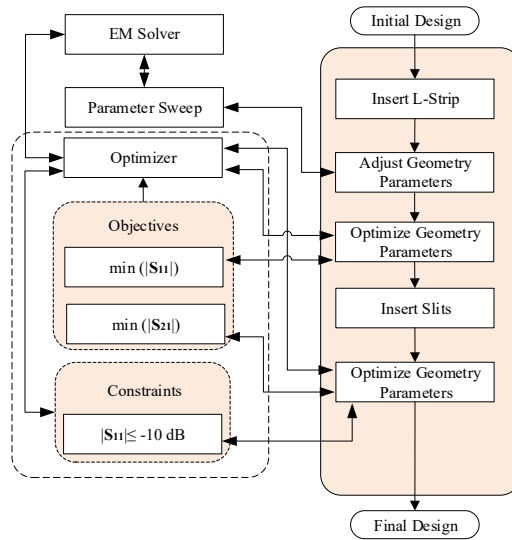


Figure 9.2: Operation of the proposed isolation enhancement technique. Here, the constraints are introduced to limit physical antenna size within a certain value. A custom-designed socket is used to interface the optimizer and the EM solver. The presented framework allows for switching between various numerical optimization setups where necessary, eventually leading to the optimum results both interms of the antenna impedance matching and isolation.

9.3 Verification case studies

The proposed optimization-based isolation enhancement procedure has been applied to four wideband MIMO antennas in a parallel configuration as shown in Figure 9.3. The antennas differ in the radiator shapes, yet, in order to demonstrate the versatility of our approach, the same ground plane technique of Section II has been used to improve isolation while maintaining small footprints. All antennas are realized on a 1.55-mm thick FR-4 substrate ($\epsilon_r = 4.4$). Computational models are implemented in CST Microwave Studio [t]. The models are equipped with SMA connectors to improve further agreement between the simulation and measurement data. The design variable vectors of Antenna I through IV are: $\mathbf{x}^I = [l_g l_0 r_1 r_2 d d_l d_w l_{g1} w_{g2} l_{g3} w_{g3} w_{01}]^T$, $\mathbf{x}^{II} = [l_g l_0 l_{01} w_{01} l_{02} w_{02} l_p w_p d d_l d_w l_{g1} w_{g2} l_{g3} w_{g3} u v]^T$, $\mathbf{x}^{III} = [l_g l_0 l_{01} w_{01} l_{02} w_{02} l_p w_p r d d_l d_w l_{g1} w_{g2} l_{g3} w_{g3} u v]^T$, and $\mathbf{x}^{IV} = [l_g l_0 l_{01} w_{01} l_{02} w_{02} l_p w_p d d_l d_w l_{g1} w_{g2} l_{g3} w_{g3} u v]^T$. All dimensions are in mm. In the first stage, following the design methodology of Section II, rigorous numerical optimization is applied to achieve the best possible matching. The results are shown in Figure 9.4(a). The numerical values corresponding to the each antenna are $\mathbf{x}_1^I = [4.0 \ 5.8 \ 6.7 \ 0.9 \ 2.9 \ 5.6 \ 3.3 \ 0.5 \ 1.5 \ 1.2 \ 1.0 \ 3.5]^T$,

$\mathbf{x}_1^{\text{II}} = [7 \ 3.4 \ 1.8 \ 2.7 \ 2.6 \ 7.4 \ 8.3 \ 8 \ 5 \ 1.8 \ 1.4 \ 1.9 \ 0.9 \ 8.4 \ 0.6 \ 2.2]^T$, $\mathbf{x}_1^{\text{III}} = [5.6 \ 3.9 \ 1.5 \ 1 \ 1.6 \ 4.3 \ 9 \ 0.9 \ 7.6 \ 5.5 \ 1 \ 1.9 \ 0.9 \ 0.3 \ 5.3 \ 0.3 \ 0.5]^T$, and $\mathbf{x}_1^{\text{IV}} = [9 \ 3.7 \ 3.4 \ 2.8 \ 3.8 \ 11.6 \ 7.5 \ 7.6 \ 4.8 \ 3.8 \ 9 \ 3 \ 1.3 \ 13 \ 0.3 \ 2]^T$. Figure 9.4(b) shows the isolation characteristics of the antennas with a plain ground. In the next stage, the slits below the feeds lines are added and the antenna parameters are re-optimized. Here, for illustration purposes, the results corresponding to both one- (Figure 9.4(c)) and two-section slits (Figure 9.4(d)) are shown. Isolation achieved for two-section slits is below -20 dB for the entire operating band. The numerical values are: $\mathbf{x}_3^{\text{I}} = [5.7 \ 7.0 \ 7.4 \ 0.8 \ 1.3 \ 5.4 \ 0.7 \ 1.0 \ 3.0 \ 4.2 \ 1.8 \ 4.2 \ 3.8 \ 0.2 \ 0.9 \ 0.8]^T$, $\mathbf{x}_3^{\text{II}} = [8.2 \ 1.6 \ 4.5 \ 2.1 \ 3.6 \ 8 \ 7.8 \ 10 \ 5 \ 3.9 \ 6.1 \ 4.4 \ 2.9 \ 13.4 \ 0.3 \ 1.6 \ 1 \ 0.3 \ 0.9 \ 0.3]^T$, $\mathbf{x}_3^{\text{III}} = [8 \ 5.8 \ 1.2 \ 2.4 \ 2.3 \ 7.2 \ 7.3 \ 0.5 \ 12.6 \ 2.8 \ 3.5 \ 6.4 \ 3 \ 15.5 \ 0.3 \ 0.6 \ 0.4 \ 3.8 \ 0.4 \ 0.2]^T$, and $\mathbf{x}_3^{\text{IV}} = [10 \ 2.5 \ 5.8 \ 1.5 \ 4.5 \ 10.7 \ 8.7 \ 15 \ 3.7 \ 1.9 \ 3.6 \ 3.9 \ 3 \ 15.4 \ 0.4 \ 1.5 \ 5.5 \ 0.7 \ 0.4 \ 0.2]^T$.

The effect of the slit can be further analyzed using surface current distributions, here shown at 5 GHz (cf. Figure 9.5). For the sake of brevity, only Antenna II is considered. It can be observed that with Port 1 excited and Port 2 is terminated with a $50 \ \Omega$ impedance load, a significant amount of current is flowing not only on the ground plane but also coupled along Port 2 as shown in Figure 9.5(a). This effect is reduced to some extent by introducing a one-section slit below the feed line as shown in Figure 9.5(b). Introduction of two-section slits improves the situation significantly, and a negligible amount of current is observed along Port 2 as shown in Figure 9.5(c). This does demonstrate that the introduction of the 2-section slits reduces the mutual coupling to the point where both ports are almost independent of each other.

In order to further validate the capability and performance of the considered MIMO antennas, envelop correlation coefficient (ECC), and diversity gain (DG) is investigated. $ECC \leq 0.5$ is considered a requirement for an uncorrelated MIMO system. ECC can be calculated using the following expression [u].

$$ECC = \frac{|\iint_{4\pi} [\vec{F}_1(\theta, \phi) \cdot \vec{F}_2(\theta, \phi)] d\Omega|^2}{\iint_{4\pi} |\vec{F}_1(\theta, \phi)|^2 d\Omega \iint_{4\pi} |\vec{F}_2(\theta, \phi)|^2 d\Omega} \quad (9.1)$$

Where, $\vec{F}_i(\theta, \phi)$ is the field radiation pattern of the MIMO antenna element when port i is excited (here, $i = 1, 2$) and other port is terminated with the $50 \ \Omega$ load. Here, ECC has been evaluated through numerical integration of the simulated farfield data. It is clear from the Figure 9.6 that the ECC values of the benchmark antennas are lower than 0.005 which confirms the capability of the antennas for reliable communication, achieved due to the proposed decoupling structure. The differential gain, evaluated using the formula as:

$$DG = 10\sqrt{(1 - ECC^2)} \quad (9.2)$$

is higher than 9.99 for the entire UWB frequency range.

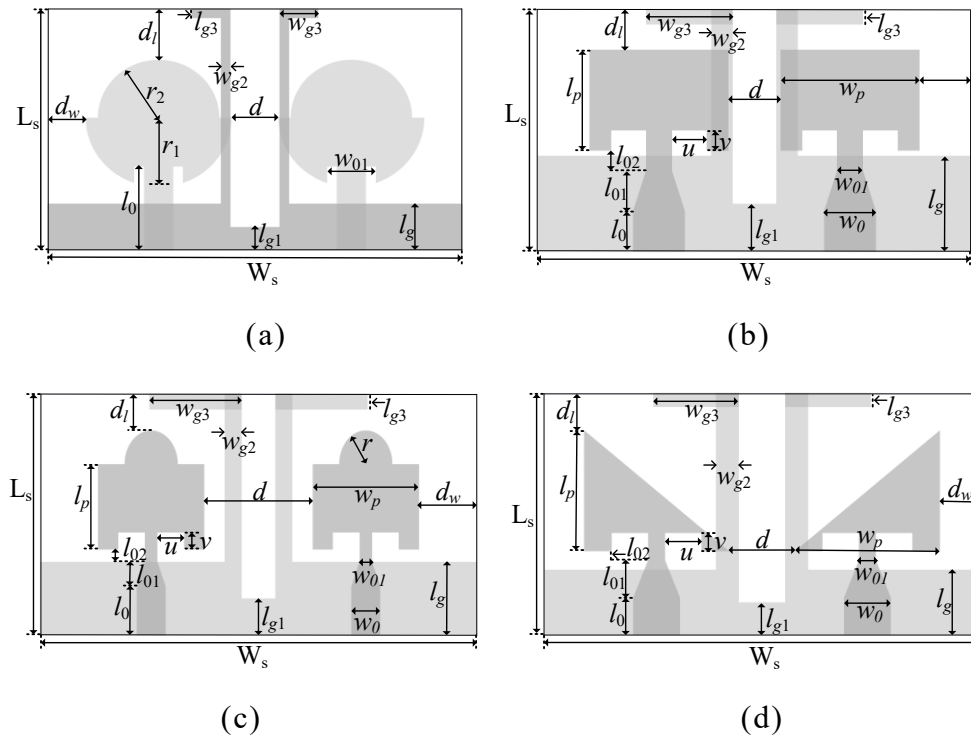


Figure 9.3: Geometries of compact UWB-MIMO antennas utilized to validate the proposed isolation enhancement technique. (a) Antenna I, (b) Antenna II, (c) Antenna III, and (d) Antenna IV. The ground plane is shown using the light gray shade.

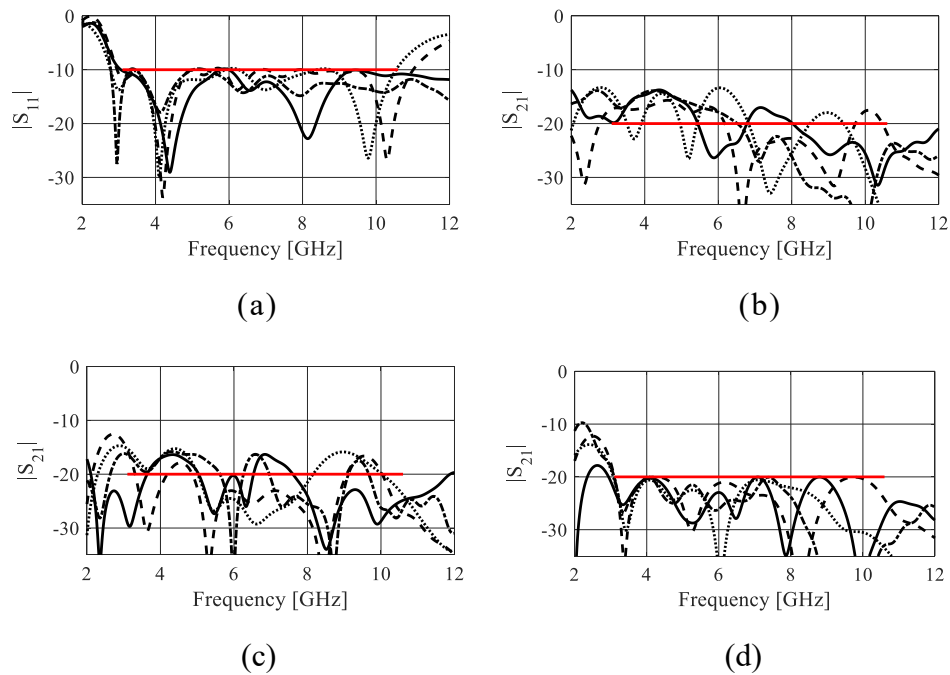


Figure 9.4: Simulated S-parameters of the optimized benchmark antennas: Antenna I (—), Antenna II (- - -), Antenna III (— · —), and Antenna IV (...): (a) $|S_{11}|$ response w. r. t. the initial design, (b) $|S_{21}|$ response w. r. t. the initial design (c) $|S_{21}|$ with one-section slit, and (d) $|S_{21}|$ with two-section slits below the feed line.

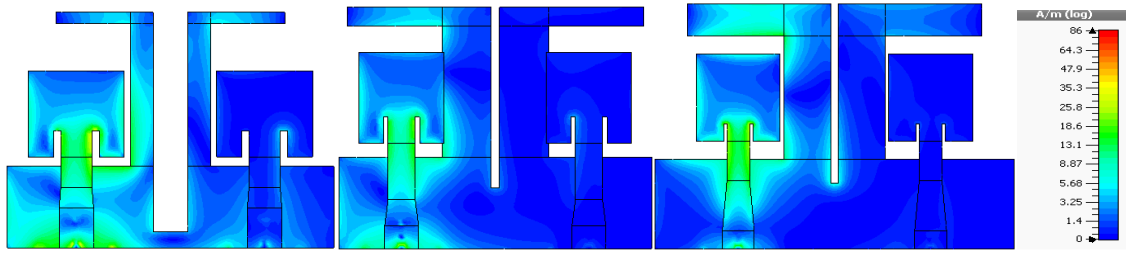


Figure 9.5: Surface current distributions over Antenna II at 5 GHz. (a) Flat ground plane, (b) one-section slit, and (c) two-section slit below the feed line.

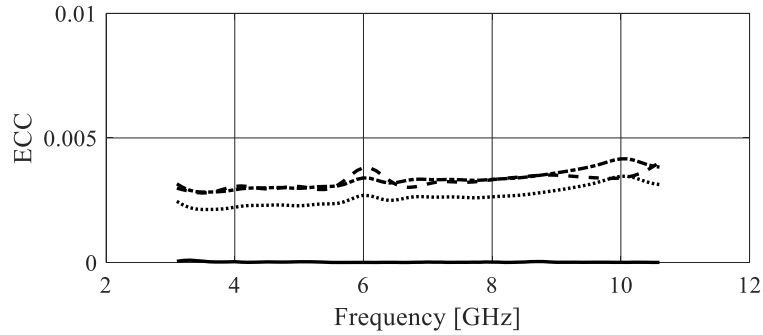


Figure 9.6: Simulated ECC characteristics of the optimized antennas: Antenna I (—), Antenna II (---), Antenna III (- - -), and Antenna IV (...).

9.4 Experimental results

Experimental validation of the simulation results have been carried out for two selected structures, Antenna I and Antenna III. Due to the parallel orientation of the MIMO antennas, the results of the Port 2 are not shown as they are identical to those for Port 1. It can be observed from Figure 9.7(a) that the simulated and measured $|S_{11}|$ response is below -10 dB which is the basic requirement for any antenna operating for the UWB frequency band. Also, Figure 9.7(b) illustrates the simulated and measured isolation $|S_{21}|$ for both antennas, which is under -20 dB. This demonstrates that the proposed isolation enhancement technique leads to adequate results in terms of reducing the mutual coupling between the antenna elements. Figure 9.8 illustrates the measured and simulated efficiencies of Antenna I and III. A good agreement is observed for the entire operating frequency range.

Figure 9.9 shows the measured and simulated MIMO antenna performance in term of ECC and DG corresponding to the Antenna I and III. It is observed that the measured ECC and DG (here, obtained from the S-parameters) are confirming our simulations. Figure 9.10 shows the radiation patterns at 6 GHz and 8 GHz. The radiation characteristics are nearly omnidirectional over the operating band.

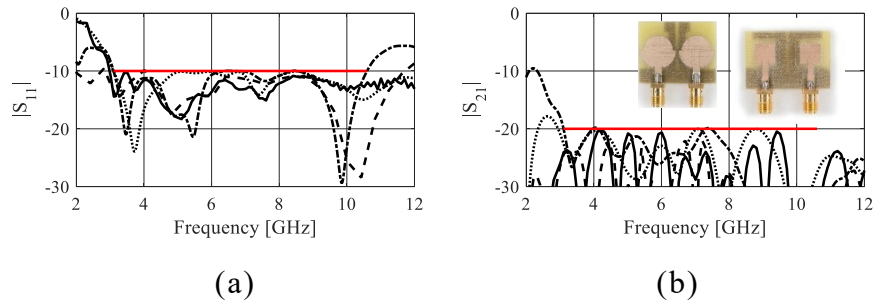


Figure 9.7: Simulated and measured S-parameters of the optimized UWB-MIMO antennas with the two-section slit below the feed line: Antenna I measured (—) and simulated (...), Antenna III measured (---), and simulated (- - -). (a) $|S_{11}|$ and (b) $|S_{21}|$.

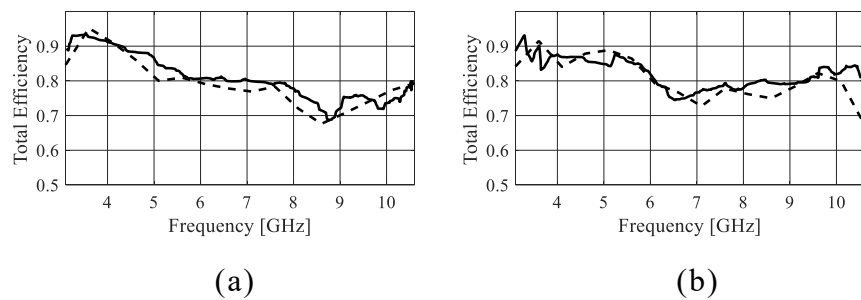


Figure 9.8: Measured (—) and simulated (---) efficiencies of the optimized MIMO antennas: (a) Antenna I and (b), Antenna III.

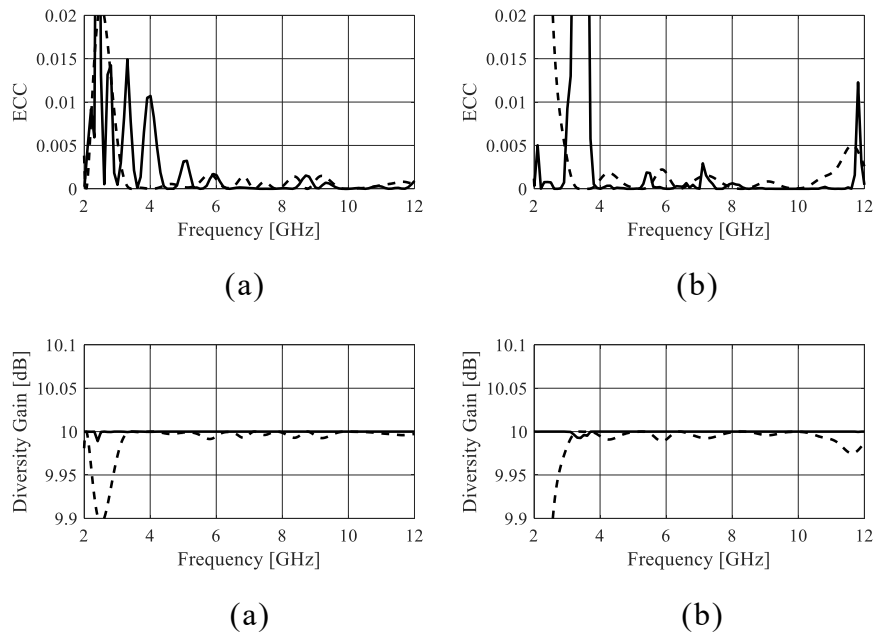


Figure 9.9: Measured (—) and simulated (---) ECC and DG response of the optimized antennas: (a) Antenna I and (b) Antenna III.

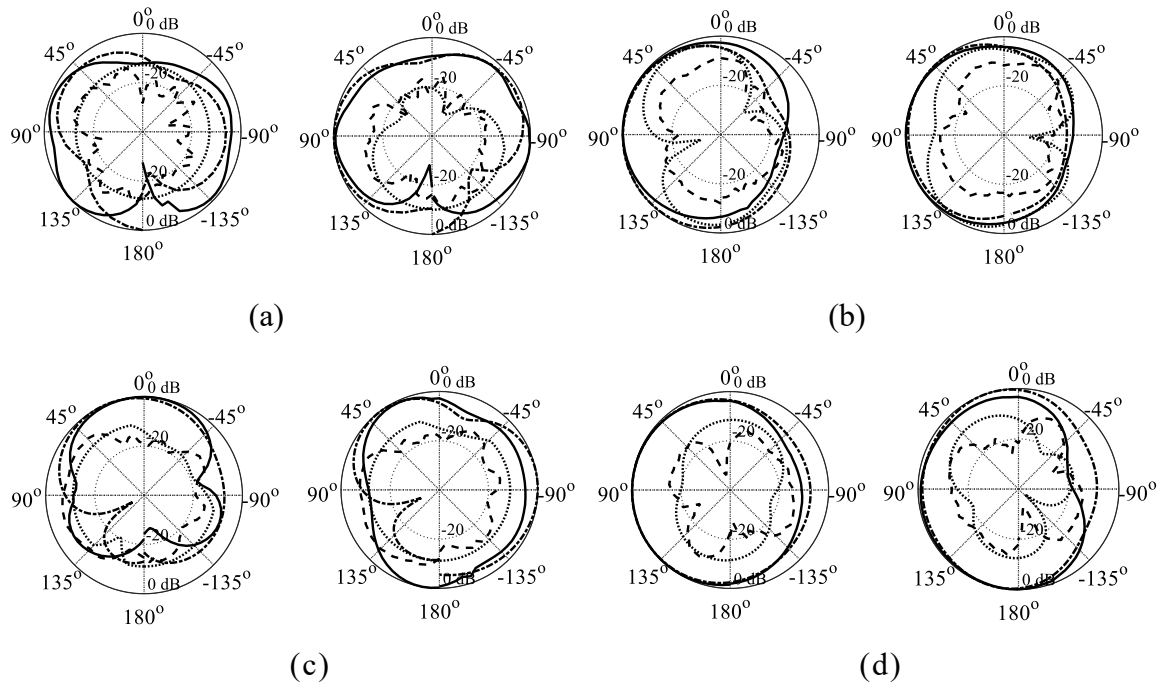


Figure 9.10: Simulated and measured radiation pattern of the optimized UWB-MIMO antennas with the two-section slit below the feed line: Simulated co-pol (---), measured co-pol (—), simulated cross-pol (...) and measured cross-pol (- - -). The plots from left- to right-hand side are for the frequencies 6 GHz and 8 GHz: (a) Antenna I E-plane (b) Antenna I H-plane, (c) Antenna III E-plane, and (d) Antenna III H-plane.

Conclusion: In this letter, a simple technique for enhancing element isolation in wideband MIMO antennas in a parallel configuration is carried out. Our approach combined topological modification of the ground plane with rigorous, multi-stage constrained optimization of antenna parameters. This does not only allow for achieving excellent performance in terms of electrical and field characteristics but also maintain a compact size of the structures. The technique has been validated using four UWB MIMO antennas exploiting various radiators. The obtained results are consistent for all cases (in particular, isolation $|S_{21}| \leq -20$ dB for the entire UWB frequency range has been achieved), which demonstrates the versatility of the approach. The proposed methodology can be used as a convenient tool for design automation and performance improvement of miniaturized MIMO antennas, as well as combined with different type of ground plane and/or radiator (or feed line) modifications.

Reference:

- S. Tripathi, A. Mohan, and S. Yadav, "A compact koch fractal UWB MIMO antenna with WLAN band-rejection," *IEEE Ant. Wireless Prop. Lett.*, vol. 14, pp. 1565-1568, 2015.
- S. Koziel and A. Bekasiewicz, "Electromagnetic-simulation-driven design of compact ultra-wideband multiple-input– multiple-output antenna," *IET Microwaves, Ant. Prop.*, vol. 10, Iss. 15, pp. 1721-1724, 2016.
- M. J. Hasan, T. A. Denidni, and A. R. Sebak, "Millimetre wave compact EBG structure for mutual coupling reduction applications," *IEEE Trans. Antennas Prop.*, vol. 63, no. 2, pp. 823–828, 2015.

- d. S. Koziel, A. Bekasiewicz, and Q. S. Cheng, "Conceptual design and automated optimisation of a novel compact UWB MIMO slot antenna," *IET Microwaves, Ant. Prop.*, vol. 3, Iss. 8, pp. 1162-1168, 2017.
- e. L. Li, S.W. Cheung, and T.I. Yuk, "Compact MIMO antenna for portable devices in UWB applications," *IEEE Trans. Antennas Propag.*, vol. 61, no. 8, pp. 4257–4264, 2013.
- f. K. J. Babu, R. W. Aldhaheri, M. Y. Talha, and I. S. Alruhaili, "Design of a compact two element MIMO antenna system with improved isolation," *Progress In Electromagnetics Research*, vol. 48, pp. 27–32, 2014.
- g. Z. Li, Z. Du, M. Takahashi, K. Saito, and K. Ito, "Reducing mutual coupling of MIMO antennas with parasitic elements for mobile terminals," *IEEE Trans. Antennas Propag.*, vol. 60, No. 2, pp. 473–481, 2012.
- h. J. F. Li, Q.-X. Chu, and T. G. Huang, "A compact wideband MIMO antenna with two novel bent slits," *IEEE Trans. Antennas Propag.*, Vol. 60, no. 2, pp. 482–489, 2012.
- i. S. Su, C. Lee, and F. Chang, "Printed MIMO-antenna system using neutralization-line technique for wireless USB-dongle applications," *IEEE Trans. Antennas Propag.*, vol. 60, no. 2, pp. 456–463, 2012.
- j. Wang, Y. and Z. Du, "A wideband printed dual-antenna with three neutralization lines for mobile terminals," *IEEE Trans. Antennas Propag.*, vol. 62, no. 3, pp. 1495–1500, 2014.
- k. L. Zhao, and K. L. Wu, "A dual-band coupled resonator decoupling network for two coupled antenna," *IEEE Trans. Antennas Propag.*, vol. 63, no. 7, pp. 2843–2850, 2015.
- l. Q. Li, A. P. Feresidis, M. Mavridou, and P. S. Hall, "Miniaturized double-layer EBG structures for broadband mutual coupling reduction between UWB monopoles," *IEEE Trans. Antennas Prop.*, vol. 63, no. 3, pp. 1168–1171, 2015.
- m. C. G. M. Ryan, and G. V. Eleftheriades, "Two compact, wideband, and decoupled meanderlin antennas based on metamateria concepts," *IEEE Antennas Wireless Propag. Lett.*, vol. 11, pp. 1277–1280, 2012.
- n. A. Iqbal, O. A. Saraereh, A. W. Ahmad, and S. Bashir "Mutual coupling reduction using F-shaped stubs in UWB-MIMO antennas," *IEEE Access.*, vol. 6, pp. 2755-2759, 2018.
- o. S. S. Jehangir and M. S. Sharawi, "A miniaturized UWB biplanar yagi-like MIMO antenna system," *IEEE Ant. Wireless Prop. Lett.*, vol. 16, pp. 2320-2323, 2017.
- p. J. Y. Deng, L. Guo, and X. Liu, "An ultrawideband MIMO antenna with a high isolation," *IEEE Ant. Wireless Prop. Lett.*, vol. 15, pp. 182-185, 2016.
- q. M. A. Haq and S. Koziel, "On topology modifications for wideband antenna miniaturization," *AEU Int. J. Electron. Commun.*, vol. 94, pp. 215-220, 2018.
- r. A. R. Conn, N.I.M. Gould, and P.L. Toint, *Trust Region Methods*, MPS-SIAM Series on Optimization, 2000.
- s. A. Bekasiewicz, and S. Koziel, "Structure and computationally-efficient simulation-driven design of compact UWB monopole antenna," *IEEE Ant. Wireless Prop. Lett.*, vol. 14, pp. 1282-1285, 2015.
- t. CST Microwave Studio, ver. 2015. CST AG, Bad Nauheimer Str. 19, D-64289

Darmstadt, Germany, 2015.

- u. S. Blanch, J. Romeu, and I. Corbella, “Exact representation of antenna system diversity performance from input parameter description,” *Electron. Lett.*, vol. 39, no. 9, pp. 705–707, May 2003.

Chapter 10

10 Conclusion and future directions

This chapter provides a brief summary of the thesis and outlines possible future research directions that might originate from the work carried out so far but also address a number of open problems related to the design of wideband antennas for modern communication systems.

10.1 Conclusion

The main focus of this work was to carry out systematic investigations related to the relevance of geometry modifications for wideband antenna miniaturization. The presented numerical and experimental results indicate that the objectives of this thesis have been achieved and the assumed hypotheses have been positively verified (cf. Section 1.7). As mentioned on several occasions, proper EM-driven optimization of all antenna parameters allows us not only to achieve small antenna footprints but also ensures that performance specifications imposed on electrical and field characteristics are fulfilled. In the course of this work, several classes of the topology alterations have been assessed and their relevance for antenna size reduction has been quantified. Furthermore, the discussed approach has led to the development of novel wideband antennas of attractive characteristics. Specific contributions in all aspects of the work have been detailed in the previous chapters.

10.2 Future directions

The work conducted for the purpose of this thesis can be extended in many different directions related to the design of wideband antennas for modern communication systems. Some important topics that might be considered include:

1. Explicit incorporation into the design process additional performance figures. For example, in mobile communication systems, omnidirectional radiation characteristics are required because of the unknown location of the user. A possible extension of the work could be an improvement of the radiation characteristics through the parametric optimization procedure;
2. Utilization of the results obtained in this thesis in the context of wideband antennas

design for 5G and/or millimeter range, as well as conducting relevant studies, among others, on suitability of particular geometry solutions/modifications for antenna miniaturization for these applications;

3. Development of algorithms for computationally-efficient EM-driven size reduction. The computational cost of the optimization process was not of a concern in this work, whereas it is generally important especially when a large number of antenna geometries and their modifications are to be tested and compared;
4. Development of algorithms for automated antenna topology development. Here, the major issue is the automated selection of appropriate geometry modifications along with dimension adjustment, which is essentially a mixed-integer problem.

Bibliography

- [1] F. J. Mann, ‘Alexander graham Bell — Scientist’, *Electr. Eng.*, vol. 66, no. 3, pp. 215–230, 1947.
- [2] T. Hattori, A. Sasaki, and K. Momma, ‘and Service Enhancement for Cordless Telephone’, vol. 26, no. 1, pp. 53–58, 1988.
- [3] M. A. Johnson and S. G. Mayer, ‘United States Patent’, 2013.
- [4] G. D. Ott, ‘Vehicle Location in Cellular Mobile Radio Systems’, *IEEE Trans. Veh. Technol.*, vol. 26, no. 1, pp. 43–46, 1977.
- [5] S. Akhtar, ‘2G-5G Networks: Evolution of Technologies , Standards , and Deployment’, *Clayt. State Univ.*, 2000.
- [6] J. W. Reed, K. J. Krizman, B. D. Woerner, and T. S. Rappaport, ‘An overview of the challenges and progress in meeting the E-911 requirement for location service’, *IEEE Commun. Mag.*, 1998.
- [7] S. Tekinay, E. Chao, and R. Richton, ‘Performance benchmarking for wireless location systems’, *IEEE Commun. Mag.*, 1998.
- [8] J. J. Caffery and G. L. Stüber, ‘Overview of radiolocation in CDMA cellular systems’, *IEEE Commun. Mag.*, 1998.
- [9] T. S. Rappaport, J. H. Reed, and B. D. Woerner, ‘Position location using wireless communications on highways of the future’, *IEEE Commun. Mag.*, vol. 34, no. 10, pp. 33–41, 1996.
- [10] C. Drane, M. Macnaughtan, and C. Scott, ‘Positioning GSM telephones’, *IEEE Commun. Mag.*, 1998.
- [11] M. A. Spirito, ‘On the accuracy of cellular mobile station location estimation’, *IEEE Trans. Veh. Technol.*, 2001.
- [12] J. M. Zagami, S. A. Parl, J. J. Bussgang, and K. D. Melillo, ‘Providing universal location services using a wireless E911 location network’, *IEEE Commun. Mag.*, 1998.
- [13] J. Laiho, K. Raivio, P. Lehtimäki, K. Hätönen, and O. Simula, ‘Advanced analysis methods for 3G cellular networks’, *IEEE Trans. Wirel. Commun.*, vol. 4, no. 3, pp. 930–942, 2005.
- [14] S. S. Soliman and C. E. Wheatley, ‘Geolocation technologies and applications for third generation wireless’, *Wirel. Commun. Mob. Comput.*, vol. 2, no. 3, pp. 229–251, 2002.
- [15] Y. Zhao, ‘Standardization of mobile phone positioning for 3G systems’, *IEEE Commun. Mag.*, 2002.
- [16] U. Varshney, ‘4G wireless networks’, *IT Prof.*, vol. 14, no. 5, pp. 34–39, 2012.
- [17] S. S. Cherian and A. N. Rudrapatna, ‘LTE location technologies and delivery solutions’, *Bell Labs Tech. J.*, vol. 18, no. 2, pp. 175–194, 2013.

- [18] J. G. Andrews *et al.*, ‘What will 5G be?’, *IEEE J. Sel. Areas Commun.*, 2014.
- [19] Gawade S., ‘Wireless Generation for 2020 -5G Technology and Introduction to Its Vital Technology Components’, *Int. J. Recent Innov. Trends Comput. Commun.*, 2015.
- [20] J. A. Del Peral-Rosado, R. Raulefs, J. A. López-Salcedo, and G. Seco-Granados, ‘Survey of Cellular Mobile Radio Localization Methods: From 1G to 5G’, *IEEE Commun. Surv. Tutorials*, vol. 20, no. 2, pp. 1124–1148, 2018.
- [21] M. A. Khan, M. A. Ul Haq, and S. Ur Rehman, ‘A practical miniature antenna design for future internet of things enabled smart devices’, in *2016, 10th International Conference on Signal Processing and Communication Systems, ICSPCS 2016 - Proceedings*, 2016.
- [22] J. L. Volakis, *Antenna Engineering Handbook, Fourth Edition*. 2012.
- [23] ‘IEEE Standard # 145 Definitions of Terms for Antennas’, *IEEE Trans. Antennas Propag.*, 1969.
- [24] C. E. Balanis, ‘Antenna Theory: Analysis and Design, 3rd Edition - Constantine A. Balanis’, *Book*. 2005.
- [25] R. Bansal, ‘Antenna theory; analysis and design’, *Proc. IEEE*, 1984.
- [26] T. A. Milligan, *Modern Antenna Design: Second Edition*. 2005.
- [27] A. Maltsev, A. Sadri, and A. Pudeyev, ‘Highly Directional Steerable Antennas’, 2016.
- [28] A. Maltsev, A. Sadri, A. Pudeyev, and I. Bolotin, ‘Highly Directional Steerable Antennas: High-Gain Antennas Supporting User Mobility or Beam Switching for Reconfigurable Backhauling’, *IEEE Veh. Technol. Mag.*, vol. 11, no. 1, pp. 32–39, 2016.
- [29] G. H. Brown and G. H. Brown, ‘Directional Antennas’, *Proc. Inst. Radio Eng.*, vol. 25, no. 1, pp. 78–145, 1937.
- [30] R. Murawski, E. Ekici, V. Chakravarthy, and W. K. McQuay, ‘Performance of highly mobile cognitive radio networks with directional antennas’, in *IEEE International Conference on Communications*, 2011.
- [31] K. L. Lau and K. M. Luk, ‘A Wideband Dual-Polarized L-Probe Stacked Patch Antenna Array’, *IEEE Antennas Wirel. Propag. Lett.*, vol. 6, pp. 529–532, 2007.
- [32] H. Vettikalladi, O. Lafond, and M. Himdi, ‘High-efficient and high-gain superstrate antenna for 60-GHz indoor communication’, *IEEE Antennas Wirel. Propag. Lett.*, 2009.
- [33] M. A. Towfiq, A. Khalat, B. A. Cetiner, O. Ceylan, and N. Biyikli, ‘Broadband high-gain 60 GHz antenna array’, in *2016 IEEE Antennas and Propagation Society International Symposium, APSURSI 2016 - Proceedings*, 2016, pp. 899–900.
- [34] H. Vettikalladi, W. T. Sethi, and M. A. Alkanhal, ‘High gain and high efficient stacked antenna array with integrated horn for 60 GHz communication systems’, *Int. J. Antennas Propag.*, vol. 2014, 2014.
- [35] H. Vettikalladi, L. Le Coq, O. Lafond, and M. Himdi, ‘Efficient and high-gain aperture coupled superstrate antenna arrays for 60 GHz indoor communication systems’, *Microw. Opt. Technol. Lett.*, vol. 52, no. 10, pp. 2352–2356, 2010.

- [36] B. Aqlan, H. Vettikalladi, and M. A. S. Alkanhal, 'High gain superstrate aperture antenna/array for 79-GHz applications', in *RFM 2015 - 2015 IEEE International RF and Microwave Conference*, 2016, pp. 194–199.
- [37] A. A. Serra, P. Nepa, G. Manara, G. Tribellini, and S. Cioci, 'A wide-band dual-polarized stacked patch antenna', *IEEE Antennas Wirel. Propag. Lett.*, 2007.
- [38] S. K. Han and H. T. Kim, 'A Dual-Polarized Wide-Band Patch Antenna for Indoor Mobile Communication Applications', vol. 108, no. September, pp. 131–140, 2010.
- [39] D. J. Jung, J. N. Hansen, and K. Chang, '60 GHz dipole antenna for short range indoor communication systems', in *IEEE Antennas and Propagation Society, AP-S International Symposium (Digest)*, 2012.
- [40] K. R. Boyle and P. J. Massey, 'Nine-band antenna system for mobile phones', *Electron. Lett.*, 2006.
- [41] R. Hussain, A. T. Alreshaid, S. K. Podilchak, and M. S. Sharawi, 'Compact 4G MIMO antenna integrated with a 5G array for current and future mobile handsets', *IET Microwaves, Antennas Propag.*, 2017.
- [42] T. Thomas, K. Veeraswamy, and G. Charishma, 'MM wave MIMO antenna system for UE of 5G mobile communication: Design', in *12th IEEE International Conference Electronics, Energy, Environment, Communication, Computer, Control: (E3-C3), INDICON 2015*, 2016.
- [43] G. Han, B. Du, W. Wu, and B. Yang, 'A Novel Hybrid Phased Array Antenna for Satellite Communication on-the-Move in Ku-band', *IEEE Trans. Antennas Propag.*, 2015.
- [44] 'PART V Integrated Antennas for Wireless'.
- [45] G.A.Deschamps, 'Microstrip Microwave Antennas', *3rd USAF Symp. Antennas*, 1953.
- [46] Y. S. H. Khraisat, 'Design of 4 elements rectangular microstrip patch antenna with high gain for 2.4 GHz applications', *Mod. Appl. Sci.*, 2012.
- [47] Y. S. Amrullah, A. A. Fathnan, F. Oktafiani, Y. Taryana, and Y. Wahyu, 'Performance enhancement of microstrip patch antenna by incorporating exponential-square patch model', *2015 Int. Conf. Radar, Antenna, Microwave, Electron. Telecommun.*, pp. 20–23, 2015.
- [48] L. Cui, W. Wu, and D. G. Fang, 'Wideband circular patch antenna with conical radiation pattern', *IEEE Antennas Wirel. Propag. Lett.*, vol. 14, pp. 458–461, 2015.
- [49] P. Squadrito, S. Zhang, and G. F. Pedersen, 'Wideband or Dual-Band Low-Profile Circular Patch Antenna With High-Gain and Sidelobe Suppression', *IEEE Trans. Antennas Propag.*, vol. 66, no. 6, pp. 3166–3171, 2018.
- [50] E. S. Alabidi, M. R. Kamarudin, T. A. Rahman, H. U. Iddi, and M. F. Jamlos, 'Dual-band Circular Patch Antenna for wideband application', in *IEEE Antennas and Propagation Society, AP-S International Symposium (Digest)*, 2013, pp. 2125–2126.
- [51] X. Zhang and L. Zhu, 'Dual-Band High-Gain Circular Patch Antenna Working in Its TM11 and TM12 Modes', *IEEE Trans. Antennas Propag.*, pp. 1–1, 2018.
- [52] Y. F. Lin, H. M. Chen, and S. C. Lin, 'A new coupling mechanism for circularly polarized annular-ring patch antenna', *IEEE Trans. Antennas Propag.*, vol. 56, no. 1,

pp. 11–16, 2008.

- [53] Y. X. Guo, L. Bian, and X. Q. Shi, ‘Broadband circularly polarized annular-ring microstrip antenna’, *IEEE Trans. Antennas Propag.*, vol. 57, no. 8, pp. 2474–2477, 2009.
- [54] M. Ji, Z. Zhang, Z. Feng, and R. Li, ‘A meander annular-ring slot antenna for circularly polarized radiation’, in *2010 International Conference on Microwave and Millimeter Wave Technology, ICMMT 2010*, 2010, pp. 1016–1019.
- [55] R. Li, Y. X. Guo, B. Zhang, and G. Du, ‘A Miniaturized Circularly Polarized Implantable Annular-Ring Antenna’, *IEEE Antennas Wirel. Propag. Lett.*, vol. 16, pp. 2566–2569, 2017.
- [56] Q. Luo *et al.*, ‘Dual Circularly Polarized Equilateral Triangular Patch Array’, *IEEE Trans. Antennas Propag.*, 2016.
- [57] T. kumar and A. Kr Aggarwal, ‘Dual band Equilateral Triangular Patch Antenna’, *IJCEM Int. J. Comput. Eng. Manag. ISSN*, vol. 15, no. 5, pp. 2230–7893, 2012.
- [58] J. T. S. Sumantyo, K. Ito, and M. Takahashi, ‘Dual-band circularly polarized equilateral triangular-patch array antenna for mobile satellite communications’, *IEEE Trans. Antennas Propag.*, vol. 53, no. 11, pp. 3477–3485, 2005.
- [59] J. P. Shinde, P. N. Shinde, and N. Y. Gondane, ‘Circularly polarized transparent equilateral triangular shaped antenna with defected ground’, in *Proceedings - 2nd International Conference on Computing, Communication, Control and Automation, ICCUBEA 2016*, 2017.
- [60] D. Q. Lai and Q. X. Chu, ‘A stacked dual-band equilateral-triangular circularly polarized microstrip antenna’, in *Proceedings of 2008 Asia Pacific Microwave Conference, APMC 2008*, 2008.
- [61] L. Boccia, G. Amendola, and G. Di Massa, ‘A shorted elliptical patch antenna For GPS applications’, *IEEE Antennas Wirel. Propag. Lett.*, 2003.
- [62] G. Amendola, L. Boccia, and G. Di Massa, ‘Surface wave radiation from a shorted elliptical patch antenna’, in *IEEE Antennas and Propagation Society International Symposium. Digest. Held in conjunction with: USNC/CNC/URSI North American Radio Sci. Meeting (Cat. No.03CH37450)*, 2003, vol. 1, pp. 601–604.
- [63] S. Ahmed, F. A. Tahir, A. Shamim, and H. M. Cheema, ‘A Compact Kapton-Based Inkjet-Printed Multiband Antenna for Flexible Wireless Devices’, *IEEE Antennas Wirel. Propag. Lett.*, vol. 14, pp. 1802–1805, 2015.
- [64] Y. L. Ban, Y. F. Qiang, Z. Chen, K. Kang, and J. H. Guo, ‘A dual-loop antenna design for hepta-band WWAN/LTE metal-rimmed smartphone applications’, *IEEE Trans. Antennas Propag.*, vol. 63, no. 1, pp. 48–58, 2015.
- [65] H. F. Abutarboush and A. Shamim, ‘A Reconfigurable Inkjet-Printed Antenna on Paper Substrate for Wireless Applications’, *IEEE Antennas Wirel. Propag. Lett.*, vol. 17, no. 9, pp. 1648–1651, 2018.
- [66] Y.-J. Chou, L.-S. Chen, M.-P. Houng, G.-S. Lin, and J.-F. Chen, ‘Design of GSM/LTE multiband application for mobile phone antennas’, *Electron. Lett.*, vol. 51, no. 17, pp. 1304–1306, 2015.

- [67] M. Naser-Moghadas, R. Ali Sadeghzadeh, M. Alibakhshi-Kenari, and B. Singh Virdee, 'Hexa-band planar antenna with asymmetric fork-shaped radiators for multiband and broadband communication applications', *IET Microwaves, Antennas Propag.*, vol. 10, no. 5, pp. 471–478, 2016.
- [68] L. Albasha, M. Ali, M. Taghadosi, and N. Qaddoumi, 'Miniaturised printed elliptical nested fractal multiband antenna for energy harvesting applications', *IET Microwaves, Antennas Propag.*, vol. 9, no. 10, pp. 1045–1053, 2015.
- [69] R. S. Aziz, A. K. Arya, and S. O. Park, 'Multiband full-metal-rimmed antenna design for smartphones', *IEEE Antennas Wirel. Propag. Lett.*, vol. 15, pp. 1987–1990, 2016.
- [70] K. K. Kishor and S. V. Hum, 'Multiport Multiband Chassis-Mode Antenna Design Using Characteristic Modes', *IEEE Antennas Wirel. Propag. Lett.*, vol. 16, pp. 609–612, 2017.
- [71] R. Khan, A. A. Al-Hadi, P. J. Soh, M. R. Kamarudin, M. T. Ali, and Owais, 'User Influence on Mobile Terminal Antennas: A Review of Challenges and Potential Solution for 5G Antennas', *IEEE Access*, vol. PP, pp. 1–1, 2018.
- [72] S. X. Ta, H. Choo, I. Park, and R. W. Ziolkowski, 'Multi-Band, Wide-Beam, Circularly Polarized, Crossed, Asymmetrically Barbed Dipole Antennas for GPS Applications', *IEEE Trans. Antennas Propag.*, 2013.
- [73] R. Pazoki, A. Kiaee, P. Naseri, H. Moghadas, H. Oraizi, and P. Mousavi, 'Circularly Polarized Monopole L-Shaped Slot Antenna With Enhanced Axial-Ratio Bandwidth', *IEEE Antennas Wirel. Propag. Lett.*, vol. 15, pp. 1073–1076, 2016.
- [74] H. F. Huang and B. Wang, 'A circularly polarized slot antenna with enhanced axial ratio bandwidth', in *2017 IEEE 6th Asia-Pacific Conference on Antennas and Propagation, APCAP 2017 - Proceeding*, 2018, pp. 1–3.
- [75] M. Nosrati and N. Tavassolian, 'A compact circularly-polarized square slot antenna with enhanced axial-ratio bandwidth using metasurface', in *2017 IEEE Antennas and Propagation Society International Symposium, Proceedings*, 2017, vol. 2017–Janua, pp. 107–108.
- [76] S. Nakao, R. Joseph, and T. Fukusako, 'Bandwidth enhancement of a circularly polarized modified L-shaped slot antenna with L-shaped probe', *Int. J. Microw. Opt. Technol.*, vol. 6, no. 2, pp. 82–87, 2011.
- [77] S. P. Pan, J. Y. Sze, and P. J. Tu, 'Circularly polarized square slot antenna with a largely enhanced axial-ratio bandwidth', *IEEE Antennas Wirel. Propag. Lett.*, vol. 11, pp. 969–972, 2012.
- [78] M. A. Ul Haq and S. Koziel, 'A miniaturized UWB monopole antenna with five-section ground plane slit', *Microw. Opt. Technol. Lett.*, 2018.
- [79] M. A. ul Haq and S. Koziel, 'Quantitative assessment of wideband antenna geometry modifications for size-reduction-oriented design', *AEU - Int. J. Electron. Commun.*, 2018.
- [80] M. Aziz Ul Haq and S. Koziel, 'On topology modifications for wideband antenna miniaturization', *AEU - Int. J. Electron. Commun.*, 2018.
- [81] M. A. U. Haq and S. Koziel, 'Simulation-based optimization for rigorous assessment of ground plane modifications in compact UWB antenna design', *Int. J. RF Microw.*

Comput. Eng., 2018.

- [82] M. A. Ul Haq, S. Koziel, and Q. S. Cheng, 'Miniaturisation of wideband antennas by means of feed line topology alterations', *IET Microwaves, Antennas Propag.*, vol. 12, no. 13, pp. 2128–2134, 2018.
- [83] Y. Li and K. M. Luk, 'A 60-GHz Wideband Circularly Polarized Aperture-Coupled Magneto-Electric Dipole Antenna Array', *IEEE Trans. Antennas Propag.*, vol. 64, no. 4, pp. 1325–1333, 2016.
- [84] X. Cui, F. Yang, M. Gao, L. Zhou, Z. Liang, and F. Yan, 'A Wideband Magnetolectric Dipole Antenna with Microstrip Line Aperture-Coupled Excitation', *IEEE Trans. Antennas Propag.*, vol. 65, no. 12, pp. 7350–7354, 2017.
- [85] S. Lung, S. Yang, A. A. Kishk, K. F. Lee, and K. M. Luk, 'E R j + j E L j', vol. 54, no. 4, pp. 1350–1352, 2006.
- [86] J. Cao, H. Wang, S. Mou, S. Quan, and Z. Ye, 'W-Band High-Gain Circularly Polarized Aperture-Coupled Magneto-Electric Dipole Antenna Array with Gap Waveguide Feed Network', *IEEE Antennas Wirel. Propag. Lett.*, vol. 16, pp. 2155–2158, 2017.
- [87] X. Cui, F. Yang, and M. Gao, 'Wideband CP magnetolectric dipole antenna with microstrip line aperture-coupled excitation', *Electron. Lett.*, vol. 54, no. 14, pp. 863–864, 2018.
- [88] K. M. Luk, C. L. Mak, Y. L. Chow, and K. F. Lee, 'Broadband microstrip patch antenna', *Electron. Lett.*, 1998.
- [89] C. L. Mak, K. M. Luk, K. F. Lee, and Y. L. Chow, 'Experimental study of a microstrip patch antenna with an L-shaped probe', *IEEE Trans. Antennas Propag.*, 2000.
- [90] A. I. Bahnacy, S. M. Elhalafawy, and Y. M. M. Antar, 'Stacked L-shaped probe fed microstrip antenna', in *Proceedings of the IEEE International Conference on Electronics, Circuits, and Systems*, 2000, vol. 1, pp. 210–213.
- [91] J. Park, H. G. Na, and S. H. Baik, 'Design of a modified L-probe fed microstrip patch antenna', *IEEE Antennas Wirel. Propag. Lett.*, vol. 3, no. 1, pp. 117–119, 2004.
- [92] K. M. Luk, L. K. A. Yeung, C. L. Mak, and K. F. Lee, 'Circular patch antenna with an L-shaped probe', *Microw. Opt. Technol. Lett.*, vol. 20, no. 4, pp. 256–257, 1999.
- [93] W. K. Lo, J. L. Hu, C. H. Chan, and K. M. Luk, 'Circularly polarized patch antenna with an L-shaped probe fed by a microstrip line', *Microw. Opt. Technol. Lett.*, vol. 24, no. 6, pp. 412–414, 2000.
- [94] H. W. Lai and K. M. Luk, 'Wideband patch antenna fed by a modified L-shaped probe', *Microw. Opt. Technol. Lett.*, vol. 48, no. 5, pp. 977–979, 2006.
- [95] M. H. Reddy, R. M. Joany, M. J. Reddy, M. Sugadev, and E. Logashanmugam, 'Bandwidth enhancement of microstrip patch antenna using parasitic patch', in *2017 IEEE International Conference on Smart Technologies and Management for Computing, Communication, Controls, Energy and Materials, ICSTM 2017 - Proceedings*, 2017, pp. 295–298.
- [96] Y. H. Cho, 'Gain enhancement of microstrip antenna using parasitic metallic patch bar', in *IEEE Antennas and Propagation Society International Symposium. Digest. Held in conjunction with: USNC/CNC/URSI North American Radio Sci. Meeting (Cat.*

- No.03CH37450*), 2003, vol. 2, pp. 728–731.
- [97] S.-T. Fan, S.-F. Zheng, Y.-M. Cai, Y.-Z. Yin, Y.-J. Hu, and J. H. Yang, ‘Design of a Novel Wideband Loop Antenna With Parasitic Resonators’, *Prog. Electromagn. Res. Lett.*, vol. 37, no. November 2012, pp. 47–54, 2013.
- [98] H. Nakano, T. Yoshida, and J. Yamauchi, ‘Metaloop antenna with a parasitic loop’, in *IEEE Antennas and Propagation Society, AP-S International Symposium (Digest)*, 2015, vol. 2015–Octob, pp. 462–463.
- [99] S. Bhaskar and A. K. Singh, ‘Meander line tag antenna with inductively coupled parasitic element and T-loop feed’, in *2017 International Symposium on Antennas and Propagation, ISAP 2017*, 2017, vol. 2017–Janua, pp. 1–2.
- [100] K. L. Wong, W. J. Chen, and T. W. Kang, ‘Small-size loop antenna with a parasitic shorted strip monopole for internal WWAN notebook computer antenna’, *IEEE Trans. Antennas Propag.*, vol. 59, no. 5, pp. 1733–1738, 2011.
- [101] H. Bin Zhang, Y. L. Ban, Y. F. Qiang, J. Guo, and Z. F. Yu, ‘Reconfigurable loop antenna with two parasitic grounded strips for WWAN/LTE unbroken-metal-rimmed smartphones’, *IEEE Access*, vol. 5, pp. 4853–4858, 2017.
- [102] T. Kawano and H. Nakano, ‘A grid array antenna with parasitic monopoles’, in *2015 International Symposium on Antennas and Propagation, ISAP 2015*, 2016.
- [103] S. S. Olokede and M. F. Ain, ‘A Multifunctional Antenna with a Small Form Factor: Designing a Novel Series-Fed Compact Triangular Microstrip Ring Resonator Antenna Array’, *IEEE Antennas Propag. Mag.*, 2018.
- [104] S.-H. Nawel and B. T. Fethi, ‘Compact triangular microstrip antenna with fractal ground’, *Int. J. Ind. Electron. Electr. Eng.*, vol. 33, no. 6, p. 433, 2016.
- [105] B. Singh, N. Sarwade, and K. P. Ray, ‘Compact series FED tapered antenna array using unequal rectangular microstrip antenna elements’, *Microw. Opt. Technol. Lett.*, vol. 59, no. 8, pp. 1856–1861, 2017.
- [106] V. Narasimha Nayak, B. Madhav, R. Sai Divya, A. Nava Sai Krishna, K. Rohith Ramana, and D. Mounika, ‘Compact microstrip rectangular edge fed antenna with DGS structure’, *Int. J. Appl. Eng. Res.*, vol. 10, no. 9, pp. 24331–24348, 2015.
- [107] S. Sengupta, D. R. Jackson, and S. A. Long, ‘A Method for Analyzing a Linear Series-Fed Rectangular Microstrip Antenna Array’, *IEEE Trans. Antennas Propag.*, vol. 63, no. 8, pp. 3731–3736, 2015.
- [108] S. Liu, W. Wu, and D. G. Fang, ‘Wideband monopole-like radiation pattern circular patch antenna with high gain and low cross-polarization’, *IEEE Trans. Antennas Propag.*, 2016.
- [109] P. S. Hall, C. Wood, and C. Garrett, ‘Wide bandwidth microstrip antennas for circuit integration’, *Electron. Lett.*, 1979.
- [110] E. H. Lim, Y. M. Pan, and K. W. Leung, ‘Dielectric resonator antennas’, in *Handbook of Antenna Technologies*, 2016.
- [111] X. L. Liang and T. A. Denidni, ‘H-shaped dielectric resonator antenna for wideband applications’, *IEEE Antennas Wirel. Propag. Lett.*, 2008.
- [112] A. Azari, A. Ismail, A. Sali, and F. Hashim, ‘A new super wideband fractal monopole-

dielectric resonator antenna', *IEEE Antennas Wirel. Propag. Lett.*, 2013.

- [113] R. K. Chaudhary, R. Kumar, and K. V. Srivastava, 'Wideband ring dielectric resonator antenna with annular-shaped microstrip feed', *IEEE Antennas Wirel. Propag. Lett.*, 2013.
- [114] M. Abedian, H. Oraizi, S. K. Abdul Rahim, S. Danesh, M. R. Ramli, and M. H. Jamaluddin, 'Wideband rectangular dielectric resonator antenna for low-profile applications', *IET Microwaves, Antennas Propag.*, 2018.
- [115] M. Ranjbar Nikkhah and A. A. Kishk, 'Compact and wideband dielectric resonator antenna', in *IEEE Antennas and Propagation Society, AP-S International Symposium (Digest)*, 2015.
- [116] U. Ullah, M. F. Ain, and Z. A. Ahmad, 'A review of wideband circularly polarized dielectric resonator antennas', *China Communications*. 2017.
- [117] H. M. R. Nurul, P. J. Soh, M. F. A. Malek, and G. A. E. Vandenbosch, 'Dual-band suspended-plate wearable textile antenna', *IEEE Antennas Wirel. Propag. Lett.*, 2013.
- [118] D. Wojcik and M. Surma, 'Low cost dual-polarized suspended microstrip antenna array for 5.8 GHz point-to-point links', ... (*RADIOELEKTRONIKA*), 2012 22nd ..., 2012.
- [119] Z. N. Chen and M. Y. W. Chia, 'Broadband suspended plate antennas fed by double L-shaped strips', *IEEE Trans. Antennas Propag.*, 2004.
- [120] M. V. Varnoosfaderani, D. V. Thiel, and J. Lu, 'A wideband capacitively fed suspended plate antenna for wearable wireless sensors', in *2015 International Symposium on Antennas and Propagation, ISAP 2015*, 2016.
- [121] I. Sfar and L. Osman, 'Development of dual-band wearable textile antenna for WLAN applications', in *Mediterranean Microwave Symposium*, 2015, vol. 2015–Janua.
- [122] M. Abbak, S. A. Rezaeieh, and I. Akduman, 'Broad-band three layer suspended plate antenna', in *2011 19th Telecommunications Forum, TELFOR 2011 - Proceedings of Papers*, 2011, pp. 951–954.
- [123] A. A. Qureshi, D. M. Klymyshyn, M. Tayfeh, W. Mazhar, M. Börner, and J. Mohr, 'Template-based dielectric resonator antenna arrays for millimeter-wave applications', *IEEE Trans. Antennas Propag.*, 2017.
- [124] Z. Ahmad and J. Hesselbarth, 'On-chip dual-polarized dielectric resonator antenna for millimeter-wave applications', *IEEE Antennas Wirel. Propag. Lett.*, vol. 17, no. 10, pp. 1769–1772, 2018.
- [125] R. Hahnel, M. Becker, B. Klein, and D. Plettemeier, 'Integrated dual polarized on-chip antenna for mm-wave applications', in *2017 IEEE Antennas and Propagation Society International Symposium, Proceedings*, 2017, vol. 2017–Janua, pp. 1817–1818.
- [126] Y. C. Tu, D. D. Ma, Y. Liu, X. H. Hu, and K. Gong, 'Broadband substrate integrated dielectric resonator antenna for millimeter-wave applications', in *2016 IEEE MTT-S International Microwave Workshop Series on Advanced Materials and Processes for RF and THz Applications, IMWS-AMP 2016 - Proceeding*, 2016.
- [127] M. Khalily, M. R. Kamarudin, M. Mokayef, and M. H. Jamaluddin, 'Omnidirectional circularly polarized dielectric resonator antenna for 5.2-GHz WLAN applications', *IEEE Antennas Wirel. Propag. Lett.*, 2014.

- [128] M. Secmen, 'Multiband and Wideband Antennas for Mobile Communication Systems', in *Recent Developments in Mobile Communications - A Multidisciplinary Approach*, 2011.
- [129] A. H. Majeed, A. S. Abdullah, F. Elmegri, K. H. Sayidmarie, R. A. Abd-Alhameed, and J. M. Noras, 'Aperture-coupled asymmetric dielectric resonators antenna for wideband applications', *IEEE Antennas Wirel. Propag. Lett.*, 2014.
- [130] M. K. Brar and S. K. Sharma, 'A wideband aperture-coupled pentagon shape dielectric resonator antenna (DRA) for wireless communication applications', in *IEEE Antennas and Propagation Society, AP-S International Symposium (Digest)*, 2011, pp. 1674–1677.
- [131] Y. Wang, Y. Bo, and D. Ben, 'Wideband aperture coupled microstrip antenna with stubs', in *Proceedings - Fourth Asia-Pacific Conference on Environmental Electromagnetics, CEEM'2006*, 2006, pp. 682–684.
- [132] R. Kumari, S. K. Behera, and S. K. Sharma, 'Aperture coupled wideband dielectric resonator antenna array with polarization reconfiguration', in *2013 IEEE Applied Electromagnetics Conference, AEMC 2013*, 2014.
- [133] M. H. Jamaluddin, G. C. Eu, S. K. A. Rahim, and N. I. Dzulkpli, 'Wideband aperture-coupled dielectric resonator antenna at 5.8 GHz', *J. Teknol. (Sciences Eng.*, vol. 69, no. 1, pp. 25–30, 2014.
- [134] R. K. Mongia and A. Ittipiboon, 'Theoretical and experimental investigations on rectangular dielectric resonator antennas', *IEEE Trans. Antennas Propag.*, 1997.
- [135] A. Gupta and R. K. Gangwar, 'Theoretical and Experimental Investigations on Rectangular Dielectric Resonator Antenna Array for Radar and Satellite Application', *Electromagnetics*, vol. 37, no. 1, pp. 27–39, 2017.
- [136] S. Solomon and R. Kumari, 'Slotted dielectric resonator antenna for broadband applications', in *Global Conference on Communication Technologies, GCCT 2015*, 2015, pp. 494–497.
- [137] E. Vinodha and S. Raghavan, 'Double stub microstrip fed two element Rectangular Dielectric Resonator Antenna for multiband operation', *AEU - Int. J. Electron. Commun.*, vol. 78, pp. 46–53, 2017.
- [138] R. K. Chaudhary, K. V. Srivastava, and A. Biswas, 'A broadband dumbbell-shaped dielectric resonator antenna', *Microw. Opt. Technol. Lett.*, 2014.
- [139] D. Guha and C. Kumar, 'Microstrip Patch versus Dielectric Resonator Antenna Bearing All Commonly Used Feeds: An experimental study to choose the right element', *IEEE Antennas Propag. Mag.*, 2016.
- [140] M. G. Durlabhji, 'Bandwidth Considerations in Miniaturized Rectangular Dielectric Resonator Antennas : Experimental Validation', no. August, 2016.
- [141] A. Rashidian and D. M. Klymyshyn, 'Compact wideband multimode dielectric resonator antennas fed with parallel standing strips', *IEEE Trans. Antennas Propag.*, 2012.
- [142] Y. M. Pan, K. W. Leung, and K. Lu, 'Compact quasi-isotropic dielectric resonator antenna with small ground plane', *IEEE Trans. Antennas Propag.*, 2014.

- [143] L. Guo and K. W. Leung, 'Compact Linearly and Circularly Polarized Unidirectional Dielectric Resonator Antennas', *IEEE Trans. Antennas Propag.*, 2016.
- [144] Y. Gao, Z. Feng, and L. Zhang, 'Compact CPW-fed dielectric resonator antenna with dual polarization', *IEEE Antennas Wirel. Propag. Lett.*, 2011.
- [145] H. M. Chen, Y. K. Wang, Y. F. Lin, S. C. Lin, and S. C. Pan, 'A compact dual-band dielectric resonator antenna using a parasitic slot', *IEEE Antennas Wirel. Propag. Lett.*, 2009.
- [146] A. Sharma, A. Sarkar, A. Biswas, and M. J. Akhtar, 'Dual-band multiple-input multiple-output antenna based on half split cylindrical dielectric resonator', *J. Electromagn. Waves Appl.*, vol. 32, no. 9, pp. 1152–1163, 2018.
- [147] A. Sharma and A. Biswas, 'Wideband multiple-input–multiple-output dielectric resonator antenna', *IET Microwaves, Antennas Propag.*, 2017.
- [148] A. Sharma and A. Biswas, 'Dual-frequency half split cylindrical dielectric resonator antenna', in *2015 IEEE Applied Electromagnetics Conference, AEMC 2015*, 2016.
- [149] S. R. Borkar, 'Multiple input multiple output dielectric resonator antenna for 4G applications', in *Proceedings - IEEE International Conference on Information Processing, ICIP 2015*, 2016, pp. 675–679.
- [150] B. Liu, J. Qiu, H. Zong, and G. Li, 'Design of dual-band pattern reconfigurable cylindrical dielectric resonator antenna', in *2017 IEEE Antennas and Propagation Society International Symposium, Proceedings*, 2017, vol. 2017–Janua, pp. 1767–1768.
- [151] R. K. Chaudhary, K. V. Srivastava, and A. Biswas, 'Wideband multilayer multi-permittivity half-split cylindrical dielectric resonator antenna', *Microw. Opt. Technol. Lett.*, vol. 54, no. 11, pp. 2587–2590, 2012.
- [152] L. D. O. E. De *et al.*, 'Rectangular ring and H-shaped microstrip antennas-alternatives to rectangular patch antenna', vol. 168, no. September, pp. 1181–1186, 2014.
- [153] T. F. A. Nayna, F. Ahmed, and E. Haque, 'Bandwidth enhancement of a rectangular patch antenna in X band by introducing diamond shaped slot and ring in patch and defected ground structure', in *Proceedings of the 2017 International Conference on Wireless Communications, Signal Processing and Networking, WiSPNET 2017*, 2018.
- [154] W. C. Chew, 'A Broad-Band Annular-Ring Microstrip Antenna', *IEEE Trans. Antennas Propag.*, 1982.
- [155] W. X. Liu, Y. Z. Yin, W. L. Xu, and S. L. Zuo, 'Compact open-slot antenna with bandwidth enhancement', *IEEE Antennas Wirel. Propag. Lett.*, 2011.
- [156] S. Genovesi, F. Costa, F. Fanciulli, and A. Monorchio, 'Wearable Inkjet-Printed Wideband Antenna by Using Miniaturized AMC for Sub-GHz Applications', *IEEE Antennas Wirel. Propag. Lett.*, 2016.
- [157] R. B. V. B. Simorangkir, A. Kiourti, and K. P. Esselle, 'UWB Wearable Antenna with a Full Ground Plane Based on PDMS-Embedded Conductive Fabric', *IEEE Antennas Wirel. Propag. Lett.*, 2018.
- [158] S. Agneessens, 'Coupled eighth-mode substrate integrated waveguide antenna: Small and wideband with high-body antenna isolation', *IEEE Access*, vol. 6, pp. 1595–1602, 2017.

- [159] Z. Hamouda, J. Wojkiewicz, A. A. Pud, L. Kone, S. Bergheul, and T. Lasri, 'Flexible UWB organic antenna for wearable technologies application', *IET Microwaves, Antennas Propag.*, 2018.
- [160] A. S. M. Alqadami, K. S. Bialkowski, A. T. Mobashsher, and A. M. Abbosh, 'Wearable Electromagnetic Head Imaging System Using Flexible Wideband Antenna Array Based on Polymer Technology for Brain Stroke Diagnosis', *IEEE Transactions on Biomedical Circuits and Systems*, 2018.
- [161] J. Laviada, M. T. Ghasr, M. Lopez-Portugues, F. Las-Heras, and R. Zoughi, 'Real-Time Multi-View SAR Imaging Using a Portable Microwave Camera with Arbitrary Movement', *IEEE Transactions on Antennas and Propagation*, 2018.
- [162] E. A. Krupinski, 'Medical imaging', in *Handbook of Visual Display Technology*, 2016.
- [163] M. Donelli, 'Microwave imaging', in *Imaging with Electromagnetic Spectrum: Applications in Food and Agriculture*, 2014.
- [164] Y. Wiaux, L. Jacques, G. Puy, A. M. M. Scaife, and P. Vandergheynst, 'Compressed sensing imaging techniques for radio interferometry', *Mon. Not. R. Astron. Soc.*, 2009.
- [165] E. C. Fear, J. Bourqui, C. Curtis, D. Mew, B. Docktor, and C. Romano, 'Microwave breast imaging with a monostatic radar-based system: A study of application to patients', *IEEE Trans. Microw. Theory Tech.*, 2013.
- [166] J. Sen Lee and E. Pottier, *Polarimetric radar imaging: From basics to applications*. 2017.
- [167] A. M. Hassan and M. El-Shenawee, 'Review of electromagnetic techniques for breast cancer detection', *IEEE Rev. Biomed. Eng.*, 2011.
- [168] T. Zwick, L. Zwirello, M. Jalilvand, and X. Li, 'Ultra wideband compact near-field imaging system for breast cancer detection', *IET Microwaves, Antennas Propag.*, 2015.
- [169] S. M. Aguilar, M. A. Al-Joumayly, M. J. Burfeindt, N. Behdad, and S. C. Hagness, 'Multiband miniaturized patch antennas for a compact, shielded microwave breast imaging array', *IEEE Trans. Antennas Propag.*, 2014.
- [170] B. Biswas, R. Ghatak, and D. R. Poddar, 'A Fern Fractal Leaf Inspired Wideband Antipodal Vivaldi Antenna for Microwave Imaging System', *IEEE Trans. Antennas Propag.*, 2017.
- [171] S. K. Hong, 'Resonance-based techniques for microwave breast cancer applications', no. September 2012, p. 195, 2012.
- [172] B. J. Mohammed, A. M. Abbosh, S. Mustafa, and D. Ireland, 'Microwave system for head imaging', *IEEE Trans. Instrum. Meas.*, 2014.
- [173] J. Jin, J. Gubbi, S. Marusic, and M. Palaniswami, 'An information framework for creating a smart city through internet of things', *IEEE Internet Things J.*, 2014.
- [174] A. Kamilaris and A. Pitsillides, 'Mobile Phone Computing and the Internet of Things: A Survey', *IEEE Internet of Things Journal*. 2016.
- [175] S. Moscato, L. Silvestri, N. Delmonte, M. Pasian, M. Bozzi, and L. Perregrini, 'SIW components for the Internet of Things: Novel topologies, materials, and manufacturing techniques', *WiSNet 2016 - Proceedings, 2016 IEEE Top. Conf. Wirel. Sensors Sens. Networks*, pp. 78–80, 2016.

- [176] S. Koziel and A. Bekasiewicz, 'Compact UWB monopole antenna for internet of things applications', *Electron. Lett.*, 2016.
- [177] Y. Mao, S. Guo, and M. Chen, 'Compact dual-band monopole antenna with defected ground plane for Internet of things', *IET Microwaves, Antennas Propag.*, vol. 12, no. 8, pp. 1332–1338, 2018.
- [178] A. M. Mansour *et al.*, 'Compact reconfigurable multi-size pixel antenna for cognitive radio networks and IoT environments', in *2016 Loughborough Antennas and Propagation Conference, LAPC 2016*, 2017.
- [179] A. Zanella, N. Bui, A. Castellani, L. Vangelista, and M. Zorzi, 'Internet of things for smart cities', *IEEE Internet Things J.*, 2014.
- [180] A. Mansour, M. Azab, and N. Shehata, 'Flexible paper-based wideband antenna for compact-size IoT devices', in *2017 8th IEEE Annual Information Technology, Electronics and Mobile Communication Conference, IEMCON 2017*, 2017.
- [181] A. Ramos, T. Varum, and J. N. Matos, 'Compact multilayer Yagi-Uda based antenna for IoT/5G sensors', *Sensors (Switzerland)*, 2018.
- [182] M. A. ul Haq and S. Koziel, 'Design optimization and trade-offs of miniaturized wideband antenna for internet of things applications', *Metrol. Meas. Syst.*, vol. 24, no. 3, pp. 463–471, 2017.
- [183] Z. N. Chen and M. Y. W. Chia, *Broadband Planar Antennas: Design and Applications*. 2006.
- [184] H. A. Wheeler, 'Fundamental limitations of small antennas', *Proc. IRE*, 1947.
- [185] L. J. Chu, 'Physical limitations of omni-directional antennas', *J. Appl. Phys.*, 1948.
- [186] R. F. Harrington, 'Effect of antenna size on gain, bandwidth, and efficiency', *J. Res. Natl. Bur. Stand. Sect. D Radio Propag.*, 1960.
- [187] J. S. McLean, 'A re-examination of the fundamental limits on the radiation Q of electrically small antennas', *IEEE Trans. Antennas Propag.*, 1996.
- [188] D. M. Grimes and C. A. Grimes, 'Radiation Q of dipole-generated fields', *Radio Sci.*, vol. 34, no. 2, pp. 281–296, 1999.
- [189] W. A. Davis, T. Yang, E. D. Caswell, and W. L. Stutzman, 'Fundamental limits on antenna size: a new limit', *IET Microwaves, Antennas Propag.*, 2011.
- [190] R. L. Fante, 'Quality Factor of General Ideal Antennas', *IEEE Trans. Antennas Propag.*, 1969.
- [191] B. F. Wang and Y. T. Lo, 'Microstrip Antennas for Dual-Frequency Operation', *IEEE Trans. Antennas Propag.*, 1984.
- [192] S. Maci, G. Biffi Gentili, P. Piazzesi, and C. Salvador, 'Dual-band slot-loaded patch antenna', *IEE Proc. Microw. Antennas Propag.*, 1995.
- [193] K. R. Carver and J. W. Mink, 'Microstrip Antenna Technology', *IEEE Trans. Antennas Propag.*, 1981.
- [194] H. Iwasaki, 'A circularly polarized small-size microstrip antenna with a cross slot', *IEEE Trans. Antennas Propag.*, 1996.

- [195] Y. Lu, Y. Huang, H. T. Chattha, and Y. Shen, 'Technique for minimising the effects of ground plane on planar ultra-wideband monopole antennas', *IET Microwaves, Antennas Propag.*, 2012.
- [196] S. Wang, H. W. Lai, K. K. So, K. B. Ng, Q. Xue, and G. Liao, 'Wideband shorted patch antenna with a modified half U-slot', *IEEE Antennas Wirel. Propag. Lett.*, 2012.
- [197] J. Wang, Q. Liu, and L. Zhu, 'Bandwidth enhancement of a differential-fed equilateral triangular patch antenna via loading of shorting posts', *IEEE Trans. Antennas Propag.*, 2017.
- [198] H. Zhu, X. Li, W. Feng, J. Xiao, and J. Zhang, 'A compact 267 GHz shorted annular ring antenna with surface wave suppression in 130 nm SiGe BiCMOS', *IEEE Antennas Wirel. Propag. Lett.*, 2018.
- [199] H. Malekpoor and S. Jam, 'Enhanced bandwidth of shorted patch antennas using folded-patch techniques', *IEEE Antennas Wirel. Propag. Lett.*, 2013.
- [200] R. Porath, 'Theory of miniaturized shorting-post microstrip antennas', *IEEE Trans. Antennas Propag.*, 2000.
- [201] R. B. Waterhouse, S. D. Targonski, and D. M. Kokotoff, 'Design and performance of small printed antennas', *IEEE Trans. Antennas Propag.*, 1998.
- [202] J. S. Kula, D. Psychoudakis, W. J. Liao, C. C. Chen, J. L. Volakis, and J. W. Halloran, 'Patch-antenna miniaturization using recently available ceramic substrates', *IEEE Antennas Propag. Mag.*, 2006.
- [203] B. Lee and F. J. Harackiewicz, 'Miniature microstrip antenna with a partially filled high-permittivity substrate', *IEEE Trans. Antennas Propag.*, 2002.
- [204] T. K. Lo, C. Ho, Y. Hwang, E. K. W. Lam, and B. Lee, 'Miniature aperture-coupled microstrip antenna of very high permittivity', *Electron. Lett.*, 1997.
- [205] J. Kapoor, 'Miniaturization of Microstrip Patch Antenna obtained by Patch Meandering and Shorting Pin Loading Technique', vol. 2, no. 1, pp. 21–24.
- [206] K. Y. Lam, K. M. Luk, K. F. Lee, H. Wong, and K. B. Ng, 'Small circularly polarized U-slot wideband patch antenna', *IEEE Antennas Wirel. Propag. Lett.*, 2011.
- [207] C. Kurter, A. P. Zhuravel, J. Abrahams, C. L. Bennett, A. V. Ustinov, and S. M. Anlage, 'Superconducting RF metamaterials made with magnetically active planar spirals', in *IEEE Transactions on Applied Superconductivity*, 2011.
- [208] C. Caloz and T. Itoh, 'Metamaterials for high-frequency electronics', in *Proceedings of the IEEE*, 2005.
- [209] A. V. Kildishev, A. Boltasseva, and V. M. Shalaev, 'Planar photonics with metasurfaces', *Science*. 2013.
- [210] S. Jahani, J. Rashed-Mohassel, and M. Shahabadi, 'Miniaturization of circular patch antennas using MNG metamaterials', *IEEE Antennas Wirel. Propag. Lett.*, 2010.
- [211] K. Rajab, R. Mittra, and M. Lanagan, 'Size reduction of microstrip patch antennas with left-handed transmission line loading', *IET Microwaves, Antennas Propag.*, 2007.
- [212] J. Liu, K. P. Esselle, S. G. Hay, and S. Zhong, 'Effects of printed UWB antenna miniaturization on pulse fidelity and pattern stability', *IEEE Trans. Antennas Propag.*,

2014.

- [213] Y. H. Chiu and Y. S. Chen, 'Multi-objective optimization for UWB antennas in impedance matching, gain, and fidelity factor', in *IEEE Antennas and Propagation Society, AP-S International Symposium (Digest)*, 2015.
- [214] L. Liu, S. W. Cheung, and T. I. Yuk, 'Compact MIMO antenna for portable devices in UWB applications', *IEEE Trans. Antennas Propag.*, 2013.
- [215] M. N. Srifi, S. K. Podilchak, M. Essaaidi, and Y. M. M. Antar, 'Planar circular disc monopole antennas using compact impedance matching networks for ultra-wideband (UWB) applications', in *APMC 2009 - Asia Pacific Microwave Conference 2009*, 2009.
- [216] B. Tian, Z. Li, and C. Wang, 'Boresight gain optimization of an UWB monopole antenna using FDTD and genetic algorithm', in *2010 IEEE International Conference on Ultra-Wideband, ICUWB2010 - Proceedings*, 2010.
- [217] W.-T. C. Chow-Yen-Desmond Sim and C.-H. Lee, 'Novel band-notch UWB antenna design with slit ground plane', *IJCAI Int. Jt. Conf. Artif. Intell.*, vol. 50, no. 8, pp. 4130–4136, 2007.
- [218] A. Bekasiewicz and S. Koziel, 'Structure and Computationally Efficient Simulation-Driven Design of Compact UWB Monopole Antenna', *IEEE Antennas Wirel. Propag. Lett.*, 2015.
- [219] S. Koziel, A. Bekasiewicz, Q. S. Cheng, and S. Li, 'On ultra-wideband antenna miniaturization involving efficiency and matching constraints', in *2017 11th European Conference on Antennas and Propagation, EUCAP 2017*, 2017.
- [220] S. Koziel and S. Ogurtsov, 'Simulation-driven design in microwave engineering: Methods', *Stud. Comput. Intell.*, 2011.
- [221] S. Koziel and S. Ogurtsov, *Antenna Design by Simulation-Driven Optimization*. 2014.
- [222] X. S. Yang, *Engineering Optimization: An Introduction with Metaheuristic Applications*. 2010.
- [223] J. Nocedal and S. J. Wright, *Numerical Optimization*.
- [224] P. L. Toint, A. R. Conn, and N. I. M. Gould, *Trust-Region Methods*.
- [225] S. F. O'Brien and K. L. Bierman, 'Conceptions and perceived influence of peer groups: interviews with preadolescents and adolescents.', *Child Dev.*, vol. 59, no. 5, pp. 1360–1365, 1988.
- [226] C. Portal, 'Ansys Hfss', *ANSYS HFSS Featur.*, 2014.
- [227] T. G. Kolda, R. M. Lewis, and V. Torczon, 'Optimization by Direct Search: New Perspectives on Some Classical and Modern Methods', *SIAM Rev.*, 2003.
- [228] D. E. Goldberg, *Genetic Algorithms in Search, Optimization, and Machine Learning*.
- [229] T. B. Fogel, David B, 'Evolutionary Computation 1: Basic Algorithms and Operators', *Compr. Chemom.*, 2000.
- [230] J. Kennedy, R. C. Eberhart, and Y. Shi, *Swarm intelligence*. 2001.
- [231] R. Storn and K. Price, 'Differential Evolution - A Simple and Efficient Heuristic for Global Optimization over Continuous Spaces', *J. Glob. Optim.*, 1997.

- [232] F. J. Ares-Pena, J. A. Rodriguez-Gonzalez, E. Villanueva-Lopez, and S. R. Rengarajan, 'Genetic algorithms in the design and optimization of antenna array patterns', *IEEE Trans. Antennas Propag.*, 1999.
- [233] P. J. Bevelacqua and C. A. Balanis, 'Optimizing antenna array geometry for interference suppression', *IEEE Trans. Antennas Propag.*, 2007.
- [234] S. Koziel, 'Computationally efficient multi-fidelity multi-grid design optimization of microwave structures', *Appl. Comput. Electromagn. Soc. J.*, vol. 25, no. 7, pp. 578–586, 2010.



School of Science and Engineering
Reykjavík University
Menntavegur 1
101 Reykjavík, Iceland
Tel. +354 599 6200
Fax +354 599
www.ru.is